

NOAA Technical Report NOS OES 002

---

# TAMPA BAY OCEANOGRAPHY PROJECT: PHYSICAL OCEANOGRAPHIC SYNTHESIS

Silver Spring, Maryland  
September 1993



FLWEST

**noaa** National Oceanic and Atmospheric Administration

---

U.S. DEPARTMENT OF COMMERCE  
National Ocean Service  
Office of Ocean and Earth Sciences  
Marine Analysis and Interpretation Division  
Coastal and Estuarine Oceanography Branch

# TAMPA BAY OCEANOGRAPHY PROJECT: PHYSICAL OCEANOGRAPHIC SYNTHESIS

Editor: Chris E. Zervas

Contributors: Kathryn T. Bosley, Richard W. Bourgerie, Marc Grossman,  
Kurt W. Hess, Leonard E. Hickman, C. Reid Nichols, and  
Chris E. Zervas

September 1993



---

**U.S. DEPARTMENT  
OF COMMERCE**  
Ronald H. Brown, Secretary

**National Oceanic and  
Atmospheric Administration**  
D. James Baker, Under Secretary

**National Ocean Service**  
W. Stanley Wilson,  
Assistant Administrator

**Office of Ocean and  
Earth Sciences**  
Melbourne G. Briscoe

**Marine Analysis and  
Interpretation Division**  
Ledolph Baer

**Coastal and Estuarine  
Oceanography Branch**  
Bruce Parker

NOAA  
NATIONAL OCEANOGRAPHIC AND  
ATMOSPHERIC ADMINISTRATION

**NOTICE**

Mention of a commercial company or product does not constitute an endorsement by NOAA. Use for publicity or advertising purposes of information from the publication concerning proprietary products or the tests of such products is not authorized.

## TABLE OF CONTENTS

LIST OF FIGURES .....	iv
LIST OF TABLES .....	vi
LIST OF ACRONYMS AND ABBREVIATIONS .....	vii
EXECUTIVE SUMMARY .....	ix
1. INTRODUCTION .....	1
1.1. The Tampa Bay Oceanography Project .....	2
1.2. General Description of Tampa Bay .....	3
1.3. Previous Oceanographic Studies of Tampa Bay .....	5
Physical Oceanographic Surveys of Tampa Bay .....	5
Physical Oceanographic Summaries of Tampa Bay .....	5
Previous Modeling Studies .....	6
1.4. Organization of This Report .....	7
2. CURRENTS .....	11
2.1. Introduction .....	11
2.2. Harmonic Analysis .....	12
Tidal Constituents .....	12
Analysis Methods .....	13
Spatial Variation of Tidal Current Constituents .....	16
Temporal Variation of Tidal Current Constituents .....	16
Tidal Current Classification .....	17
Rotary Character of Offshore Stations .....	17
Greenwich Intervals and Mean Maximum Flood and Ebb Currents .....	18
2.3. Nontidal Circulation .....	18
Mean Currents .....	20
Residual Currents .....	21
2.4. Towed ADCP Transects .....	23
Method of Analysis .....	24
Cross Sectional Velocity Contour Plots .....	24
2.5. Conclusions .....	25
3. WATER LEVELS .....	51
3.1. Introduction .....	51
3.2. Harmonic Analysis .....	51
Spatial Variation of Tidal Constituents .....	52
Tidal Classification .....	53
Greenwich Intervals and Tidal Ranges .....	54
Temporal Variation .....	56

3.3. Nontidal Water Levels .....	57
Residual Analysis .....	57
Storm Events .....	58
3.4. Conclusions .....	59
4. METEOROLOGY AND HYDROLOGY .....	71
4.1. Introduction .....	71
4.2. Local Climate .....	71
4.3. Windfield Characteristics .....	72
Data Collection and Analysis .....	72
Spatial Variability .....	73
Temporal Variability .....	75
4.4. Rainfall and Waterway Discharge Analysis .....	76
Data Sources and Processing .....	76
Rainfall Analysis .....	76
Waterway Discharge .....	77
4.5. Conclusions .....	78
5. WATER MASS CHARACTERISTICS .....	91
5.1. Introduction .....	91
Measurement Program .....	91
Background Information .....	91
5.2. Data Processing and Plotting .....	93
The CTD Transects .....	93
Tidal Stage Determination .....	94
The Moored CTs .....	94
General Characteristics .....	95
5.3. Temporal Variability of Salinity and Temperature .....	95
Tidal Scale .....	95
Weekly Scale .....	96
Seasonal Scale .....	97
Interannual Scale .....	98
5.4. Spatial Variability of Salinity and Temperature .....	98
Vertical .....	98
Horizontal .....	98
5.5. Conclusions .....	99
6. NONTIDAL CIRCULATION .....	119
6.1. Shelf Water Level Effect .....	119
Energy Density Spectra .....	120
Cross Spectral Analysis .....	121
Filtered Time Series .....	121
Prediction of the Shelf Effect .....	122

6.2. Density Gradient Effect .....	123
Observed Long-Term Current .....	124
Model/Data Comparison .....	124
6.3. Predictability of Currents and Water Levels .....	126
Currents .....	126
Water Levels .....	127
6.4. Conclusions .....	128
7. MODELED HYDRODYNAMICS .....	143
7.1. Introduction .....	143
7.2. Model Formulation .....	143
Boundary Conditions .....	144
Model Accuracy .....	145
7.3. The Natural Period .....	145
7.4. Semidiurnal Tidal Currents .....	146
7.5. Semidiurnal Tides .....	147
7.6. Response to Winds .....	148
7.7. Salinity Distribution .....	149
7.8. Mean Buoyancy-Driven Currents .....	150
7.9. Conclusions .....	150
8. OVERVIEW OF THE CIRCULATION OF TAMPA BAY .....	163
8.1. Tidal Circulation .....	163
8.2. Nontidal Circulation .....	164
Meteorologically Forced Currents .....	164
Hydrologically Forced Currents .....	165
Summary .....	166
ACKNOWLEDGEMENTS .....	167
REFERENCES .....	169
APPENDIX A    DEPLOYMENT TIME LINES FOR TOP DATA SETS .....	175
APPENDIX B    TYPICAL TIDAL AND TIDAL CURRENT CONSTITUENTS .....	181

## LIST OF FIGURES

Figure 1.1.	Tampa Bay area map . . . . .	8
Figure 1.2.	Bathymetry of Tampa Bay . . . . .	9
Figure 2.1.	Location of TOP current meter stations. . . . .	26
Figure 2.2.	Location of the towed ADCP transects . . . . .	27
Figure 2.3.	Sample tidal current records at C-2 . . . . .	28
Figure 2.4.	Amplitude of the major axis of the constituent ellipses . . . . .	29
Figure 2.5.	Epoch of the major axis of the constituent ellipses. . . . .	30
Figure 2.8.	Annual variation of tidal current constituent amplitudes . . . . .	33
Figure 2.9.	Annual variation of tidal current constituent epochs . . . . .	34
Figure 2.10.	Tidal current classification ratio $(K_1 + O_1)/(M_2 + S_2)$ . . . . .	35
Figure 2.11.	Tidal current ellipses for $M_2$ , $S_2$ , $K_1$ , and $O_1$ . . . . .	36
Figure 2.12.	Greenwich intervals . . . . .	37
Figure 2.13.	Mean maximum flood and ebb currents . . . . .	38
Figure 2.14.	Mean current at a depth of 10 m . . . . .	39
Figure 2.15.	Mean current at a depth of 5 m . . . . .	40
Figure 2.16.	Mean current at a depth of 2 m . . . . .	41
Figure 2.20.	CT-1 towed ADCP transects . . . . .	45
Figure 2.21.	CT-2 towed ADCP transects . . . . .	46
Figure 2.22.	CT-3 towed ADCP transects . . . . .	47
Figure 2.23.	CT-4 towed ADCP transects . . . . .	48
Figure 2.24.	CT-5 towed ADCP transects . . . . .	49
Figure 3.1.	Water level station locations during the TOP . . . . .	60
Figure 3.2.	Amplitude of the tidal constituents . . . . .	61
Figure 3.3.	Epoch of the tidal constituents . . . . .	62
Figure 3.4.	Tidal amplitude ratio $(K_1 + O_1)/(M_2 + S_2)$ . . . . .	63
Figure 3.5.	Greenwich intervals and ranges . . . . .	64
Figure 3.6.	Monthly mean sea level for St. Petersburg and Clearwater Beach . . . . .	65
Figure 3.7.	Annual mean sea level at St. Petersburg and Clearwater Beach . . . . .	66
Figure 3.8.	Residual water levels . . . . .	67
Figure 3.9.	Spectra of observed and residual water levels . . . . .	68
Figure 3.10.	Residual water level during three storms . . . . .	69
Figure 4.1.	Meteorological station locations in Tampa Bay . . . . .	79
Figure 4.2.	The Tampa Bay watershed . . . . .	80
Figure 4.3.	Air temperature and barometric pressure . . . . .	81
Figure 4.4.	Tampa Bay winds . . . . .	82
Figure 4.5.	Rotary cross spectral analysis of winds at TPA . . . . .	83
Figure 4.6.	Synoptic scale winds at TPA, M-3, M-2, and M-1. . . . .	84
Figure 4.7.	Rotary spectral analysis of the wind at TPA. . . . .	85
Figure 4.8.	Sea breeze system over Tampa Bay. . . . .	86
Figure 4.9.	The wind vector pattern observed during the passage of three storms . . . . .	87
Figure 4.10.	Monthly total rainfall observed at TPA. . . . .	88
Figure 4.11.	Monthly total rainfall at eight NCDC weather stations . . . . .	88
Figure 4.12.	Mean monthly discharge for eleven rivers which drain into Tampa Bay. . . . .	89

Figure 4.13.	Mean monthly discharge for eleven Tampa Bay waterways. . . . .	89
Figure 5.1.	Location of the TOP CTD transects. . . . .	101
Figure 5.2.	Location of 31 moored CT/CTD stations. . . . .	102
Figure 5.3.	Temperature vs salinity diagram . . . . .	103
Figure 5.4.	Temporal variation of water mass characteristics at Egmont Channel . . . .	104
Figure 5.5.	Salinity versus depth along Transect 6 during Cruise 1 . . . . .	105
Figure 5.6.	Salinity and temperature energy density spectra for C-2 and C-4 . . . . .	106
Figure 5.7.	Salinity and temperature energy density spectra for C-46 and C-41 . . . . .	107
Figure 5.8.	Cross spectral analysis of density and currents . . . . .	108
Figure 5.9.	Surface salinity and temperature for August 17-18, 1990. . . . .	109
Figure 5.10.	Surface salinity and temperature for Nov. 9-15, 1990 . . . . .	110
Figure 5.11.	Surface salinity and temperature for Feb. 26-Mar. 5, 1991 . . . . .	111
Figure 5.12.	Surface salinity and temperature for May 24-June 4, 1991. . . . .	112
Figure 5.13.	Surface salinity and temperature for August 17-30, 1991. . . . .	113
Figure 5.14.	Comparison of monthly mean seawater and air temperature . . . . .	114
Figure 5.15.	Salinity and temperature versus depth along Transect 5 . . . . .	115
Figure 5.16.	Vertical salinity and temperature difference . . . . .	116
Figure 5.17.	Salinity versus depth along Transect 2 . . . . .	117
Figure 5.18.	The variation of the strength of the salinity gradient . . . . .	118
Figure 6.1.	Energy density spectra . . . . .	129
Figure 6.2.	Cross spectral analysis between longshore wind and water level . . . . .	130
Figure 6.3.	Cross spectral analysis between water levels . . . . .	131
Figure 6.4.	Cross spectral analysis between change of water levels and currents . . . .	133
Figure 6.5.	36-hour low-pass filtered time series for summer 1990 . . . . .	134
Figure 6.6.	36-hour low-pass filtered time series for winter 1991 . . . . .	135
Figure 6.7.	36-hour low-pass filtered time series for summer 1991 . . . . .	136
Figure 6.8.	36-hour low-pass filtered time series during a storm . . . . .	137
Figure 6.9.	Water levels at St. Petersburg after subtraction . . . . .	138
Figure 6.10.	Vertical profiles of along-channel currents at mid Bay . . . . .	139
Figure 6.11.	The mid Bay long-term current at C-4. . . . .	140
Figure 6.12.	Density difference from the mouth to the head . . . . .	140
Figure 6.13.	Total river discharge into Tampa Bay. . . . .	141
Figure 6.14.	Comparison of the mean along-channel flow at mid-Bay stations . . . . .	141
Figure 6.15.	Reduction of variance in currents at mid Bay . . . . .	142
Figure 6.16.	Diurnal and semidiurnal energy in the windfield . . . . .	142
Figure 6.17.	Reduction of variance in water levels at St. Petersburg. . . . .	143
Figure 7.1.	Plan view of the orthogonal curvilinear grid . . . . .	152
Figure 7.2.	The vectors representing the maximum flood current . . . . .	153
Figure 7.3.	Contours of the maximum flood speed at prediction depth . . . . .	154
Figure 7.4.	Contours of the time of maximum flood . . . . .	155
Figure 7.5.	Contours of the tide range . . . . .	156
Figure 7.6.	Contours of the time of maximum tide . . . . .	157
Figure 7.7.	Contours of the mean surface salinity for climatological river flow . . . . .	158
Figure 7.8.	Mean near-surface buoyancy-driven circulation . . . . .	159
Figure 7.9.	Mean near-bottom buoyancy-driven circulation . . . . .	160
Figure 7.10.	Mean baroclinic currents and mean isohalines at the Sunshine Skyway . .	161

## LIST OF TABLES

Table 1.1.	Characteristics of some major U. S. estuaries . . . . .	4
Table 2.1.	Amplitude and epoch of five tidal current constituents . . . . .	14
Table 2.2.	Amplitude and epoch of five tidal current constituents . . . . .	15
Table 2.3.	Vertical variation of tidal current constituents . . . . .	17
Table 2.4.	Greenwich intervals and mean maximum flood and ebb speeds . . . . .	19
Table 2.5.	Standard deviations of observed and residual currents . . . . .	22
Table 3.1.	Amplitude and epoch of the primary semidiurnal constituents . . . . .	52
Table 3.2.	Amplitude and epoch of the primary diurnal constituents . . . . .	53
Table 3.3.	Greenwich intervals and mean and great diurnal ranges . . . . .	55
Table 3.4.	Epoch and Greenwich interval differences. . . . .	56
Table 3.5.	Standard deviations of observed and residual water levels . . . . .	57
Table 4.1.	Monthly prevailing wind direction and mean barometric pressure . . . . .	72
Table 4.2.	TOP meteorological station winds. . . . .	74
Table 4.3.	Average monthly river discharge into Tampa Bay . . . . .	78
Table 5.1.	TOP CTD Transect information . . . . .	92
Table 5.2.	Variation of observed water mass characteristics . . . . .	100
Table 7.1.	Modeled water level characteristics at two locations . . . . .	149
Table 7.2.	Mean along-channel vertically-averaged current . . . . .	149
Table A.1.	Current meter deployments . . . . .	176
Table A.2.	Water level gauge deployments . . . . .	177
Table A.3.	Meteorological instrument deployments . . . . .	178
Table A.4.	CT and CTD deployments . . . . .	179
Table B.1.	Harmonic constituents for Egmont Channel . . . . .	182
Table B.2.	Harmonic constituents for St. Petersburg . . . . .	183

## LIST OF ACRONYMS AND ABBREVIATIONS

ADCP	Acoustic Doppler Current Profiler
ASCII	American Standard Code for Information Interchange
BASIS	Bay Area Scientific Information Symposium
CEOB	Coastal and Estuarine Oceanography Branch
cfs	Cubic Feet per Second
cpd	cycles per day
CT	Conductivity-Temperature
CTD	Conductivity-Temperature-Depth
DOI	Department of the Interior
FL	Florida
HP	Hewlett-Packard
HCEPC	Hillsborough County Environmental Protection Commission
LORAN	Long Range Navigation
NCDC	National Climatic Data Center
NOAA	National Oceanic and Atmospheric Administration
NODC	National Oceanographic Data Center
NOS	National Ocean Service
MAID	Marine Analysis and Interpretation Division
MEC	Maximum Ebb Current
MFC	Maximum Flood Current
MLLW	Mean Lower Low Water
MSL	Mean Sea Level
OES	Office of Ocean and Earth Sciences
OLLD	Ocean and Lake Levels Division
PORTS	Physical Oceanographic Real-Time System
psu	practical salinity unit
rms	root mean square
SBE	Slack Before Ebb
SBF	Slack Before Flood
SWFWMD	Southwest Florida Water Management District
TOP	Tampa Bay Oceanography Project
TPA	Tampa International Airport
USCG	United States Coast Guard
USGS	United States Geological Survey
UT	Universal Time

## EXECUTIVE SUMMARY

NOS's Tampa Bay Oceanography Project (TOP) collected a large and diverse set of physical oceanographic and meteorological data between June 1990 and September 1991. This report presents the results of the data analysis and synthesizes these results in order to characterize the hydrodynamics of Tampa Bay. The TOP data set includes: (1) current meter data from 40 fixed stations (20 occupied by acoustic Doppler current profilers (ADCPs) and 20 occupied by electromagnetic current meters), (2) current meter data from a downward-facing towed ADCP along five transects in the Bay, (3) water levels at 16 stations along the shores of the Bay and the Gulf of Mexico, (4) meteorological (wind, temperature, and atmospheric pressure) data at five stations in the Bay, (5) time series of salinity and temperature data at 36 fixed sites, and (6) salinity and temperature profiles over depth along six transects. The following is a summary of the major findings of the synthesis:

- Tidal currents account for most of the variability of the currents in Tampa Bay. The tidal constituents of the water level and current signals were obtained by harmonic analysis methods. Both the tide and the tidal currents are classified as mixed, mainly semidiurnal throughout the Bay and on the adjacent continental shelf. Tidal currents are rectilinear, having a minor ellipse axis less than 5% of the major ellipse axis, at most locations in the Bay. Tidal currents are rotary on the continental shelf.
- The strongest tidal currents were found in Egmont Channel (where a peak speed of 1.63 m/s was measured), in lower Tampa Bay, and at the entrance to Old Tampa Bay. The weakest tidal currents were found in Hillsborough Bay. Seasonal variation was seen in several tidal current constituents, with the amplitudes and epochs of  $K_1$  and  $S_2$  having the greatest variability.
- Towed, downward-looking ADCP measurements showed that the location of the maximum current, which was usually centered over the deepest part of the natural channel, can vary by as much as 1.5 km. There may be small-scale (100 m or less) features in the current field due to the influence of dredged channels, spoil islands, and submerged spoil mounds.
- The tide in Tampa Bay is a damped progressive wave that is reflected at the head of the Bay. The tide has the characteristics of a standing wave in Hillsborough Bay (uniform water level epochs and a 90° lag of water level epoch relative to current epoch). Tidal ranges increase by about 30% from Egmont Channel to the head of Old Tampa Bay. The tidal constituent epochs show that the tide requires four to five hours to reach the head of Old Tampa Bay.
- Synoptic-scale winds were highly coherent over Tampa Bay, while higher frequency winds were more variable from station to station. Wind speeds were higher for stations closer to the Gulf of Mexico. There was significant windfield energy at the diurnal and semidiurnal frequencies due to the daily sea breeze cycle, which often intensified into

afternoon thunderstorm activity during the summer. Currents induced by sea breezes may have influenced the tidal current constituents with periods closest to 12 and 24 hours ( $S_2$  and  $K_1$ , respectively).

- The water mass distribution of Tampa Bay exhibited a high degree of temporal and spatial variability. On the tidal scale, salinity increased during flood and decreased during ebb. Seasonal and interannual variability was also evident in the water mass structure. The highest precipitation and river discharge occurred during the summer months when afternoon thunderstorms were common. Because of the higher river flow in the summer, the salinity in the upper Bay was depressed, resulting in a strong head-to-mouth density gradient. The head-to-mouth density gradient drives a long-term estuarine flow with saline inflow near the bottom and fresher outflow near the surface.
- Both salinity and temperature were relatively uniform vertically, although slight vertical stratification can occur in Hillsborough Bay during the summer. The water temperature of the Bay was relatively uniform spatially and closely tracked the monthly mean air temperature.
- Significant nontidal signals (17% to 90% of the total signal amplitude) were present in the water levels and currents recorded during TOP. The water level fluctuations at Clearwater Beach were found to be coherent with longshore winds over the continental shelf which raise or lower coastal water levels by transport perpendicular to the coast. Subtidal water levels at Clearwater Beach were found to be highly coherent with subtidal water levels at St. Petersburg; the rate of change of water level at Clearwater Beach was found to be coherent with along-channel currents at mid-Bay.
- Prediction schemes were developed to quantify the shelf effect on water levels at St. Petersburg and on currents at mid-Bay, using water levels at Clearwater Beach. The subtraction of the shelf prediction resulted in a large reduction in variability of the water level signal at St. Petersburg, especially during the winter months when synoptic-scale storms were more frequent. A smaller reduction in variability, mainly during the winter months, was observed when the shelf effect was subtracted from the mid-Bay current.
- A prediction scheme was also developed for the estuarine circulation profile at mid-Bay, depending on the strength of the density gradient between the head and the mouth of the Bay. The subtraction of the density-driven current resulted in a significant reduction in variability for the summer of 1991 when a strong head-to-mouth density gradient was present in the Bay.
- The three-dimensional numerical circulation model showed that the natural period of the Bay was 10.7 hours, the highest tide range was in upper Old Tampa Bay, and the lowest tide range was in mid-Tampa Bay near Pinellas Point. The barotropic current at the Sunshine Skyway due to a steady 10 m/s wind from the southwest was 6 cm/s toward the southwest. In the upper Bay, south of the Interbay Peninsula, there were westward buoyancy currents in the upper layer, driven by east-west salinity differences.

# 1. INTRODUCTION

Kurt W. Hess, Chris E. Zervas, and Kathryn T. Bosley

The primary goal of the Tampa Bay Oceanography Project (TOP), undertaken by the National Ocean Service (NOS) during 1990 and 1991, was to improve NOS's tide and current predictions and thereby increase navigational safety in the Bay. This report is a synthesis of the scientific knowledge gained from TOP and it incorporates the results of the analysis of several different types of data collected by NOS with some results from previous investigations. Although the synthesis focuses mainly on tidal phenomena, it also considers atmospheric forcing, fresh-water inflows, and the influence of the Gulf of Mexico on the circulation in the Bay. The results are used to characterize the hydrodynamics of Tampa Bay and to draw conclusions about the relative importance of the driving forces operating on Tampa Bay and their influence on the predictability of the tidal and nontidal water levels and currents.

Tampa Bay is the largest estuary and the largest port in Florida and is the seventh largest U. S. commercial port in terms of tonnage handled (Estevez et al., 1985). The Bay has mixed (i.e., semidiurnal and diurnal) tides and tidal currents. Winds and horizontal density gradients due to fresh-water inflow are also factors in determining local currents. Since the previous NOS circulation survey in 1963, numerous changes in the Bay's bathymetry, wetlands, runoff patterns, shoreline, marine terminal configurations, and bridge pier placements have caused changes in the circulation pattern. In response, NOS initiated the multi-year TOP to collect oceanographic data sufficient to update NOS predictions of tides and tidal currents, provide real-time current information, and to develop and validate a three-dimensional model of the Bay's circulation. These data augment those collected in previous investigations.

The extensive oceanographic data set collected in Tampa Bay during TOP consists of (1) current meter data from 40 fixed stations, including both acoustic Doppler current profilers (ADCPs) and electromagnetic current meters; (2) current meter data from a downward-facing towed ADCP at five transects in the Bay; (3) water levels from 16 stations along the shore of the Bay and Gulf; (4) wind, temperature, and atmospheric pressure measurements at five meteorological stations in the Bay and additional temperature, solar radiation, and humidity measurements at one station; (5) time series of salinity and temperature data at three mooring sites with near-bottom and near-surface measurements; (6) near-bottom measurements at 33 of the fixed current meter sites; and (7) salinity and temperature profiles over depth at 684 stations along six transects.

The following strategy for analysis and synthesis of the data is used in this report. First, the currents and water levels are analyzed using harmonic analysis techniques to determine the constituent amplitudes and epochs that are required for prediction. Then, predicted currents and water levels are removed from the observed signal and a determination is made about the size of the nontidal residual current. Next, the meteorology, hydrology, and water mass characteristics are analyzed as separate phenomena, but with the knowledge that they are important in determining the residual or nontidal part of the circulation. The period of observation in TOP is analyzed for differences from mean climatological conditions. Next, there is a detailed analysis of the nontidal currents and their relation to nontidal water levels on the west Florida

shelf and horizontal buoyancy forcing. Model results are analyzed to augment the observational data.

## **1.1. THE TAMPA BAY OCEANOGRAPHY PROJECT**

TOP was initiated in response to mariners' observations that NOAA's published current predictions often do not reflect actual conditions, particularly near the Sunshine Skyway. Concerns regarding NOAA's tide predictions and tidal current charts for Tampa Bay were also expressed. At present, the published NOAA tidal current predictions are computed from measurements acquired in 1963. Results from a 2-month quality assurance miniproject carried out in 1988 and 1989 (Williams et al., 1989) confirmed that improved circulation information was required, leading to the initiation of TOP. TOP was planned and carried out by scientists from the Office of Ocean and Earth Sciences (OES) in the Coastal and Estuarine Oceanography Branch (CEOB) with assistance from the Ocean and Lake Levels Division (OLLD) and the Ocean Systems Data Group (OSDG). TOP consists of three major components: (1) the circulation survey, (2) the development and application of a numerical circulation model, and (3) the development and installation of a Physical Oceanographic Real-Time System (PORTS). The TOP Plan (NOS, 1990a) and annual progress reports (Hess, 1990; Hess, 1992b) contain details of the project.

An intensive 16-month circulation survey of currents, water levels, water temperature, salinity, winds, and other meteorological parameters began in June 1990 and was successfully completed in September 1991. The TOP circulation survey resulted in the greatest volume of circulation measurements acquired from one estuary in the 100-year history of NOAA's Coastal Ocean Circulation Program; details of the measurement program, instrument locations, and data availability can be found in Nowadly (1992). Data from the circulation survey are being used to revise and expand NOAA's tide and current prediction tables, beginning with the 1994 tables. The new data will also be used to estimate prediction uncertainties due to wind and river effects.

A three-dimensional, time-varying, curvilinear grid numerical circulation model for the Bay has been run and its skill has been assessed (Hess and Bosley, 1992; Hess, 1993). The model, when fully calibrated and validated, will be used to produce a circulation and water level atlas, an information product that is far more advanced than the traditional tidal current charts. The model, combined with information from the 16-month survey, will provide important new information about the physical processes in Tampa Bay resulting from the combined effects of astronomical tides, winds, and density gradients.

The installation of the Nation's first fully-integrated PORTS began in Tampa Bay with a prototype in September 1990. During the course of the TOP survey, PORTS was developed and became fully operational in October 1991, with information available both as a single-call, voice-response telephone message and as either a text message or a data file via modem. This system, which is now in continuous operation, was the first of its kind anywhere in the world (Frey, 1991; Appell et al., 1991; Bethem and Frey, 1991; Nichols, 1993). PORTS consists of ADCP current meters located at the Sunshine Skyway and the mouth of Old Tampa Bay, a

meteorological station located near Cut B and Manatee Channel, and water level and wind sensors located at Port Tampa, St. Petersburg, Port Manatee, and the McKay Bay entrance. Data available in real time from the PORTS include currents at all ADCP locations, winds and water levels from the corresponding sensors, and a nowcast of currents at the intersection of the navigation channel and the Port Manatee Channel (Williams, 1993). Ongoing maintenance and operation of the PORTS is made possible through a cooperative agreement with the Greater Tampa Bay Marine Advisory Council.

Data and information products and services resulting from TOP include (1) quality-controlled circulation survey data and a survey report describing the field data, (2) revision of NOAA's tide and current prediction tables, (3) a model-generated circulation and water level forecast atlas, (4) model-generated simulations of circulation and water levels for various scenarios on magnetic media, and (5) a technical report on the physical oceanography of Tampa Bay.

In addition to improving the safety and efficiency of navigation within the Bay, TOP was also planned to provide circulation and water level data to aid in rapid response to hazardous material spills, aid in search and rescue missions, and assist environmental management of the Bay.

## **1.2. GENERAL DESCRIPTION OF TAMPA BAY**

Tampa Bay is the largest estuary in Florida and has been widely described in the literature (Figure 1.1). Compared to other estuaries, the Bay has relatively little fresh-water inflow as compared to its tidal prism (NOS, 1985), indicating that salinities should be relatively high since the Bay contains little fresh water. Table 1.1 lists several major U.S. estuaries and their important characteristics as compiled by NOAA (NOS, 1985). Independent estimates of the area are 1,031 km<sup>2</sup> (Lewis and Whitman, 1985) for the Bay and 4,623 km<sup>2</sup> (Clark and MacAuley, 1989) for the watershed. The Bay has a length of 53 km from Passage Key Inlet to the mouth of the Hillsborough River and a width of 10.5 km near Port Manatee. The Bay's average depth is 3.7 m (Goodwin, 1987). The maximum depth of 27 m occurs just north of Egmont Key, although inside the Bay the greatest depths are 9 m in the broad natural channel that extends from Mullet Key northeast up to the mouth of the Little Manatee River. Another deep area runs east-west and lies just south of the Interbay Peninsula. A contour plot the bathymetry is shown in Figure 1.2. The dredging of an extensive system of shipping channels has resulted in the creation of large spoil islands and submerged disposal areas. Extensive filling has created the land approaches to four major bridges across Tampa Bay: three in Old Tampa Bay and one (the Sunshine Skyway) in the lower Bay.

Tides in Tampa Bay are driven by the tides of the adjacent Gulf of Mexico. They have a small amplitude (the diurnal range is 70 cm in the NOS Tide Tables) and are mixed (i.e. having diurnal and semidiurnal components of about the same size). Tidal currents are generally the reversing type, have flood and ebb directions nearly parallel to the isobaths, and reach maximum speeds of 200 cm/s in Egmont Channel according to the NOS Tidal Current Tables. Tidal currents on the adjacent Florida shelf are rotary in nature. The net shelf currents set generally to the north at speeds up to 50 cm/s (U.S. Navy Pilot Charts).

**Table 1.1. Characteristics of some major U. S. estuaries ranked by surface area (NOS, 1985). The flow ratio is the annual mean volume of fresh water entering the estuary during a semidiurnal tidal cycle divided by the mean tidal prism.**

Estuary	Surface Area (km <sup>2</sup> )	Watershed Area (km <sup>2</sup> )	Mean Flowrate (m <sup>3</sup> /s)	Flow Ratio
Narragansett Bay	427	3,444	91	.006
Apalachicola Bay	554	45,405	8,234	.133
Tampa Bay	893	6,729	68	.006
Mobile Bay	1,059	102,888	2,244	.449
San Francisco Bay	1,171	113,558	917	.032
Pamlico-Albemarle Sound	7,638	46,568	1,274	.050
Chesapeake Bay	9,920	122,572	2,428	.063

Climatologically, Tampa Bay lies in a transition zone between the temperate climate to the north and the tropical climate to the south (Wooten, 1985). Summers are long and humid and winters are mild. The sun shines approximately 66% of the daylight hours, with maximums occurring during April and May (NOAA, 1990). Thunderstorms are common from June through September. Prevailing winds in Florida are easterly and average 3.7 m/s in Tampa Bay, although winds are northerly during winter (October through January). The maximum monthly averaged wind speed of 4.2 m/s occurs during March when the winds are southerly. Westerly sea breezes are also prominent. The highest winds occur in the June-October hurricane season and during thunderstorms.

Fresh-water inflow from the Hillsborough, Alafia, Manatee, and Little Manatee Rivers, which comprises approximately 80% of the total runoff (Flannery, 1989), mixes with Gulf of Mexico water to give Tampa Bay water its estuarine character. Most of the discharge is along the eastern side of the Bay. Annual river flow generally follows the precipitation cycle, although rainfall is highly spatially variable and discharge is modified by impoundments and withdrawals. The total annual mean discharge was approximated to be 57 m<sup>3</sup>/s by Flannery (1989) and 54 m<sup>3</sup>/s by Goodwin (1987). Peak river discharge occurs during the June-September thunderstorm season.

Salinities in the Bay vary from highs of 30 or more practical salinity units (psu) at the entrance, which is dominated by conditions in the Gulf, to lows of 20 psu in the northern and eastern parts of Hillsborough Bay, in McKay Bay, and in the northwest part of Old Tampa Bay (Boler, 1992). South of the Little Manatee River, vertically-averaged salinities are generally higher on the eastern side due to the deeper natural channel, while north of the Little Manatee River salinities are lower on the east side due to the larger fresh-water discharge. Salinities in the Bay are lowest in summer, when discharge is greatest, and highest in winter. Outside Tampa Bay on the west Florida shelf, the seasonal range is approximately 5 psu and the annual variation is just the opposite of that inside the Bay, with minimums of 31 occurring at the surface in January and

maximums of 36 psu at the bottom occurring in summer (Dragovich and Sykes, 1967). Vertical stratification is slight but is strongest in Hillsborough Bay.

Water temperatures are relatively uniform baywide and vary from 11.7°C in winter to 32.8°C in summer (Boler, 1992). The shelf temperature varies from a minimum of 14°C in winter to a maximum of 30°C in summer, with maximum stratification of at most 2°C (Dragovich and Sykes, 1967).

### **1.3. PREVIOUS OCEANOGRAPHIC STUDIES OF TAMPA BAY**

Numerous oceanographic studies of Tampa Bay have been conducted by NOAA, U.S Geological Survey (USGS), Department of Interior (DOI), Florida state agencies, universities, and others.

#### **Physical Oceanographic Surveys of Tampa Bay**

Dragovich and Sykes (1967) reported on a physical and chemical oceanographic survey of Tampa Bay and the adjacent shelf (out to about 83 km) carried out during 1958 - 1961 by DOI. They depicted monthly sections of temperature, salinity, density ( $\sigma_t$ ), inorganic phosphorus, total phosphorous, nitrogen, and copper along the occupied transects.

Dinardi (1978) described an extensive circulation survey of the Bay carried out by the Coast and Geodetic Survey (NOS's predecessor) in 1963. These data were used for the NOAA Tidal Current Tables and the Tidal Current Charts for Tampa Bay. The most recent NOS bathymetric surveys of the Bay occurred during 1957 and 1958.

Boler (1992) described the ongoing data collection program of the Hillsborough County Environmental Protection Commission (HCEPC). Although directed at measuring water quality variables, the HCEPC surveys salinity and temperature on a regular basis and monitors meteorological and river discharge data.

#### **Physical Oceanographic Summaries of Tampa Bay**

In a major survey produced by the State University System of Florida, Jones et al. (1973) summarized the oceanography of the eastern Gulf of Mexico and Florida shelf, especially as it relates to the Loop Current. They discuss currents, water mass structure, and hydrographic sections for the Florida shelf and deeper waters. Climatic features for Florida and Tampa are discussed by Jordan (1973). Ross (1973) summarized Florida estuaries in terms of tide range, drainage area, and mean fresh-water inflow.

Goodwin and Michaelis (1976) of USGS reported on a water level study carried out by USGS from 1971 to 1973. During the study period, the maximum tide at St. Petersburg was recorded at 1.5 m during Hurricane Agnes and the minimum tide was recorded at 0.9 m below mean sea level.

In a NOAA Estuarine Programs Office symposium, Flannery (1989) summarized the hydrography of the Bay's watershed and discussed the character of fresh-water discharge and its role in supplying sediments and nutrients to the estuary. Goodwin (1989) summarized the circulation in Tampa Bay by comparing the tidal prism to the mean fresh-water inflow (with a ratio equalling 200) to indicate an unstratified estuary. He also hypothesized that a set of tidally-induced residual current gyres, which resulted from the interaction of tidal currents with the topography, were important for mixing in the Bay.

Many aspects of the Bay were discussed at the Bay Area Scientific Information Symposiums (BASIS and BASIS II). Weisberg and Williams (1992) described preliminary results from the analysis of TOP data. (The first author was supported by a NOAA Sea Grant.) Even though the Bay is nearly homogeneous in the vertical, large horizontal density gradients can give rise to strong buoyancy forcing. Also, the ADCP located under the Sunshine Skyway recorded currents that have a net up-estuary flow from the bottom to 3.6 m from the surface; the authors hypothesized that the necessary flux balance would occur in the upper 3.6 m and/or in the shallow, shoreward limbs of the cross section that were not sampled. Finally they found that in the 5- to 8-day period band the along-axis winds (toward 60°) were highly correlated to along-axis (outward) deep currents at the Sunshine Skyway.

### **Previous Modeling Studies**

There have been several modeling studies focused on understanding the Bay's circulation. Goodwin and Ross (1984) made comparisons of tidal amplitudes, residual tidal circulation, and storm surges in Tampa Bay using vertically averaged numerical models. They simulated the changes in circulation that occurred after the completion of pier protection islands near the new Sunshine Skyway. Based on model results, they concluded that the overall circulation in the Bay was not altered significantly and that there were negligible changes in the pattern of current vectors near the bridge.

USGS has performed several modeling studies of the Bay. Goodwin (1977, 1980, 1987, 1989) made highly-detailed, two-dimensional numerical simulations of currents to estimate the effects of dredging on the flushing of Tampa Bay and Hillsborough Bay. These studies demonstrated the importance of residual circulation, especially the effects of gyres, in flushing the Bay.

Galperin et al. (1992a), at the University of South Florida, described initial results from three-dimensional modeling of the Bay with the Mellor-Blumberg model formulation. They found that, for the barotropic case, net currents were about 2 to 3 cm/s. For the baroclinic case, however, the time-averaged, two-layered estuarine (buoyancy-driven) circulation was strong and could reach values as large as 10 cm/s. Winds were also shown to have a profound effect on the three-dimensional circulation and hence on the salinity structure. In a following study, supported in part by a NOAA Sea Grant, Galperin et al. (1992b) looked at the system of gyres that are thought to exist and found that the location and number of gyres produced by a model is profoundly different depending on whether a two-dimension barotropic or a three-dimensional baroclinic model is used.

## 1.4. ORGANIZATION OF THIS REPORT

In Sections 2 and 3, the currents and water levels respectively are analyzed using harmonic analysis techniques to determine the constituent amplitudes and phases that are required for prediction. Greenwich intervals are also determined. Then, the currents and water levels are examined in plots of time series and spectra and a determination is made about the size of the nontidal component. The residual (observed minus predicted) currents and water levels are displayed for correlations with wind and other forcing. For the currents, towed ADCP data are analyzed and plotted to show regions along the transects with high velocities.

In Section 4, the wind data are analyzed to find the degree of spatial coherence and the important time scales. Rotary spectral analysis of wind data shows the time scales of wind events that are likely to contribute to the circulation. Cross spectral analysis of wind speed and direction at different stations shows the spatial pattern of the wind over the water. Sea breezes are discussed. Precipitation and river discharge are introduced because they are important for water mass characterization.

Then, in Section 5, salinity and temperature are analyzed to determine the spatial variability and the temporal variability at diurnal, weekly, seasonal, and annual time scales. Horizontal and vertical density gradients are computed.

Section 6 describes the analysis of the nontidal current and water levels and their relationship to changes in the shelf water level and to horizontal buoyancy forcing. Furthermore, some conclusions are made about the total variability of the current and water level signals and our ability to predict nontidal currents and water levels.

In Section 7, results from the model relating to tides, currents, winds, and density are discussed. The model simulates an idealized tide and computes the currents over the entire grid. Flood speeds and times are normalized and compared to constituent amplitudes and times given in Section 2. Water level ranges and times of high water are normalized and compared to constituent amplitudes and times given in Section 3. The distribution of mean baroclinic currents is discussed. A case of a gradually-imposed wind stress is examined, and salt transport variability is also simulated.

Finally, an overview of the tidal and nontidal circulation in the Bay is presented in Section 8.

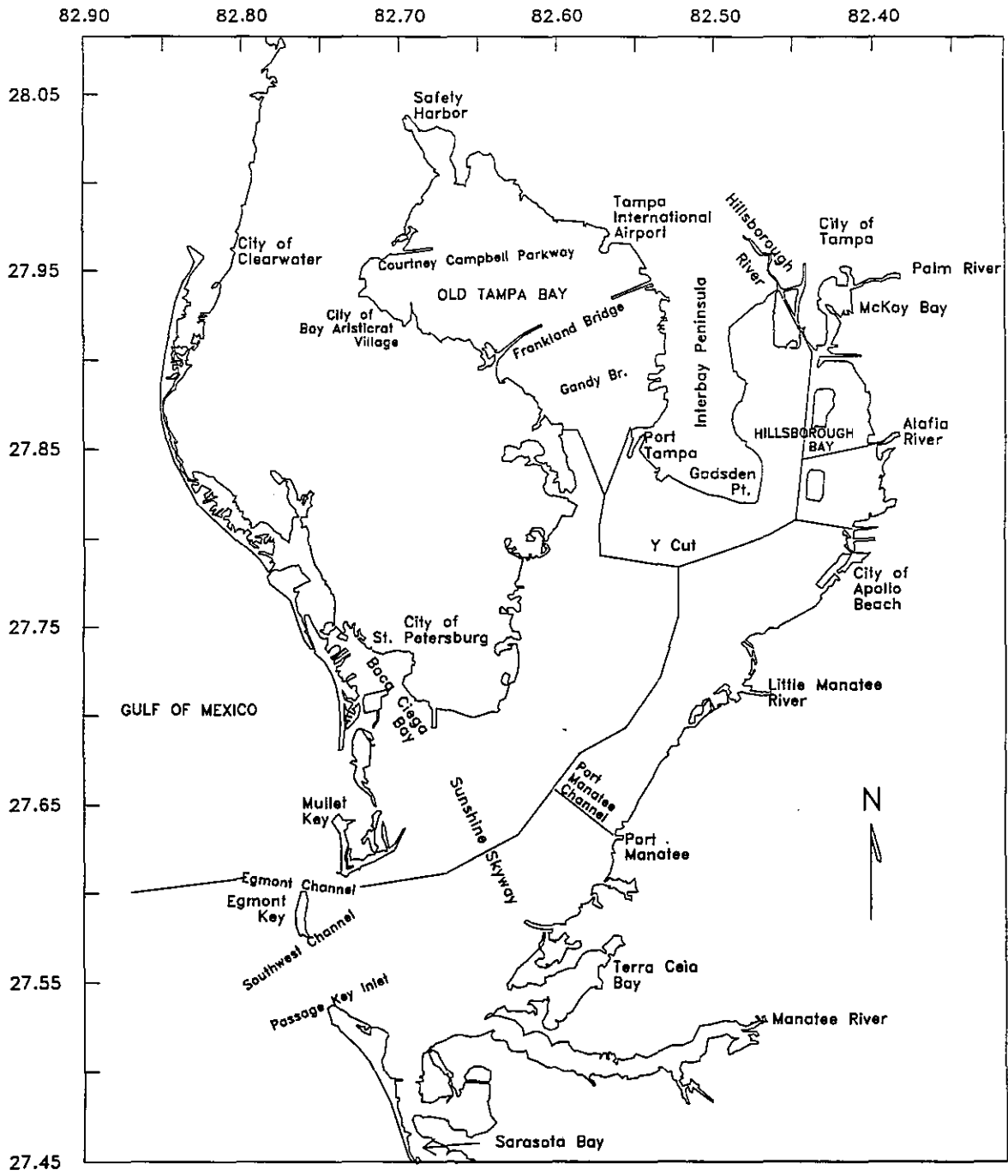


Figure 1.1. Tampa Bay area map, showing many of the locations mentioned in this report.

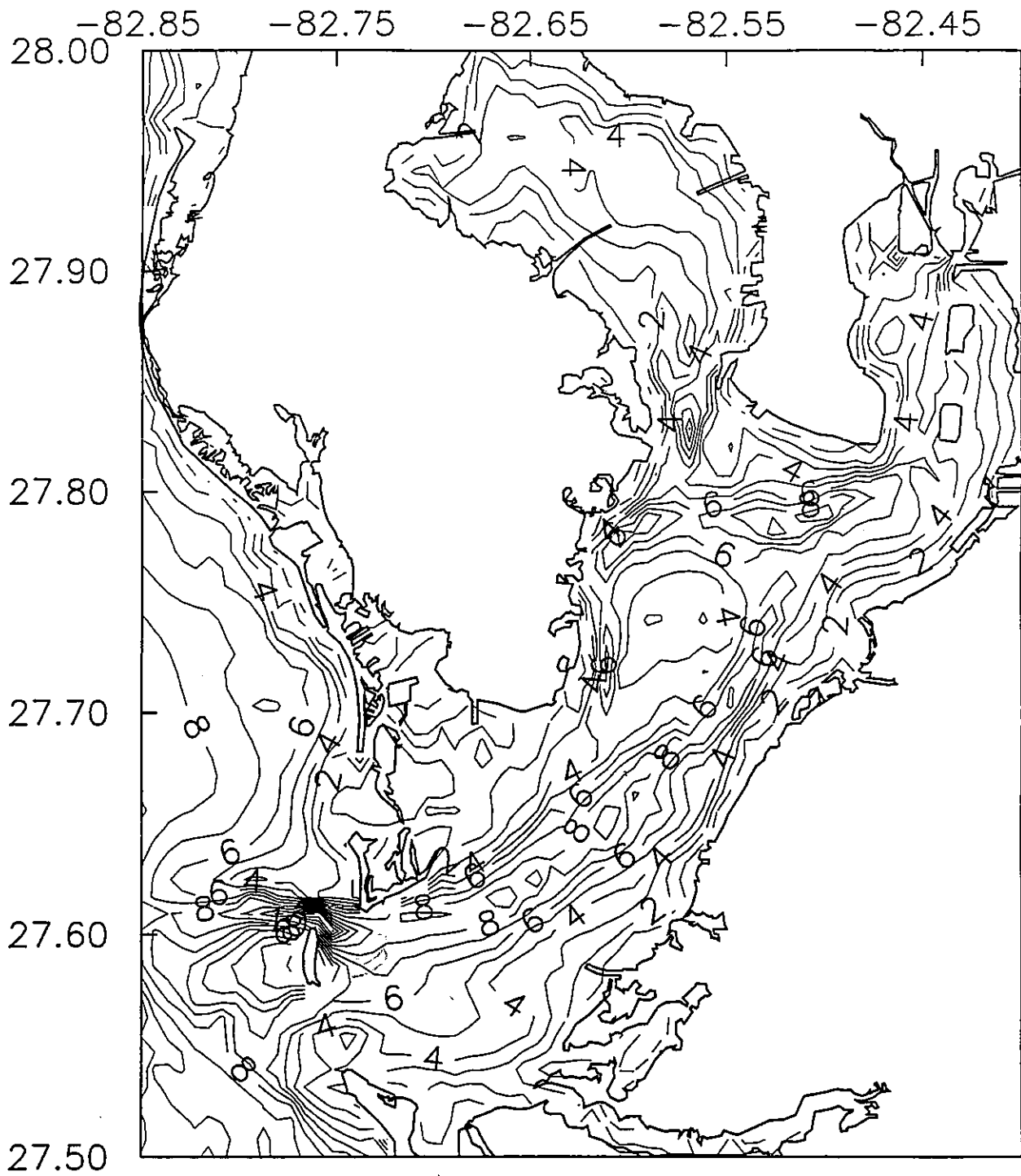


Figure 1.2. Bathymetry of Tampa Bay. Isobath units are meters.



## **2. CURRENTS**

Chris E. Zervas and Richard W. Bourgerie

### **2.1. INTRODUCTION**

Since the last NOS physical oceanographic survey of Tampa Bay in 1963 (Dinardi, 1978), there have been major changes to the bathymetry of the Bay including the construction of the new Sunshine Skyway and Port Manatee, the dredging of the shipping channels, and the deposition of dredge spoils. The 1990-1991 circulation survey of Tampa Bay (NOS, 1990a) was undertaken in order to update the NOS Tidal Current Tables to reflect the changes in Tampa Bay since 1963 and to measure the nontidal circulation.

In order to accomplish these goals, current meters were deployed throughout Tampa Bay (Figure 2.1). In this section, the current data collected from Tampa Bay and its subembayments are used to characterize the tidal and nontidal circulation. In Section 6, the nontidal circulation is related to meteorological and hydrological driving forces. The current data are also important for the calibration and validation of the numerical model described in Section 7.

Two types of current meters were used: the acoustic Doppler current profiler (ADCP) manufactured by RD Instruments and the InterOcean S4 electromagnetic current meter. The ADCP acoustically measures current velocity in a number of vertical bins chosen to be 1 m thick. These current meters were deployed on the seafloor in an upward-facing configuration. The S4 electromagnetic current meters were deployed in shallow areas of Tampa Bay and measured currents at only one level (1 to 3 m above bottom). Bottom depths at the instrument locations are listed in Table A.1 in Appendix A. Current velocity cross sections were obtained from a downward-facing ADCP mounted on a catamaran towed along a number of selected transects (Figure 2.2).

Planned current meter deployments were for long-term (over a year) and short-term (60 days) time periods. There were six long-term stations (C-1 to C-6). C-1 was located 10 km offshore to provide a boundary condition for numerical modeling (Figure 2.1). C-2 was in Egmont Channel, the main entrance to Tampa Bay, and is the reference station presently used in the NOS Tidal Current Tables. C-3 was located in the main shipping channel near the Sunshine Skyway, while C-4 was further up the channel near the turn to Port Manatee. C-5 was at the entrance to Old Tampa Bay near Port Tampa and C-6 was about 50 km offshore on the continental shelf. Acceptable data for the planned periods were not obtained for all instruments. Table A.1 in Appendix A shows the time periods for which data were obtained.

The short-term instrument deployments (C-10 to C-60) were grouped into a series of five periods concentrating on different sections of the Bay. The first and second periods covered middle and lower Tampa Bay, respectively. During the third period, the focus was on Old Tampa Bay and Hillsborough Bay. Periods 4 and 5 were planned to examine small-scale processes near Port Tampa and Port Manatee, respectively.

A typical tidal current record at C-2 (Egmont Channel) during November-December, 1990 is displayed in Figure 2.3. The polar plot of velocity (Figure 2.3a) shows the rectilinear character of the current in Egmont Channel. The greatest part of the signal is tidal. When a 36-hour low-pass filter was applied, the long-period current was generally aligned along the channel (Figure 2.3b). The amplitude of the long-period current can be as large as 25% of the range of the total current at this station.

A 10-day record of the current is displayed in Figures 2.3c and 2.3d as the along-channel component ( $118^\circ$ ) and the across-channel component ( $208^\circ$ ). Positive values for the along-channel component indicate the current is flooding while negative values indicate the current is ebbing. In most of the Bay, flood and ebb currents are in two opposite directions with negligible currents in the perpendicular directions. This situation is known as a reversing current. In larger bodies of water (Gulf of Mexico, Atlantic Ocean) the currents are essentially rotary (i.e. the current vector rotates clockwise or counter-clockwise with only small changes in amplitude).

Figures 2.3e and 2.3f show the along-channel current record at C-2 after low-pass and high-pass filtering at 36 hours. The high-pass filtered current is dominated by the tidal flow although it also contains short period wind-driven currents and high frequency turbulent noise. The low-pass filtered current is lower in amplitude and is driven by wind, river discharge, density gradients, and nontidal water levels in the Gulf of Mexico.

The towed ADCP transects were planned to delineate the small-scale velocity structure in the vicinity of the shipping channels (Figure 2.2). CT-1 was a transect across the entrance to Tampa Bay. CT-2 crossed the Bay parallel to the Sunshine Skyway. CT-3 was oriented along the channel to Port Manatee while CT-4 was along the channel to Port Tampa. CT-5 was a transect along the main shipping channel from below the Sunshine Skyway to the turn to Port Manatee.

## **2.2. HARMONIC ANALYSIS**

Circulation in Tampa Bay is driven primarily by the astronomical tides of the Gulf of Mexico. However, there are other forces which affect the Bay's circulation, including wind stress, river discharge, nontidal water level variations on the continental shelf, and density gradients due to water salinity and temperature variations. Since the tidal currents predominate and are predictable, they will be analyzed before the other currents are discussed.

### **Tidal Constituents**

The astronomical tides consist of a set of sinusoidal waves, known as constituents, at a finite number of discrete frequencies. To describe the tidal currents, the directions, amplitudes, and epochs of the tidal current ellipse axes are determined for each constituent. If  $h(t)$  is a 2-dimensional vector describing the horizontal current as a function of time  $t$ , then

$$h(t) = H_0 - \sum_n f_n H_n \cos[a_n t - (\kappa'_n - (V_0 + u)_n)] \quad (2.1)$$

where  $H_0$  is the mean current velocity,  $n$  indicates the constituent,  $f_n$  is the node factor,  $H_n$  is the constituent amplitude,  $a_n$  is the constituent speed,  $\kappa'_n$  is the modified epoch, and  $(V_0 + u)_n$  is the equilibrium constituent argument (Dennis and Long, 1971). The modified epoch for Tampa Bay is in degrees relative to the 75°W time meridian. To convert the modified epoch to the Greenwich epoch, add 5 hours multiplied by the constituent speed  $a_n$ . To convert the epoch into a time interval in hours, divide by the constituent speed  $a_n$ .

Since  $H_n$  and  $\kappa'_n$  are both vectors, they describe a tidal current ellipse for each constituent in the horizontal plane. Where the tidal currents are rectilinear, the current ellipses are approximately aligned with each other and the minor axis amplitudes are a small fraction of the major axis amplitudes. Where the tidal currents are rotary, the current ellipses are not necessarily aligned with each other and the minor axis amplitudes are a substantial fraction of the major axis amplitudes.

## Analysis Methods

Two harmonic analysis methods were used. The Fourier harmonic analysis method (Schureman, 1958; Dennis and Long, 1971) calculates the amplitudes and epochs for ten major constituents and infers 14 additional constituents from the first ten. This method requires 29 continuous days of current data. If longer data records are available, the results for a number of 29-day periods are averaged.

Fourier harmonic analyses were performed for 36 current stations in Tampa Bay (20 ADCP stations and 16 S4 stations). For the ADCP stations, current data from the bin at 15 feet (4.57 m) below mean lower low water (MLLW) were analyzed. This depth represents half the average draft of ocean-going ships using major U.S. ports and will be used in the NOS Tidal Current Tables. The largest tidal current constituents are the lunar ( $M_2$ ,  $N_2$ ) and solar ( $S_2$ ) semidiurnal constituents and the lunar ( $O_1$ ) and lunisolar ( $K_1$ ) diurnal constituents. The major axis amplitude and epoch of the five major constituents are presented in Table 2.1 along with the analysis depths.

An alternate method called least squares harmonic analysis (Harris et al., 1963) calculates the amplitude and epoch of any number of specified constituents. The time period of current data required must be longer than the synodic period of the two closest constituents in frequency. The synodic period is the amount of time needed for the higher frequency constituent to complete exactly one more cycle than the lower frequency constituent. The least squares method requires one year of data to resolve the constituents  $K_2$ ,  $R_2$ ,  $S_2$ , and  $T_2$ . Only three of the long-term stations in Tampa Bay (C-2, C-4, and C-5) collected more than one year of data. Although there were short data gaps between instrument deployments, the least squares method is capable of handling such gaps. Least squares harmonic analysis was carried out to resolve the 37 standard constituents used by NOS. However, the five long-term constituents (Sa, Ssa, Mm, MSf, and Mf)

are generally unreliable without several years of data.  $S_a$  and  $S_{sa}$  are primarily a result of meteorological forcing which may vary from year to year.

Results for the least squares harmonic analysis are comparable to the results obtained using Fourier harmonic analysis. The 37 tidal current constituents for C-2 are listed in Table B.1 in Appendix B and the five major constituents for C-2, C-4, and C-5 are shown in Table 2.2. The maximum difference between the two methods is 0.6 cm/s in amplitude (constituent  $N_2$  at C-2) and  $6.2^\circ$  in epoch (constituent  $S_2$  at C-4). Because the differences are small, all future discussion of harmonic constituents for C-2, C-4, and C-5 will refer to those obtained by averaging the Fourier harmonic analysis results of a number of 29-day periods (Table 2.1).

**Table 2.1. Amplitude (cm/s) and epoch ( $^\circ$ ) of five tidal current constituents from Fourier harmonic analysis.**

Station	Depth (m)	$M_2$		$S_2$		$N_2$		$K_1$		$O_1$	
		Amp	Epoch								
C-1	4.6	9.21	276.0	3.81	283.5	1.90	266.6	5.66	244.1	4.78	225.2
C-2	4.6	53.40	335.9	18.88	341.7	10.19	328.8	31.59	251.6	26.70	244.7
C-3	4.6	48.87	337.7	17.65	345.1	9.00	335.6	27.21	250.6	21.50	246.6
C-4	4.6	34.57	344.4	11.94	357.2	6.28	345.0	19.70	258.5	16.56	251.9
C-5	4.6	42.70	6.2	13.99	24.9	7.41	5.0	19.39	265.2	16.98	258.6
C-6	4.6	7.05	257.2	2.68	265.7	1.44	252.2	2.62	203.0	2.73	172.6
C-10	3.8	13.94	347.2	4.89	26.9	3.19	347.3	6.07	258.0	4.73	249.3
C-12	0.9	16.00	327.7	5.61	15.2	3.04	352.5	4.48	245.4	5.09	235.2
C-13	4.8	26.85	335.3	9.77	10.3	7.15	331.9	12.35	254.2	10.96	244.0
C-14	4.6	29.63	338.4	9.21	5.4	5.45	329.3	14.82	260.6	14.51	248.8
C-15	4.6	29.12	350.6	8.54	17.2	4.68	340.0	13.84	268.3	13.84	257.3
C-20	4.6	41.98	313.3	15.90	320.2	6.89	320.2	20.53	237.7	18.93	229.1
C-21	6.5	37.04	299.0	15.38	311.9	6.02	278.3	17.80	229.5	15.43	222.6
C-22	0.2	11.99	320.3	4.73	316.2	3.70	289.6	6.28	249.8	6.89	248.1
C-23	4.6	39.56	331.1	14.82	338.0	6.69	337.2	19.39	254.0	18.31	244.6
C-27	4.6	4.99	332.1	2.21	343.2	.62	354.2	1.70	244.8	1.75	268.2
C-30	4.6	37.97	8.5	13.94	10.6	7.20	11.9	22.74	270.2	16.72	255.2
C-31	4.6	11.99	345.0	5.14	9.6	2.21	325.6	6.33	256.9	6.69	267.9
C-32	3.1	19.14	14.7	7.51	41.3	2.78	0.7	10.13	263.6	8.80	265.8
C-33	1.9	23.66	10.8	9.16	35.4	3.55	348.9	12.14	259.5	10.60	265.7

**Table 2.1 (continued). Amplitude (cm/s) and epoch (°) of five tidal current constituents from Fourier harmonic analysis.**

Station	Depth (m)	M <sub>2</sub>		S <sub>2</sub>		N <sub>2</sub>		K <sub>1</sub>		O <sub>1</sub>	
		Amp	Epoch								
C-34	2.6	12.96	15.3	5.20	43.0	1.59	3.6	7.25	266.5	6.28	268.6
C-36	4.6	9.36	325.7	3.60	338.5	1.70	308.4	4.37	234.0	4.22	245.7
C-40	4.7	24.49	8.0	9.77	15.1	5.35	30.6	13.89	263.6	9.47	245.5
C-41	4.6	41.72	8.5	15.43	12.0	7.92	11.4	23.72	269.0	15.43	255.4
C-42	3.7	10.49	338.8	3.76	342.2	2.88	346.1	6.17	249.2	3.96	239.2
C-43	7.0	21.45	8.2	8.23	8.7	4.84	11.9	10.34	262.9	7.10	248.0
C-44	4.6	8.75	350.7	3.40	354.9	1.85	341.6	6.89	255.4	5.04	252.5
C-46	2.5	10.75	324.2	3.86	328.0	2.01	312.7	4.58	241.3	3.60	225.8
C-50	2.7	17.85	332.4	4.68	356.9	3.04	312.0	7.36	246.6	5.66	237.0
C-51	5.7	23.46	336.1	5.45	359.0	4.48	341.2	11.47	254.9	10.29	244.8
C-52	4.6	13.89	323.5	2.73	345.2	1.90	309.4	6.64	251.0	6.79	246.9
C-53	2.7	23.20	333.9	6.17	359.7	3.70	316.4	9.31	248.1	8.90	240.9
C-54	3.6	16.87	315.2	3.50	342.8	2.83	332.7	9.72	248.0	7.61	235.0
C-55	4.6	40.54	343.3	13.79	7.6	7.72	339.8	19.34	259.1	19.14	242.7
C-56	4.6	55.82	327.1	19.91	340.9	9.93	323.3	24.38	256.2	25.67	237.6
C-60	4.6	10.49	274.6	4.17	288.4	2.31	273.8	5.30	253.3	5.40	204.0

**Table 2.2. Amplitude (cm/s) and epoch (°) of five tidal current constituents from least squares harmonic analysis.**

Station	Depth (m)	M <sub>2</sub>		S <sub>2</sub>		N <sub>2</sub>		K <sub>1</sub>		O <sub>1</sub>	
		Amp	Epoch								
C-2	4.6	53.76	337.6	18.93	343.8	9.62	333.9	31.43	250.8	26.49	247.2
C-4	4.6	34.72	349.0	12.04	3.4	6.07	347.5	19.60	258.0	16.62	255.9
C-5	4.6	43.06	9.9	13.84	25.8	7.25	9.3	19.60	265.3	17.08	261.3

## **Spatial Variation of Tidal Current Constituents**

Contour plots were made of the amplitude and epoch for  $M_2$ ,  $S_2$ ,  $K_1$ , and  $O_1$  (Figures 2.4 and 2.5). The highest constituent amplitudes are found at the entrances to Tampa Bay. The greatest volume of water transported during a tidal cycle in an enclosed bay must be through the entrance. The narrow width of the entrances relative to the width of Tampa Bay acts to increase the current through these constrictions. Egmont Channel is considerably deeper than the other two entrances to the Bay (Southwest Channel and Passage Key Inlet). Therefore, due to a reduction in the effect of bottom friction, the current through Egmont Channel is greater than the current through the other entrances. Another area of relatively high amplitudes is at the narrow entrance to Old Tampa Bay. The lowest amplitudes are found in Hillsborough Bay.

The epoch contour plots show the progression of each constituent up the Bay (Figure 2.5). An epoch difference of  $30^\circ$  represents approximately 1 hour for a semidiurnal constituent and approximately 2 hours for a diurnal constituent. Tidal currents at Egmont Channel lag the currents at Southwest Channel and Passage Key Inlet by as much as one hour. Given the distribution of station locations, it is hard to get a complete picture of the epoch pattern in the Bay. However, Hillsborough Bay epochs are significantly in advance of epochs near the entrance to Old Tampa Bay. C-34 near the Frankland Bridge in Old Tampa Bay has the latest epochs (2.5-3.0 hours after C-21 at Passage Key Inlet).

The  $M_2$  and  $K_1$  current ellipses for the stations in the Bay are plotted in Figures 2.6 and 2.7 to show the orientation of the ellipses and the relative amplitudes of the major and minor axes. At all stations except C-44 at the Y-Cut, the minor axis amplitude of the ellipse is negligible (less than 10% of the major axis amplitude). The tidal currents can be considered to be rectilinear at all stations except at C-44 where they are rotary.

Tidal current constituents often show a variation with depth in the water column with earlier epochs and smaller amplitudes closer to the bottom (Browne and Fisher, 1988). In Tampa Bay, this depth dependence is relatively small, probably due to the shallowness of the Bay. Table 2.3 shows the direction, amplitude, and epoch of the major ellipse axis for the  $M_2$  and  $K_1$  constituents at C-4 during one deployment. The tidal current constituents display a high degree of vertical homogeneity. Weisburg and Williams (1992) reached a similar conclusion by performing an empirical orthogonal function analysis of current data from C-3 at the Sunshine Skyway.

## **Temporal Variation of Tidal Current Constituents**

Fourier harmonic analysis was carried out for the six long-term stations for a number of 29-day time periods to show how constituent amplitudes and epochs varied over the course of the project (Figures 2.8 and 2.9). It is evident that the amplitudes and epochs can vary substantially. The amplitudes and epochs of the four stations in Tampa Bay (C-2 to C-5) appear to be closely correlated with each other but are not correlated with the offshore stations (C-1 and C-6). Since the astronomical driving forces do not change, the tidal response of the Bay must be changing over the course of the year. This could be due to the changing density structure of the Bay

**Table 2.3. Vertical variation of tidal constituents along the major ellipse axes at C-4 for January 4 - February 2, 1991.**

Depth below MLLW (m)	M <sub>2</sub>			K <sub>1</sub>		
	Direction	Amplitude	Epoch	Direction	Amplitude	Epoch
1.7	35.0	35.4	346.5	35.9	20.8	251.8
2.7	34.3	34.8	346.0	35.5	20.5	251.6
3.7	33.7	34.2	345.7	35.1	20.3	251.6
4.7	32.8	32.8	345.0	34.7	19.6	251.9
5.7	32.4	31.9	344.7	34.6	19.0	251.9
6.7	32.3	31.1	344.7	34.3	18.6	251.8

which in turn is due to changes in its salinity and temperature structure. Alternatively, there could be some interference from a wind-driven current with a period of 24 hours and its overtones. The two constituents that show the greatest variability are S<sub>2</sub> and K<sub>1</sub>. The period of S<sub>2</sub> is exactly 12 hours and K<sub>1</sub> is the diurnal tidal constituent closest to 24 hours.

### Tidal Current Classification

The ratio of constituent amplitudes  $(K_1+O_1)/(M_2+S_2)$  was computed for each station and is contoured in Figure 2.10. This ratio is used to classify tides and currents (Defant, 1961) and indicates the degree of similarity between tidal waveforms. If it is less than 0.25, the tide is semidiurnal. If it is between 0.25 and 1.5, the tide is mixed, mainly semidiurnal. Between 1.5 and 3, the tide is mixed, mainly diurnal and if it is greater than 3, the tide is diurnal. All of Tampa Bay has mixed, mainly semidiurnal tidal currents. The lowest ratios (most semidiurnal) are 0.44 at C-12 and 0.48 at C-27. The highest ratio (most diurnal) is 0.98 at C-44.

As the diurnal and semidiurnal tides propagate in shallower water on continental shelves and in estuaries, they are distorted due to the relative differences in water depths and, therefore, wave speeds during flood and ebb. As a consequence, higher order overtides can become more prominent. Although Tampa Bay is relatively shallow, the amplitude ratio of the M<sub>4</sub> constituent to the M<sub>2</sub> constituent is always less than 15%. It exceeds 10% only at the Y-Cut (C-44) and at the stations in Hillsborough Bay (C-27, C-31, C-36, and C-46).

### Rotary Character of Offshore Stations

The tidal currents at the three offshore stations (C-1, C-6, and C-60) have small amplitudes and are rotary in character. The minor axis amplitude of most of the constituent ellipses are a substantial fraction of the major axis amplitude. The axis directions of each constituent do not necessarily line up with each other as they do in the Bay. Figure 2.11 shows the four major tidal

current ellipses for the offshore stations (C-1 and C-6) and for two Tampa Bay stations (C-2 and C-4). At C-6, the ratios of the minor to major axis amplitude for constituents  $K_1$  and  $O_1$  are 0.75 and 0.66, respectively. These nearly circular ellipses make the direction of the major axis indeterminate and causes the large variation in  $K_1$  and  $O_1$  epochs in Figures 2.9c and 2.9d.

### **Greenwich Intervals and Mean Maximum Flood and Ebb Currents**

In the NOS Tidal Current Tables, the times of slack before flood (SBF), maximum flood current (MFC), slack before ebb (SBE), and maximum ebb current (MEC) are given for every day of the year at a limited number of reference stations. Tidal currents can be calculated by the user for a much larger number of stations listed in Table 2 of the Tidal Current Tables. Every station in Table 2 is associated with a reference station in Table 1 through time differences for SBF, MFC, SBE, and MEC and speed ratios for MFC and MEC. Table 2 stations are referenced to a Table 1 station with a similar tidal classification ratio.

The time differences are obtained by subtracting the Greenwich interval of the reference station from the Greenwich intervals of the secondary stations. The Greenwich interval is the time period between the moon's transit over the Greenwich meridian and the occurrence of SBF, MFC, SBE, and MEC at a given location. It is a measure of the delay of the ocean's response to astronomical tidal forces caused by the topography of the earth's surface. The mean Greenwich intervals were obtained for all of the current meter stations by averaging the Greenwich intervals calculated for each SBF, MFC, SBE, and MEC. They are presented in tabular form in Table 2.4 and as contour plots (Figure 2.12).

The contour plots show early arrivals at most stations in lower Tampa Bay. Stations near the shores of the Bay generally have earlier arrivals than those in the main shipping channel. This pattern is similar to the results of the NOS Chesapeake Bay survey (Browne and Fisher, 1988). The earliest arrivals are at Passage Key Inlet (C-21) and near Boca Ciega Bay (C-24). The arrivals in mid-Tampa Bay and Old Tampa Bay get progressively later with C-34 at the Frankland Bridge being 2 to 3 hours later than C-21. Stations in Hillsborough Bay are generally earlier than the Old Tampa Bay stations.

The mean maximum flood and ebb speeds (MFC and MEC) for each station are also shown in Table 2.4 and displayed as contour plots (Figure 2.13). The flood and ebb contour plots are similar in appearance. The highest speeds are in Egmont Channel, under the Sunshine Skyway, and at the entrance to Old Tampa Bay. The lowest speeds are in Hillsborough Bay.

### **2.3. NONTIDAL CIRCULATION**

The tidal currents are only one part of the circulation in Tampa Bay. Nontidal currents have smaller amplitudes and are composed of a broad band of frequencies. They are driven by winds, river discharge, nontidal water level variations in the Gulf of Mexico, and horizontal density gradients in the Bay. The nontidal circulation is a complex phenomenon and will be examined by different methods in Section 6 to resolve the effects of the various driving forces.

**Table 2.4. Greenwich intervals (hours) and mean maximum flood and ebb speeds (cm/s).**

Station	SBF	MFC	MFC speed	SBE	MEC	MEC speed
C-1	11.63	0.97	10.29	4.81	8.69	14.20
C-2	13.70	4.25	67.19	7.19	10.20	68.88
C-3	13.59	4.08	64.92	7.44	10.18	55.66
C-4	13.69	4.38	42.90	7.59	10.58	42.49
C-5	14.62	4.65	49.28	8.21	11.32	47.89
C-6	10.94	1.27	7.46	4.60	6.87	8.90
C-10	13.93	4.45	14.66	7.59	10.43	17.13
C-11	13.56	3.65	36.68	7.03	10.29	40.07
C-12	13.31	3.93	18.31	7.38	9.80	14.92
C-13	13.10	4.15	34.62	7.36	9.97	27.93
C-14	13.54	3.97	31.33	7.25	10.53	38.79
C-15	13.89	4.76	35.86	7.79	10.95	34.26
C-20	12.93	3.36	40.43	6.51	9.70	60.55
C-21	12.22	2.41	41.41	5.97	9.06	47.07
C-22	12.91	4.68	15.69	6.85	10.30	12.40
C-23	13.47	4.14	44.91	7.09	10.30	50.72
C-24	12.36	3.43	43.93	6.60	9.29	31.59
C-26	13.30	4.25	18.06	6.52	10.02	16.10
C-27	11.70	5.51	10.13	8.14	10.56	3.29
C-30	14.76	4.98	43.01	8.17	11.36	50.42
C-31	13.39	5.16	19.60	7.88	10.94	11.63
C-32	14.90	5.01	26.13	8.19	11.49	21.45
C-33	14.78	4.99	31.79	8.36	11.44	26.39
C-34	15.26	5.06	12.86	8.04	11.69	18.47
C-36	13.07	4.75	12.96	7.28	10.43	10.19
C-40	14.64	4.97	31.79	8.29	10.95	25.57
C-41	14.80	4.89	53.24	8.28	11.31	48.05
C-42	14.00	4.46	10.55	7.25	10.63	13.12
C-43	14.91	5.27	33.54	8.27	10.94	22.64

**Table 2.4 (continued). Greenwich intervals (hours) and mean maximum flood and ebb speeds (cm/s).**

Station	SBF	MFC	MFC speed	SBE	MEC	MEC speed
C-44	14.12	5.27	10.44	7.59	10.97	11.73
C-46	13.09	4.99	15.33	7.09	10.39	16.10
C-50	13.01	3.87	23.46	7.47	10.06	16.51
C-51	13.42	4.15	30.76	7.27	10.43	24.18
C-52	13.13	4.07	10.96	6.81	10.21	21.04
C-53	13.40	4.00	29.84	7.35	10.06	27.93
C-54	12.80	3.68	24.18	6.83	9.67	20.47
C-55	13.55	4.39	48.20	7.40	10.45	48.51
C-56	13.32	3.99	55.87	7.02	10.20	73.77
C-60	11.08	1.14	12.45	5.32	9.33	13.94

In this section, we characterize the magnitude of the nontidal circulation by examining the mean and the residual currents.

### Mean Currents

Permanent currents are induced by driving forces that have a time-invariant component. Permanent currents in Tampa Bay may be a combination of a density-driven current and a tidally-induced residual current. A time series long enough to average out long-period currents is necessary to accurately measure the permanent current since density-driven currents can have seasonal and interannual variability. Most of the stations in this survey do not have a long enough record to obtain the permanent current. However, the mean current can be calculated for each deployment to give an approximation of the speed and direction of the permanent current. If the mean currents are similar at stations with multiple deployments, the permanent current vector may be estimated.

The mean currents for each ADCP station were obtained by vector averaging the current in each bin over an entire deployment. In general, there is a mean current into the Bay at depth and a mean current out of the Bay near the surface at most stations. This is a typical circulation pattern in an estuary where denser, salty water from the ocean enters the Bay at depth and lighter, fresher water leaves the Bay closer to the surface. Stations with multiple deployments (C-1 to C-6) have reasonably consistent depth profiles.

Mean current vectors for each deployment at all of the ADCP stations were plotted on maps of Tampa Bay (Figures 2.14, 2.15, and 2.16). The 2-m plot includes mean velocities from 0 to 3 m

depths below MLLW. The 5-m plot covers 4 to 6 m depths below MLLW and the 10-m plot covers 9 to 11 m depths below MLLW. Stations with multiple deployments have consistent mean currents from season to season; therefore, the mean current vectors were all plotted together even though deployments occurred in different seasons.

All of the 10-m velocity vectors (Figure 2.14) are from ADCPs deployed in the shipping channels. They all show currents toward the head of the Bay. At a depth of 5 m (Figure 2.15), there is a mixture of currents toward the head and toward the mouth of Tampa Bay. Mean currents are generally toward the head of the Bay in the main shipping channels up into Hillsborough Bay; however, mean currents run out of Old Tampa Bay. C-56 in Egmont Channel is only 0.5 km north of C-2, but the mean current is in the opposite direction (out of the Bay). C-20 at Southwest Channel also has a mean current out of the Bay. At 2-m depth (Figure 2.16), the mean currents are almost all toward the mouth of the Bay. The only exceptions are C-44 in upper Tampa Bay, C-31 in Hillsborough Bay, and at C-3 under the Sunshine Skyway. At C-1 offshore, the mean currents are toward the northwest for all deployments at all levels.

## **Residual Currents**

The tidal current constituents obtained by harmonic analysis can be used to predict the tidal currents for any specified time period. The tidal currents were predicted for the periods during which data were collected and then subtracted from the observed current to obtain the residual current. The standard deviation of the observed and the residual currents from the mean current along the principal component direction are presented in Table 2.5 along with the ratio of the standard deviations.

The standard deviations of the observed currents range from 7.28 to 54.46 cm/s. The standard deviations of the residual currents range from 4.88 to 14.05 cm/s. The ratio of residual to observed standard deviation ranges between 17.2% and 88.2%. The largest residual currents are at the reference station (C-2) in Egmont Channel. This is also the station with the largest observed currents. The smallest residual currents are at C-52.

The ratio of the residual to the observed standard deviation is high at the offshore stations (C-1, C-6, and C-60), where the tidal currents are rotary and have small amplitudes. The magnitude of long-term shelf currents are comparable to the tidal currents. The residual current is also large relative to the observed current at stations in the Bay with small-amplitude tidal currents, especially C-27 in Hillsborough Bay. In the rest of the Bay, the residual currents are 20% to 60% of the observed currents.

Along-channel residual currents for November and December, 1990, at the four long-term stations in the Bay (C-2, C-3, C-4, and C-5) are plotted in Figure 2.17. They show that there is substantial high frequency variability over the whole time period with distinct events of lower frequency which show up at all stations. In Sections 3 and 4, these events will be shown to be the result of winter storms. The four stations appear to be well correlated.

**Table 2.5. Standard deviations (S.D.) of observed and residual currents from the mean current along the principal component direction.**

Station	Principal Component Direction	Observed S.D. (cm/s)	Residual S.D. (cm/s)	Ratio (Res/Obs)
C-1	17	13.26	10.84	.817
C-2	118	54.46	14.05	.258
C-3	58	47.55	12.64	.266
C-4	35	34.14	8.80	.258
C-5	28	39.47	11.03	.279
C-6	358	9.75	8.60	.882
C-10	6	13.39	6.27	.469
C-12	61	14.04	6.37	.454
C-13	57	24.36	6.81	.279
C-14	41	28.90	5.78	.200
C-15	45	27.84	6.39	.230
C-20	88	39.82	9.58	.240
C-21	73	35.51	8.14	.229
C-22	210	12.82	8.55	.667
C-23	74	37.40	7.72	.206
C-27	28	7.28	5.85	.804
C-30	13	37.13	9.45	.254
C-31	6	15.15	9.14	.603
C-32	356	19.04	6.33	.333
C-33	359	23.51	12.64	.538
C-34	318	13.38	5.01	.375
C-36	37	10.57	6.09	.576
C-41	359	40.21	11.28	.281
C-42	27	10.91	5.46	.500
C-43	9	20.64	9.18	.445
C-44	46	9.66	5.47	.566
C-46	347	11.35	6.81	.600
C-50	38	17.58	7.98	.454

**Table 2.5 (continued). Standard deviations (S.D.) of observed and residual currents from the mean current along the principal component direction.**

Station	Principal Component Direction	Observed S.D. (cm/s)	Residual S.D. (cm/s)	Ratio (Res/Obs)
C-51	42	22.41	7.15	.319
C-52	61	13.79	4.88	.354
C-53	50	22.02	7.62	.346
C-54	84	17.96	7.32	.407
C-55	34	38.24	6.78	.177
C-56	114	50.17	8.64	.172
C-60	48	10.96	5.94	.542

The energy density spectra in Figure 2.18 show the relative distribution of energy in different frequency bands for the along-channel observed and residual current at C-2 during a deployment in the fall of 1990. The diurnal and semidiurnal frequencies dominate the observed spectrum; in the residual spectrum, they have been reduced to the level of long-period nontidal frequencies by removing the predicted tidal current. Higher-order harmonics are visible in both spectra.

The two along-channel observed time series for C-2 and C-5 were subjected to cross spectral analysis to determine how coherent the signals were in different frequency bands (Figure 2.19). The coherence is very high in the low frequency subtidal bands where the phase lag of C-5 relative to C-2 is near zero and the amplitude of C-5 is about 50% of C-2. The coherence is near 1.0 in the diurnal and semidiurnal tidal bands where the phase lag of C-5 relative to C-2 can be converted to a time lag of about 1 hour. The only other bands with significant coherence are the overtones at 3, 4, and 5 cpd. The transfer amplitude is greater than 1.0 for 3 and 5 cpd, indicating that these overtones have increased in amplitude between C-2 and C-5.

## **2.4. TOWED ADCP TRANSECTS**

In order to map the smaller-scale horizontal variability of current velocity, a 600-kHz ADCP mounted on a catamaran in a downward-facing configuration was towed along five transects. Although a towed ADCP will not be able to make simultaneous measurements of the currents across the whole transect, a reasonable approximation of the spatial variability can be obtained if several transect crossings can be made during a flood or ebb period. The transects were occupied during flood and ebb phases several times during the year. The transects (Figure 2.2) were located across-channel near the entrance to the Bay and the Sunshine Skyway (CT-1 and CT-2) and along segments of the major shipping channels (CT-3, CT-4, and CT-5). The time, bottom depth, bottom tracking velocity (north and east), LORAN position, and the north and east current velocities in every bin were recorded every 10-20 s.

## Method of Analysis

The following procedure was used to make velocity contour plots from the towed ADCP data. A least squares line was fitted to the LORAN ship positions. A selected number of cells were formed along the least squares fitted line. Each data point was sorted into one of the cells and the velocity perpendicular or parallel to the fitted line was calculated for each depth bin. For along-channel lines, the velocity parallel to the trackline was obtained; for across-channel lines, the velocity perpendicular to the trackline was obtained. An average velocity was determined for each depth bin in each cell, based on all the sorted data available.

The averaged velocities were gridded and plotted. Each of the contour plots was based on several passes along the transect. They are displayed as vertical-plane cross sections with the depth bin converted to meters and the cells converted to kilometers along the trackline. Positive velocities indicate flood currents and negative values indicate ebb currents. The averaged bottom topography along the transect is also displayed. The bottom topography may vary between cross sections of the same transect due to small variations in the ship's tracklines.

## Cross Sectional Velocity Contour Plots

CT-1 extends across the two main entrances to Tampa Bay (Egmont Channel and Southwest Channel), but not across Passage Key Inlet. The two flood periods (Figures 2.20a and 2.20c) have strong currents centered in Egmont Channel at depth and slightly south of the deepest part of the channel closer to the surface. One of the flood cross sections has a weaker but well-developed core near the Southwest Channel; the other flood cross section does not have such a feature. The ebb cross section (Figure 2.20b) has the highest speeds slightly to the north of the center of the channel and the lowest speeds just south of Egmont Channel. This shift in the position of maximum flood and ebb currents may explain the opposite directions of the mean currents at C-2 and C-56 in Figure 2.15.

CT-2 extends across the deeper part of lower Tampa Bay parallel to the Sunshine Skyway. There is a spoil area just south of the main channel at 2.5 km (Figure 2.21). The flood cross section has a high velocity core centered in the main shipping channel. There are two lower velocity regions just north and south of the edges of the channel. The velocity is slower over the spoil area. There are two higher velocity regions over 1 km north and south of the channel. One of the ebb cross sections has a very symmetrical pattern of strong currents centered on the shipping channel axis and a lower velocity region over the spoil area. The other ebb cross section has a similar structure at depth. However, near the surface, the fastest velocity region has been displaced about 1.5 km to the north.

CT-3 is aligned along the Port Manatee channel from the intersection with the main shipping channel to Port Manatee. The velocity cross sections display velocities perpendicular to the Port Manatee channel (Figure 2.22). All the cross sections show a lateral gradient from nearly zero velocity near Port Manatee to maximum velocities centered in the main shipping channel which crosses CT-3 between 1 and 2 km. One of the flood cross sections also has a high velocity

region between 3 and 4 km along the section, which may be due to a gap in the spoil areas which border the Port Manatee channel to the north and south.

CT-4 is along the shipping channel to Port Tampa at the entrance to Old Tampa Bay. The velocities displayed are along-channel velocities (Figure 2.23). The fastest velocities for the flood and two ebb cross sections are between 4 and 5 km. This area is the narrowest part of the entrance to Old Tampa Bay. There are also slightly higher velocities where the channel ends at Port Tampa and the bottom depth shoals abruptly.

CT-5 follows the main shipping channel from a point west of the Sunshine Skyway to the Port Manatee channel. CT-5 was carried out in order to evaluate the accuracy of the PORTS velocity values (Nichols et al., 1992). There is a 25° bend in the channel half way between the Sunshine Skyway and the intersection with the Port Manatee Channel (Figure 2.2). The along-channel velocities were plotted for the section of CT-5 below the bend (Figure 2.24). All CT-5 cross sections have their highest along-channel velocities close to the Sunshine Skyway. The position of the bridge is at 2.9 km on the contour plots. Note that during the flood periods, the greatest velocities extend from the bridge up the channel. During the ebb period, the greatest velocities extend from the bridge toward the mouth of the Bay. This indicates that turbulent flow caused by the bridge pilings may have a focusing effect on flow in the shipping channel resulting in faster velocities after the flow passes under the bridge. Since the position of the current meter (C-3) was slightly up the channel from the bridge, it would measure stronger flood currents than ebb currents due to this focusing effect. This is supported by the consistent mean currents into the Bay at shallow depths at C-3 (Figure 2.16) in contrast to the mean currents out of the Bay at most other stations.

## 2.5. CONCLUSIONS

The current meter deployments and towed ADCP transects carried out during TOP have contributed to a detailed picture of the circulation in Tampa Bay. Tidal current constituents and Greenwich intervals were computed and indicate that tidal currents in Tampa Bay are mixed, mainly semidiurnal. The strongest tidal currents occur at Egmont Channel and the weakest tidal currents are in Hillsborough Bay. Some of the tidal current constituents at the long-term stations show considerable variation over the course of the project. Mean currents reveal a typical estuarine circulation pattern in the Bay. Residual currents are a substantial fraction of the observed currents and are highly coherent between the lower Bay and upper Bay. The towed ADCP transects show that currents are fastest where the cross sectional areas perpendicular to the current are narrowest and the largest velocities are located near the surface above the deepest part of the cross section.

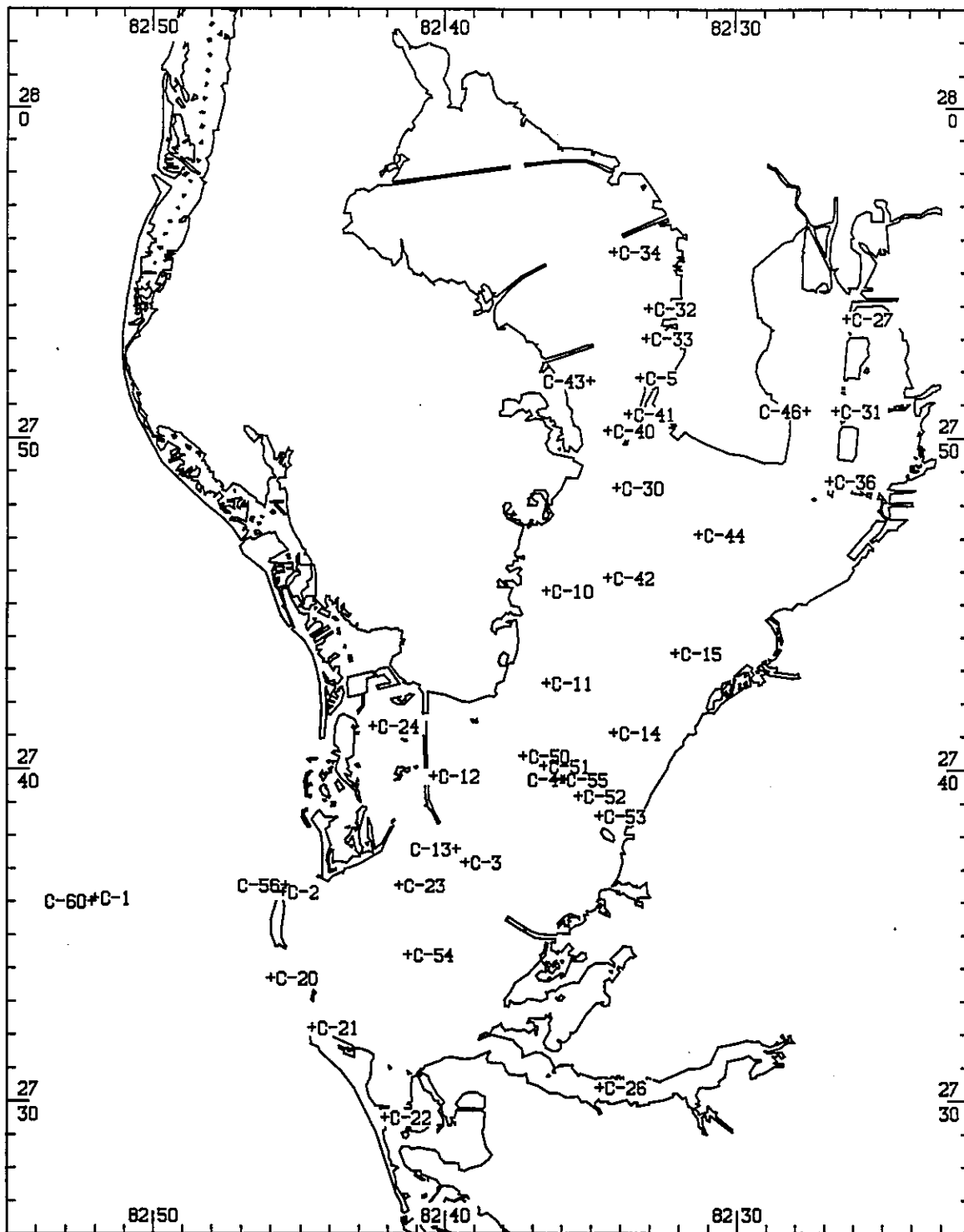


Figure 2.1. Location of TOP current meter stations. C-6 is located 50 km offshore.

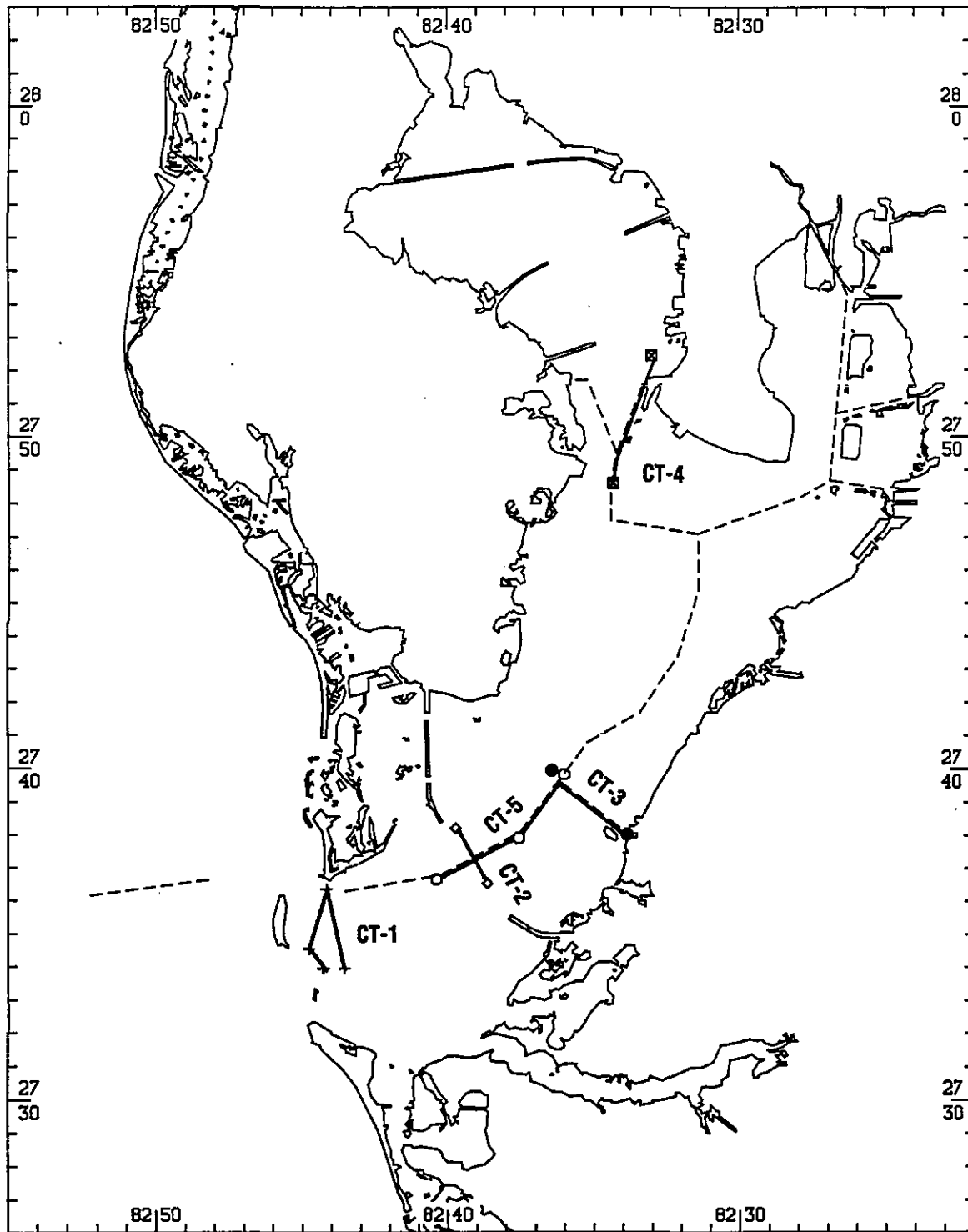
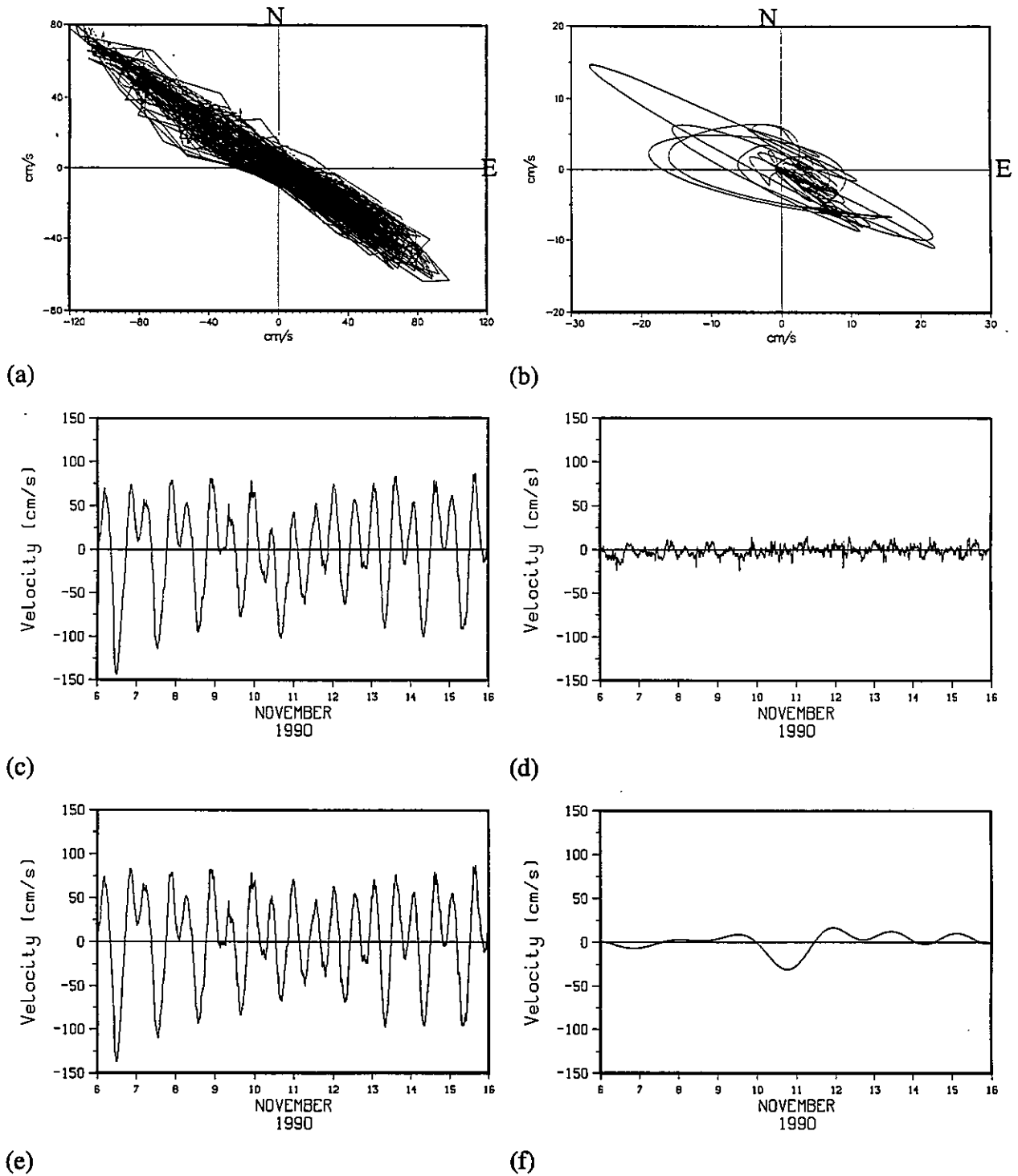


Figure 2.2. Location of the towed ADCP transects. Dashed lines indicate dredged shipping channels.



(a) (b) (c) (d) (e) (f)  
 Figure 2.3. Sample tidal current records at C-2 (Egmont Channel) at a depth of 4.5 m. (a) Polar plot of current from October 28 - December 27, 1990. (b) Figure a) after 36-hour low-pass filtering. (c) Current in the principal component direction ( $118^\circ$ ). (d) Current perpendicular to the principal component direction ( $208^\circ$ ). (e) 36-hour high-pass filtered current along  $118^\circ$ . (f) 36-hour low-pass filtered current along  $118^\circ$ .

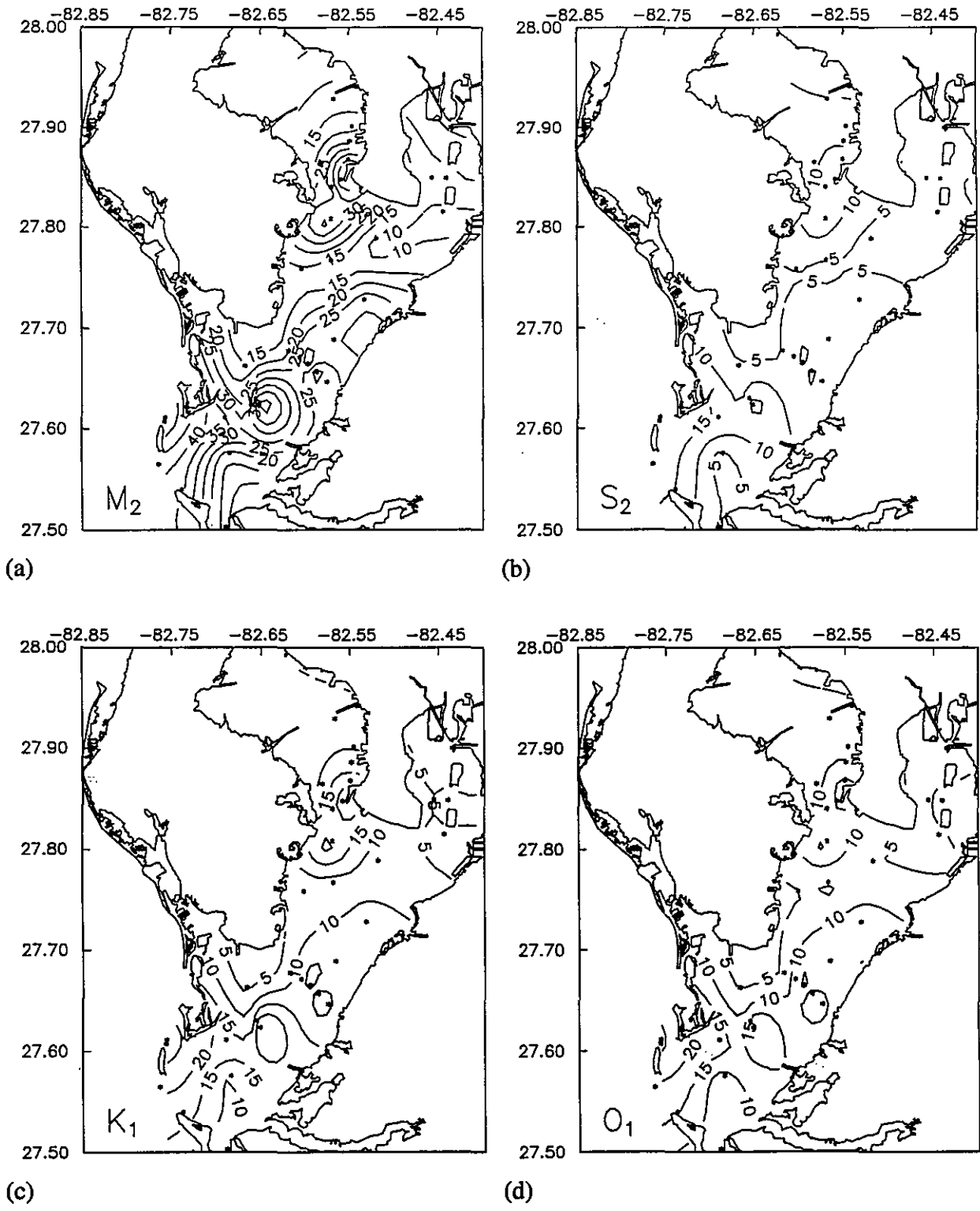


Figure 2.4. Amplitude (cm/s) of the major axis of the constituent ellipses. Tidal constituents (a)  $M_2$ , (b)  $S_2$ , (c)  $K_1$ , and (d)  $O_1$ . Contour interval is 5 cm/s. Dots indicate station locations.

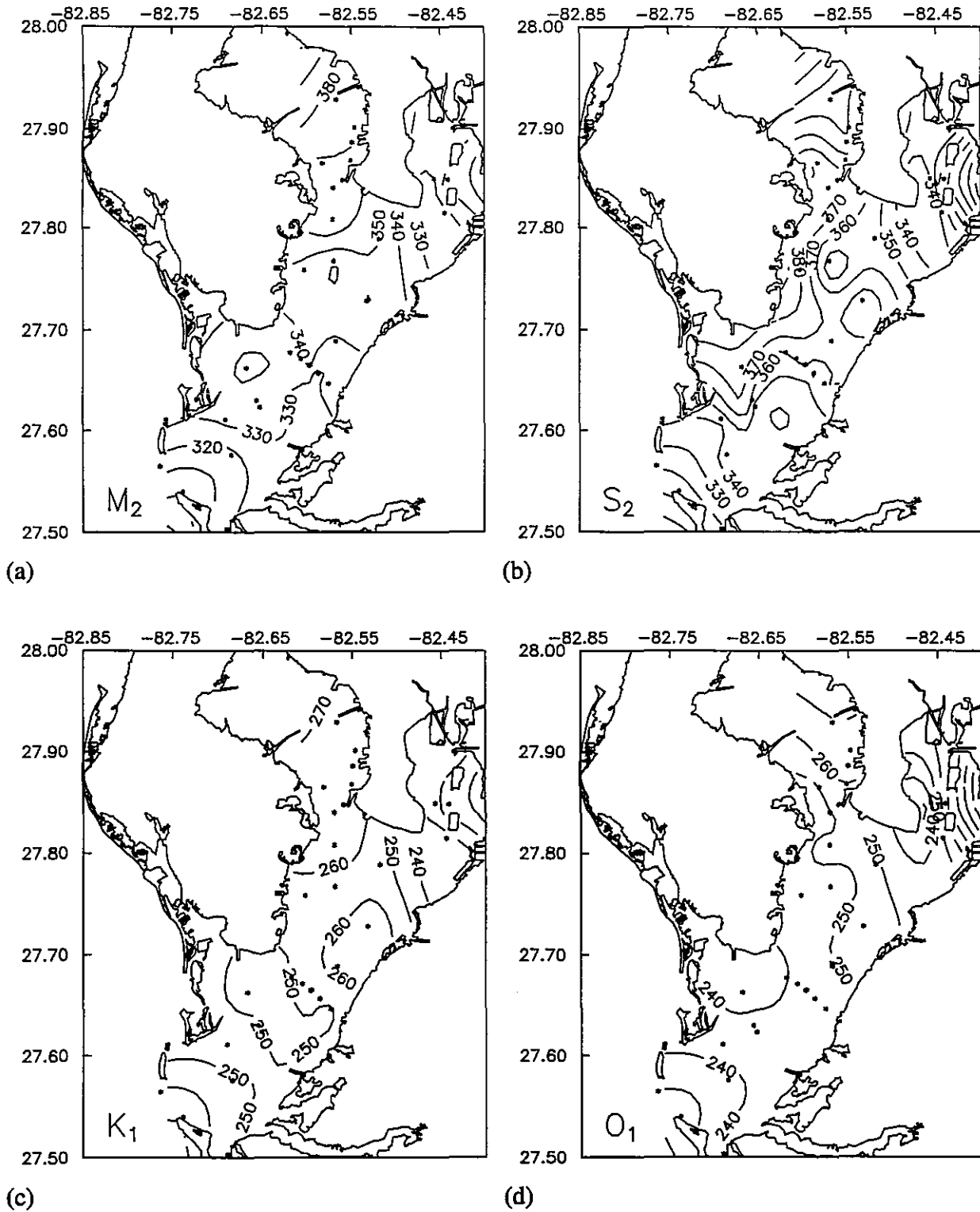


Figure 2.5. Epoch (degrees) of the major axis of the constituent ellipses. Tidal constituents (a)  $M_2$ , (b)  $S_2$ , (c)  $K_1$ , and (d)  $O_1$ . Contour interval is 10 degrees. Dots indicate station locations.

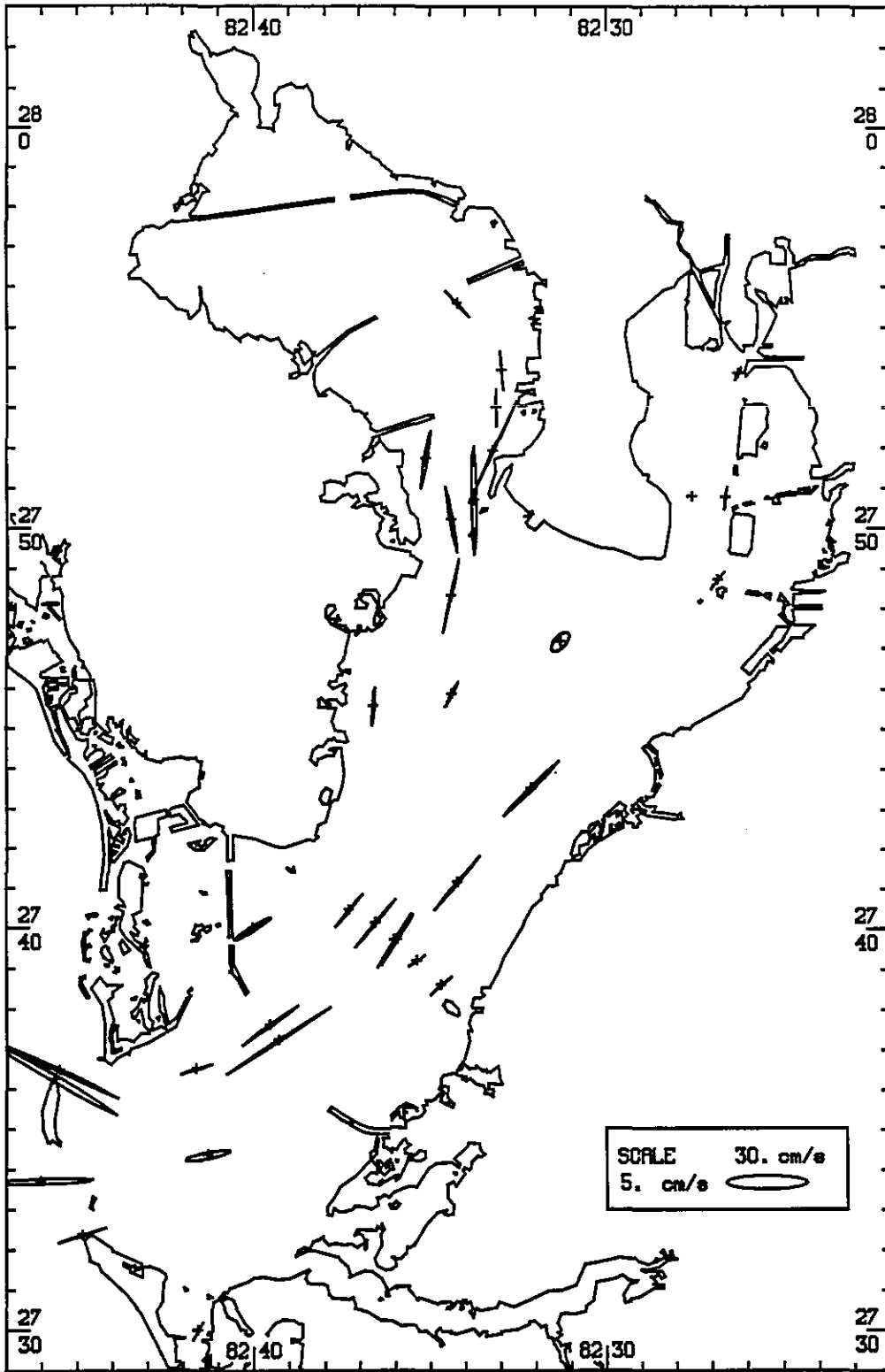


Figure 2.6. M<sub>2</sub> tidal current ellipses.

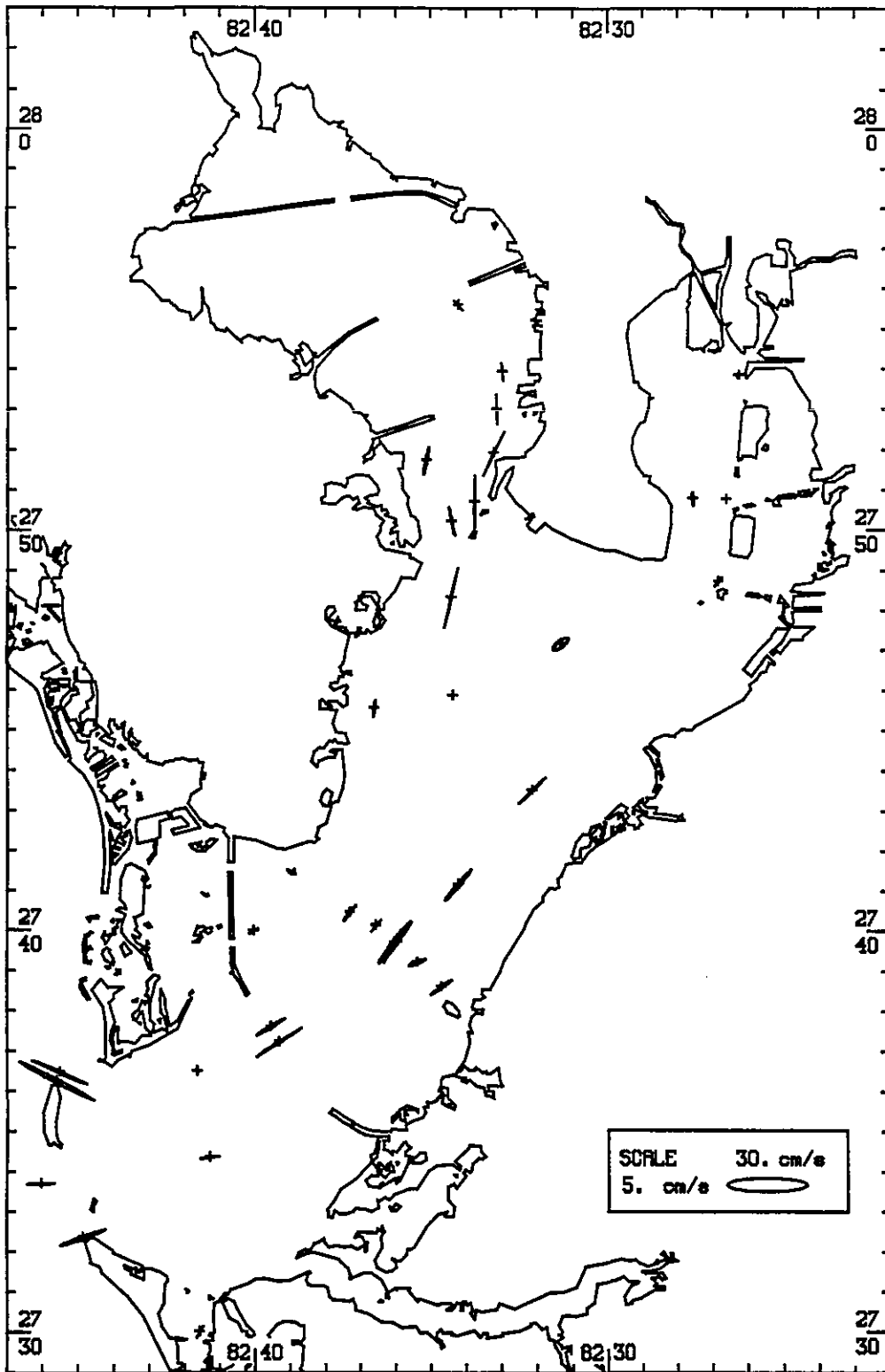
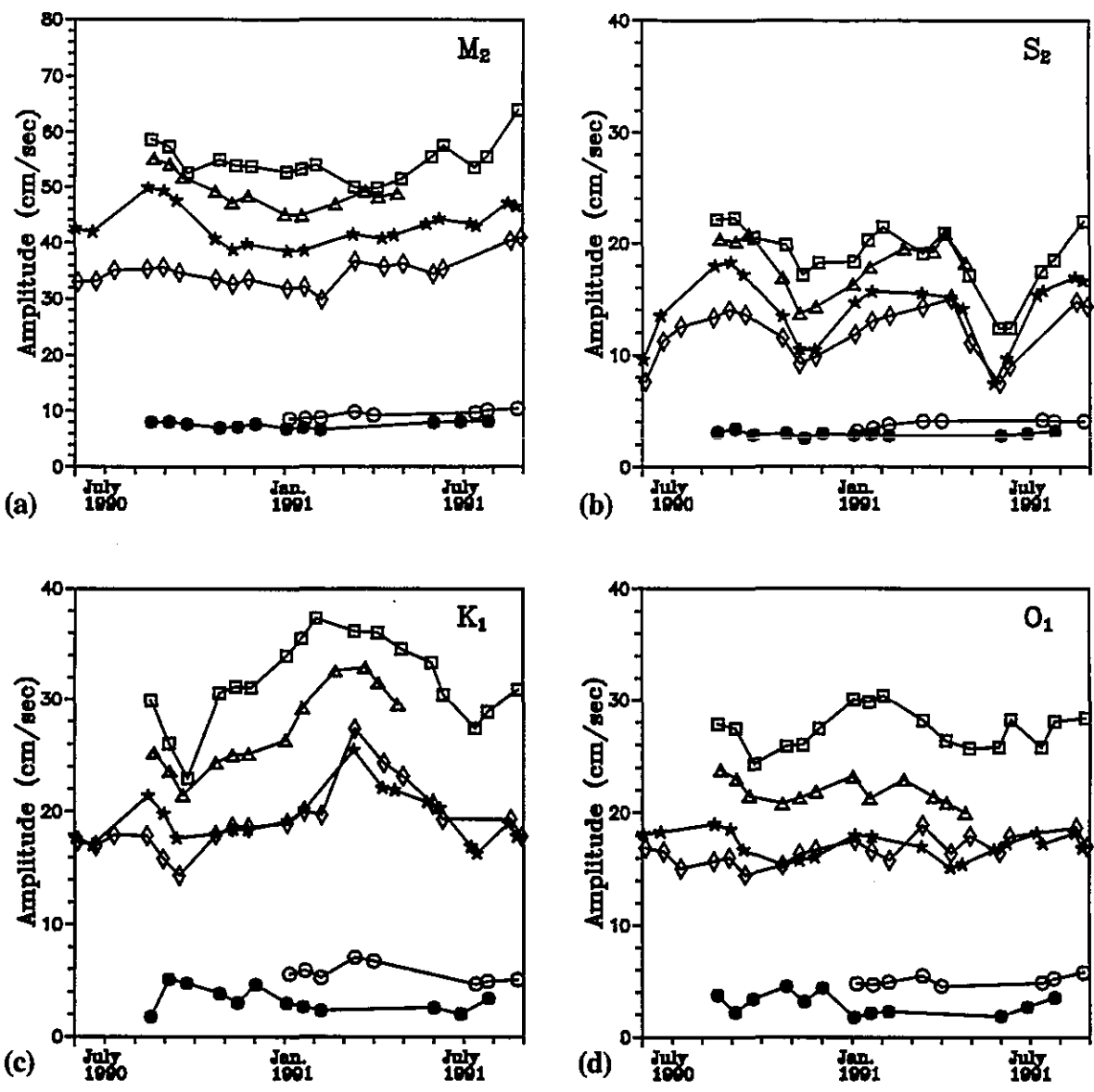
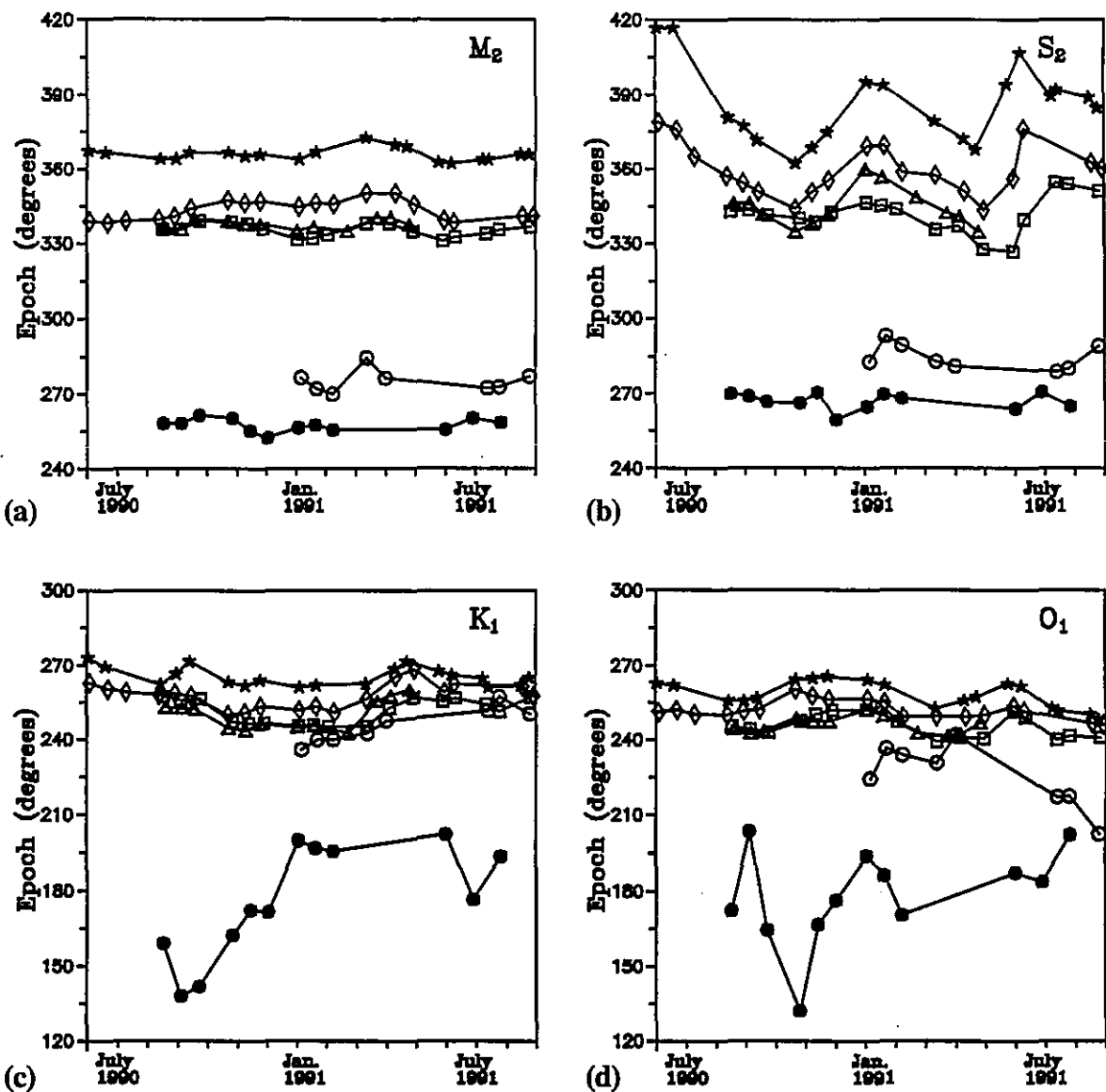


Figure 2.7. K<sub>1</sub> tidal current ellipses.



○○○○○ Station C-1 (Outer Egmont)  
 □□□□□ Station C-2 (Inner Egmont)  
 ▲▲▲▲▲ Station C-3 (Sunshine Skyway)  
 ◇◇◇◇◇ Station C-4 (Port Manatee)  
 ★★★★★ Station C-5 (Port Tampa)  
 ●●●●● Station C-6 (Gulf of Mexico)

Figure 2.8. Annual variation of tidal current constituent amplitudes from 29-day harmonic analysis periods. Constituents displayed are (a)  $M_2$ , (b)  $S_2$ , (c)  $K_1$ , and (d)  $O_1$ . Note that the stations in Tampa Bay are correlated with each other but not with the offshore stations (C-1 and C-6).



○○○○○ Station C-1 (Outer Egmont)  
 □□□□□ Station C-2 (Inner Egmont)  
 ▲▲▲▲▲ Station C-3 (Sunshine Skyway)  
 ◇◇◇◇◇ Station C-4 (Port Manatee)  
 ★★★★★ Station C-5 (Port Tampa)  
 ●●●●● Station C-6 (Gulf of Mexico)

Figure 2.9. Annual variation of tidal current constituent epochs from 29-day harmonic analysis periods. Constituents displayed are (a)  $M_2$ , (b)  $S_2$ , (c)  $K_1$ , and (d)  $O_1$ . Note that the stations in Tampa Bay are correlated with each other but not with the offshore stations. The epochs of  $K_1$  and  $O_1$  for the offshore station (C-6) vary greatly because the current ellipses are nearly circular making the major axis indeterminate.

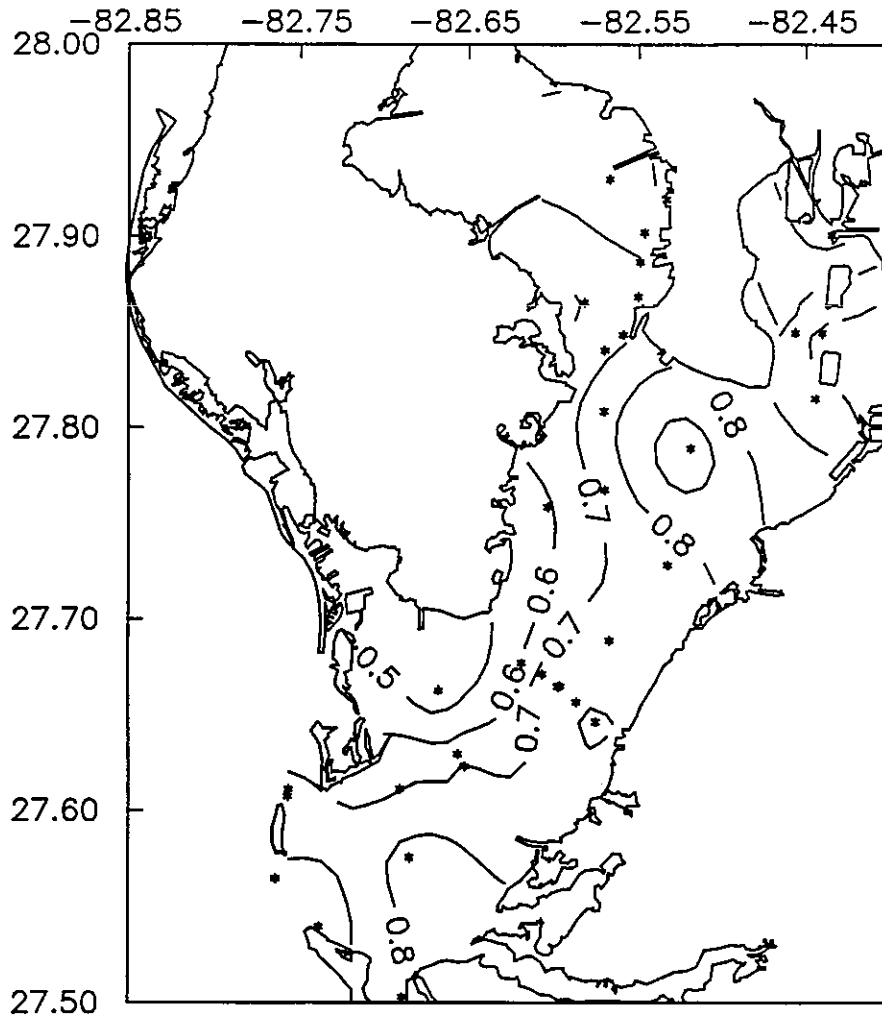
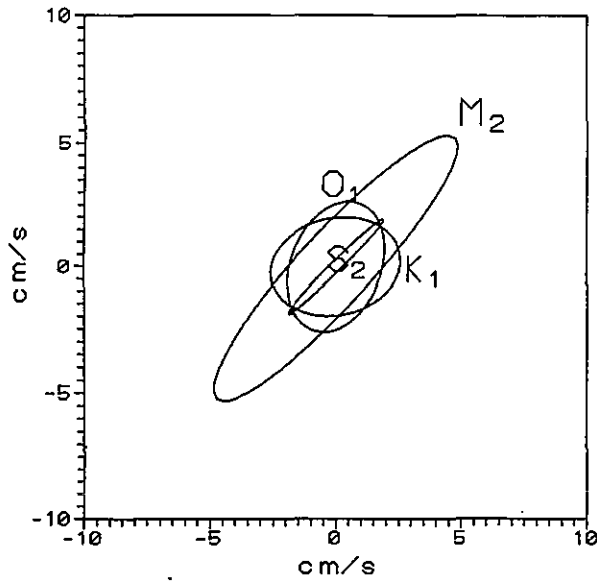
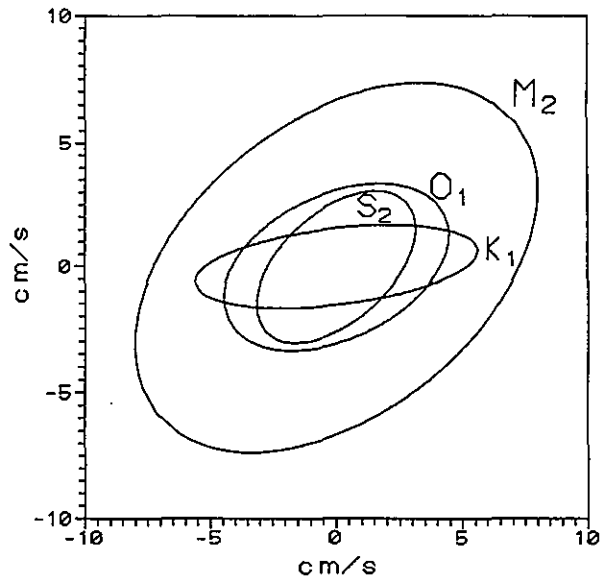


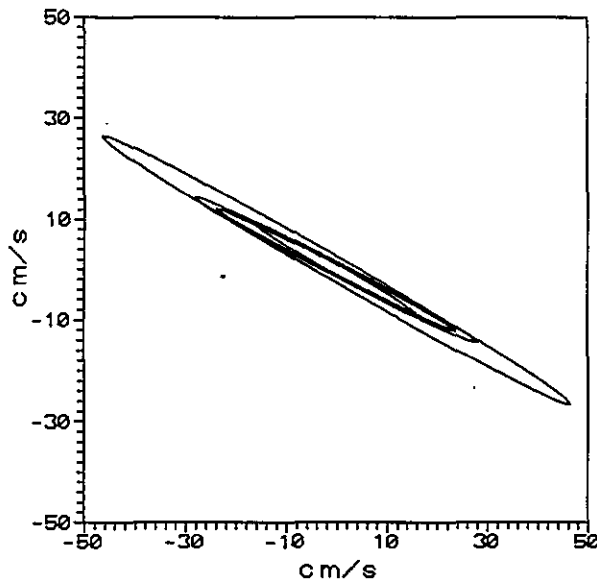
Figure 2.10. Tidal current classification ratio  $(K_1 + O_1)/(M_2 + S_2)$ . Contour interval is 0.1. Tampa Bay currents are classified as mixed, mainly semidiurnal since all of the ratios are between 0.25 and 1.5.



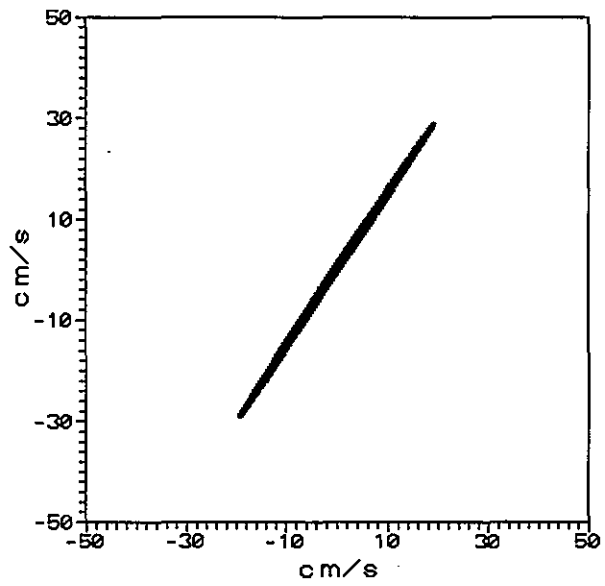
(a)



(b)



(c)



(d)

Figure 2.11. Tidal current ellipses for  $M_2$ ,  $S_2$ ,  $K_1$ , and  $O_1$  at offshore stations (a) C-6 and (b) C-1 and Tampa Bay stations (c) C-2 and (d) C-4. The ellipses for C-2 and C-4 are not labeled. The width of the offshore current ellipses indicates that shelf currents are rotary.

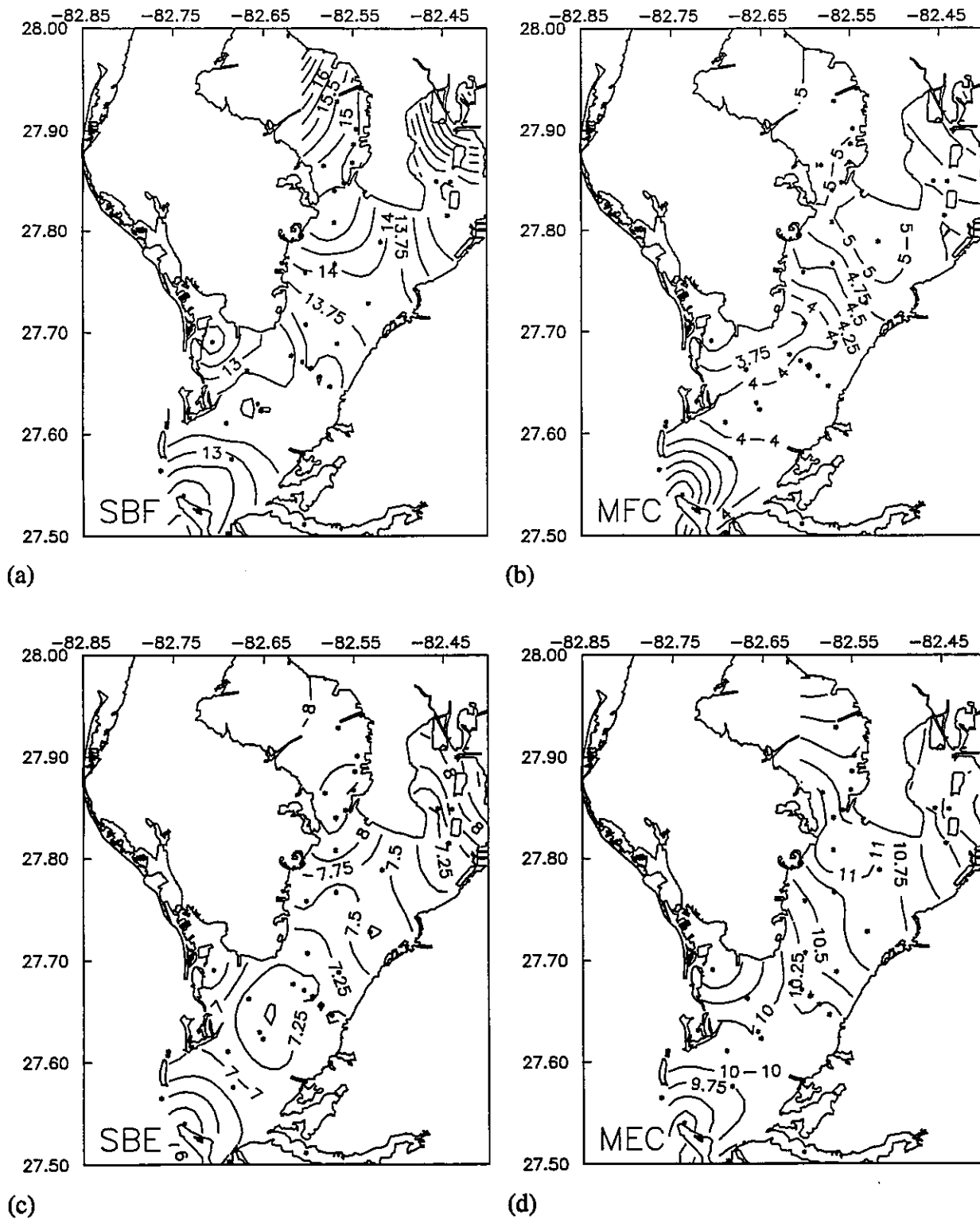
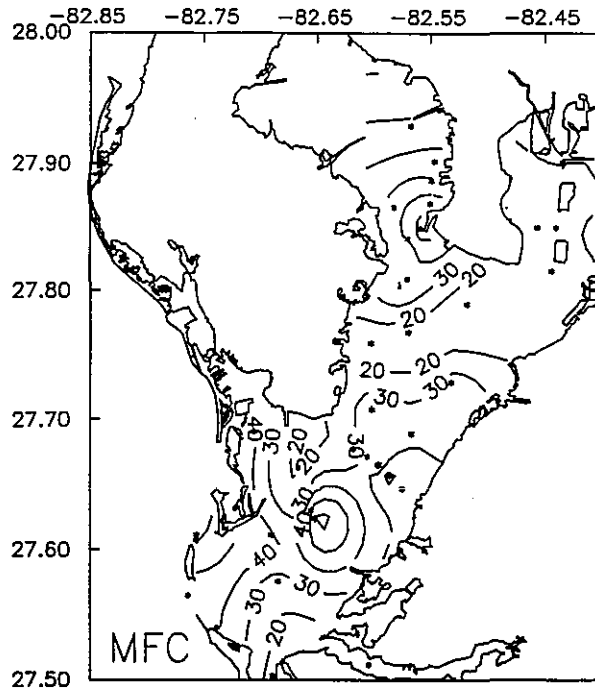
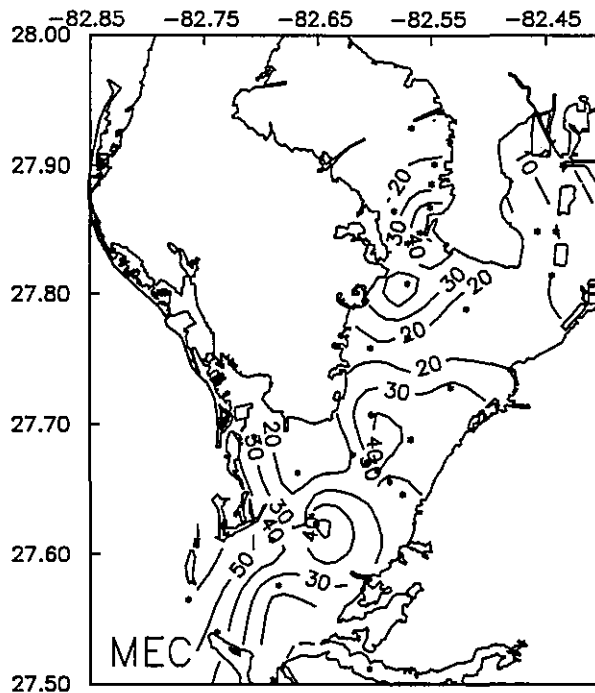


Figure 2.12. Greenwich intervals for (a) slack before flood (SBF), (b) maximum flood current (MFC), (c) slack before ebb (SBE), and (d) maximum ebb current (MEC). Contour interval is 0.25 hour. Dots indicate station locations.



(a)



(b)

Figure 2.13. Mean maximum (a) flood (MFC) and (b) ebb (MEC) currents in cm/s. Contour interval is 10 cm/s. Dots indicate station locations.

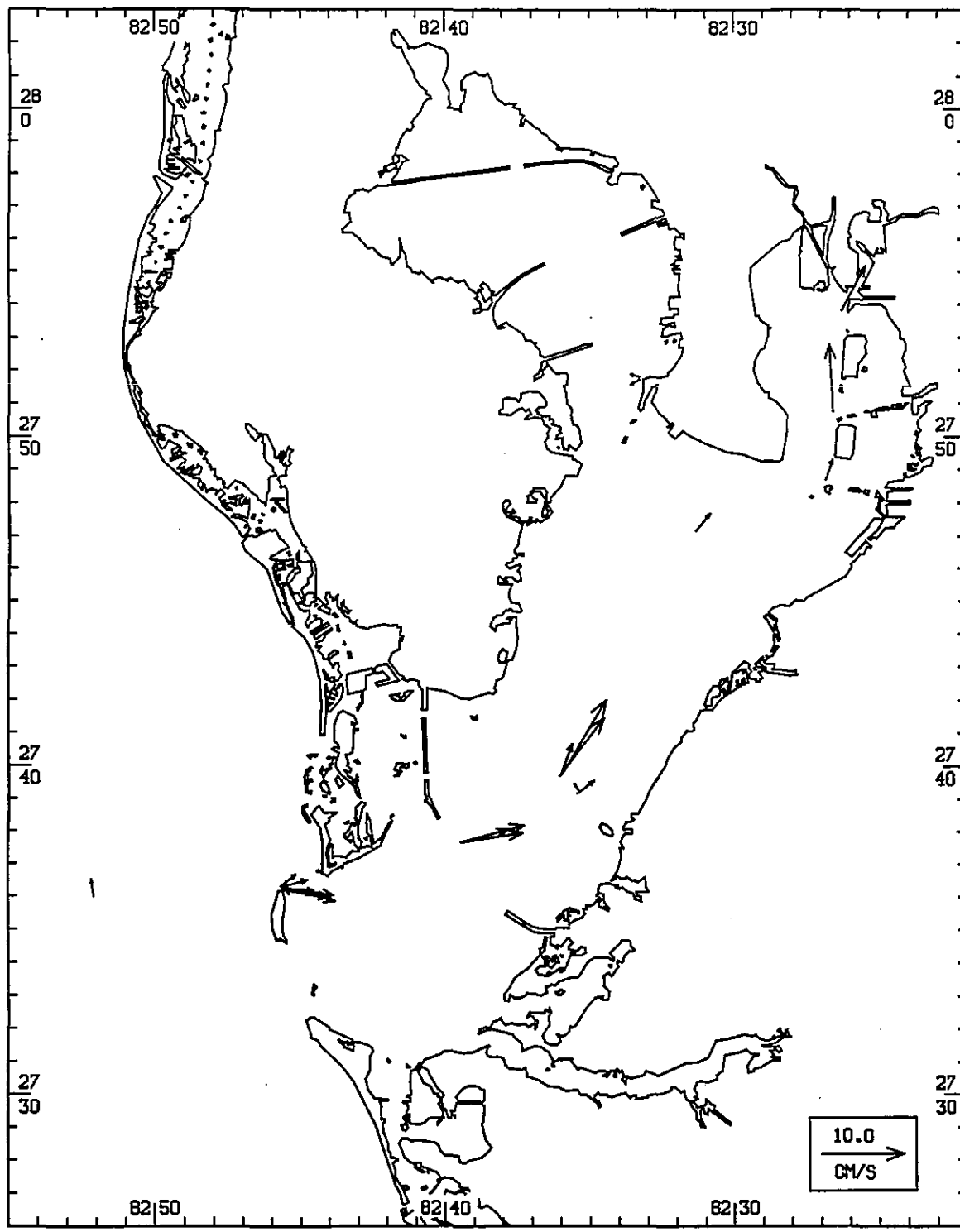


Figure 2.14. Mean current at a depth of 10 m. All data for each deployment were vector averaged.

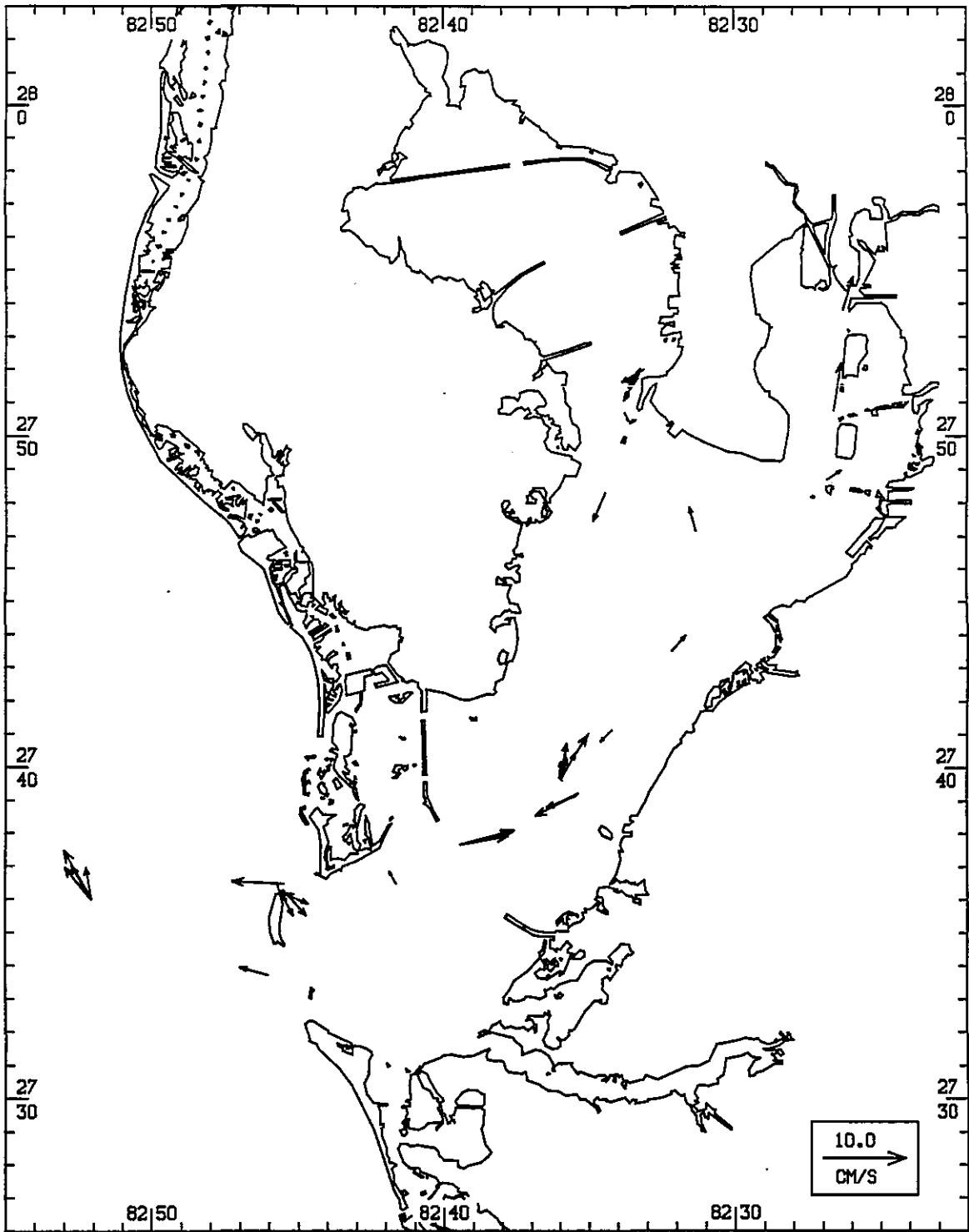


Figure 2.15. Mean current at a depth of 5 m. All data for each deployment were vector averaged.

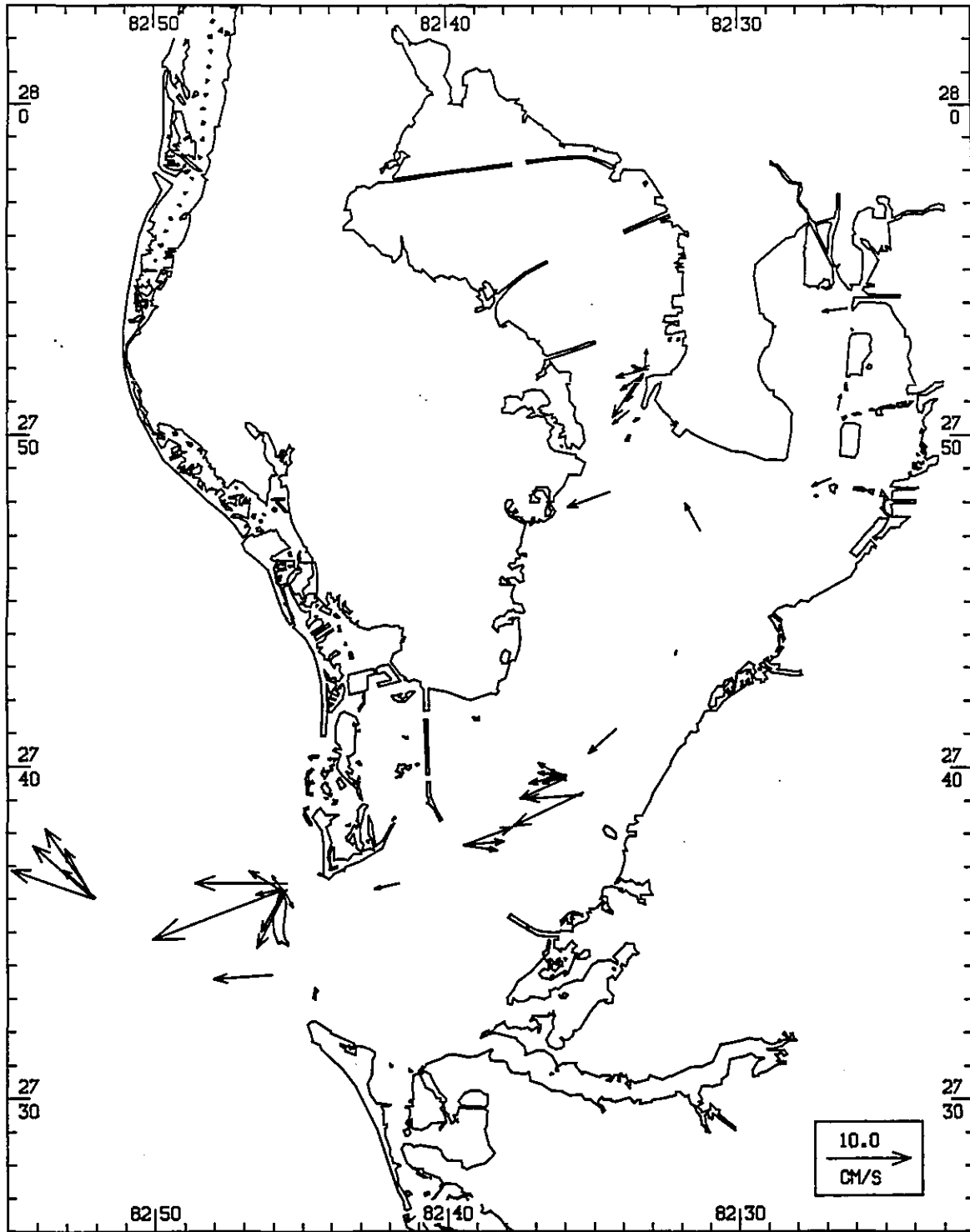
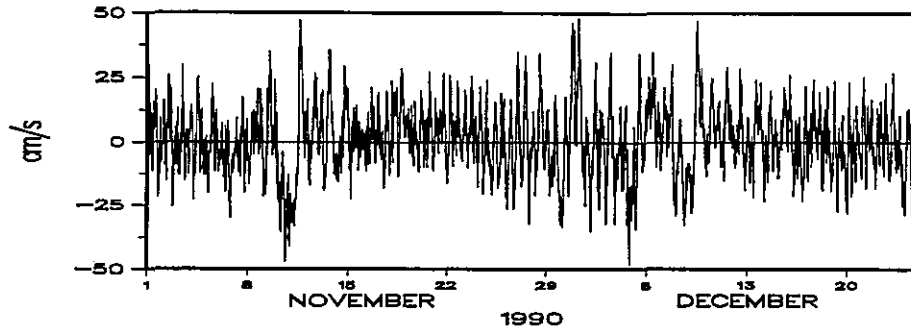
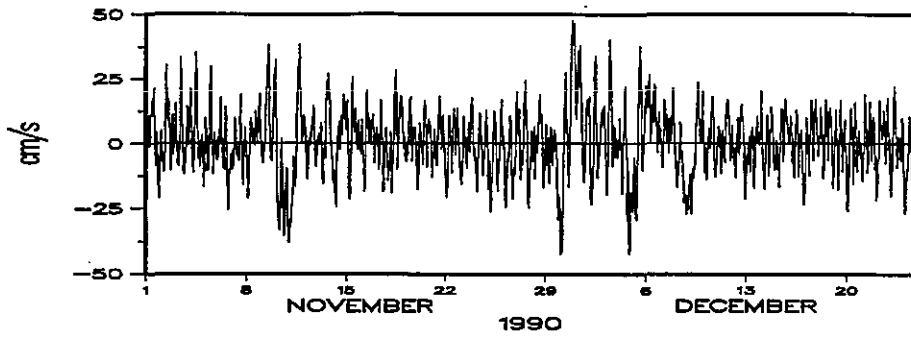


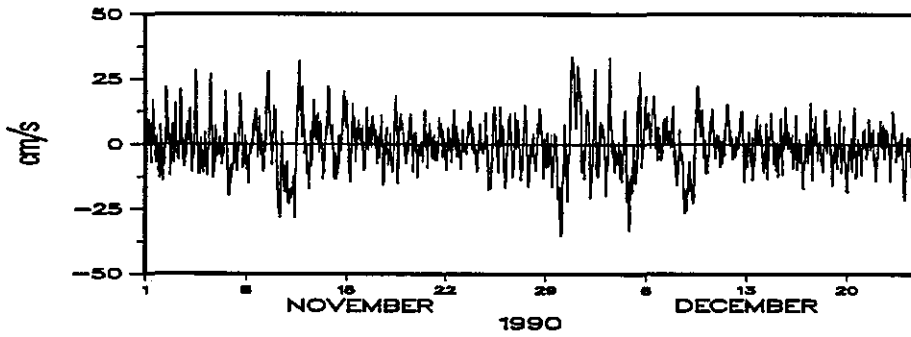
Figure 2.16. Mean current at a depth of 2 m. All data for each deployment were vector averaged.



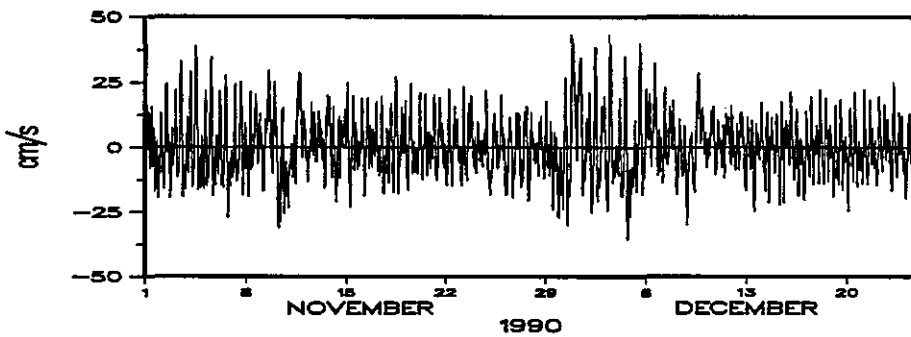
(a)



(b)



(c)



(d)

Figure 2.17. Residual along-channel currents for (a) C-2, (b) C-3, (c) C-4, and (d) C-5.

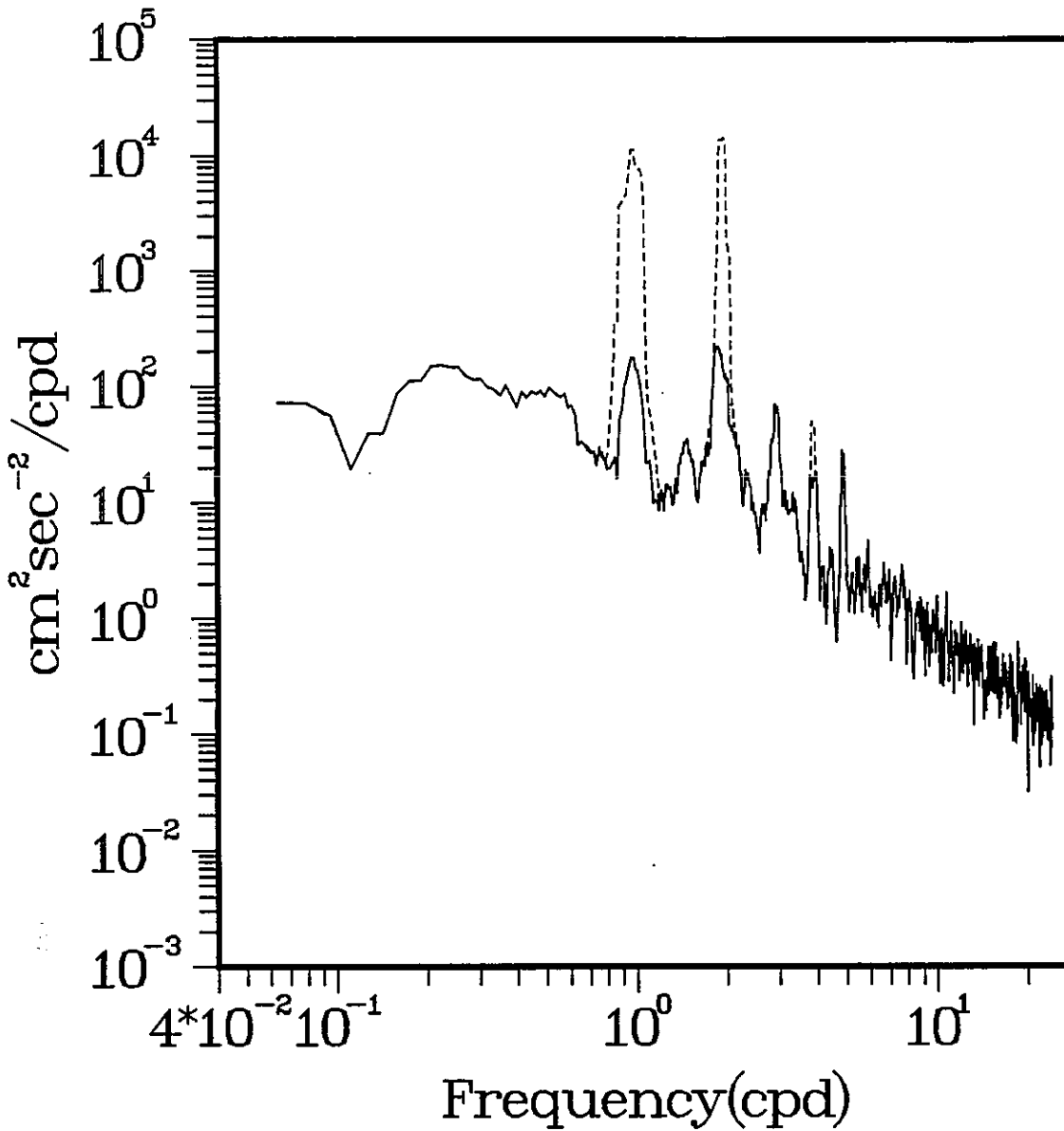


Figure 2.18. Observed (dashed) and residual (solid) spectra of along-channel current velocity at C-2 during October 27 - December 27, 1990. The bandwidth is 0.016 cpd.

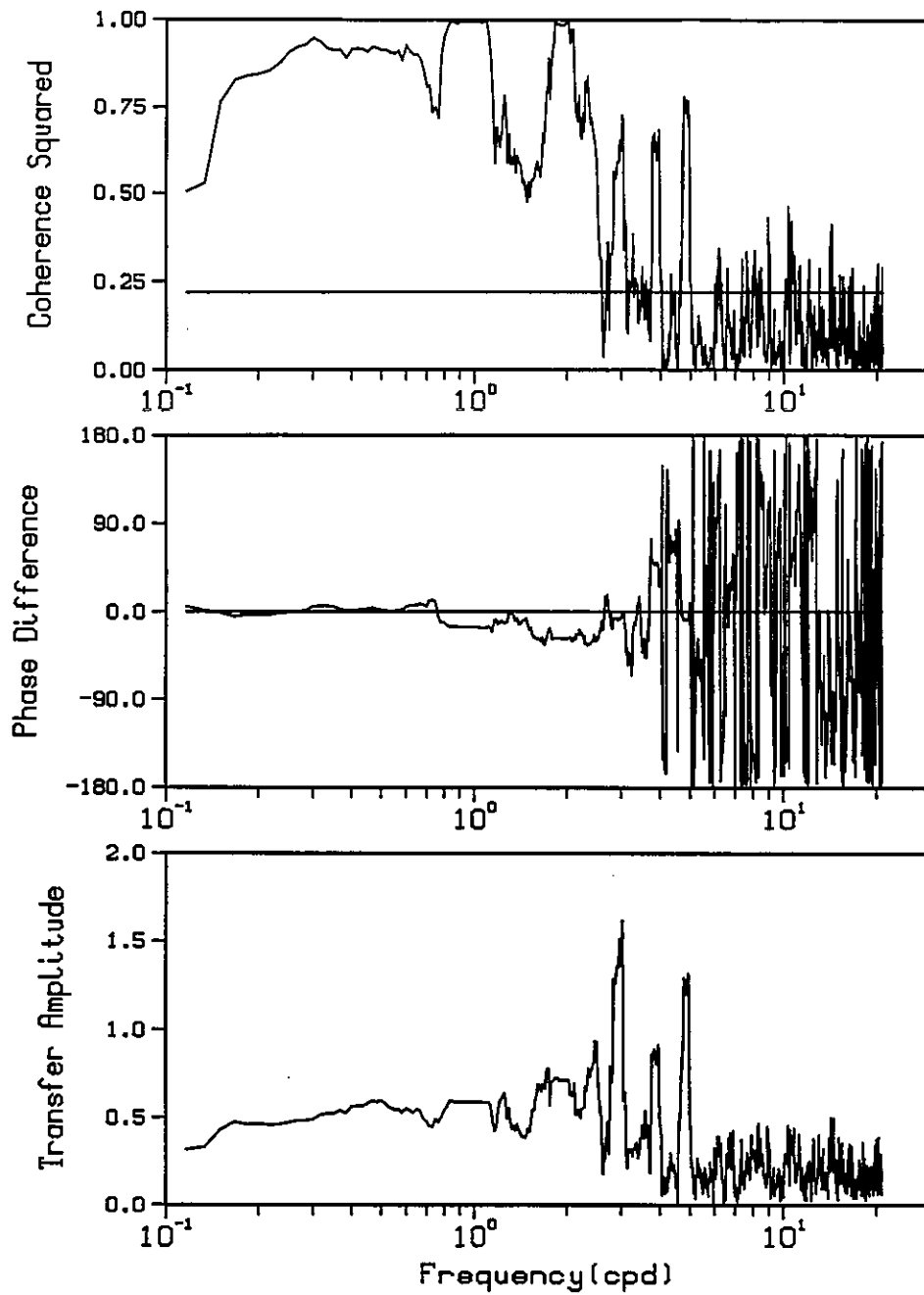
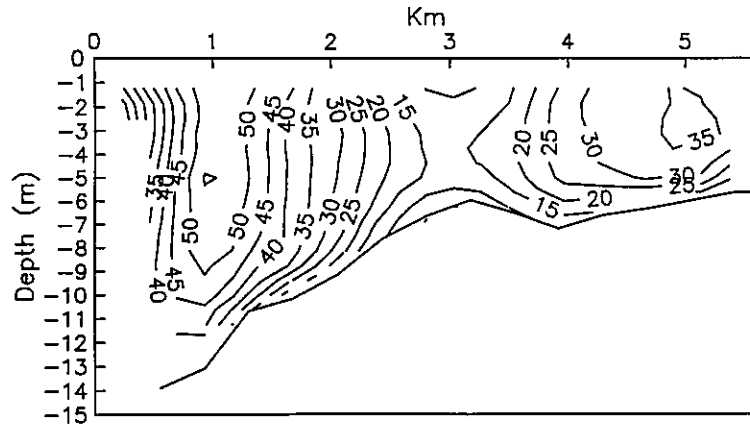
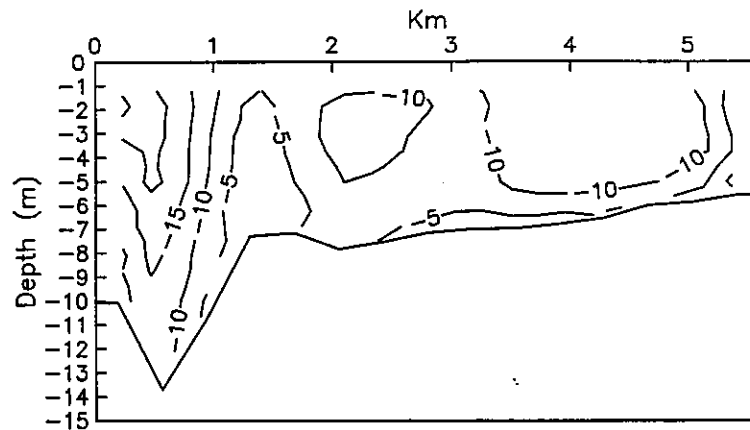


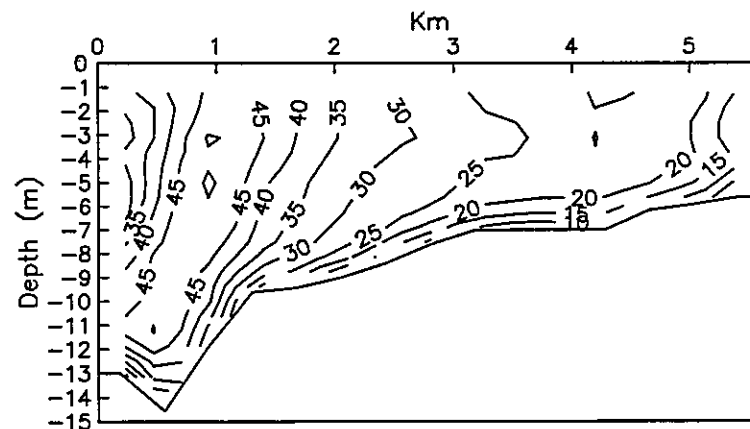
Figure 2.19. Results of cross spectral analysis of along-channel current velocity at C-2 and C-5 during October 28 - December 25, 1990. The figure shows coherence squared (with the 95% significance level), phase difference ( $^{\circ}$ ) [C-2 - C-5], and transfer amplitude [C-5/C-2]. The bandwidth is 0.0167 cpd.



(a) North FLOOD South

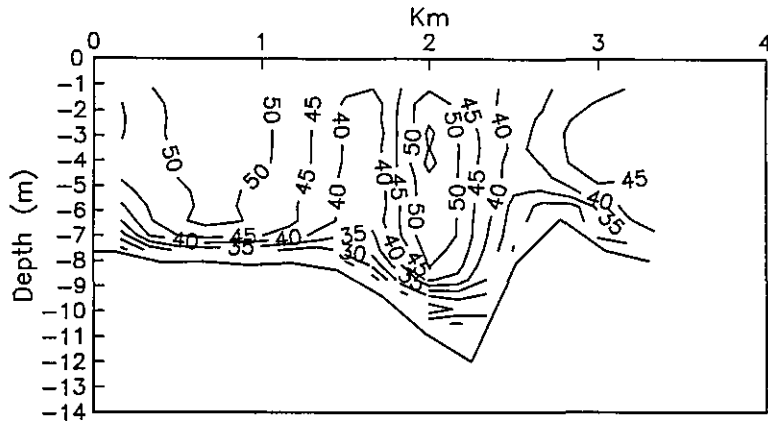


(b) North EBB South

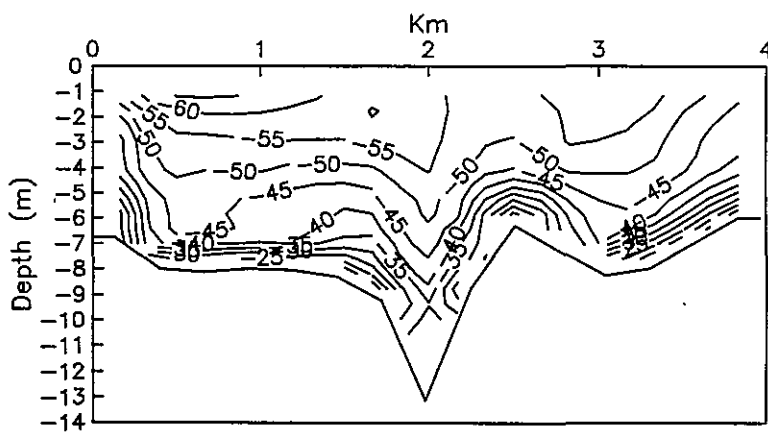


(c) North FLOOD South

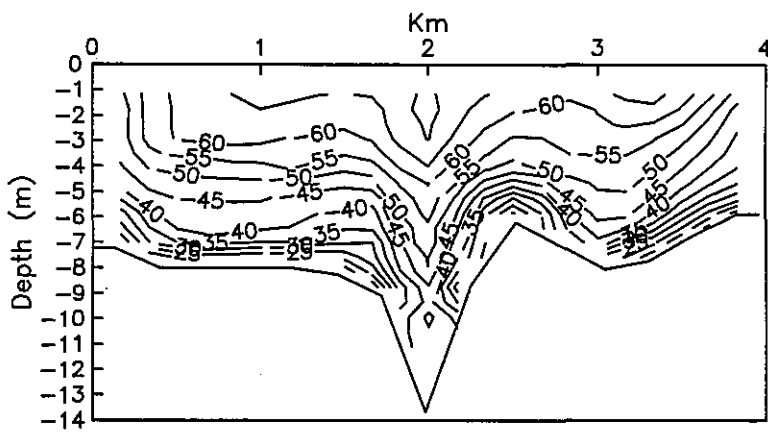
Figure 2.20. CT-1 towed ADCP transects for velocity perpendicular to the vertical plane. Contour interval is 5 cm/s. Negative values indicate ebb flow. (a) Flood period 11/14/90 1321-1702 UT. (b) Ebb period 3/5/91 1122-1421 UT. (c) Flood period 3/5/91 1626-2001 UT.



(a) Northwest FLOOD Southeast

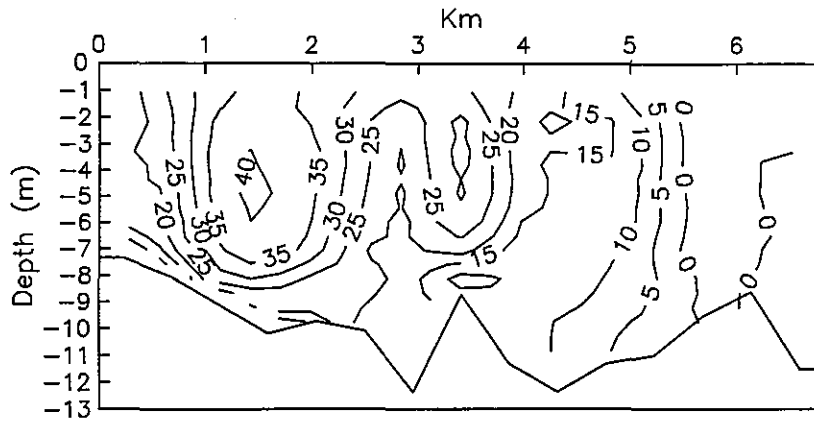


(b) Northwest EBB Southeast

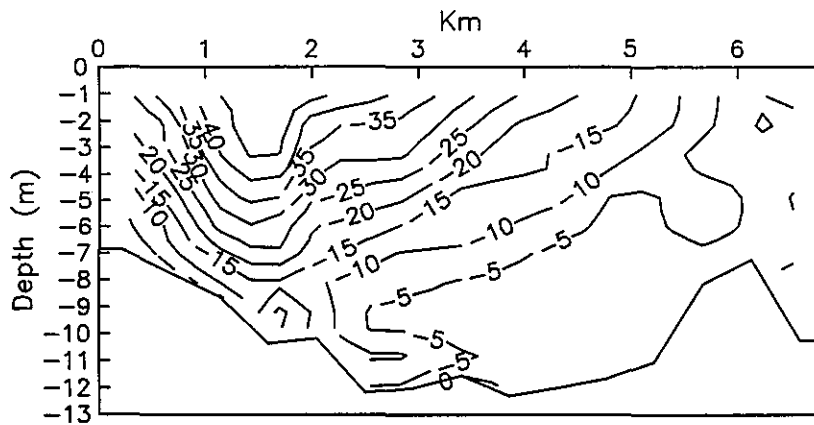


(c) Northwest EBB Southeast

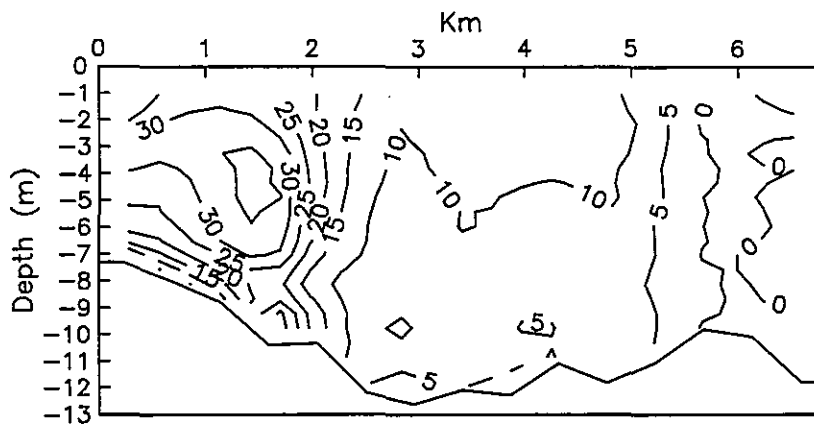
Figure 2.21. CT-2 towed ADCP transects for velocity perpendicular to the vertical plane. Contour interval is 5 cm/s. Negative values indicate ebb flow. (a) Flood period 11/13/90 1234-1621 UT. (b) Ebb period 8/17/91 1342-1535 UT. (c) Ebb period 8/18/91 1625-1816 UT.



(a) Northwest FLOOD Southeast



(b) Northwest EBB Southeast



(c) Northwest FLOOD Southeast

Figure 2.22. CT-3 towed ADCP transects for velocity perpendicular to the vertical plane. Contour interval is 5 cm/s. Negative values indicate ebb flow. (a) Flood period 11/15/90 1427-1810 UT. (b) Ebb period 8/16/91 1602-1802 UT. (c) Flood period 8/16/91 2023-0027 UT.

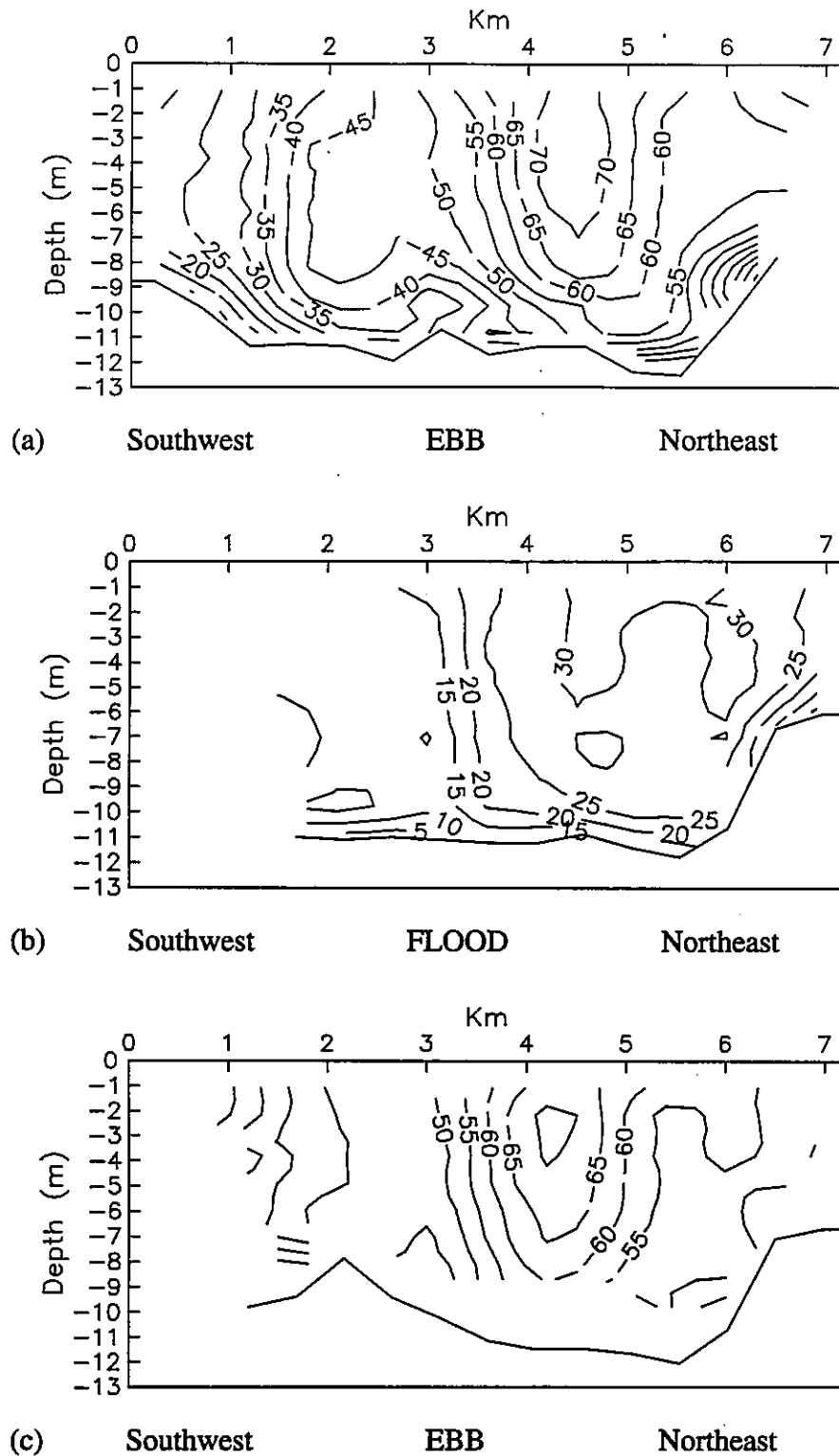
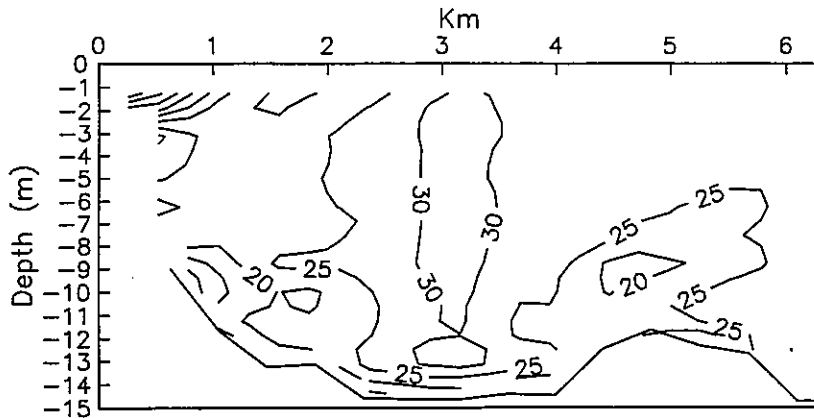
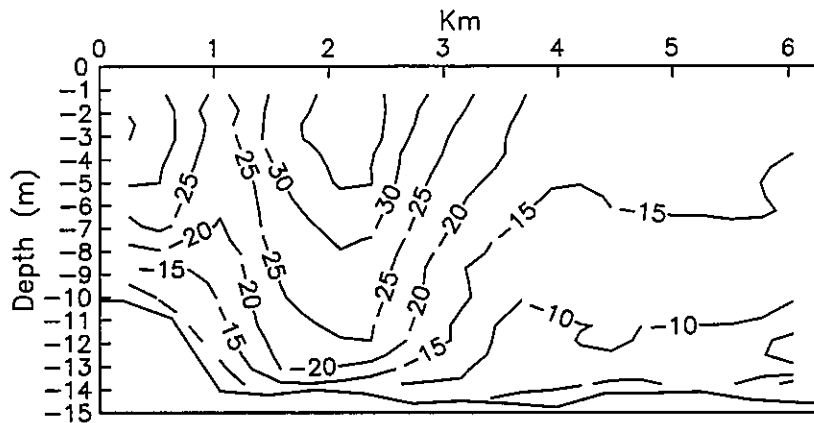


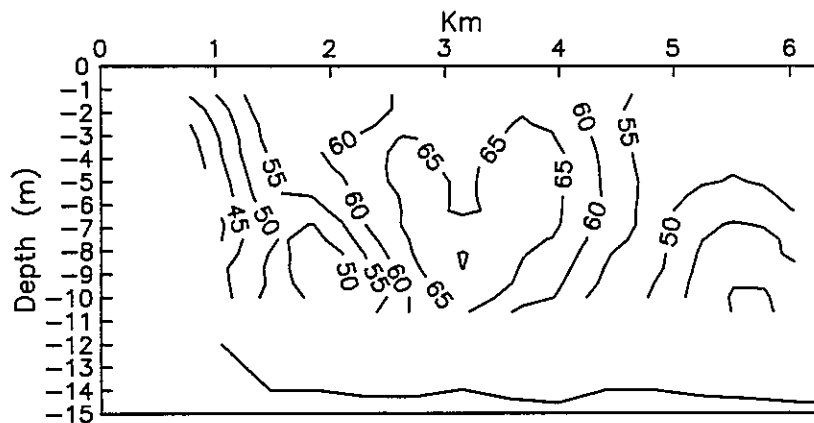
Figure 2.23. CT-4 towed ADCP transects for velocity parallel to vertical plane. Contour interval is 5 cm/s. Negative values indicate ebb flow. (a) Ebb period 11/10/90 1428-1752 UT. (b) Flood period 2/27/91 1525-1626 UT. (c) Ebb period 6/3/91 0021-0257 UT.



(a) Southwest FLOOD Northeast



(b) Southwest EBB Northeast



(c) Southwest FLOOD Northeast

Figure 2.24. CT-5 towed ADCP transects for velocity parallel to vertical plane. (a) Flood period 11/12/90 1210-1544 UT. (b) Ebb period 11/12/90 1706-2017 UT. (c) Flood period 8/26/91 1533-1741 UT. The Sunshine Skyway crosses this transect at 2.9 km.



### 3. WATER LEVELS

Leonard E. Hickman, Chris E. Zervas, and Richard W. Bourgerie

#### 3.1. INTRODUCTION

The last update of the secondary Tide Table stations in Tampa Bay was based on data collected at nine locations in 1977-1979. As a part of the TOP plan (NOS, 1990a), water level data were collected concurrently with the current data in order to update the Tide Tables. In this section, tidal and nontidal water level characteristics are discussed and related to the results for currents presented in Section 2. In Section 6, the nontidal water level signal is related to meteorological driving forces. The tidal and nontidal water levels at the entrance to the Bay are used to drive the numerical model described in Section 7. The water level data in the Bay are used for the calibration and validation of the numerical model.

Water level measurements were collected from 16 stations throughout Tampa Bay and along the Gulf Coast. The stations at St. Petersburg (E-520) and Clearwater Beach (E-724) are permanent NOS tide stations while the other 14 were temporary stations occupied during TOP (Figure 3.1). The permanent station at Clearwater Beach and the temporary stations at Venice Pier (E-858) and Anna Maria Island (E-243) were on the Gulf Coast north and south of Tampa Bay, while the remaining stations were inside the Bay. St. Petersburg is the reference station for Tampa Bay in the NOS Tide Tables. The acquisition of water level data for TOP was conducted in two phases to minimize the number of instruments required to complete the project. The periods when data were collected at each station are shown in Table A.2 of Appendix A.

#### 3.2. HARMONIC ANALYSIS

Continuous hourly water level data sets for periods of at least 29 days and less than 180 days were analyzed using the Fourier harmonic analysis technique described in Section 2.2. Multiple sets of 29-day analyses were averaged to produce the tidal constituents. For data sets longer than 180 days, the least squares harmonic analysis method was used (Harris et al., 1963). NOS routinely analyzes time series for a standard set of 37 values that include diurnal and semidiurnal constituents, shallow-water constituents that are made up of combinations of the diurnal and semidiurnal constituents (overtides and compound tides), and the meteorological constituents  $S_a$ ,  $S_{sa}$ , and  $S_1$ . The long-period constituents are unstable from year to year because their amplitudes and phases depend upon seasonal meteorological forcing rather than periodic tidal forcing. The definition of the five primary diurnal and semidiurnal constituents used in this report are: (1) the lunisolar diurnal  $K_1$ , (2) the lunar diurnal  $O_1$ , (3) the principal lunar semidiurnal  $M_2$ , (4) the larger lunar elliptic semidiurnal  $N_2$ , and (5) the principal solar semidiurnal  $S_2$  constituents. The harmonic analysis results are presented in Tables 3.1 and 3.2 which show the amplitudes and epochs of these constituents and the method used to calculate their values. The amplitudes and epochs for all 37 constituents at the Tide Tables reference station at St. Petersburg are shown in Table B.2 in Appendix B.

## Spatial Variation of Tidal Constituents

Tidal amplitudes and epochs are displayed as contour plots in Figures 3.2 and 3.3 for the constituents  $M_2$ ,  $S_2$ ,  $K_1$ , and  $O_1$ . The highest tidal amplitudes are at the head of Old Tampa Bay. These amplitudes are about 20% to 35% higher than amplitudes at the entrance to Tampa Bay. The lowest amplitudes of the diurnal constituents occur at the mouth of the Bay (Figures 3.2c and 3.2d); however, the semidiurnal constituent amplitudes are lowest in the middle section of Tampa Bay (Figures 3.2a and 3.2b).

The epoch contour plots (Figure 3.3) show the steady progression of the tidal constituents up Tampa Bay and into Old Tampa Bay. An epoch difference of  $30^\circ$  represents approximately 1 hour for a semidiurnal constituent and approximately 2 hours for a diurnal constituent. Epochs in Hillsborough Bay are somewhat earlier than epochs at the entrance to Old Tampa Bay. The latest epochs occur at the head of Old Tampa Bay and are 3 to 4 hours after the epochs at Egmont Key.

**Table 3.1. Amplitude (cm) and epoch ( $^\circ$ ) of the primary semidiurnal constituents  $M_2$ ,  $S_2$ , and  $N_2$ .**

Station	$M_2$		$S_2$		$N_2$	
	Amp	Epoch	Amp	Epoch	Amp	Epoch
E-217	16.1	0.0	6.0	9.3	3.6	359.5
E-243	18.5	331.2	7.3	336.5	4.1	328.3
E-273	16.7	4.1	5.9	11.7	3.6	1.6
E-347	16.3	345.7	6.5	351.0	3.4	340.7
E-364	15.3	352.8	6.2	355.7	3.2	351.7
E-384	15.1	26.4	5.2	35.3	2.8	24.9
E-428	16.7	1.2	6.3	10.9	3.6	359.9
E-520	16.4	53.5	5.2	64.2	3.0	49.8
E-537	18.9	52.4	6.2	60.5	3.4	49.9
E-641	18.0	83.0	6.5	97.8	3.4	82.1
E-657	18.8	62.7	6.6	72.5	3.0	49.3
E-667	18.7	55.9	7.2	66.5	3.8	53.1
E-689	21.9	90.5	6.6	111.5	3.9	88.4
E-724	24.3	338.4	9.5	350.6	5.0	338.4
E-738	20.6	97.3	7.4	112.4	3.9	98.2
E-858	16.9	332.8	6.6	337.4	4.0	330.5

**Table 3.2. Amplitude (cm) and epoch (°) of the primary diurnal constituents  $K_1$  and  $O_1$ . HA29 indicates Fourier harmonic analysis and LSQHA indicates least squares harmonic analysis. The number in parenthesis is the number of separate analyses that were vector averaged for HA29 or the number of days of data used for LSQHA.**

Station	$K_1$		$O_1$		Source
	Amp	Epoch	Amp	Epoch	
E-217	13.2	314.5	13.5	308.8	HA29 (5)
E-243	13.6	296.8	13.4	292.5	HA29 (4)
E-273	13.1	315.6	13.8	308.8	HA29 (4)
E-347	14.3	304.9	13.8	300.7	LSQHA(196)
E-364	14.6	310.3	13.7	305.0	LSQHA(203)
E-384	15.6	323.4	14.3	319.3	LSQHA(304)
E-428	13.6	314.1	13.8	308.5	HA29 (5)
E-520	15.7	335.8	14.8	329.4	LSQHA(365)
E-537	15.9	335.1	14.9	330.2	LSQHA(237)
E-641	19.8	347.4	15.5	340.8	HA29 (5)
E-657	18.0	340.0	15.5	333.2	LSQHA(232)
E-667	19.9	335.9	15.4	330.0	HA29 (5)
E-689	16.7	349.4	16.1	346.5	HA29 (8)
E-724	15.3	297.0	14.6	294.4	LSQHA(365)
E-738	19.9	354.2	16.1	347.4	HA29 (5)
E-858	13.4	297.1	13.4	293.0	HA29 (5)

### Tidal Classification

The tidal amplitude ratio  $(K_1 + O_1)/(M_2 + S_2)$  for all the water level stations in Tampa Bay is displayed as a contour plot in Figure 3.4. This ratio (Defant, 1961) is used to classify tides and currents. Two tidal signals with similar tidal amplitude ratios will have similar waveforms. The tide is (1) semidiurnal if it is less than 0.25, (2) mixed, mainly semidiurnal if it is between 0.25 and 1.5, (3) mixed, mainly diurnal if it is between 1.5 and 3, or (4) diurnal if it is greater than 3. The amplitude ratio ranges from 0.88 at Clearwater Beach (E-724) to 1.48 at Port Manatee (E-384), which means that the type of tide observed at all locations is mixed, mainly semidiurnal. A station with a higher ratio has more diurnal days per month than a station with a lower ratio.

The tidal current amplitude ratios in Figure 2.10 are about half of the tidal amplitude ratios in Figure 3.4. While the tidal amplitude ratio indicates the ratio of volumes transported in and out of the Bay, the tidal current amplitude ratio indicates the ratio of the transport rates. For example, if the tidal amplitude ratio in an enclosed bay is 1, the same volume of water is transported by the diurnal and the semidiurnal tide. However, the transport rate for a semidiurnal constituent must be double the rate for a diurnal constituent to transport a comparable volume of water in half the time. Therefore, the tidal current amplitude ratio is 0.5.

### **Greenwich Intervals and Tidal Ranges**

Other indicators of temporal and spatial differences are the Greenwich high and low water intervals and the mean and great diurnal ranges. Greenwich intervals are referenced to the transit of the moon over the meridian of Greenwich. The mean range is the difference between mean high water and mean low water; the great diurnal range is the difference between the mean higher high water and the mean lower low water. Values used in this report were calculated using formulae based on the relationships of the amplitudes and epochs of several harmonic constituents. The Greenwich intervals and the ranges were calculated for each station (Table 3.3) and are displayed as contour plots in Figure 3.5.

There is a clear trend of epoch and amplitude as the tide progresses from the mouth of Tampa Bay up into Old Tampa Bay and Hillsborough Bay. The Greenwich intervals show the consistent progression of the tide up the Bay. Arrivals in Hillsborough Bay are earlier than arrivals at the entrance to Old Tampa Bay. Four to five hours are required for high and low tide to travel from Egmont Key to the head of Old Tampa Bay. The tidal range increases steadily toward the head of the Bay. The lowest tidal ranges are in lower Tampa Bay with the greatest ranges (about 30% greater than Egmont Key) at the head of Old Tampa Bay.

The tidal response of an enclosed bay can often be understood as the sum of an incident wave entering the bay and a wave reflected at the head of the bay (Redfield, 1980). The wave will not necessarily be completely reflected; some energy may travel up rivers or be dissipated by an irregular shoreline. The wave will also experience frictional damping as it travels up the bay with stronger damping occurring in shallower areas.

The pure progressive wave and the standing wave are two idealized examples. A pure progressive wave travels up the bay undamped and is not reflected. In this case, tides and tidal currents are in phase, with high water occurring at the same time as flood and low water occurring at the same time as ebb. A standing wave is found when an undamped wave is completely reflected at the head of the bay. In this case, tides and tidal currents are 90° out of phase, and high and low waters lag the flood and ebb currents, respectively, by a quarter of a tidal cycle. High and low water will occur simultaneously throughout the bay. There will be a node where the incident and reflected waves are 180° out of phase; the tidal range there will be zero and the current range will be maximum.

At most locations, the tide is somewhere between these two end members and is a combination of a damped incident wave and a damped partially-reflected wave. A comparison of the epochs

and the Greenwich intervals for nearby current and water level stations can be used to characterize each constituent of the tide. Table 3.4 shows the  $M_2$ ,  $S_2$ ,  $K_1$ , and  $O_1$  epochs and the Greenwich interval lag times for several pairs of nearby current and water level stations.

**Table 3.3. Greenwich intervals (hours) and mean and great diurnal ranges (cm)**

Station	Greenwich interval		Range	
	High water	Low water	Mean	Great
E-217	5.771	11.983	37.7	61.8
E-243	4.834	11.001	42.3	66.2
E-273	5.950	12.217	38.9	63.2
E-347	4.725	10.702	38.4	62.8
E-364	4.940	11.020	37.3	63.3
E-384	5.932	12.169	37.0	63.9
E-428	5.925	12.009	39.3	63.6
E-520	6.794	13.074	39.1	66.7
E-537	6.792	13.186	44.0	72.0
E-641	8.478	14.860	43.7	75.9
E-657	7.156	13.665	44.8	75.6
E-667	7.652	14.185	45.1	77.9
E-689	8.718	15.200	50.0	79.9
E-724	4.246	10.527	54.8	81.9
E-738	8.944	15.462	48.8	82.0
E-858	4.818	11.036	39.5	63.5

The semidiurnal tide gradually changes from a progressive wave near the entrance to the Bay to a standing wave in the upper reaches of Hillsborough Bay. In contrast, the diurnal tide is about halfway between a progressive and a standing wave at the entrance and approaches a standing wave in Hillsborough Bay. At the mouth of the Bay, the water level lags the current by about half an hour. The lag increases farther into the Bay to about three and a half hours in Old Tampa Bay.

In Figure 3.2, the amplitudes of the diurnal constituents increase steadily from the mouth to the head of the Bay, while the semidiurnal constituent amplitudes are lowest in the middle part of Tampa Bay. The epoch contour plots in Figures 3.3a and 3.3b show that there is a  $90^\circ$  phase

difference between the location of the lowest semidiurnal amplitudes and the head of Old Tampa Bay. This position is where the incident and reflected waves would be 180° out of phase. If there were no damping and complete reflection, a standing wave node would be located at this position. In contrast, for the diurnal epoch plots (Figures 3.3c and 3.3d) there is only a 55° phase difference between the mouth and the head of the Bay, so that there is no position in the Bay where the incident and reflected wave would be 180° out of phase.

**Table 3.4. Epoch differences (°) and Greenwich interval differences (hours) between water level and current at nearby stations.**

Tide Station	Current Station	M <sub>2</sub>	S <sub>2</sub>	K <sub>1</sub>	O <sub>1</sub>	High water - Flood	Low water - Ebb
E-347	C-2	9.8	9.3	53.3	56.0	0.475	0.502
E-364	C-23	21.7	17.7	56.3	60.4	0.800	0.720
E-384	C-53	52.5	35.6	75.3	78.4	1.932	2.109
E-520	C-10	66.3	37.3	77.8	80.1	2.344	2.644
E-641	C-32	68.3	56.5	83.8	75.0	3.468	3.370
E-537	C-36	86.7	82.0	101.1	84.5	2.042	2.756
E-657	C-27	90.6	89.3	95.2	65.0	1.646	3.105

### Temporal Variation

There are large seasonal fluctuations in the water level, primarily due to the meteorological constituents S<sub>a</sub> and S<sub>sa</sub>. Monthly mean sea levels for St. Petersburg and Clearwater Beach during TOP are shown along with 19-year averages of monthly mean sea level (Figure 3.6). The 19-year period is used because the period of variation in obliquity of the moon's orbit is close to 19 years. The 19-year averages show that monthly mean sea levels peak in September and are lowest in January and February. The annual range is about 20 cm which is a substantial fraction of the tidal range (see Table 3.3 and Table B.2). The water levels in Tampa Bay appear to be highly correlated with the water levels on the Gulf Coast over the 19-year period 1973-1991 and for 1990-1991.

Figure 3.7 is a plot of the yearly mean sea level values relative to accepted mean sea level computed over the 1960-1978 Tidal Datum Epoch to show the interannual variability at St. Petersburg and Clearwater Beach. The trend for the common time period of 1974 to 1991 is 0.4 cm/year. A linear least squares fit to both data sets shows almost no difference in the apparent secular (long-term) sea level rise. However, between 1990 and 1991, the mean sea level rise was 5.5 cm at Clearwater Beach and 1.1 cm at St. Petersburg.

### 3.3. NONTIDAL WATER LEVELS

#### Residual Analysis

The tidal constituents obtained by harmonic analysis were used to produce predicted water level time series for all of the stations during their deployment periods. The predicted time series were then subtracted from the observed data to obtain the residual water levels. The standard deviations from the mean of the observed and residual time series provide an estimate of the absolute and relative magnitudes of these signals. The standard deviations of the observed and residual water levels are shown in Table 3.5 along with the ratio of the residual to the observed standard deviation. The observed standard deviations range from 20.1 cm to 29.6 cm and the residual standard deviations range from 5.9 cm to 16.4 cm. The ratio of residual to observed standard deviations range between 29% and 55.7%, indicating the relative importance of nontidal forcing. Residual standard deviations are low for E-217, E-243, E-273, E-428, and E-858 because their deployment periods ended in late October 1990. Examination of residuals at other stations shows increased variability during the late fall and winter months.

**Table 3.5. Standard deviations (S.D.) from the mean of observed and residual water levels.**

Station	Year	Observed S. D. (cm)	Residual S. D. (cm)	Ratio (Res/Obs)
E-217	1990	20.1	5.9	.293
E-243	1990	21.9	6.7	.305
E-273	1990	20.7	6.2	.300
E-347	1990-1	22.7	10.1	.445
E-364	1990-1	22.1	9.7	.440
E-384	1990-1	22.9	10.4	.455
E-428	1990	20.8	6.3	.304
E-520	1990-1	24.1	10.4	.431
E-537	1990-1	25.7	11.7	.455
E-641	1991	27.8	15.5	.557
E-657	1990-1	26.6	12.9	.486
E-667	1991	28.2	15.7	.556
E-689	1990-1	28.0	12.7	.452
E-724	1990-1	27.7	10.0	.363
E-738	1991	29.6	16.4	.556
E-858	1990	20.5	6.0	.290

Figure 3.8 shows the residual water levels at four stations in Tampa Bay from June through December, 1990. Bay Aristocrat Village (E-689) is in upper Old Tampa Bay, Davis Island (E-657) is in upper Hillsborough Bay, St. Petersburg (E-520) is a mid-Bay station, and Egmont Key (E-347) is near the entrance to the Bay. Residual water levels appear to be well-correlated from station to station around the Bay; however, the stations in Old Tampa Bay and Hillsborough Bay are more responsive to high-frequency nontidal forcing than are stations closer to the mouth of the Bay. These upper Bay stations were also more responsive to tidal forcing as seen in Figure 3.2.

The spectra of observed and residual water levels at St. Petersburg for May to December, 1990, are shown in Figure 3.9. In the observed spectrum, the diurnal and semidiurnal tidal frequencies have more energy than all nontidal frequencies. After the predicted tides have been removed, most of the energy in the spectrum is at frequencies longer than 5 days (0.2 cpd). Although higher order harmonics of the tidal frequencies are visible, their energy is far lower than the energy in the longer-period bands.

### **Storm Events**

One of the primary reasons for analyzing the residual series is to investigate the response of the water levels to short- and long-term meteorological forcing (i.e., thunderstorms and cold fronts). The effects of three specific events are shown in Figure 3.10. The first is a wind event that occurred on October 25-26, 1990, the second is the passage of cold front on November 9-11, 1990, and the third is a strong thunderstorm event on January 19-20, 1991. The wind vectors during these events will be discussed in Section 4.

The October event occurred during a period when high water was predicted at Clearwater Beach and St. Petersburg. The highest wind speeds occurred on October 25 and were toward the south-southeast. The height of the expected high water was reduced by 25 to 45 cm at all locations. Stations in the Bay such as St. Petersburg and Bay Aristocrat Village showed a greater response to the storm than the Clearwater Beach station.

During the storm on November 9-11, 1990, water levels rose to a peak early on November 10 and then fell 75 cm over a 36-hour period. The wind direction rotated clockwise by nearly 360° during this event. All three stations showed a similar response to the storm with a slightly stronger response at the stations in the Bay.

The winter thunderstorm event occurring on January 19-20, 1991, created a significant storm surge (almost 1 m) at Clearwater Beach. This storm also arrived at predicted high water but, unlike the event of October 25-26, the winds increased the height of the astronomical high water. Wind speeds gradually increased on January 19 and were directed toward the north-northeast. Early on January 20, the wind speed suddenly doubled, the wind direction rapidly rotated clockwise, and then abruptly diminished. This occurred in less than four hours and produced the storm surge at Clearwater Beach. Clearwater Beach had a much stronger response to the storm surge than the stations inside Tampa Bay such as St. Petersburg and Bay Aristocrat Village.

### 3.4. CONCLUSIONS

The geographical distribution of the water level stations has resulted in a data set providing good spatial resolution of the tidal and nontidal response of Tampa Bay. Harmonic analysis of the data shows the steady progression of the tide into the Bay and into Hillsborough and Old Tampa Bays. The tidal ranges gradually increase from the mouth to the head of the Bay. The tide is classified as mixed, mainly semidiurnal throughout the Bay. The tide resembles a progressive wave near the entrance to the Bay and a standing wave in Hillsborough Bay. Three storm events were examined to illustrate the response to meteorological forcing. The residual water level signal is a significant fraction of the observed water level signal and has a major effect on the ability to accurately predict the tides using traditional harmonic analysis and prediction techniques.

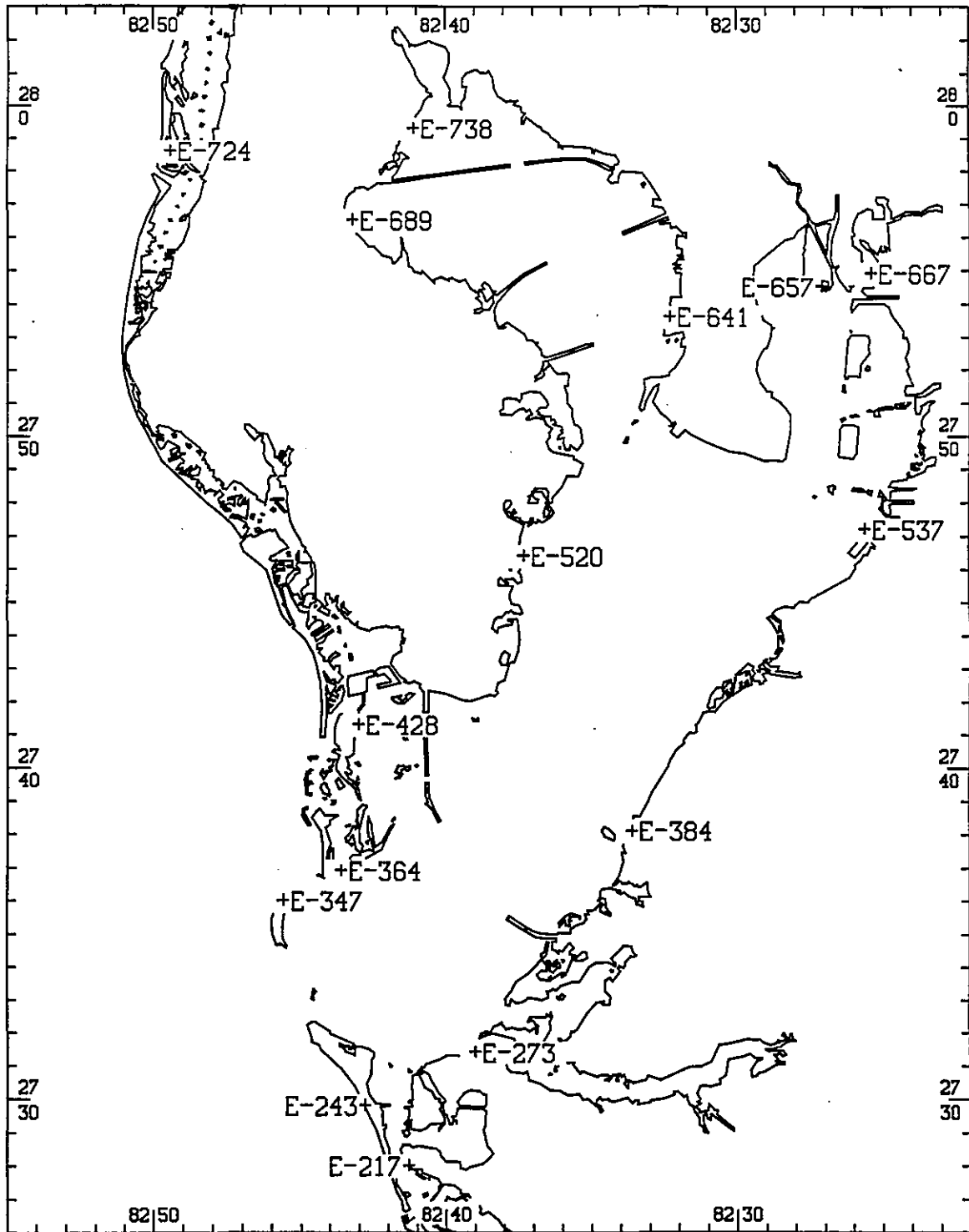


Figure 3.1. Water level station locations during the Tampa Bay Oceanography Project. Venice Pier (E-858) is about 50 km south of the entrance to Tampa Bay.

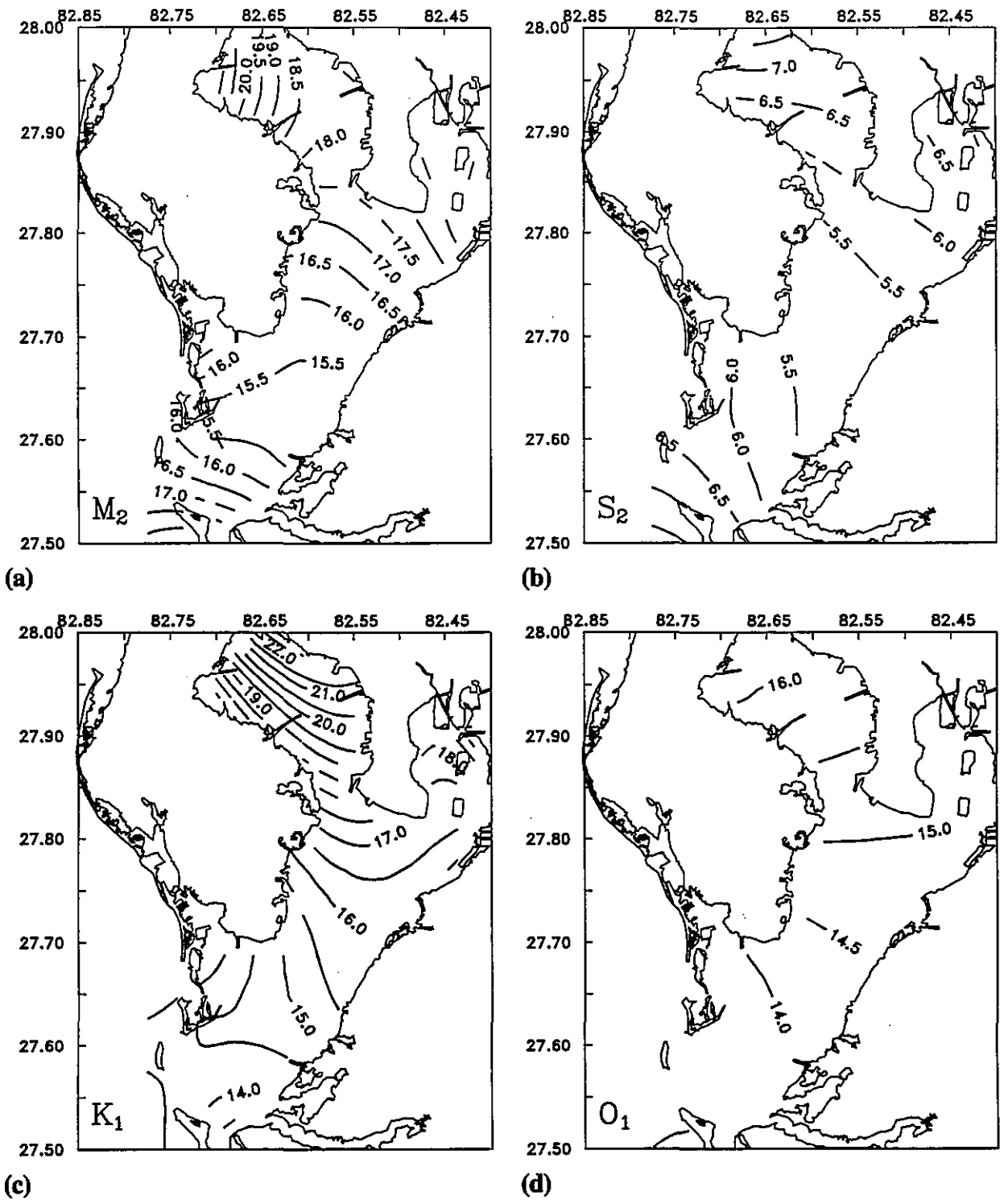


Figure 3.2. Amplitude (cm) of the tidal constituents (a)  $M_2$ , (b)  $S_2$ , (c)  $K_1$ , and (d)  $O_1$ . Contour interval is 0.5 cm.

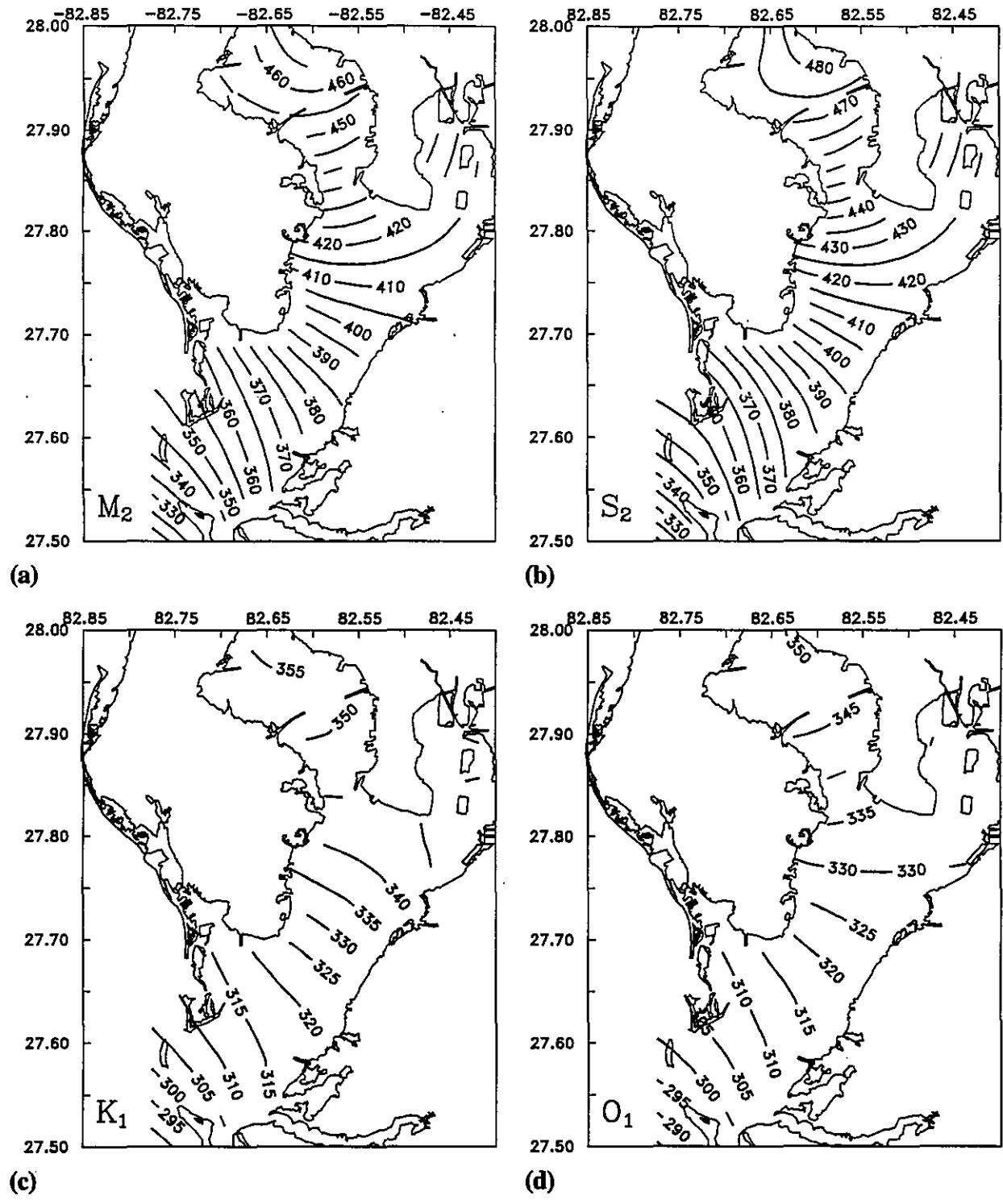


Figure 3.3. Epoch (degrees) of the tidal constituents (a)  $M_2$ , (b)  $S_2$ , (c)  $K_1$ , and (d)  $O_1$ . Contour interval is 5 degrees.

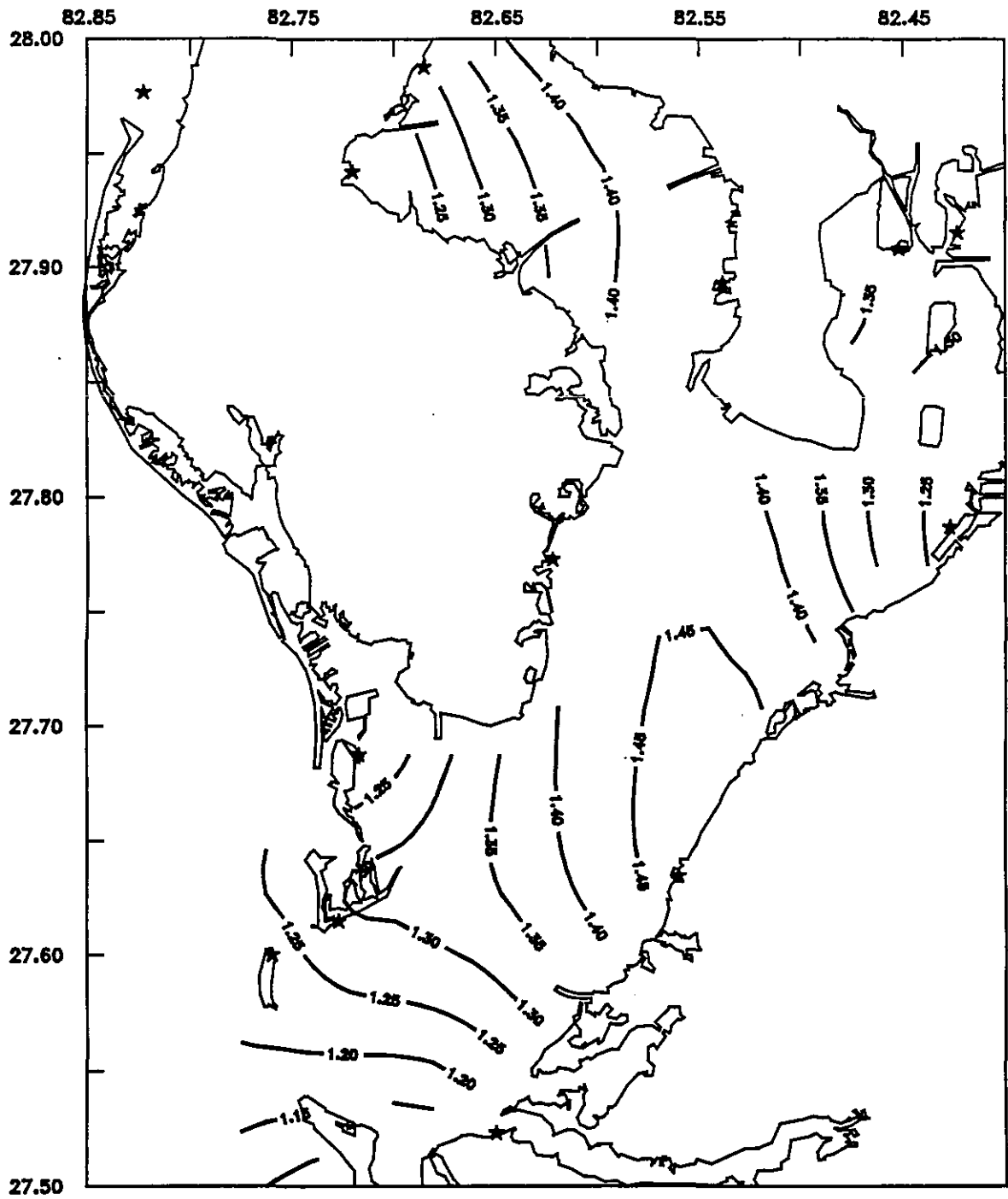
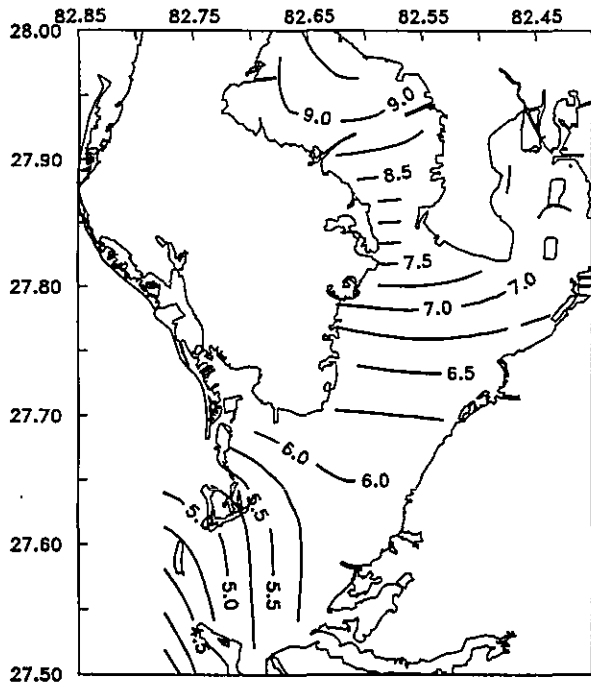
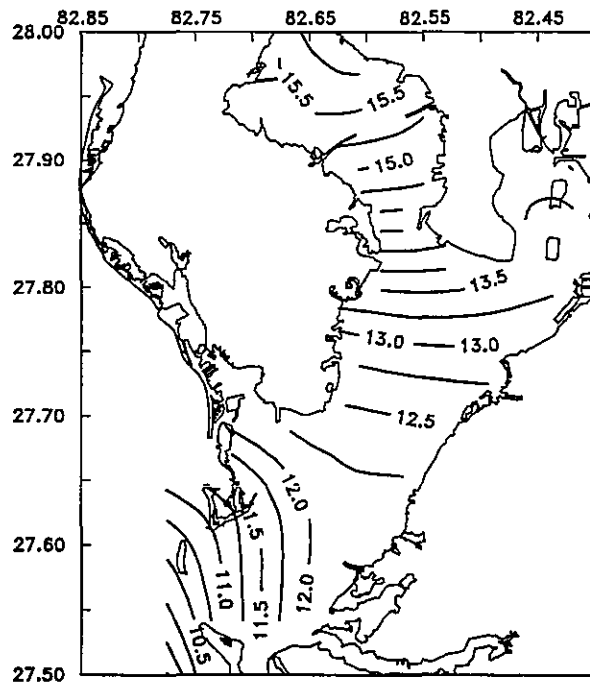


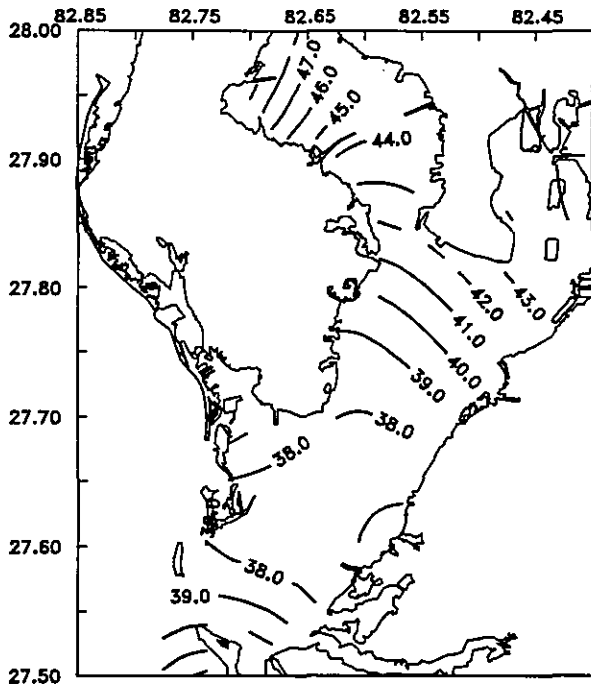
Figure 3.4. Tidal amplitude ratio  $(K_1 + O_1) / (M_2 + S_2)$ . Contour interval is 0.05. Tide stations are denoted by a star. Tampa Bay is classified as mixed, mainly semidiurnal since all of the ratios are between 0.25 and 1.5.



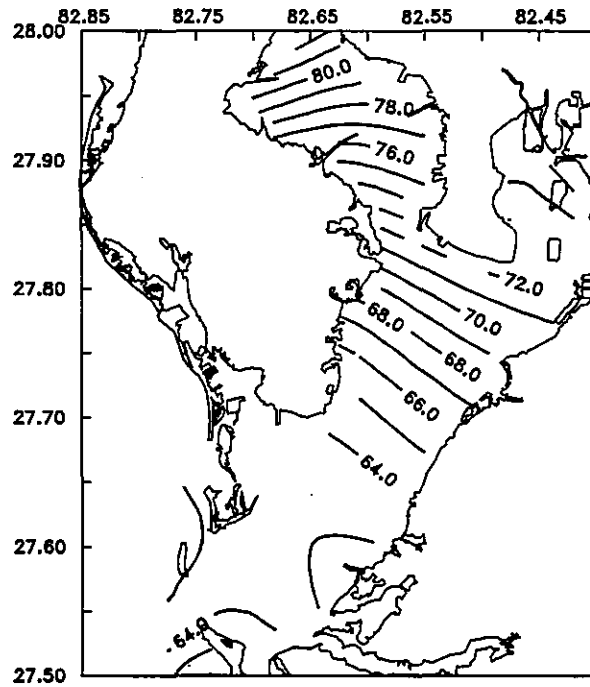
(a)



(b)

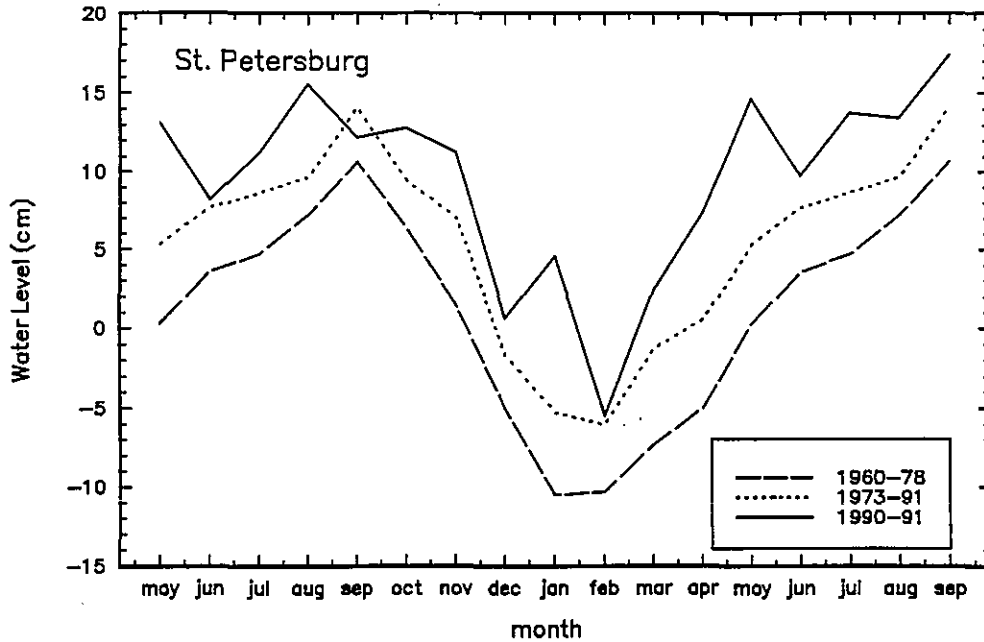


(c)

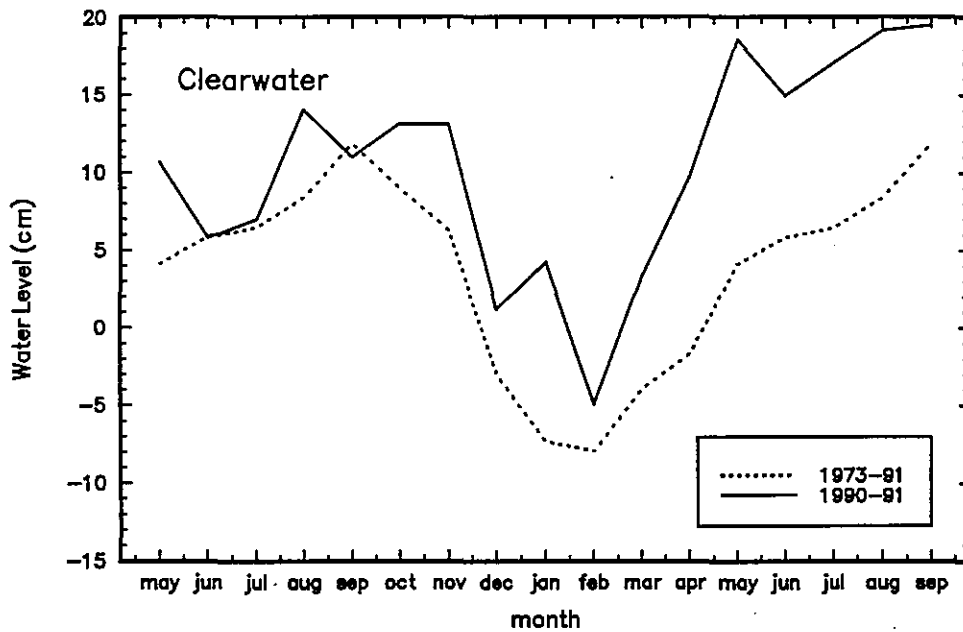


(d)

Figure 3.5. Greenwich intervals and ranges - (a) high water interval (hours), (b) low water interval (hours), (c) mean range (cm), and (d) great diurnal range (cm). Panels a & b have contour intervals of 0.25 hours, panels c & d have contour intervals of 1 cm.



(a)



(b)

Figure 3.6. Monthly mean sea level for (a) St. Petersburg and (b) Clearwater Beach. The solid line depicts the monthly mean values during TOP, the dotted line is the mean for 1973-1991, and the dashed line represents the mean for the 19-year Tidal Datum Epoch (1960-1978). All months during TOP except September 1990 show an increase in mean sea level over 1973-1991.

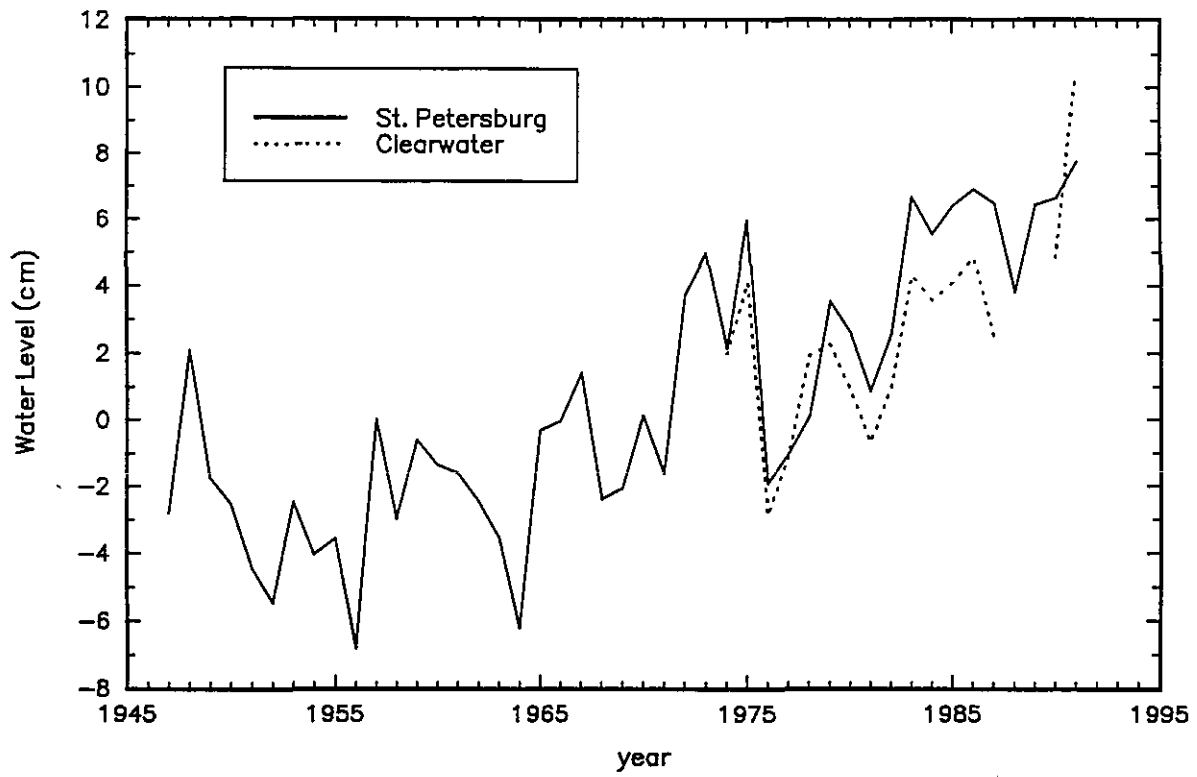
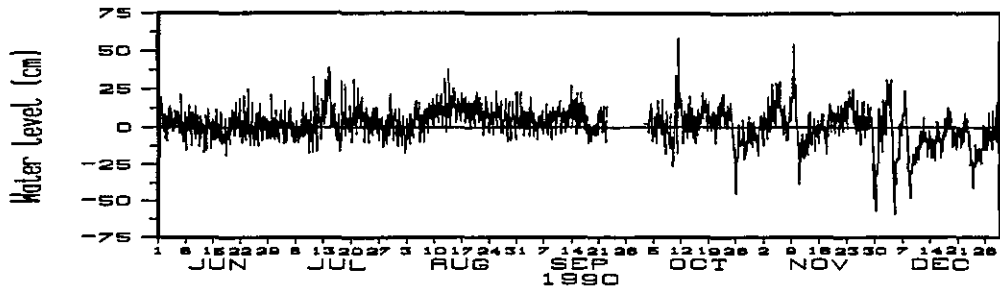
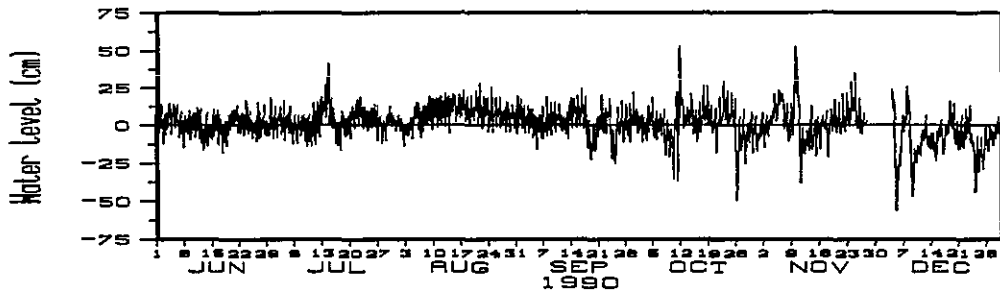


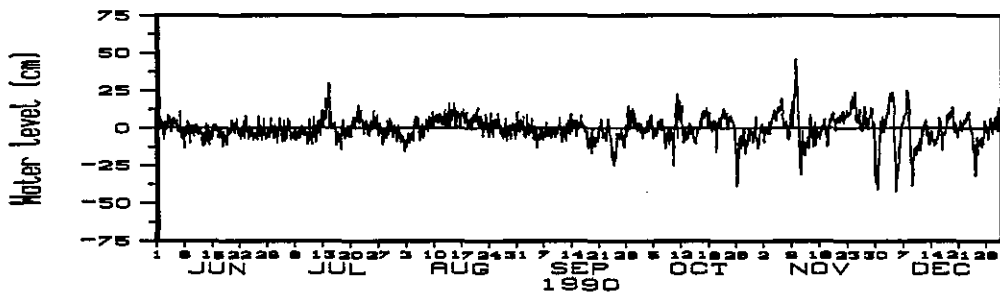
Figure 3.7. Annual mean sea level at St. Petersburg and Clearwater Beach. The general trend of sea level rise is 0.4 cm/year.



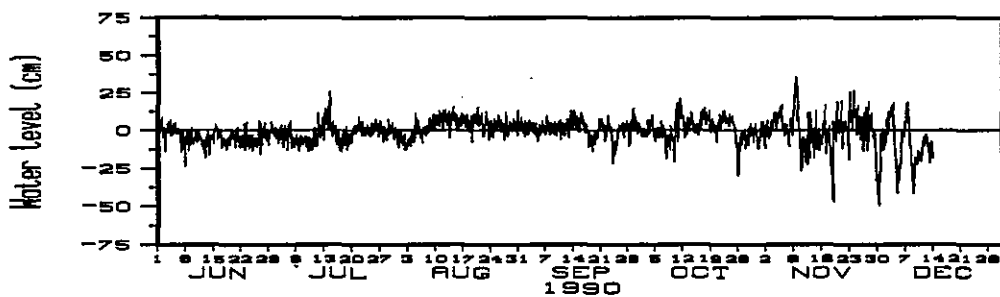
(a)



(b)



(c)



(d)

Figure 3.8. Residual water levels for (a) Bay Aristocrat Village (E-689), (b) Davis Island (E-657), (c) St. Petersburg (E-520), and (d) Egmont Key (E-347).

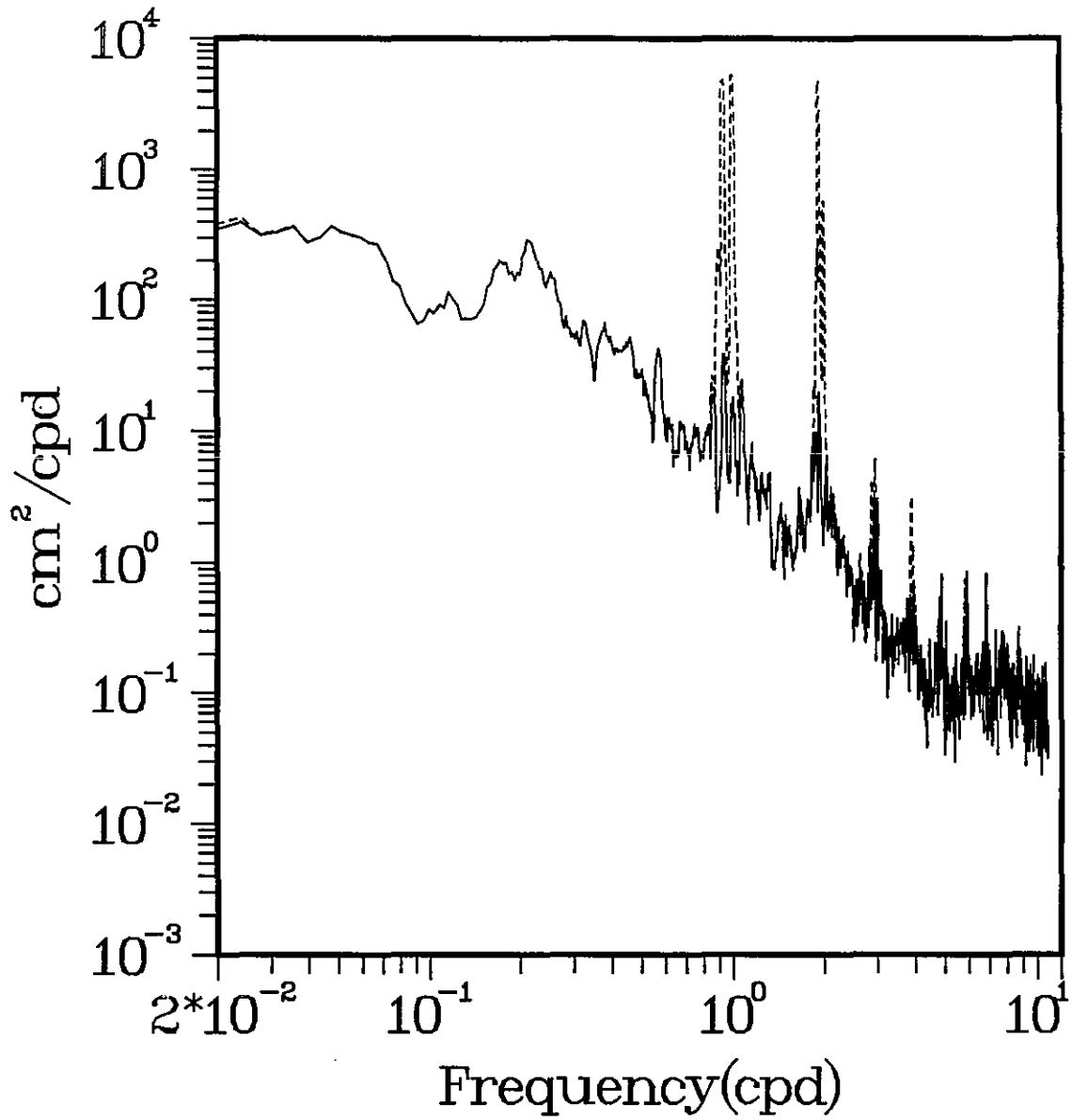
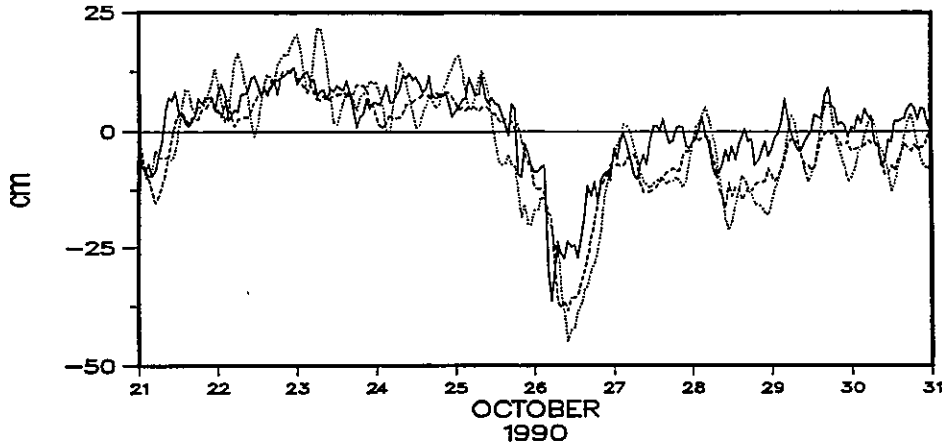
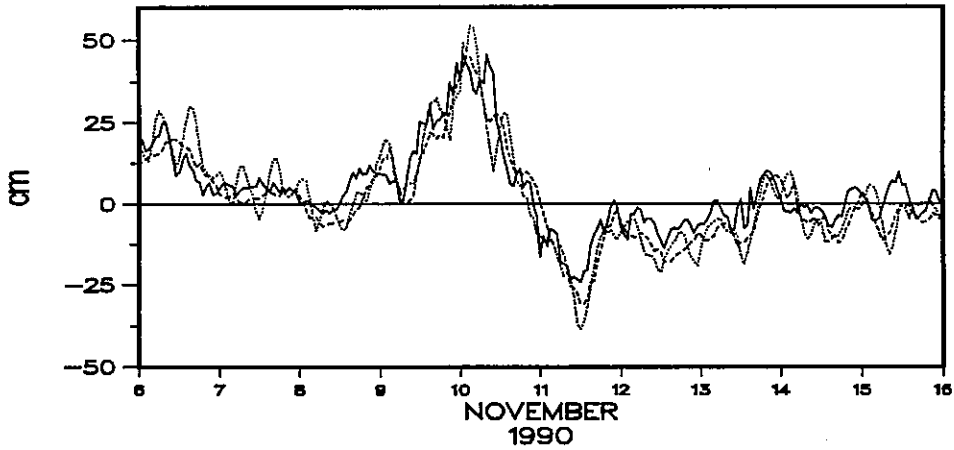


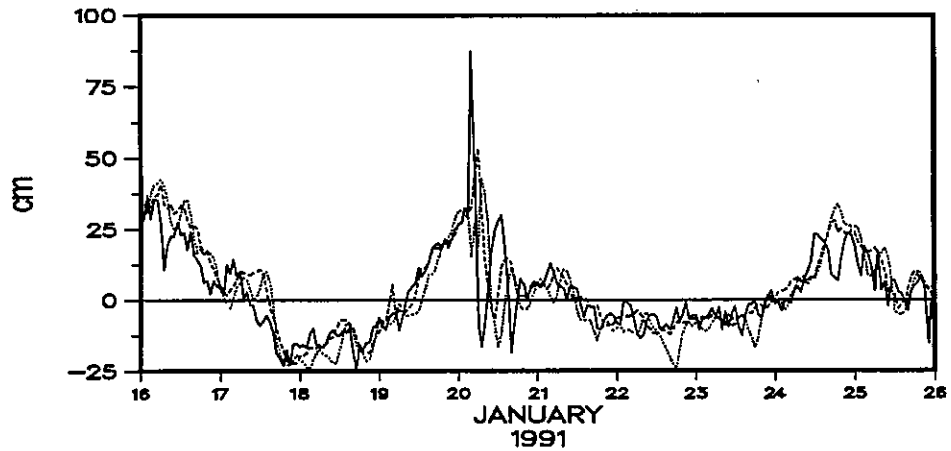
Figure 3.9. Observed (dashed) and residual (solid) spectra of water level at St. Petersburg (E- 520) during May 1 - December 31, 1990. The bandwidth is 0.004 cpd.



(a)



(b)



(c)

Figure 3.10. Residual water level values at Clearwater Beach (solid), St. Petersburg (dashed), and Bay Aristocrat Village (E-689) (dotted) during three storms. Clearwater Beach experienced a storm surge of almost 1 m during the January 19 - 21, 1991 storm.



## 4. METEOROLOGY AND HYDROLOGY

C. Reid Nichols, Kathryn T. Bosley, and Marc Grossman

### 4.1. INTRODUCTION

Wind and waterway discharge are the main forces behind nontidal circulation. Time series of meteorological data allow investigators to characterize the Tampa Bay climate and windfield while establishing relationships between winds and water circulation. Wind measurements are used to determine surface wind stress, wind-induced water level set-up, and current shear. Waterway discharge enhances estuarine circulation by establishing horizontal density gradients. Accurate representations of the wind field and riverine discharge are essential inputs for coastal circulation models.

Meteorological data in support of TOP were collected from five weather stations deployed from the mouth to the upper reaches of Tampa Bay (Figure 4.1). Measurement parameters include wind speed and direction, air temperature, and barometric pressure. Additionally, relative humidity and solar radiation were measured at M-2 as part of the Tampa Bay Physical Oceanographic Real-Time System (PORTS) and were provided to the National Weather Service (Hess, 1992b). Meteorological data collected from December 1989 through June 1991 at Tampa International Airport (TPA) were obtained from NOAA's National Climatic Data Center (NCDC).

The Tampa Bay watershed, which includes rivers, tidal creeks, mangrove swamps, marshes, canals, springs, and streams, encompasses an area of approximately 5000 km<sup>2</sup> (Clark and MacAuley, 1989). Hydrological data from the main rivers were available from the U.S. Geological Survey (USGS) at eleven waterway discharge stations (Figure 4.2).

Following a brief discussion of average climatic conditions in the Tampa Bay area, this section will highlight the spatial and temporal characteristics of the windfield over the Bay. Next a description of the hydrology of the Bay is presented. Both of these sections are intended to characterize the winds and hydrology of Tampa Bay with an emphasis on their importance in driving nontidal circulation.

### 4.2. LOCAL CLIMATE

The west coast of Florida has a subtropical climate that is affected by close proximity to the Gulf of Mexico and by weather phenomena such as sea breezes and frequent thunderstorms. Winds are generally from the northeast quadrant with the average wind speed in the Tampa Bay area of approximately 3.4 m/s. Synoptic scale ( $10^4$  to  $10^7$  m) winds are light and variable. Table 4.1 lists monthly prevailing wind directions, based on data collected since 1963 (NOAA, 1991). By meteorological convention, wind direction is the direction from which the wind is blowing. Gusts above 16 m/s tend to occur during the summer and result from thunderstorms, tropical storms, and hurricanes. Thunderstorms and squall lines are small scale phenomena occurring

about 90 days out of the year, generally during the late afternoons from June through September (Wooten, 1982). The average total annual precipitation since 1890 is 1.23 m, occurring primarily during the thunderstorm season. Summers are hot and humid while winters are mild due to dominating warm and moist maritime air masses. The average annual air temperature is 22.2°C and has ranged from -7.8°C in December, 1962, to 37.2°C in June, 1985 (NOAA, 1991). The monthly average barometric pressure fluctuates around the annual mean of 1017.6 (Table 4.1).

**Table 4.1. Monthly prevailing wind direction and mean barometric pressure based on data collected since 1963 at TPA (NOAA, 1991). Wind direction is from the indicated direction and pressure is in millibars.**

Month	Direction	Pressure	Month	Direction	Pressure
January	N	1020.1	July	E	1017.7
February	E	1019.2	August	ENE	1016.9
March	S	1017.9	September	ENE	1015.4
April	ENE	1016.8	October	NNE	1016.7
May	E	1015.7	November	NNE	1018.3
June	E	1016.3	December	N	1020.2

Storm systems which pass through the Tampa Bay area present a variety of meteorological signals (Figure 4.3). On October 10 and 11, 1990 (Julian dates 283-284), tropical storm Marco traversed the Gulf of Mexico. Due to its large scale, this storm caused a large pressure signal at mid Bay (M-2) and the airport (TPA); however, because of its warm, tropical nature there was no noticeable temperature signal at either station. The passage of a cold front a few days later, however, is clearly evident in the temperature records of both stations. Fluctuation patterns are quite similar between the two sites, indicating a high degree of spatial uniformity in Tampa Bay.

### 4.3. WINDFIELD CHARACTERISTICS

#### Data Collection and Analysis

Weather stations (Coastal Climate WeatherPaks) were deployed at various locations (Figure 4.1) and elevations throughout the Tampa Bay study area (Nowadly, 1992). M-1 (elevation 8.2 m) was located near Egmont Key and M-2 (elevation 17.4 m), part of the Tampa Bay PORTS, was located on the lower C-cut range marker. M-3 (elevation 19.5 m) was located just south of Gadsden Point, M-4 (elevation 15.2 m) was located in upper Hillsborough Bay, and M-5 (elevation 5.5 m) was located on the USGS platform in Old Tampa Bay north of the Howard Frankland Bridge. The Tampa International Airport (TPA) station (elevation 6.7 m) is located just north of the Courtney Campbell Parkway. To compare the six meteorological data sets,

the winds were extrapolated to a common level of 10 m using the power-profile law (Arya, 1988).

$$\frac{U}{U_r} = \left( \frac{z}{h} \right)^m \quad (4.1)$$

where

- U = measured wind speed,
- U<sub>r</sub> = wind speed at 10 m reference height,
- z = height of anemometer,
- h = 10 m height, and
- m = momentum flux constant of 0.15

None of the five TOP meteorological stations were occupied continuously during the survey. The deployment lengths of the stations are shown in Table A.3 in Appendix A. Several of the stations returned data in November 1990 and April 1991; therefore, these months are used in the discussions of spatial coherency of the windfield.

### **Spatial Variability**

Winds are caused by pressure gradients that develop in response to unequal heating of the earth's surface. Generally, synoptic scale overland and overwater winds result from semipermanent or seasonal pressure gradients. Local or mesoscale (10<sup>2</sup> to 10<sup>4</sup> m) winds may be caused by topography or differences in surface composition. Consequently, winds fluctuating at time scales on the order of several days are expected to be similar at each of the TOP stations while 10-min records are expected to show the highest variability. Descriptive statistics were computed for each station. Prevailing wind conditions are represented by vector-averaged quantities from 10-min data at M-1 through M-5 and hourly data from TPA (Table 4.2).

In general, meteorological sites located on the open bay recorded wind speeds which are up to twice as fast as measurements taken at TPA. Wind speeds increase with increasing distance from the upper Bay toward the Bay's mouth. Speed and direction at M-2 were closely correlated with speed and direction values from site M-1 when their deployment periods overlapped. Vector-averaged winds were easterly from September through January and southerly during the spring months.

November 1990 was the first period when simultaneous data from several sites were available for comparison. Wind speeds and directions are consistent from station to station during this period (Figure 4.4). To take advantage of the continuous time series of wind data available at TPA, it is necessary to establish how well TPA represents winds over the Bay.

**Table 4.2. TOP meteorological station winds. Speed and direction values from five sites and TPA were converted to 10-m east and north components for vector averaging. Vector-averaged speed and direction are provided for each month at each station. Shaded regions indicate that data were not available for analysis.**

Year	M-1		M-2		M-3		M-4		M-5		TPA	
	spd (m/s)	dir (°T)										
July 1990			0.5	343							0.1	101
August			0.5	223							0.3	219
September			2.4	67							1.5	57
October			3.2	54							2.0	50
November	2.7	40	3.2	53			2.2	44			1.6	35
December	1.9	75	2.0	78			1.5	81			1.3	81
Jan. 1991	1.7	93	1.5	91							1.1	76
February	1.4	73	2.3	73			1.2	316			1.0	8
March	1.2	200	1.2	203			1.2	240	1.7	208	1.0	204
April	2.0	159	1.1	138			2.0	117	2.2	114	0.9	129
May	2.8	130			1.6	127					1.7	109
June	0.8	39			0.7	78	0.6	55			0.3	6
July	1.8	235			1.8	198	1.4	206				
August	0.7	237			0.9	182						
September	2.6	79			2.6	64						

The results of rotary cross spectral analysis show a high degree of spatial coherence for synoptic scale winds (Figure 4.5). A comparison of winds at TPA and M-1 reveals that the signals are very coherent for periods greater than one day. The wind speeds at TPA are approximately 60% of those observed at M-1.

Mid-April through May 1991 meteorological data depict a typical springtime weather pattern. Wind records were low-pass filtered at 36 hours to illustrate that winds lasting on the order of days affect the entire Tampa Bay area. Such synoptic scale winds have length scales that are large compared to the study area. The 36-hour, low-pass-filtered winds at M-1, M-3, and TPA are strikingly similar (Figure 4.6). Higher magnitude winds occur at M-1, the closest weather station to the Gulf of Mexico, yet the direction and relative strength of individual events is common to all the series. In general, the winds recorded at Tampa International Airport provide a good representation of the long-period (>36 hours) windfield over Tampa Bay.

## Temporal Variability

Winds over Tampa Bay are usually light and variable. Sporadic stronger wind events are caused by thunderstorms and synoptic scale storms. Rotary spectral analysis of the TPA winds shows significant energy in the diurnal and semidiurnal bands (1 cpd and 2 cpd) and at synoptic time scales (less than 0.5 cpd) (Figure 4.7a and b). The clockwise component is generally larger than the counterclockwise component. The daily sea breeze and thunderstorms account for much of the diurnal energy, while the energy at 12 hours is likely to be a higher harmonic of the 24-hour peak. Thunderstorms are more prevalent during the summer, hence the diurnal band contains more energy in July/August than in November/December. The high, clockwise, synoptic-period energy level in the winter spectra is due to the passage of large-scale storms, which rarely occur in the summertime.

The land and sea breeze system brings a cooling breeze from the sea during late afternoon and a breeze from land during the remainder of the day. If the land cannot cool below the ocean temperature, the land breeze may be missing or poorly developed. In Florida, sea breezes can focus convection and lead to intense thunderstorm activity (Pielke, 1974). The convergence of sea breezes from the Atlantic and Gulf Coasts contribute in part to Florida's summertime precipitation maximum. When the sea breeze is well developed, it can be observed along the coast from Old Tampa Bay to Sarasota, Florida (Young and Winchester, 1980). The late spring and summer months have pronounced sea breeze circulation due to large overland and overwater heating differentials.

Sea breeze circulation was well developed during the early part of May 1991. In the spring, the land warms more quickly than the water; so, the air temperature gradient between the air masses overlying the two is intensified. The air temperature difference between land and water changes sign daily as the land warms and cools (Figure 4.8a). A land breeze dominates the spring windfield, although there were several hours of sea breeze late each afternoon (Figure 4.8b).

In Section 3.3, three storm events that had significant effects on the water levels in Tampa Bay and the nearby Gulf Coast were discussed (Figure 3.10). The wind vector plots from the same three time periods are shown in Figure 4.9. There is a clear connection between the wind direction and the rise or fall of sea level. When there were strong winds from the north on October 25-26, 1990 (Figure 4.9a), water levels fell below normal at all stations. From November 9 to November 11, the wind direction rotated nearly 360° (see Figures 4.4 and 4.9b). Water levels were higher than normal when the wind had a component from the south and were lower than normal when the wind had a component from the north. The same relationship holds for the January 16 - 26, 1991, time period (Figure 4.9c). However, the sharp storm surge that occurred on January 20 was associated with strong cross-shore winds when there was a sudden doubling of wind strength, rapid clockwise rotation, and an abrupt decrease in wind strength over a 4-hour period. This short-term phenomenon had a greater effect on the coast than in Tampa Bay and was associated with a powerful thunderstorm.

In general, the windfield over Tampa Bay exhibits significant temporal variability. The time scale of wind variability ranges from minutes to days. Thunderstorms and sea breezes

concentrate energy at the diurnal period, while synoptic scale storms are associated with 2- to 10-day variations in the windfield.

#### **4.4. RAINFALL AND WATERWAY DISCHARGE ANALYSIS**

River discharge and precipitation are two principle sources of freshwater into Tampa Bay. Through their role in establishing density gradients, these freshwater inputs have an effect on the long-term residual flow within the Bay. Rainfall data from NOAA's National Climatic Data Center (NCDC) and river discharge data compiled by the United States Geological Survey (USGS) were analyzed to establish the nature of the mean annual signal and to highlight the deviation of the TOP study period from the normal climatic conditions in Tampa Bay. Precipitation and runoff data will also be used as inputs to the TOP numerical circulation model.

##### **Data Sources and Processing**

Rainfall data were acquired from NCDC for eight stations in the Tampa Bay watershed. Of these eight stations, five are located along the periphery of the watershed and three are in close proximity to the Bay's shoreline. The five remote stations are Tarpon Springs, St. Leo, Hillsborough, Bradenton, and Fort Green; the three stations located near the Bay are St. Petersburg, TPA, and Parrish. Daily values of precipitation were totaled for each month during the TOP survey period (May 1990 through September 1991) and compared to the 100-year (1890-1989) mean of monthly total rainfall observed at TPA. These data were also obtained from the NCDC.

Discharge data were acquired from the USGS and the Southwest Florida Water Management District (SWFWMD) for ten of the largest Tampa Bay waterways. Discharge gage locations for the ten waterways are displayed in Figure 4.2. The USGS provided daily average discharge data for Hillsborough River, Sulphur Springs, Alafia River, Little Manatee River, Manatee River, Braden River, Rocky Creek, Sweetwater Creek, and Bullfrog Creek. The SWFWMD furnished daily average elevations during the TOP study period for the Hillsborough River at a site upstream from the Tampa Bypass Canal. SWFWMD also provided a formula from which daily average elevations at the Tampa Bypass Canal could be converted to daily average discharges. Daily values of discharge were averaged for each month during the TOP survey period. The long-term averages of discharge were taken directly from USGS records. The length of historical records ranged from 22 years for the Hillsborough River to only 3 years for the Braden River.

##### **Rainfall Analysis**

One hundred years of precipitation data collected near the present site of TPA were used to provide historical perspective of the rainfall regime in the vicinity of Tampa Bay. The mean historical value of monthly total rainfall is presented as the open bars in Figure 4.10. Typically, nearly sixty percent of the annual total rainfall occurs between June and September, with the maximum occurring in August. Relatively little precipitation is observed in October through May; November is historically the driest month.

Values for total rainfall recorded during the 17 months of TOP reveal a strikingly different pattern than the historical average (hatched bars on Figure 4.10). The driest month during the survey was December 1990, while both Julys show very high precipitation. With the exception of July, the summer of 1990 was much drier than normal.

Significant spatial variability in rainfall is the result of the local sea-breeze/convection circulation pattern which dominates Tampa weather during the summer wet season (Flannery, 1989). Strong localized thunderstorms occur frequently in response to the convergence of moist Gulf air advected inshore by daytime sea breezes and convective currents resulting from heating over the land surface. For example, Tarpon Springs and Tampa Airport are located approximately 25 km apart; yet, in August of 1991, the former recorded 38.9 cm of rainfall while the latter received only 18.7 cm (Figure 4.11). The standard deviation of the eight August, 1991, precipitation records was 7.8 cm, about a mean of 20.3 cm, again indicating little spatial coherence. In contrast, the passage of large frontal systems dominates the winter weather of Tampa. These systems produce a pattern of rainfall with a greater degree of spatial coherency. The precipitation recorded in February, 1991 provides a good illustration of this pattern. Tarpon Springs received 2.2 cm of precipitation and TPA received 1 cm. The standard deviation in February was much lower than in August (0.8 cm about a mean of 2.3 cm), suggesting higher spatial coherence.

### **Waterway Discharge**

Eleven of the waterways which drain into Tampa Bay combine to produce a historical average annual mean discharge of nearly 35 m<sup>3</sup>/s (Table 4.3). Of these ten, the five largest waterways (Hillsborough, Alafia, Little Manatee, Tampa Bypass Canal and Manatee, respectively) contribute over 80% of the average monthly discharge. The historical mean monthly signal of discharge is similar to rainfall; nearly 55% of the total occurs between June and September (Figure 4.12). The winter dry season discharge maximum occurs in March, coincident with the winter rainfall maximum; however, during the summer, the discharge maximum occurs in September, lagging the rainfall maximum by about a month. The discharge values recorded during TOP vary significantly from the long-term mean. During May through August of 1991, the discharge into the Bay was on average 51% greater than normal, while for the rest of the study period, discharge was on average 45% less than normal.

In general, the rivers draining into Tampa Bay have similar seasonal discharge signals. All four of the largest rivers showed a significant discharge increase in July 1991 (Figure 4.13). The small waterways such as Rocky, Bullfrog and Sweetwater Creeks, and Tampa Bypass Canal all exhibited much smaller percentage increases during the summer of 1991.

Comparison between Figures 4.11 and 4.13 reveals little correspondence between monthly total rainfall and monthly mean discharge recorded during TOP. The amount of summer rainfall is similar during both summers, yet the discharge was much greater during the summer of 1991. Human factors including controlled withdrawal and impoundment combined with environmental factors such as previous rainfall, topography, and solar radiation confound the relationship.

**Table 4.3. Average monthly river discharge into Tampa Bay. The first five rivers listed account for over 80% of the total runoff. All averages were computed using 17 months of data: May - September.**

River	Historical Average (m <sup>3</sup> /s)	Averaging Period	Average for TOP (m <sup>3</sup> /s)	% Difference TOP to Historical
Hillsborough	8.69	1969-90	5.46	-37.2
Alafia	8.61	1969-90	5.72	-33.6
Little Manatee	4.51	1969-90	4.32	-4.2
Tampa Bypass	4.30	1975-90	2.56	-40.5
Manatee	2.09	1969-90	2.18	+4.3
Lake Tarpon	1.35	1975-90		
Braden	1.31	1988-90	1.41	+7.6
Bullfrog Creek	1.25	1977-90	1.39	+11.2
Rocky Creek	1.15	1969-90	1.22	+6.1
Sulphur Springs	1.05	1969-90	0.94	-10.5
Sweetwater Creek	0.61	1986-90	0.54	-11.5
Total	34.92		25.74	

#### 4.5. CONCLUSIONS

Winds over Tampa Bay are generally light and variable. Occasional strong winds are produced by thunderstorms and synoptic scale storms. A relatively high degree of spatial coherency is evident between stations. A well-developed sea breeze system exists in the spring and fall. During the winter, the passage of synoptic scale storms results in periods of high winds.

Over 60% of the annual rainfall and 55% of the discharge occur between June and September. June, August, and September of 1990 were dry compared with the historical average. Although the rainfall in the summer of 1990 was similar to that in the summer of 1991, the river discharge was considerably greater during the summer of 1991.

The relationship between meteorological forcing and the nontidal circulation of Tampa Bay is discussed in Section 6. Winds, particularly longshore winds associated with synoptic scale storms, drive significant residual circulation in the winter. River discharge establishes strong summer horizontal density gradients, which in turn forces long-term residual flow.

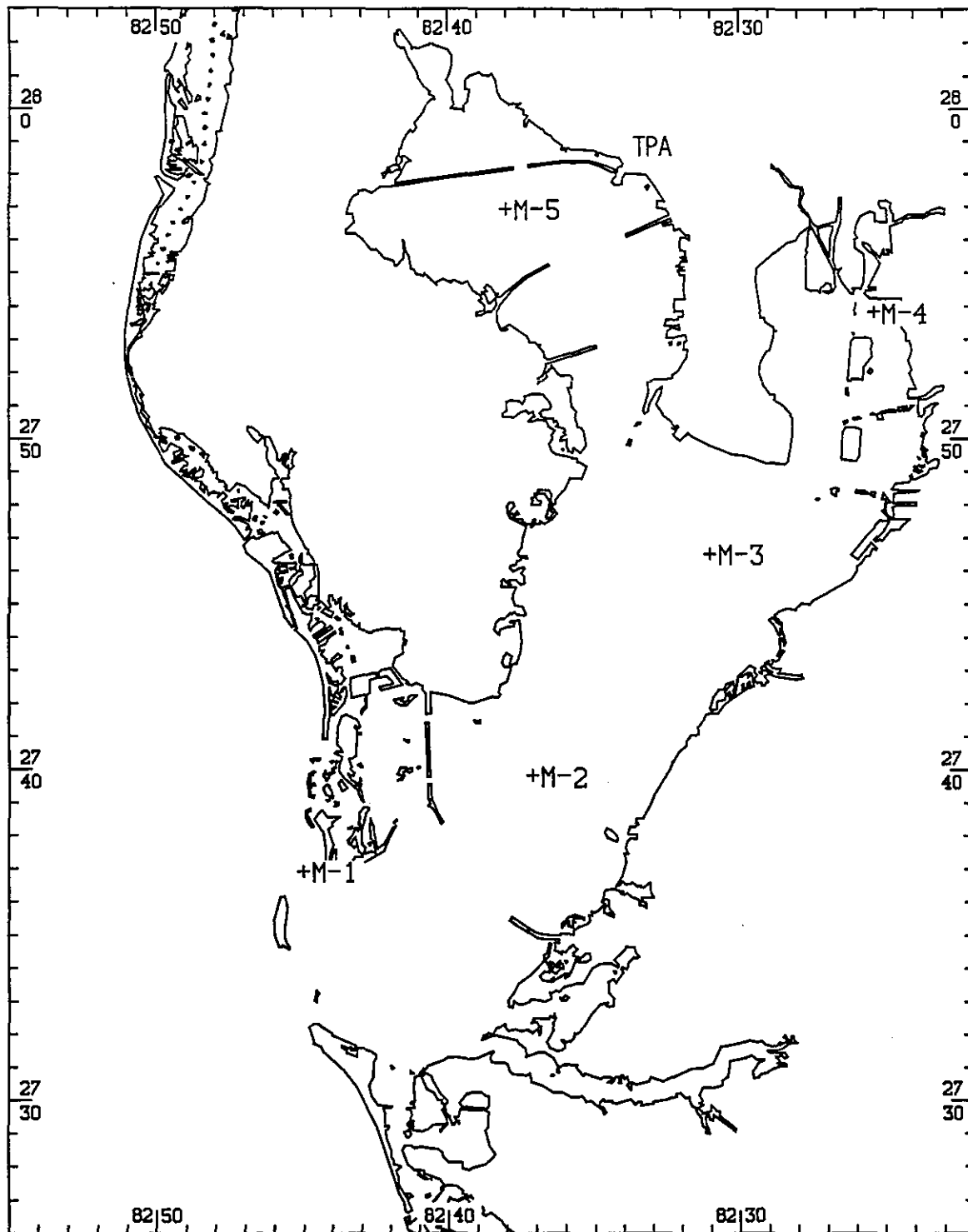


Figure 4.1. Meteorological station locations in Tampa Bay. M-2 is the PORTS location.

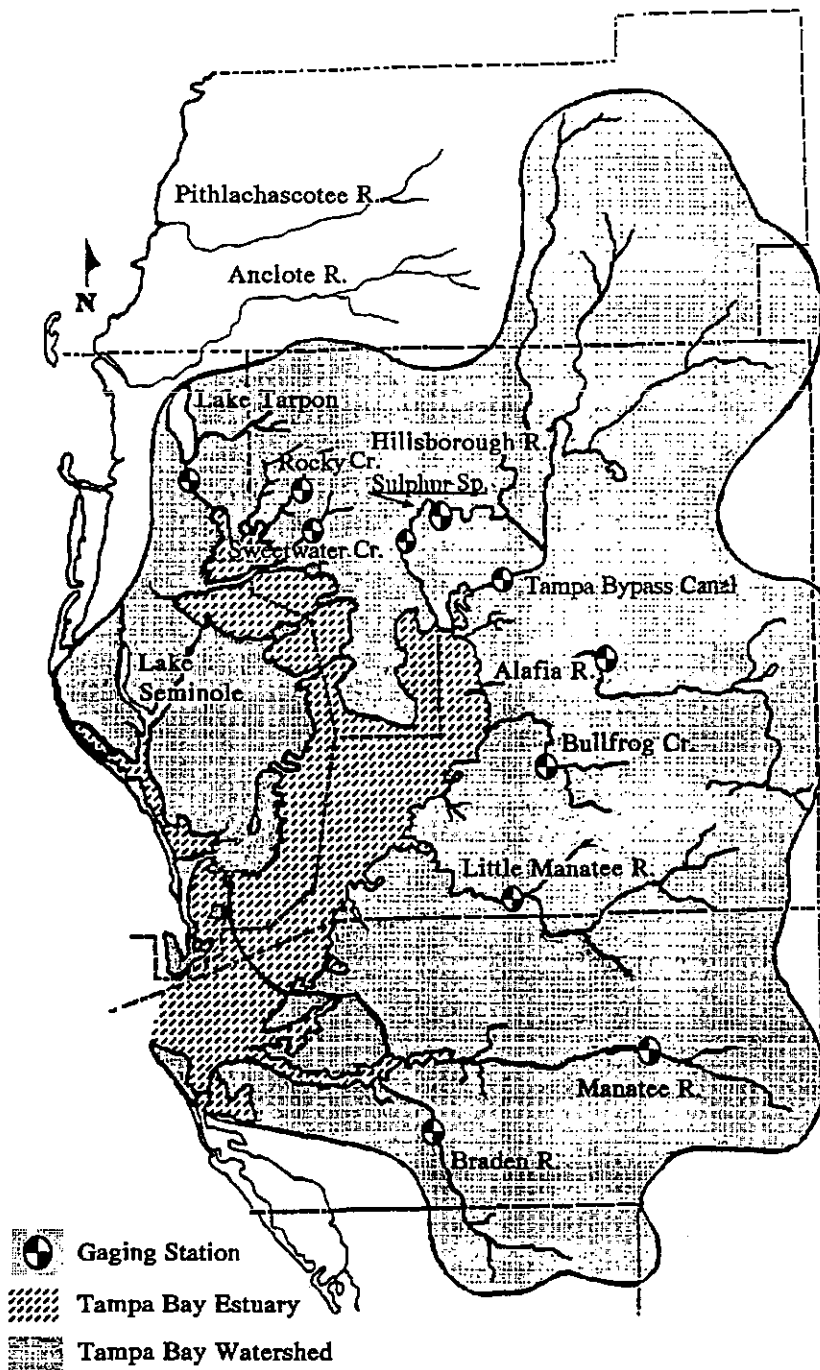


Figure 4.2. The Tampa Bay estuary and watershed (adapted from Clark and MacAuley, 1989). Selected USGS waterway discharge gaging stations are indicated by a .

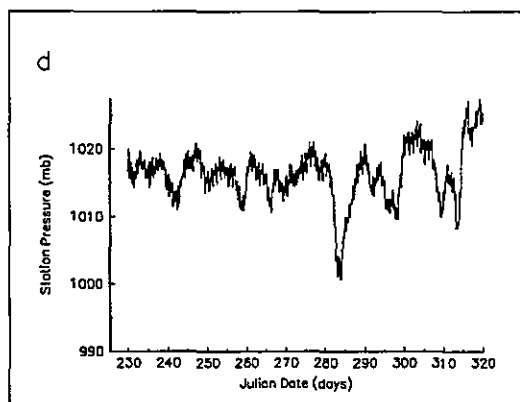
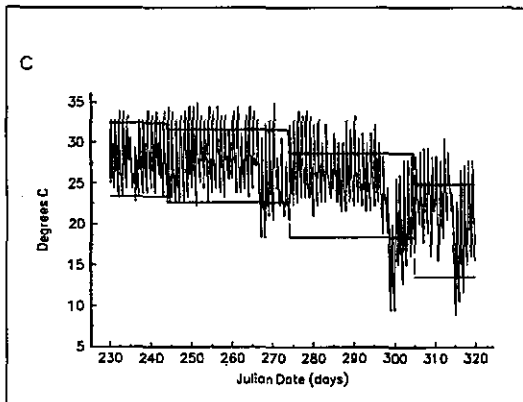
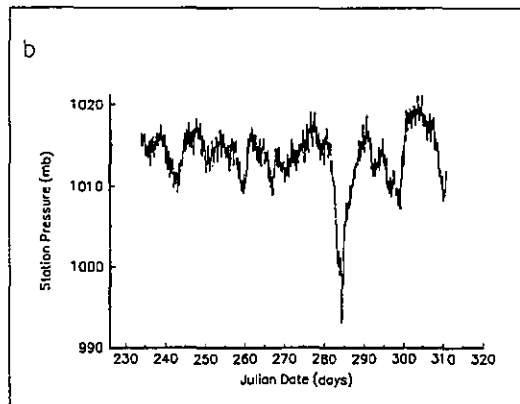
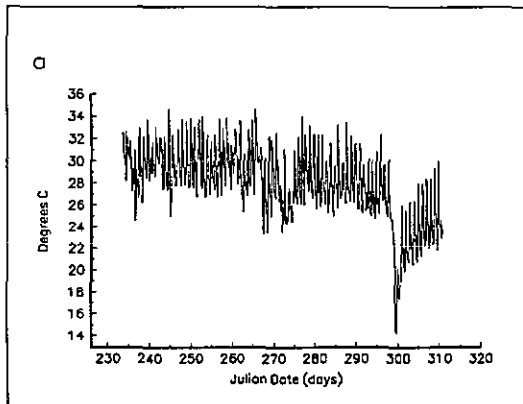


Figure 4.3. Air temperature and pressure from August 17 through November 16, 1990. (a) Hourly averaged temperature at M-2. (b) Hourly averaged barometric pressure at M-2. (c) Hourly averaged temperature at TPA. (d) Hourly averaged pressure at TPA.

# November 1990

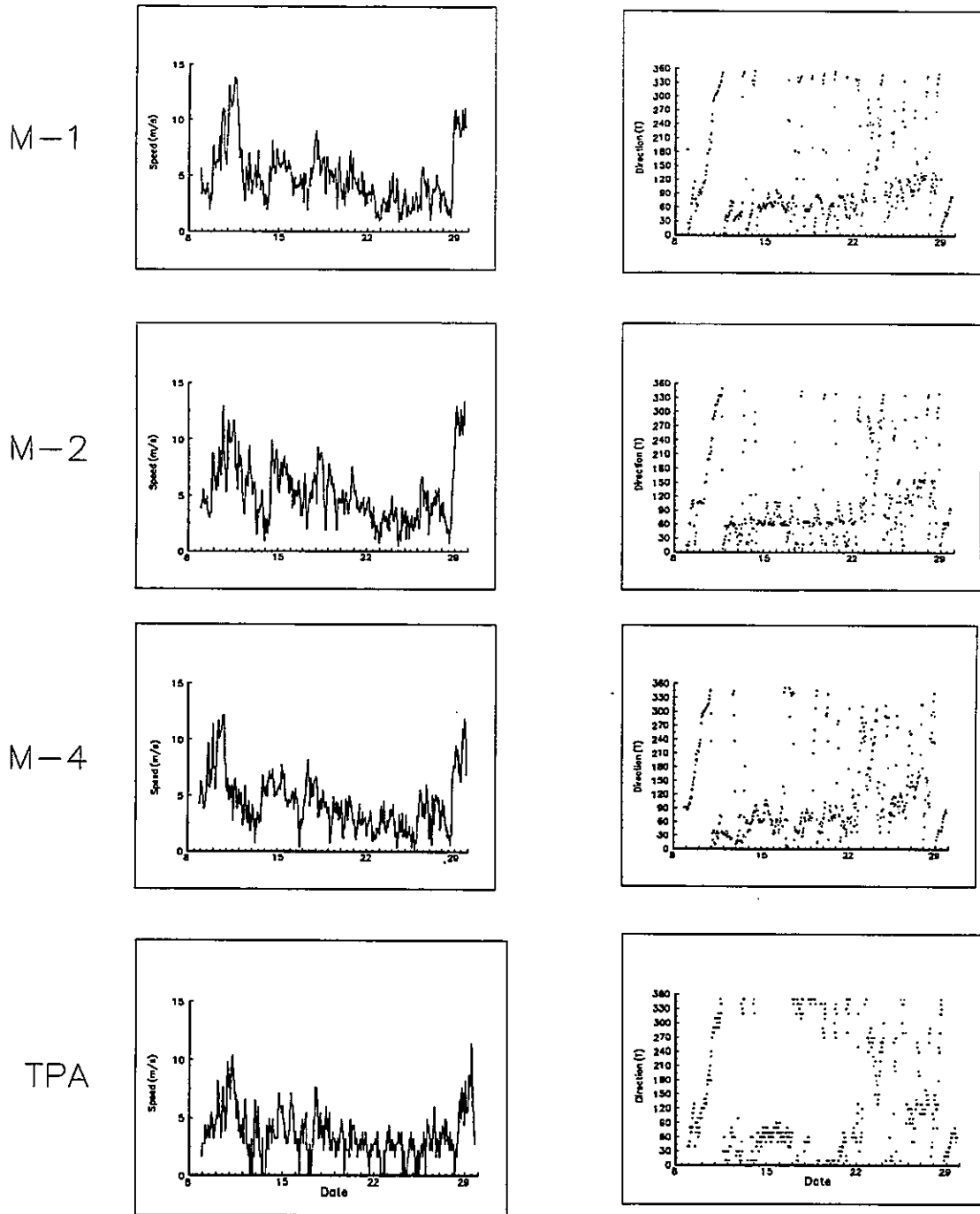


Figure 4.4. Tampa Bay winds during November 1990, wind patterns are similar at all of the stations, indicative of spatial coherence. Speeds increase with distance from TPA toward the Gulf of Mexico. In agreement with historical data, NNE is the prevailing wind direction.

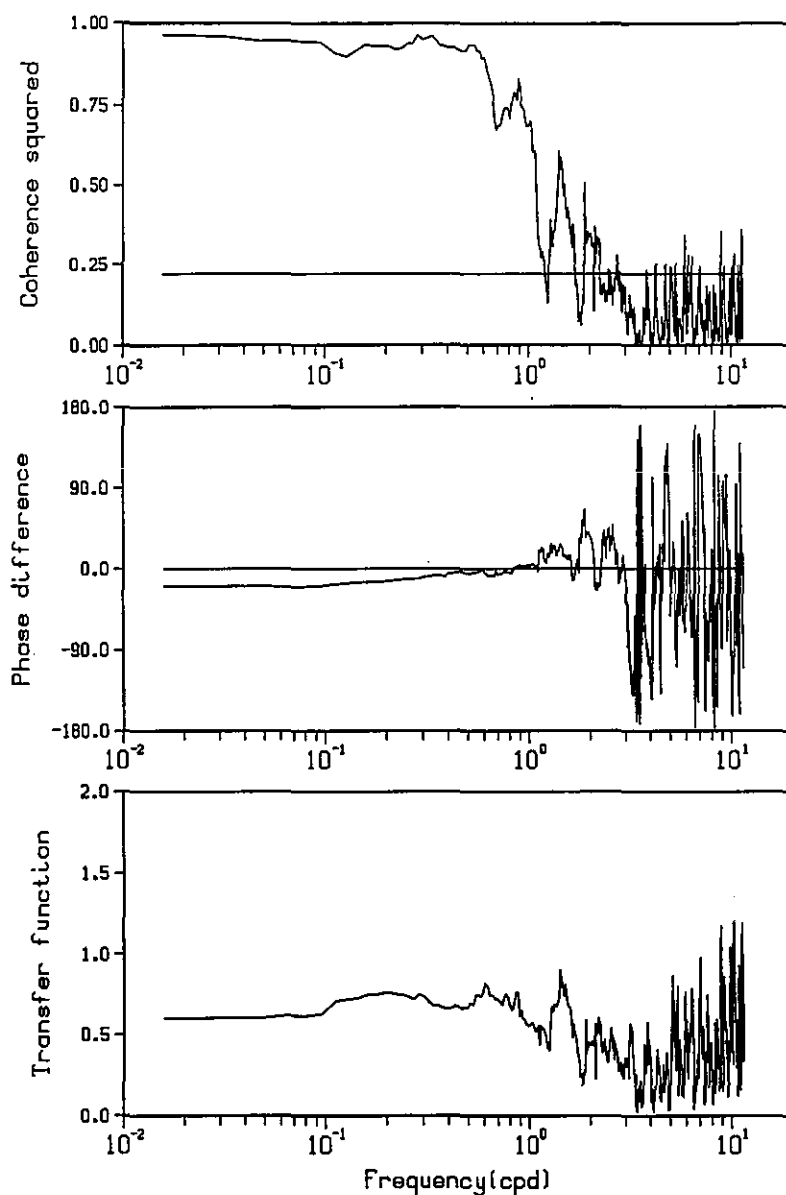


Figure 4.5. Results of rotary cross spectral analysis of winds over Tampa Bay. Fifty-nine days of wind observations (November 8, 1990 - January 6, 1991) at M-1 and TPA were compared. The spectra shown are the relationships between the clockwise component at each station. The coherence is high for winds with a period longer than 1 day. Wind speeds at TPA are approximately 60% of those at M-1. The analysis bandwidth is 0.017 cpd.

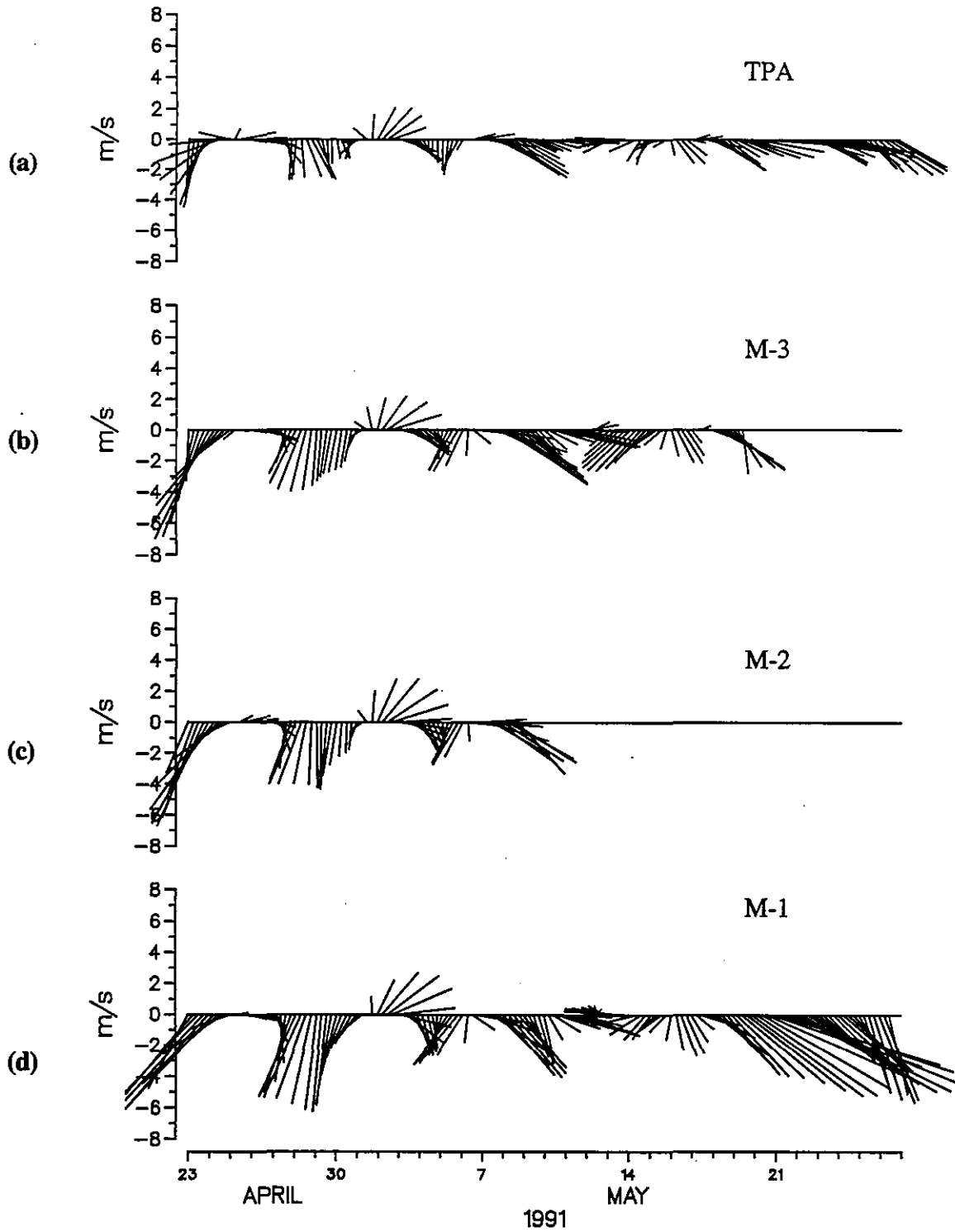
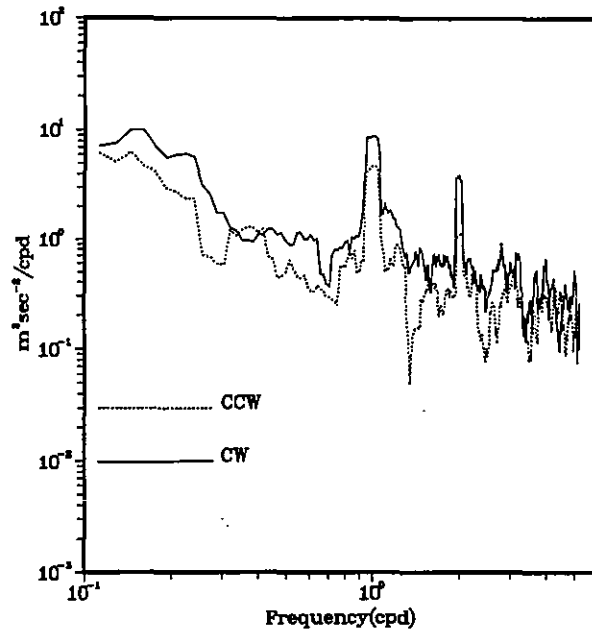
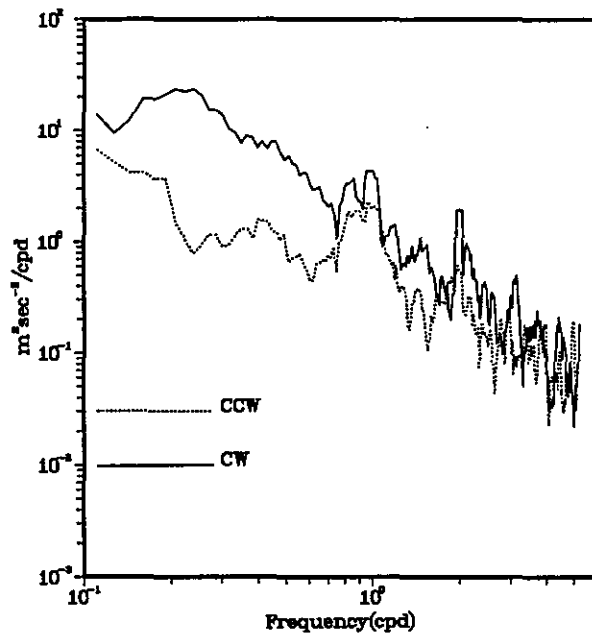


Figure 4.6. The 36-hour, low-pass-filtered wind field at (a) TPA, (b) M-3, (c) M-2, and (d) M-1. Similar synoptic scale events are evident in each series, although the magnitude of the events decreases with distance from the mouth of the Bay. The synoptic scale winds over the Bay are relatively spatially coherent. The wind is from the directions shown.



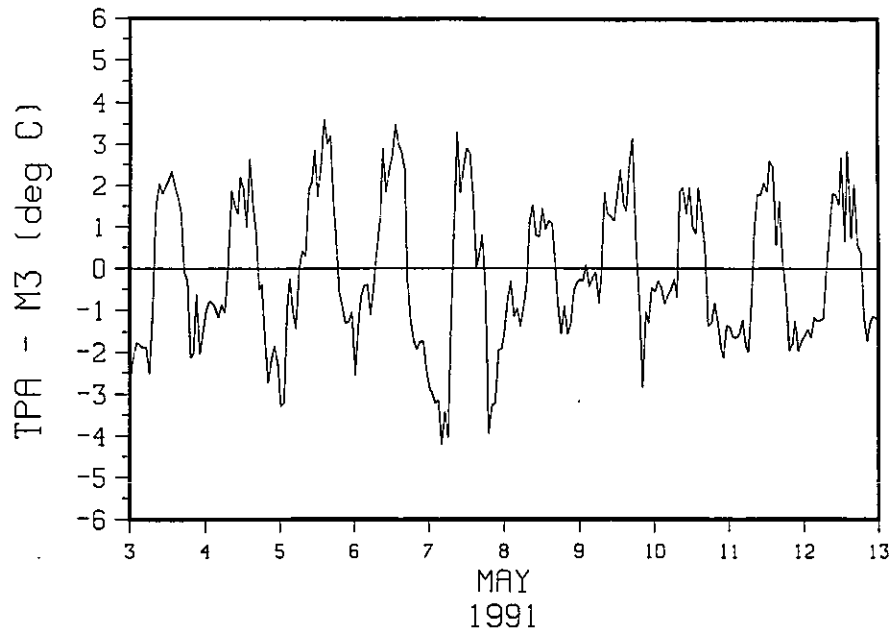
(a)



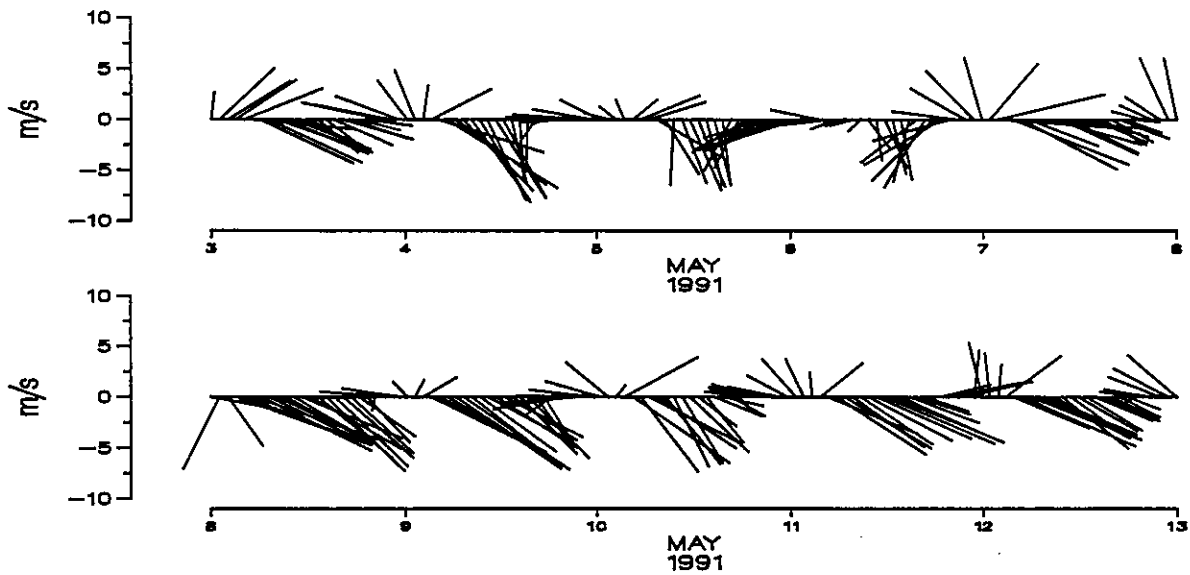
(b)

Figure 4.7. Rotary spectral analysis of the wind at TPA. The solid line indicates the energy in the clockwise component and the dotted line represents the counterclockwise component. Sixty days of data were analyzed for each spectra, the analysis bandwidth is 0.017 cpd.

(a) The spectra for July/August 1990 show a strong peak at 24 hours, with an overtone at 12 hours, as well as broad energy throughout the synoptic band. In contrast, (b) the synoptic band contains higher energy in the November/December 1990 spectra, with less diurnal and semidiurnal energy.



(a)



(b)

Figure 4.8. Sea breeze system over Tampa Bay. (a) The air temperature difference between TPA and station M-3. Negative values indicate the air over the Bay is warmer than the land. (b) Wind vectors at station M-1 (wind is from the direction shown). Both the land-sea air temperature gradient and the winds show a strong diurnal seabreeze pattern.

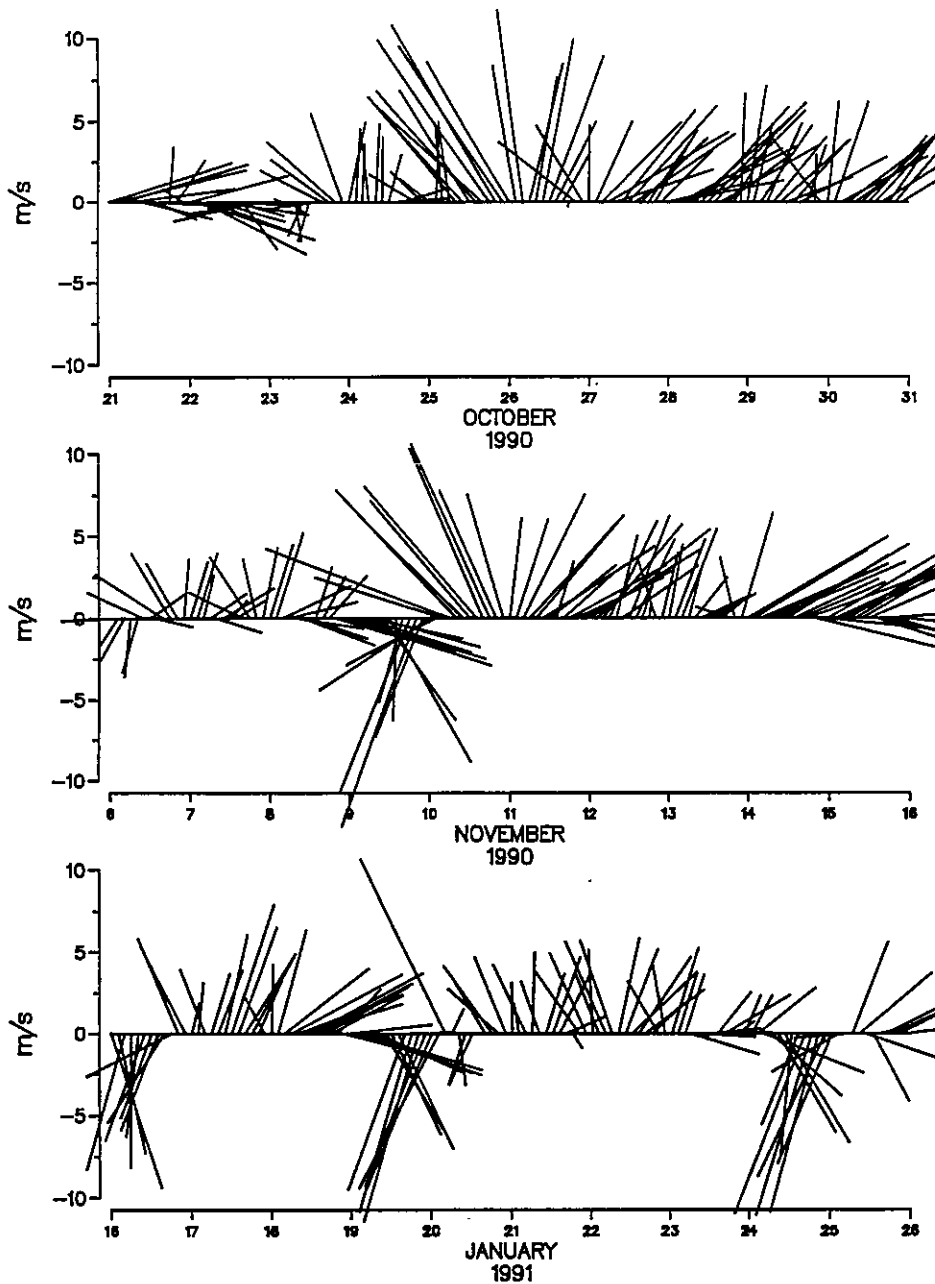


Figure 4.9. The wind vector pattern observed mid-Bay (M-2) during the passage of three separate storms. Water levels during these three storms are shown in Figure 3.10. The sticks show the direction from which the wind is blowing.

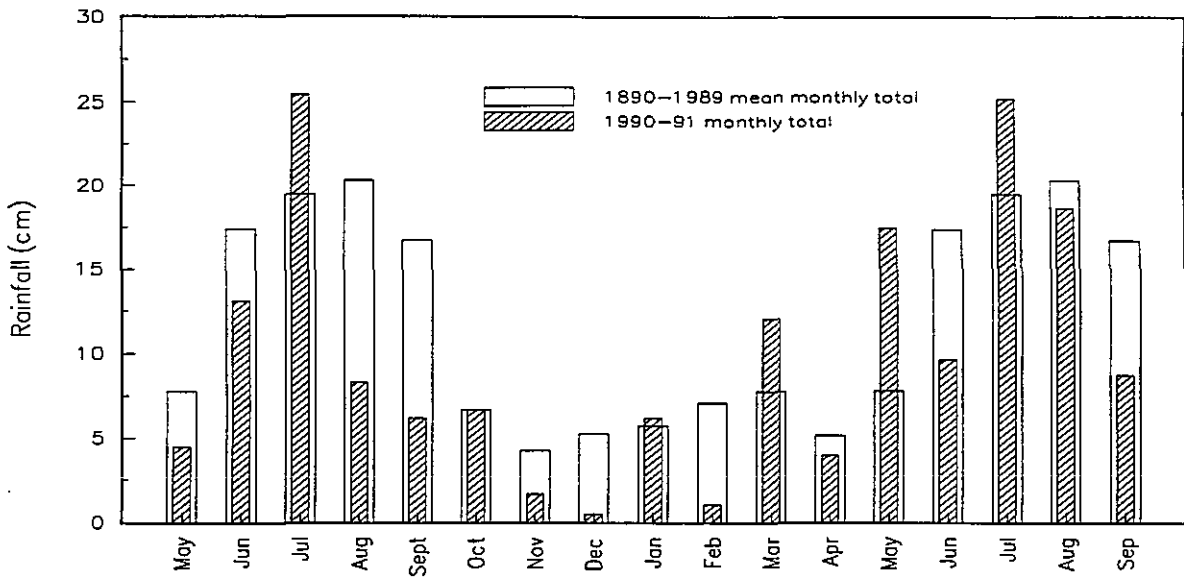


Figure 4.10. Monthly total rainfall observed at TPA. The open bars represent the historical record averaged for 100 years between 1890 and 1989. The hatched bars are the monthly total rainfall measured during TOP. Notice that although the general pattern of wet summers and dry winters is common to both observation periods, the rainfall recorded at TPA was significantly below the normal for many months during TOP.

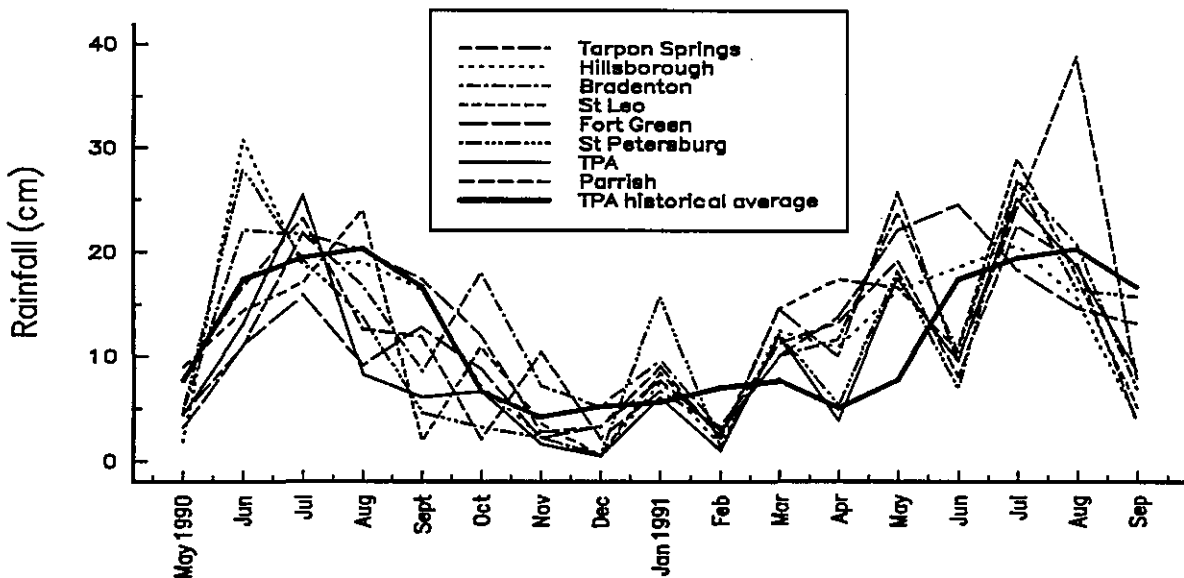


Figure 4.11. Monthly total rainfall at eight NCDC weather stations in the Tampa Bay watershed. The heavy solid line is the mean monthly total rainfall at TPA based on historical data (1890-1989). Although observations vary between stations, the general trend of wet summers and dry winters is evident.

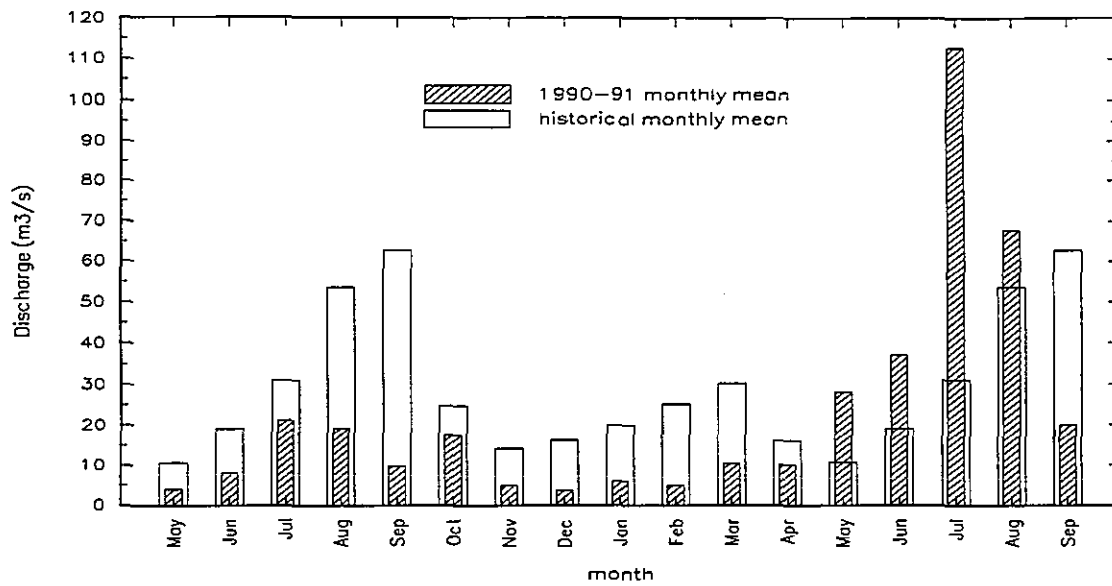


Figure 4.12. Mean monthly discharge for eleven rivers which drain into Tampa Bay. The open bars represent the historical monthly mean, while the hatched bars are the mean values observed during TOP. May, June, July, and August of 1991 show large positive departures from the mean discharge conditions.

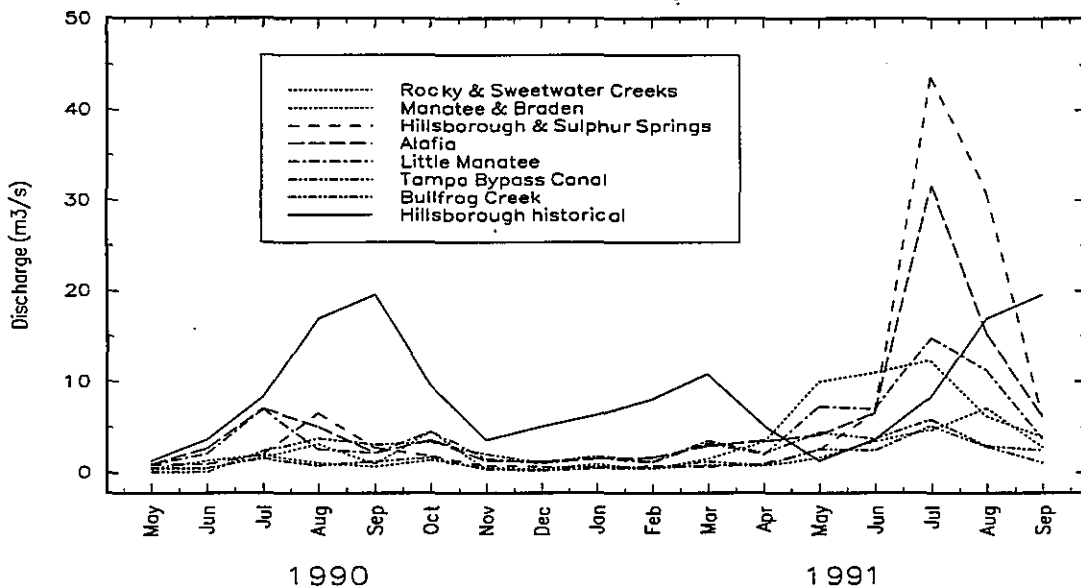


Figure 4.13. Mean monthly discharge for eleven Tampa Bay waterways. Three small waterways in the proximity of large rivers were combined with those rivers. The heavy solid line indicates the historical mean discharge for the Hillsborough River. The annual and interannual signals are similar for all the waterways.



## 5. WATER MASS CHARACTERISTICS

Kathryn T. Bosley and Richard W. Bourgerie

### 5.1. INTRODUCTION

#### Measurement Program

An extensive oceanographic survey comprised of both hydrographic cruises and the deployment of moored sensors was undertaken as part of TOP to provide water mass characterization. In addition to significantly increasing the knowledge of the physical oceanographic setting of Tampa Bay, analysis of hydrographic data is crucial to understanding the buoyancy forces driving nontidal circulation. Many of these measurements also serve as initialization, calibration, and validation values for the TOP numerical circulation model.

One component of the oceanographic survey consisted of five hydrographic cruises conducted from August 1990 to August 1991. These five seasonal cruises were performed in summer (August 1990 and 1991), fall (November 1990), winter (February/March 1991), and spring (May/June 1991). During these cruises, 684 individual conductivity-temperature-depth (CTD) casts were taken at stations along six transects (Figure 5.1). Transect 1 extended south-southeastward from just off Mullet Key across Egmont and Southwest Channels. Transect 2 ran northwest-southeast parallel to the Sunshine Skyway. Transect 3 extended east-west south of the Y Cut. The Outer Egmont transect, Transect 4, began outside the Tampa Bay entrance and continued east along the channel between Egmont and Mullet Keys. Running from the Sunshine Skyway to the Y Cut, Transect 5 covered the main navigation channel. Finally, Transect 6 extended north from the Y Cut to the head of Hillsborough Bay. The time of occupation of each transect and the number of individual hydrographic stations occupied are listed in Table 5.1.

In addition to the transect data, moored CTDs and CTs provided salinity and temperature time series of varying length at 36 locations throughout the Bay. Four mooring locations had a near-surface and a near-bottom CT; the remaining CTs and CTDs were moored at current meter stations. The locations of these moorings are shown on Figure 5.2. The length of each time series is presented in Table A.4 in Appendix A.

#### Background Information

Tampa Bay is primarily a tidally driven estuary; both the salinity and the temperature change temporally in response to the tides and tidal currents. The results of the TOP hydrographic survey support previous findings that Tampa Bay is relatively well mixed vertically (Dragovich, and Sykes, 1967). Although both salinity and temperature are nearly constant with depth, strong horizontal salinity gradients exist in Tampa Bay. The most saline water was found near the entrance to the Bay, while the least saline water was observed in upper Hillsborough Bay. At any given time, the temperature was nearly constant throughout the Bay. Following Pritchard's (1955) classification scheme based on salinity stratification, Tampa Bay is a vertically

homogenous, laterally inhomogeneous estuary. This is a typical situation for an estuary where the tidal flow is much larger than the river flow. Previous modeling efforts assumed that the horizontal gradients of density did not make a significant contribution to the flow (Goodwin, 1987); however, this work supports Weisburg and Williams (1991) hypothesis that the horizontal density gradients are dynamically significant and must be considered when modelling the Bay.

Following a brief description of the hydrographic data acquisition, processing, and general characteristics, this discussion will highlight the temporal and spatial variability of the water masses, as well as put forth possible explanations for that variability. Finally, a synthesis of the water mass characteristics of Tampa Bay is presented.

**Table 5.1. TOP CTD Transect information. Listed are the date and elapsed time (hours) of occupancy of a transect, the number of stations taken and the tidal condition during the transect. P# indicates pass number; W&V - current was weak and variable. <sup>P</sup> - indicates tidal stage derived from NOAA tidal current predictions.**

Cruise	Date	Casts	Elapsed Time	Passes	Tidal Stage
<b>Transect 1 - Egmont Channel</b>					
1	Aug. 17-18, '90	133	23.0	6	P1,P2 Ebbing <sup>P</sup> ; P3,P4 Flooding <sup>P</sup> ; P5,P6 W&V <sup>P</sup>
2	Nov. 14, '90	12	1.8	1	Flooding
3	March 5, '91	25	2.8	5	Flooding <sup>P</sup>
4	June 3, '91	20	3.4	4	Weak Ebb
5	Aug. 18, '91	30	3.8	6	Flooding
<b>Transect 2 - Sunshine Skyway Bridge</b>					
1	Aug. 18, '90	24	3.1	3	All Passes W&V <sup>P</sup>
2	Nov. 13, '90	11	0.2	2	Flooding
3	March 4, '91	28	3.3	5	Slack Before Flood
4	June 1, '91	9	1.0	2	Flooding
5	Aug. 26, '91	23	2.8	4	Slack Before Ebb
<b>Transect 3 - St. Petersburg to Mangrove Point</b>					
1	Aug. 18, '90	25	4.2	2	P1 Slack Before Ebb <sup>P</sup> ; P2 ebbing <sup>P</sup>
2	Nov. 15, '90	15	2.4	1	Slack Before Ebb
3	March 2, '91	31	5.1	4	Slack Before Flood
4	May 24, '91	21	3.5	2	Slack Before Ebb
5	Aug. 24, '91	20	4.2	2	Slack Before Flood

**Table 5.1 (continued). TOP CTD Transect information.** Listed are the date and elapsed time (hours) of occupancy of a transect, the number of stations taken and the tidal condition during the transect. P# indicates pass number; W&V - current was weak and variable. <sup>P</sup> - indicates tidal stage derived from NOAA tidal current predictions.

Cruise	Date	Casts	Elapsed Time	Passes	Tidal Stage
<b>Transect 4 - Main Channel: Outer Egmont</b>					
1	Aug. 17-18, '90	28	22.7	2	P1 flooding <sup>P</sup> ; P2 W&V <sup>P</sup>
2	Nov. 12, '90	4	0.7	1	Flooding
3	March 1, '91	12	4.1	2	Slack Before Flood
4	June 4, '91	16	3.4	2	Slack Before Ebb
5	Aug. 17, '91	20	4.5	2	Ebbing
<b>Transect 5 - Main Channel: Central Bay</b>					
1	Aug. 17-18, '90	44	16.0	2	P1 Ebbing <sup>P</sup> ; P2 W&V <sup>P</sup>
2	Nov. 9, '90	9	4.0	1	Slack Before Flood
3	Feb. 28, '91	18	4.3	2	Slack Before Flood
4	May 26, '91	17	4.2	2	Slack Before Ebb
5	Aug. 30, '91	15	2.5	2	Flooding
<b>Transect 6 - Main Channel: Hillsborough Bay</b>					
1	Aug. 17-18, '90	20	6.2	2	P1 Ebbing <sup>P</sup> ; P2 Flooding <sup>P</sup>
2	Nov. 10, '90	8	1.9	1	Ebbing
3	Feb. 26, '91	14	4.1	2	Slack Before Flood
4	June 2, '91	17	3.4	2	Slack Before Ebb
5	Aug. 24 '91	15	3.7	2	Slack Before Ebb

## 5.2. DATA PROCESSING AND PLOTTING

The purpose of this section is to synthesize the enormous body of data collected during TOP; therefore, a detailed description of data acquisition and pre-processing is not included. These aspects of the CTD data are presented in the NOS Oceanographic Circulation Survey Report (Nowadly, 1992).

### The CTD Transects

All six transects were occupied at least once during each of the five seasonal cruises. The 684 individual CTD profiles were stored as separate cast files. During most of the cruises, several passes were made over a transect, so that a particular geographic location was often sampled more than once. The station casts were grouped by transect, cruise, and pass number. Often, the repeated passes of a transect were completed in a short period of time, and little difference

is apparent between the water mass fields observed at each pass. Average salinity and temperature depth profiles were calculated for each location where more than one sampling was obtained. For Cruises 2, 3, 4, and 5, this was accomplished by taking the arithmetic mean of all the values at a single depth from each pass. The transects of Cruise 1 were not time-averaged because the sampling strategy employed during Cruise 1 was significantly different from the other four cruises. During Cruise 1, the passes up the Bay and across the mouth of the Bay (Transects 4, 5, 6 and 1) took place over a 2-day period, rendering the averaging time unacceptably large. All of the passes from Cruise 1 were plotted individually.

The vertical plane contour plots of salinity and temperature are presented as depth versus horizontal distance along the transect (for example Figure 5.5). Distance was used as the abscissa to standardize the appearance of horizontal gradients. The portion of a transect not occupied during a given cruise was blanked out as well as the area below the depth of the deepest data record.

The seasonal (as represented by each cruise) horizontal plane views of salinity and temperature were produced by contouring all of the surface or bottom values of salinity and temperature (for example, Figure 5.9). The surface was chosen to be 1.5 m although many of the casts collected the first sample at a shallower depth than 1.0 m. The CTD used during TOP is approximately 1 m long and needed to be fully submerged for at least 30 s at the beginning of each cast to prime the conductivity pump. In order to map vertical stratification, the vertical temperature differences were calculated by subtracting the bottom value from the surface value at each station, and the vertical salinity differences were calculated by subtracting the surface value from the bottom value.

### **Tidal Stage Determination**

Because Tampa Bay is primarily a tidally-driven estuary it is important to know the tidal condition during the transects in order to understand and characterize water mass patterns. Although the TOP plan called for the hydrographic stations to be taken during slack water, some of the transects were occupied during other tidal stages. The approximate tidal condition during each transect was estimated from TOP current measurements or from the tidal current predictions (NOS, 1989 and 1990b) for Tampa Bay (Table 5.1). Following the NOS Tidal Current Tables, the current measurements taken at Egmont Channel (C-2; Figure 5.1) were used as the reference for other positions in the Bay. There was no current record at Egmont Channel during Cruise 1; therefore the prediction of tidal stage given in the NOS Tidal Current Tables was used for all of the Cruise 1 transects.

### **The Moored CTs**

Conductivity and temperature time series were collected at 31 different stations throughout Tampa Bay (Figure 5.2). The times of occupation for each station are shown in Table A.4 in Appendix A. Data were collected at 10-min intervals using SeaBird Electronics (SBE), Inc., model SBE-16 instruments at all stations. Three of the stations (S-1, S-2, and S-3) were long-term salinity and temperature stations, and data were collected at two depths (near-bottom and

near-surface). The remaining 28 CT stations were located throughout the Bay and were occupied for various lengths of time, ranging from 30 days to 15 months. The instruments at each of these stations were mounted to ADCP or S4 platforms and are considered near-bottom measurements.

SBE's software package, SEASOFT, was used to compute salinity and density from the measured values of temperature and conductivity and convert the data to ASCII engineering units (see Nowadly, 1992). The data were quality controlled by plotting out all of the time series and performing statistical analyses.

## **General Characteristics**

A temperature versus salinity diagram of the CTD transect data highlights the rich nature of water mass variability within Tampa Bay (Figure 5.3). In general, water temperature depends on the time of year; as expected the Bay is warmest in the summer (August 1990-yellow, August 1991-green) and coldest in the winter (February/March 1991-purple). In contrast, the magnitude of salinity is most dependent on the location within the Bay; high salinities are observed, regardless of season, near the mouth (Transects 1, 2, and 4-○, △, and •, respectively), the salinity gradually decreases with increasing distance up the Bay (Transects 3 and 5-▽ and ▲), and the lowest salinities are found in Hillsborough Bay (Transect 6-■). Temporal variability is seen in the range of salinities observed during a cruise. Interestingly, the largest range of salinity is observed during the summer season when temperature is least variable (compare yellow and green - summers with the purple symbols - winter). Details of the temporal and spatial variability of the water mass characteristics will be discussed in the following sections.

## **5.3. TEMPORAL VARIABILITY OF SALINITY AND TEMPERATURE**

### **Tidal Scale**

Fluctuations of the tidal current in Tampa Bay cause significant temporal variations in both the extreme values and the gradients of the salinity field. In general, the salinity at a given location increases during flood and is highest near Slack Before Ebb (SBE). Similarly, the salinity decreases during ebb, and the lowest salinity is observed near Slack Before Flood (SBF). The increasing salinity is a result of bayward advection of more saline Gulf of Mexico water, while the decreasing salinity reflects the seaward transport of the freshwater input (Figure 5.4a and b).

The two passes taken along Transect 6 during Cruise 1 illustrate the effect of tidal stage on the strength of the local horizontal salinity gradients (Figure 5.5a and b). Pass 1 was obtained while the Bay was ebbing and pass 2 was taken during flood. The strong horizontal salinity gradient in the upper 5 m of the water column between 5 and 10 km along the transect is displaced northward (to the right in the figure) during flood. This movement is the direct result of the influence of higher salinity Gulf water advecting from lower in the Bay.

Salinity variations are the result of the progression of floods and ebbs which alternatively transport saline water from the Gulf of Mexico and fresher riverine input from the upper Bay.

Plots of the frequency distribution of energy density highlight the dominance of tidal scale variability. Strong diurnal and semidiurnal energy peaks are observed in the salinity time series at four separate locations throughout the Bay (Figures 5.6 and 5.7). Spectral analyses of concurrent 70-day time series (March 13 - May 21, 1991) at the entrance to Tampa Bay (C-2), mid Bay (C-4), Hillsborough Bay (C-46), and Old Tampa Bay (C-41) show that the predominant short-period frequencies of salinity variability are the diurnal (1 cpd) and semidiurnal (2 cpd) frequencies.

The amplitude of the tidal variation in salinity is greatest at mid-Bay (C-4). Larger variations of salinity occur at mid-Bay, where the effects of the salty Gulf water and the fresh river water are equally strong. As will be discussed later, the horizontal salinity gradients are very strong in the middle of the Bay. The salinity at the other three locations are more strongly affected by one of the two water mass sources. In the upper Bay, the effect of river input is dominant, whereas, at Egmont Channel, the Gulf water influence dominates. In general, the short-term temporal variability of salinity may be explained by the variation of the tides and tidal current.

Significant tidal scale temperature variability is also observed in Tampa Bay. In the fall and winter, warmer Gulf water is advected into the Bay during flood, while cooler Bay water flows out during ebb. During the late spring and early summer months, the opposite trend is evident (Figure 5.4a and c). The water temperature of the Bay is generally different from that of the Gulf because the Bay is shallower and is more influenced by radiational heating and cooling. All four of the temperature energy density spectra show significant diurnal and semidiurnal peaks (Figures 5.6 and 5.7). The strength of the diurnal peak in each of the spectra is likely related to the effect of diurnal heating which augments the tidal signal. As with the salinity, the short-term temporal temperature variations are clearly driven by tidal current variability.

Confirmation of the importance of tidal forcing of the density field in Tampa Bay is provided by cross spectral analysis of the along-channel current speed and density observed at mid-Bay. The highest coherence is evident in the diurnal and semidiurnal bands (Figure 5.8). As observed in the time series, currents lead the density by approximately a quarter tidal cycle ( $90^\circ$ ) (Figure 5.4a and d).

### **Weekly Scale**

All of the eight energy density spectra show a general increase of energy at the synoptic scale (2 to 7 days), indicating that both the salinity and the temperature records exhibit significant sub-tidal variability. A subtidal maximum coherence squared is present at approximately 5 days in the relationship between density and along-channel current speed (Figure 5.8). As in the tidal band, the synoptic-scale phase difference between the two observations is constant at nearly  $90^\circ$ .

### **Seasonal Scale**

Seasonal variability in the horizontal salinity field is clearly evident in a series of horizontal plane views of surface salinity. The strength of the along-channel salinity gradient is influenced by the mouth-to-head difference in salinity which varies seasonally in proportion to the amount of

freshwater input. Consistently strong, along-channel gradients are observed during the two summer cruises when the mouth-to-head salinity range at 1.5 m is 25.5 psu to 35.4 psu ( $\Delta S = S_{\text{mouth}} - S_{\text{head}} = 9.887$ ) for August 1990 and 19.133 psu to 33.818 psu ( $\Delta S = 14.685$ ) for August 1991 (Figure 5.9a and 5.13a). Summer is a period of high rainfall in the Tampa Bay area (see Figure 4.10); thus the large river runoff significantly depresses the salinity near the inputs to the Bay and increases the mouth-to-head salinity difference. Weak along-channel gradients were observed during the February/March 1991 cruise. The mouth-to-head salinity range at 1.5 m is 34.448 psu to 29.885 psu ( $\Delta S = 4.563$ ) (Figure 5.11a). The low rainfall and associated small runoff of this time period serve to lower the mouth-to-head salinity difference and the associated horizontal salinity gradient.

The change in the location of the 30 psu isohaline (a median value of salinity throughout the Bay) is another indication of the seasonal change of salinity. During Cruise 1 (August 1990), the 30 psu isohaline was located near  $27^{\circ}43'$  (Figure 5.9a). In November, during Cruise 2, the 30 psu isohaline was displaced northward, near  $27^{\circ}50'$ , indicating a relatively higher proportion of Gulf water (Figure 5.10a). In the winter (Cruise 3), the 30 psu isohaline was located at its most northerly observed position, at approximately  $27^{\circ}51'$  (Figure 5.11a), indicating the lack of freshwater input. Tampa Bay receives the least amount of precipitation during the winter; therefore the influence of the saline Gulf water is most prominent then. As rainfall and river discharge increase in the spring (see Figures 4.10 and 4.12), the location of the isohaline is displaced southward, reflecting the increasing presence of fresh water (Cruise 4 - Figure 5.12a). Finally, during the second summer season sampled during TOP (August 1991, Cruise 5), the 30 psu isohaline was at its most southern observed location, near  $27^{\circ}36'$  (Figure 5.13a).

Comparison of the seasonal map views of surface temperature reveals the significant seasonal variation in the temperature of Tampa Bay (Figures 5.9b, 5.10b, 5.11b, 5.12b, and 5.13b). As expected, the Bay is warmest during the summer and early fall and coldest in the winter. The minimum temperature ( $18.0^{\circ}\text{C}$ ) was observed at mid-Bay in early March during Cruise 3. The maximum temperature ( $32.1^{\circ}\text{C}$ ) was seen off of Mullet Key in mid-August during Cruise 5.

The seasonal change in the water temperature throughout Tampa Bay closely follows the seasonal air temperature change. The seasonal variation of the monthly mean seawater temperature observed at four stations (C-1 and S-1, 10 km from the entrance, C-2 at the entrance to Tampa Bay, C-4 at mid Bay, and C-5 in Old Tampa Bay) all mirror the variation of the monthly mean air temperature observed at M-2 (Figure 5.14). The seasonal cycle of water temperature is reduced on the shelf (C-6); the shelf is warmer than the Bay in late fall and winter and cooler in the late spring and summer. Dramatic changes in the mean monthly water temperature occur during the transition seasons - spring and fall. This energy is evident in the spring density spectra at individual stations (Figures 5.6 and 5.7). All the temperature spectra are "red"; that is, they show significant energy at low frequencies.

### **Interannual Scale**

The repetition of the six CTD transects in August 1990 and August 1991 provides some information on the interannual variability of the water masses of Tampa Bay. A significant

difference in the salinity of Tampa Bay is evident in a comparison of the two August depictions of the surface salinity (Figures 5.9a and 5.13a). The diminished salinity values observed in August 1991 reflect the unusually high runoff in the summer of 1991.

A larger horizontal temperature gradient is also evident in August 1991. Warmer surface water was observed during the August 1991 cruise near the Bay entrance (Figures 5.9b and 5.13b). The monthly average temperature at C-6 was 26.2°C in August 1990 as compared with 29.3°C in 1991 (Figure 5.14). The warm water measured at the entrance likely resulted from the advection of warmer shelf water during the summer of 1991.

## **5.4. SPATIAL VARIABILITY OF SALINITY AND TEMPERATURE**

### **Vertical**

In general, both the salinity and the temperature of Tampa Bay are well mixed vertically. Isohalines and isotherms are nearly vertical in the majority of the transects (Figure 5.15a and b). Slight vertical stratification is evident only during the summer season (Figure 5.5). Maps of the surface-to-bottom salinity difference also indicate the presence of summer stratification (Figure 5.16a). Hillsborough Bay exhibited vertical salinity differences in excess of 2 psu; these stronger vertical gradients reflect the presence of fresher surface water. Hillsborough Bay receives approximately three fourths of the total freshwater input to Tampa Bay (Flannery, 1989). The surface-to-bottom temperature difference maps reveal little vertical temperature variation.

### **Horizontal**

Although the salinity of Tampa Bay is relatively well mixed vertically, significant horizontal salinity gradients exist. The positions of the minimum and maximum salinity as well as the strength of the salinity gradient are controlled by the proximity of fresh and salt water sources.

In general, the minimum along-channel salinity values (minimum equals 19.060 psu for all cruises) are found at the head of Hillsborough Bay, while the highest values (maximum = 36.908 psu) are located near the mouth at Outer Egmont Channel (Figures 5.9a, 5.10a, 5.11a, 5.12a, and 5.13a). The maximum cross-channel salinity values are observed deep in the navigation channel, while the lowest values occur at the surface at or near the boundaries (Figure 5.17). Table 5.2 indicates the range of salinity values observed during the five TOP cruises. Note that the salinity standard deviations (or root-mean-square of the deviations from the mean) are large and, in the summer of 1991, exceeded 4 psu.

Transect 4 at Outer Egmont Channel exhibits generally weak salinity gradients because the salinity in this region is dominated by the consistently more saline shelf water (Figure 5.18a). The salinity at the westernmost portion of this transect is generally in excess of 35 psu, similar to that observed at the shelf station (S-1). The mean end-to-end gradient at 5 m for the six profiles of Transect 4 is 0.072 psu/km, standard deviation equals 0.066 psu/km. In contrast, Transect 5, which runs up the navigation channel through the center of the Bay, exhibits

generally strong salinity gradients. The mean end-to-end gradient for Transect 5 is 0.218 psu/km, standard deviation equals 0.076 psu/km, (Figure 5.18b). A notable exception to the trend of weak gradients at Transect 4 occurs during August 1991, when strong gradients resulted from the high river runoff discussed earlier.

In addition to vertical homogeneity, the horizontal variation in the temperature of Tampa Bay is quite small as well (Figures 5.9b, 5.10b, 5.11b, 5.12b, and 5.13b). Using standard deviation as a proxy for variability of the data indicates that the temperature varies about the mean temperature by approximately 1°C over the five cruises (Table 5.2). The means and standard deviations listed in Table 5.2 are for all depths and all positions during each cruise, emphasizing that the temperature within Tampa Bay is relatively constant throughout the Bay in a given season.

## **5.5. CONCLUSIONS**

The water mass characteristics of Tampa Bay exhibit both temporal and spatial variations. Tidal fluctuations are a significant portion of the time variability; however, there is also a significant seasonal signal. On the tidal scale, salinity increases during flood and decreases during ebb. Summer is the warm, rainy season in Tampa Bay; the salinity of Tampa Bay is depressed and the water temperature is increased during the summer months. Data from the 17-month hydrographic survey indicate that the interannual variability of water mass characteristics of Tampa Bay may also be significant.

Spatially, the horizontal variations in the water mass characteristics dominate over vertical variations. Both the salinity and the temperature of Tampa Bay are relatively well mixed vertically, although slight vertical stratification is occasionally evident in Hillsborough Bay during the summer season. The along-channel density gradient results from and fluctuates primarily in response to freshwater input. This horizontal density gradient is expected to drive a long-term residual estuarine flow which influences the net transport of the Bay (Weisburg and Williams, 1991). The characteristics of this residual flow as a function of the along-channel density gradient is discussed in Section 6.

**Table 5.2. Variation of observed water mass characteristics. Listed are the minimum, mean, maximum, range, and standard deviation of salinity (upper number) and temperature (lower number) for each cruise.**

Minimum	Mean	Maximum	Range	Standard Deviation
<b>Cruise 1 - August 17-18, 1990</b>				
24.074 psu 29.692 °C	33.369 psu 30.394 °C	35.716 psu 31.614 °C	11.642 psu 1.922 °C	2.690 psu .233 °C
<b>Cruise 2 - November 9-15, 1990</b>				
27.921 psu 21.383 °C	33.000 psu 23.119 °C	36.908 psu 26.862 °C	8.987 psu 5.479 °C	2.234 psu 1.238 °C
<b>Cruise 3 - February 26 - March 5, 1991</b>				
29.593 psu 18.001 °C	32.591 psu 19.409 °C	35.747 psu 21.955 °C	6.154 psu 3.954 °C	1.515 psu 1.027 °C
<b>Cruise 4 - May 24 - June 4, 1991</b>				
26.571 psu 26.409 °C	32.853 psu 28.169 °C	35.784 psu 30.157 °C	9.213 psu 3.748 °C	2.558 psu .691 °C
<b>Cruise 5 - August 17-30, 1991</b>				
19.060 psu 28.612 °C	29.275 psu 30.332 °C	35.347 psu 32.084 °C	16.287 psu 3.472 °C	4.264 psu .948 °C

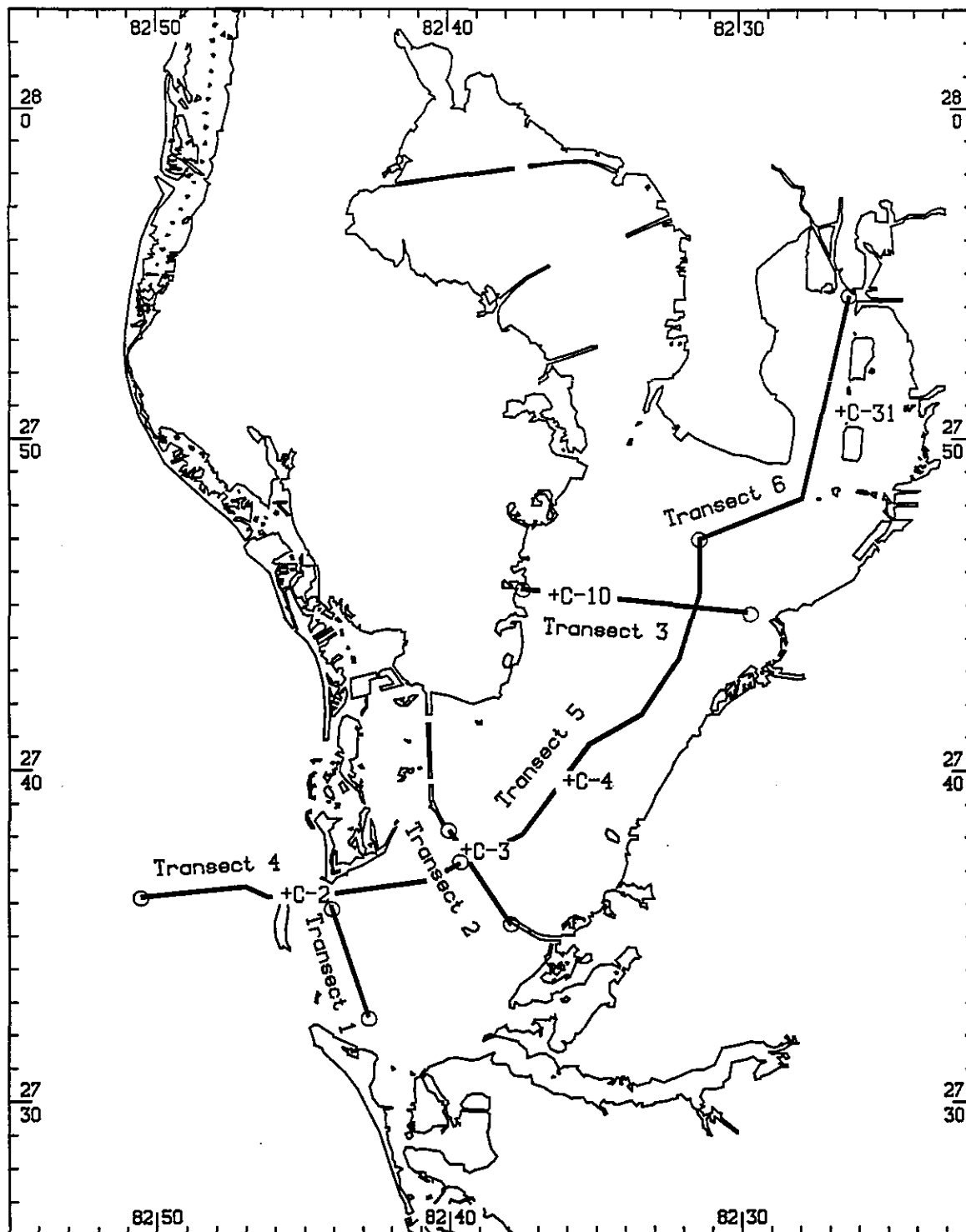


Figure 5.1. Location of the TOP CTD Transects. The beginning and ending of each transect are marked by open circles. Also shown are the locations of the five current meter stations (marked with a +) used to determine the tidal stage for each transect.

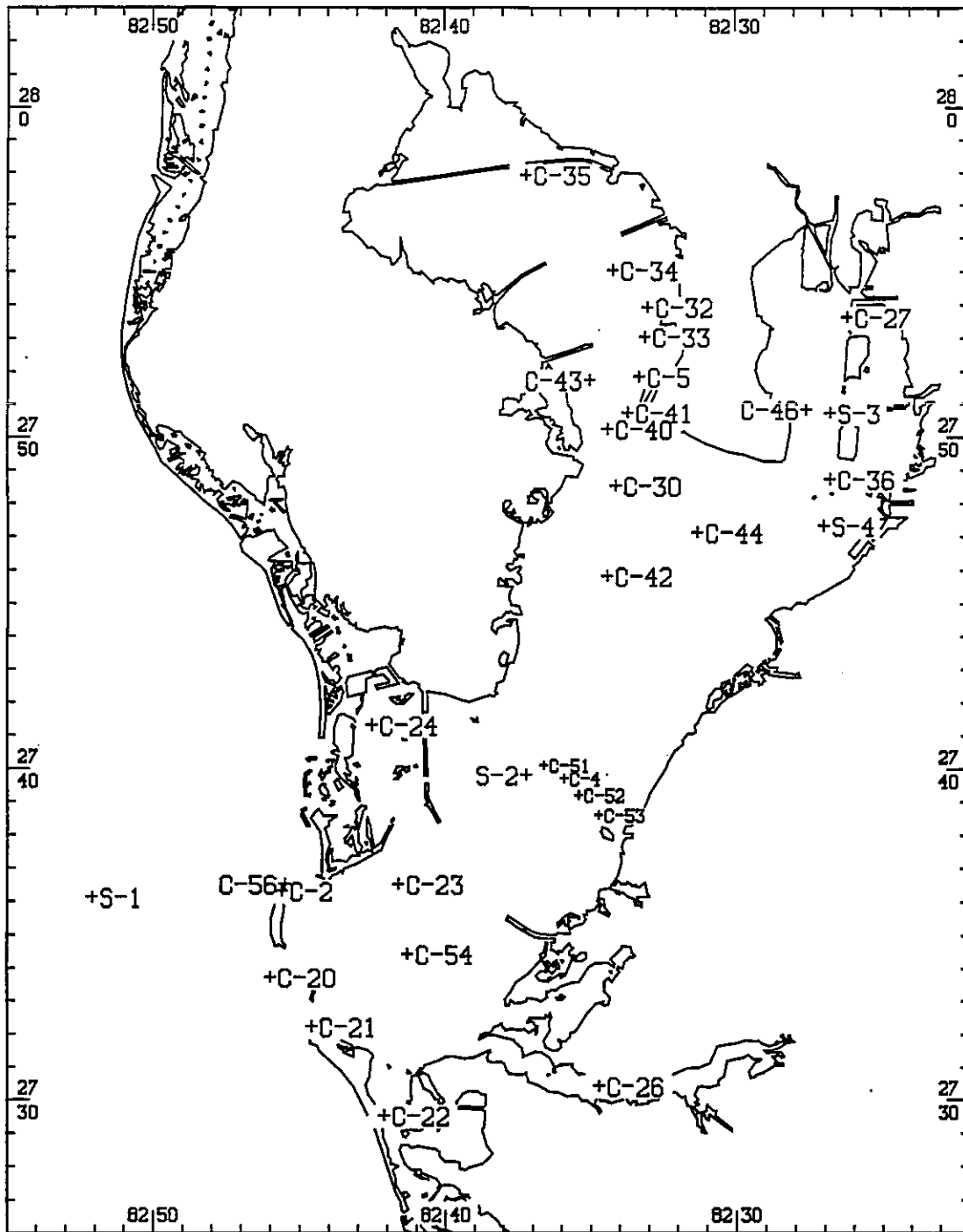


Figure 5.2. Location of 31 moored CT/CTD stations. Moorings with a near-surface and a near-bottom CT are denoted by an "S". Bottom-mounted CTs (associated with current meter platforms) are denoted by a "C". Not shown are stations C-1 and C-60, which are co-located with station S-1, station C-6 which is 50 km offshore of Egmont Key, and station C-31 co-located with S-3.

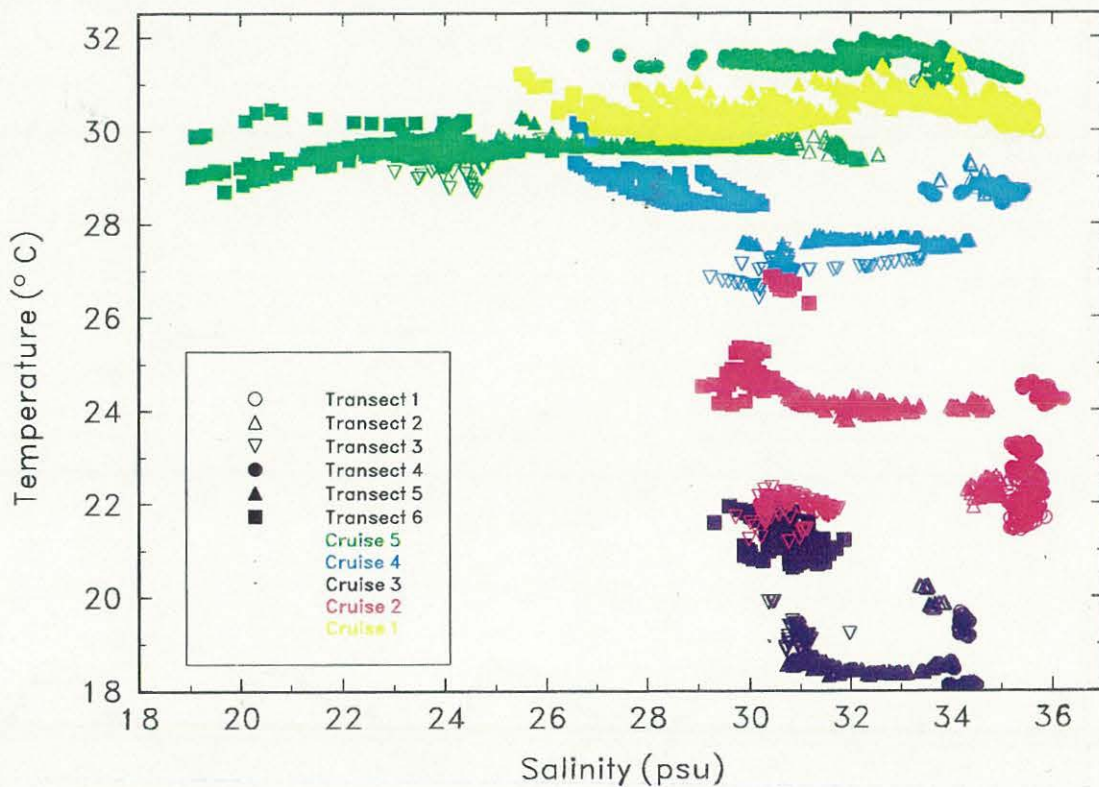


Figure 5.3. Temperature vs salinity diagram for all the CTD transect data taken during TOP. Color is used to indicate season (yellow - Cruise 1 August 1990; magenta - Cruise 2 November 1990; purple - Cruise 3 February/March 1991; cyan - Cruise 4 May/June 1991; and green - August 1991). Transect number is represented by symbol shape (○-Transect 1; △-Transect 2; ▽-Transect 3; ●-Transect 4; ▲-Transect 5; ■-Transect 6). Salinity is most variable during the summer when the water temperature is nearly constant.

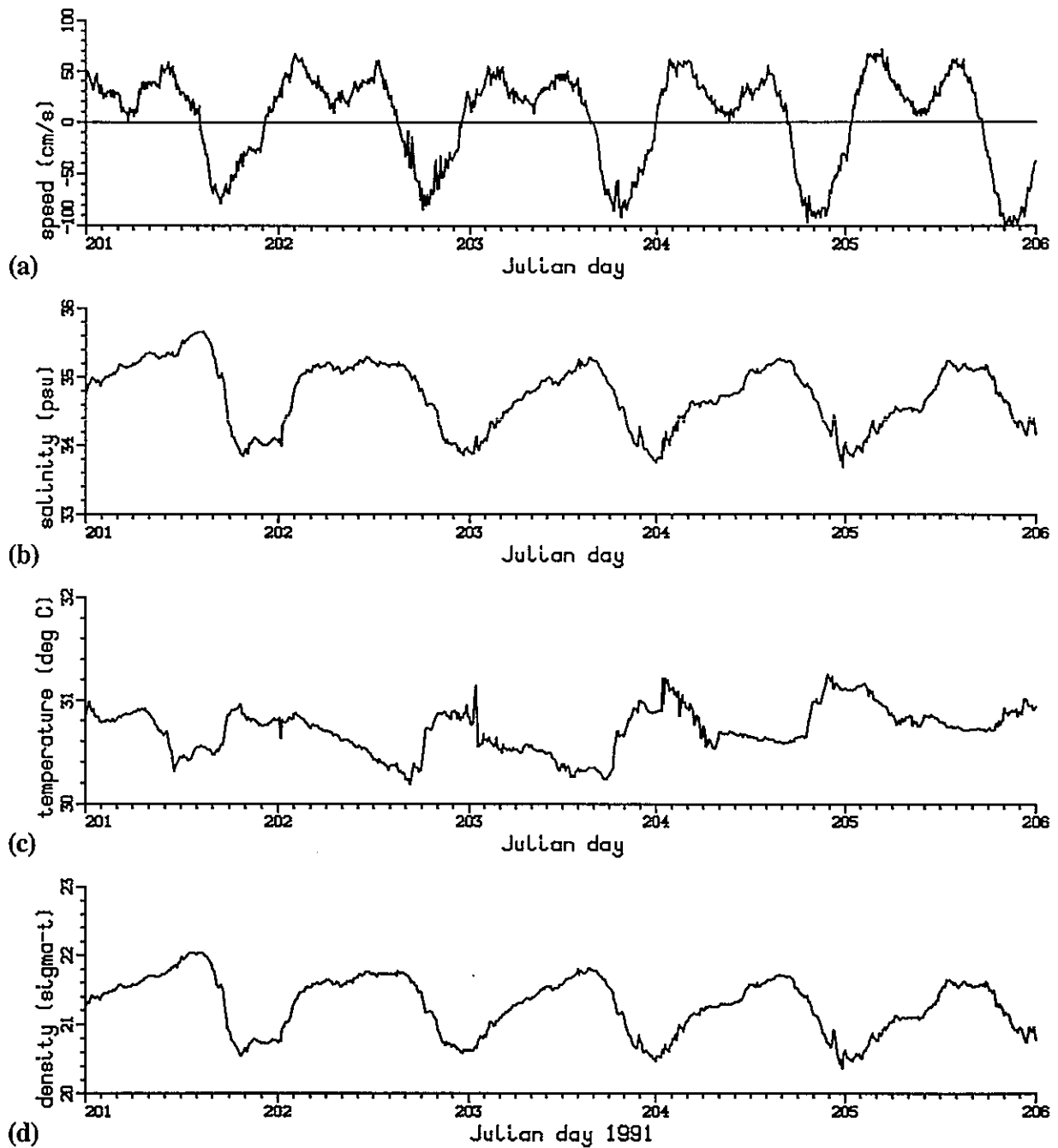
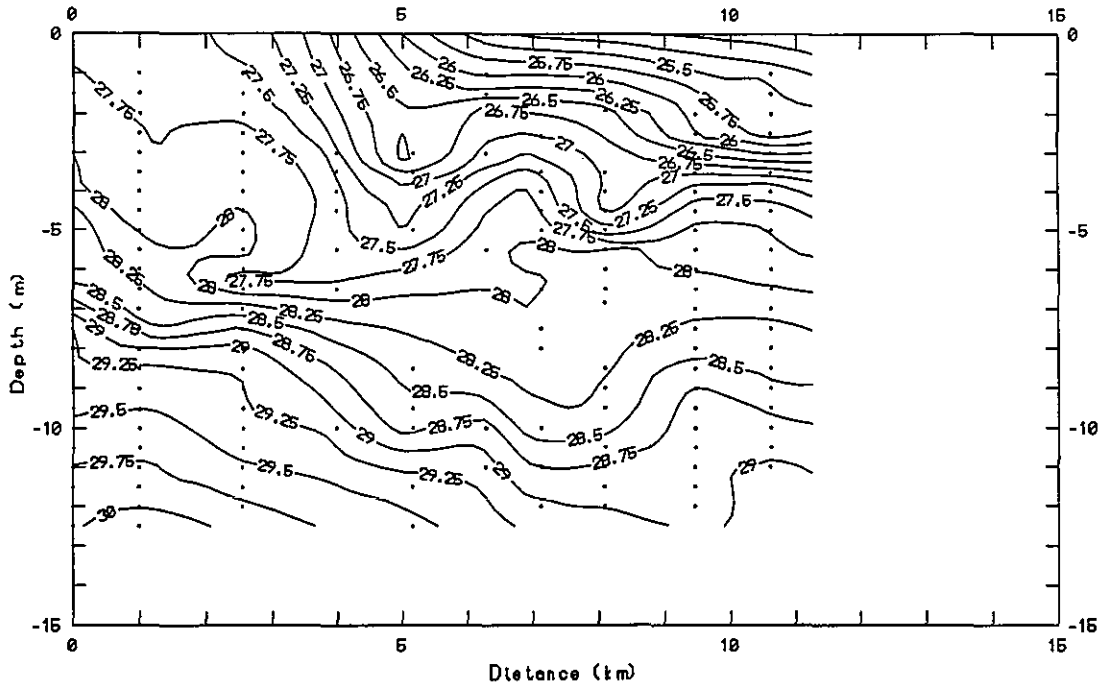
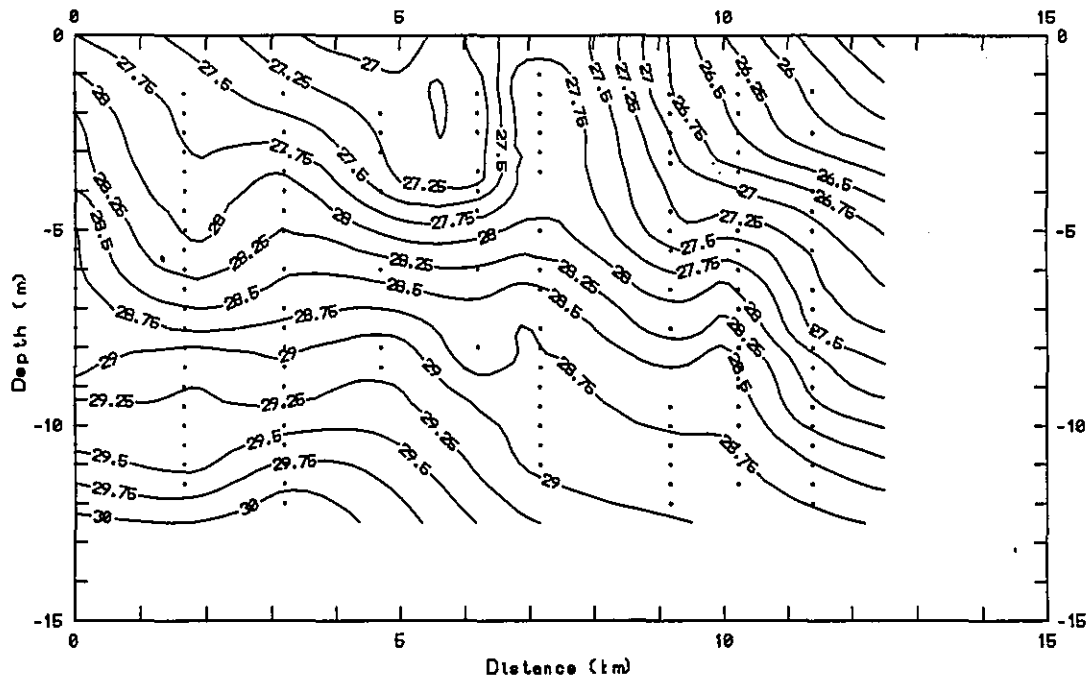


Figure 5.4. Temporal variation of near-bottom water mass characteristics at Egmont Channel ( $27.562^{\circ}$ ,  $82.731^{\circ}$ ) from July 20 to July 25, 1991. The variation of (a) the tidal current (flood is positive) is compared to the (b) salinity, (c) temperature, and (d) density variations. The salinity decreases during ebb and increases during flood; the converse is true of the temperature. Peak salinity occurs at SBE and minimum salinity at SBF.



(a)



(b)

Figure 5.5. Salinity versus depth along Transect 6 (Hillsborough Bay) during Cruise 1. The contour interval is 0.25 psu. (a) Pass 1 was taken on August 17, 1990, from 2052 UT to 2247 UT during ebb. The section begins at 27.789°N, 82.504°W and ends at 27.855°N, 82.447°W. (b) Pass 2 was taken on August 18, 1990, from 0114 UT to 0306 UT during flood. The section begins at 27.787°N, 82.512°W and ends at 27.857°N, 82.446°W.

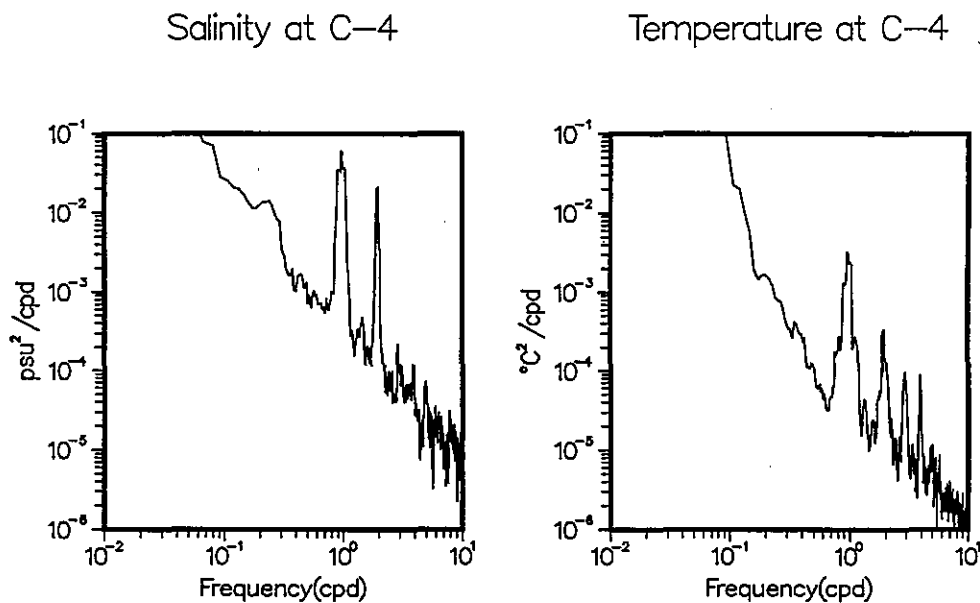
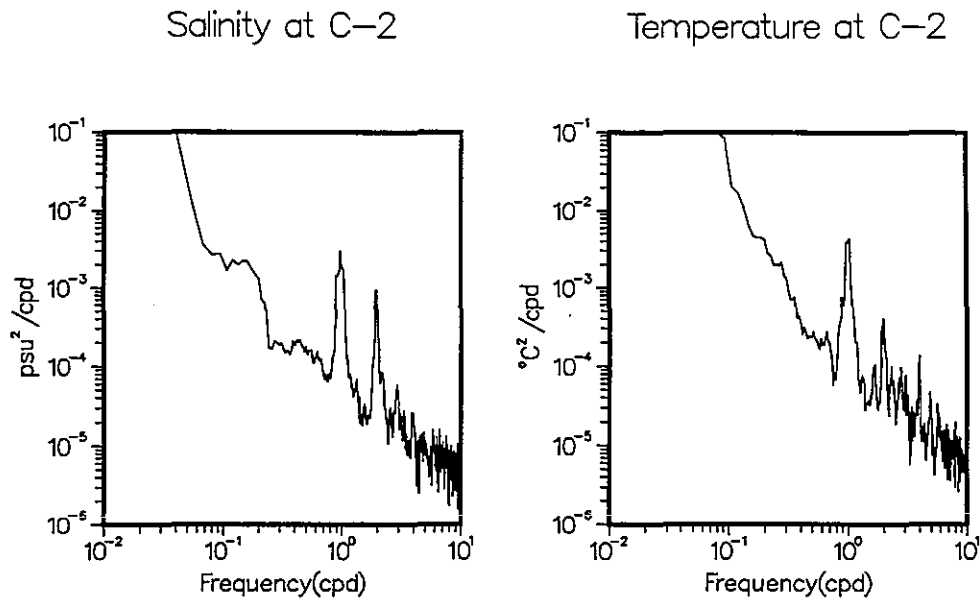
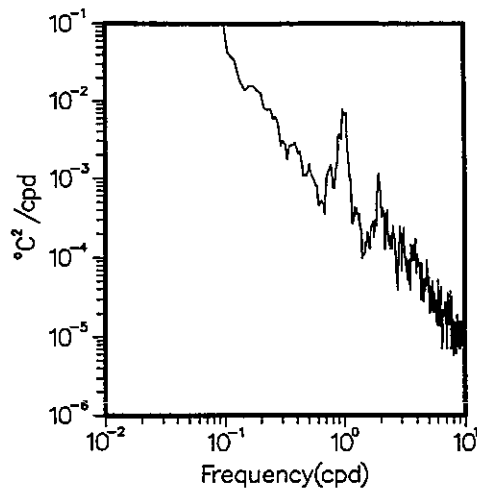
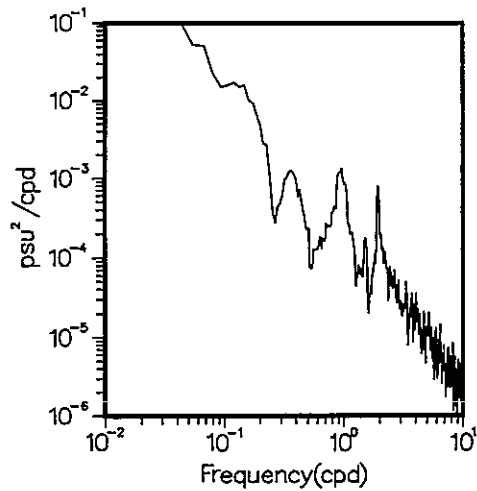


Figure 5.6. Salinity and temperature energy density spectra for (a) C-2 Egmont Channel (deployment t02041 at 23 m depth) and (b) C-4 Manatee Channel (deployment t04041 at 11 m depth). Results of analysis of a 70-day time period from March 13 to May 21, 1991. The analysis bandwidth is 0.014 cpd. Significant diurnal (1 cpd) and semidiurnal (2 cpd) energy is evident, as well as energy in the broad synoptic-scale (0.1-0.5 cpd) band.

Salinity at C-46

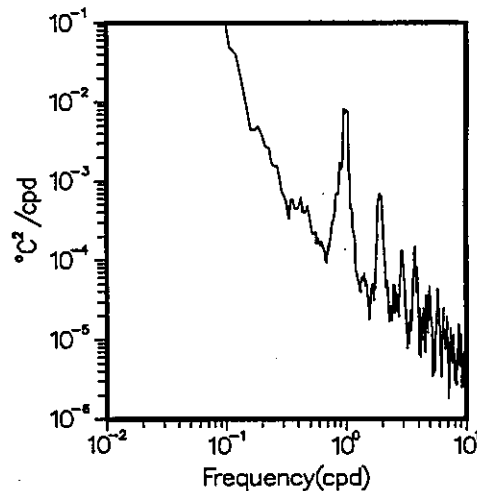
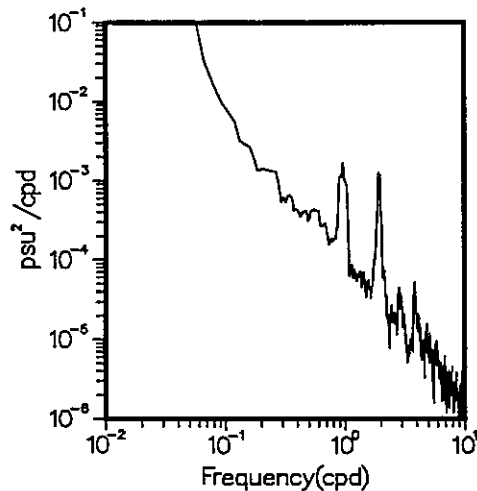
Temperature at C-46



(a)

Salinity at C-41

Temperature at C-41



(b)

Figure 5.7. Salinity and temperature energy density spectra for (a) C-46 Hillsborough Bay (deployment t46011 at 3 m depth) and (b) C-41 Port Tampa (deployment t41011 at 8 m depth). Results of analysis of a 70-day time period from March 13 to May 21, 1991. The analysis bandwidth is 0.014 cpd. Significant diurnal (1 cpd) and semidiurnal (2 cpd) energy is evident, as well as energy in the broad synoptic-scale (0.1-0.5 cpd) band.

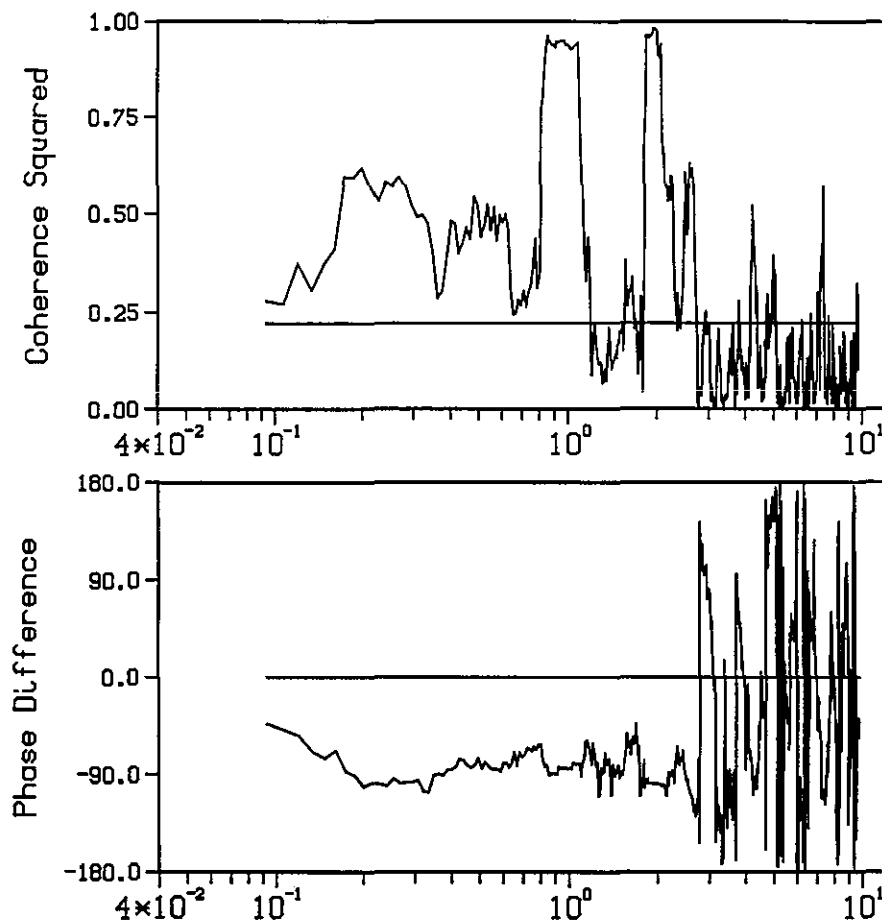


Figure 5.8. Results of cross spectral analysis of the along-channel current speed and the density observed at mid-Bay. A 70-day time period from March 13 to May 21, 1991 was used. The analysis bandwidth is 0.014 cpd. Density lags the along-channel current by 90°.

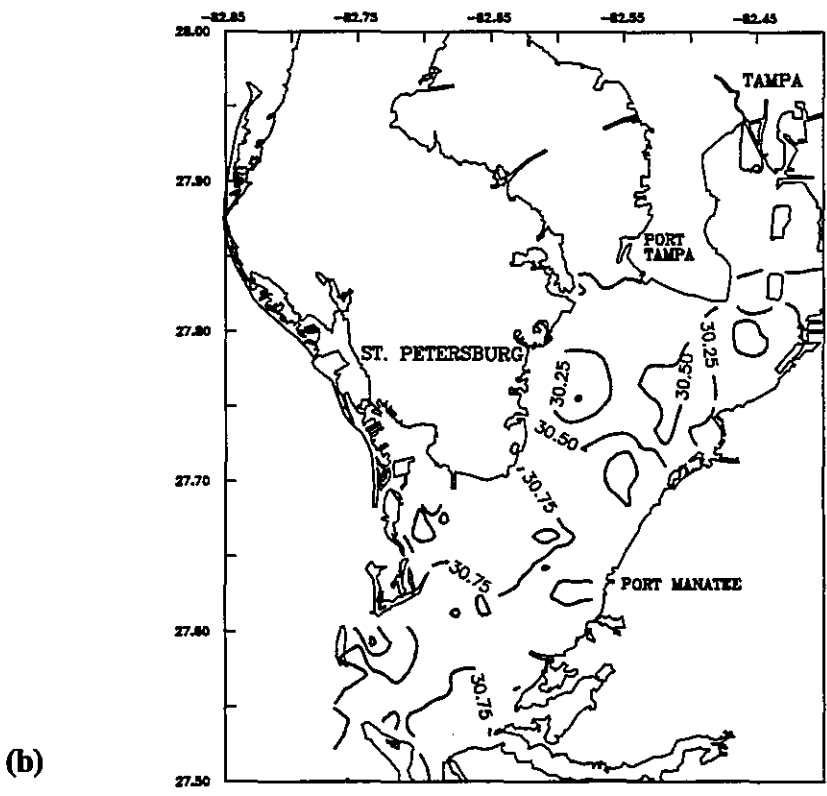
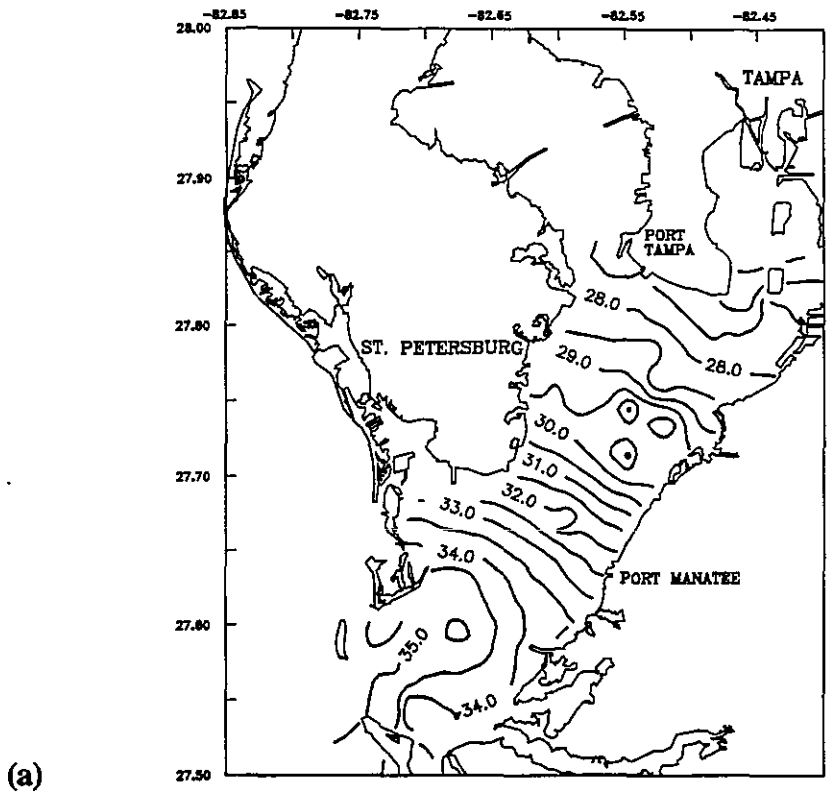


Figure 5.9. (a) Surface salinity (psu) and (b) surface temperature (°C) for August 17-18, 1990.

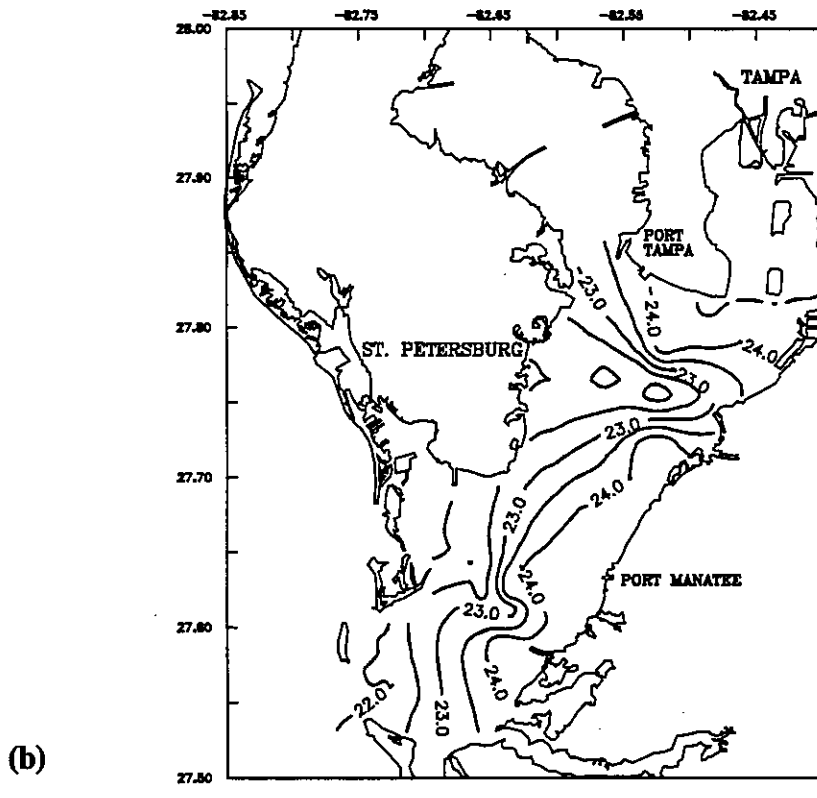
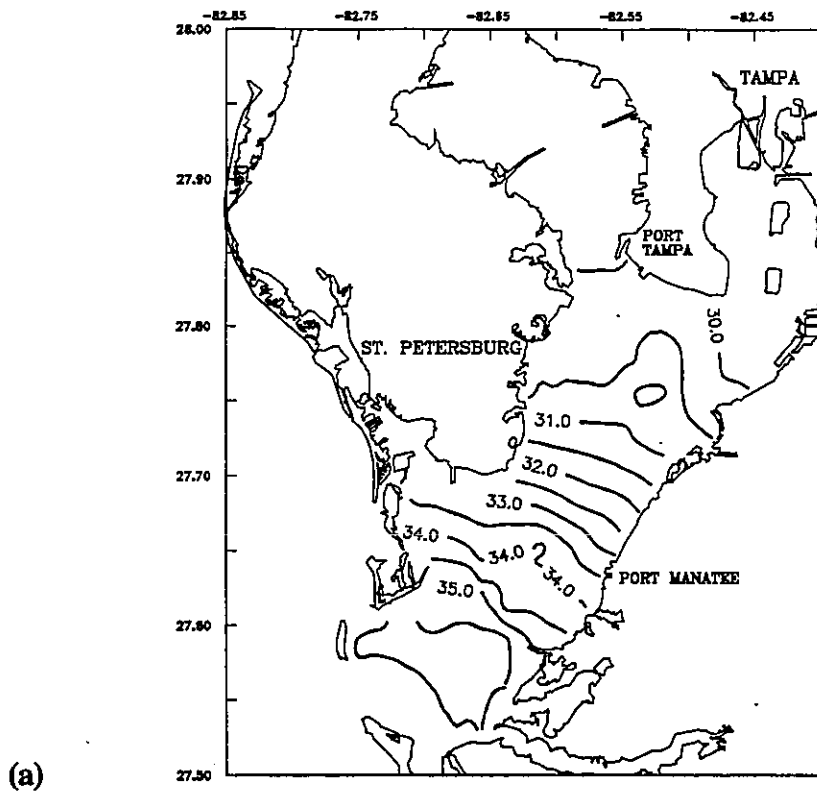


Figure 5.10. (a) Surface salinity (psu) and (b) surface temperature ( $^{\circ}\text{C}$ ) for Nov. 9-15, 1990.

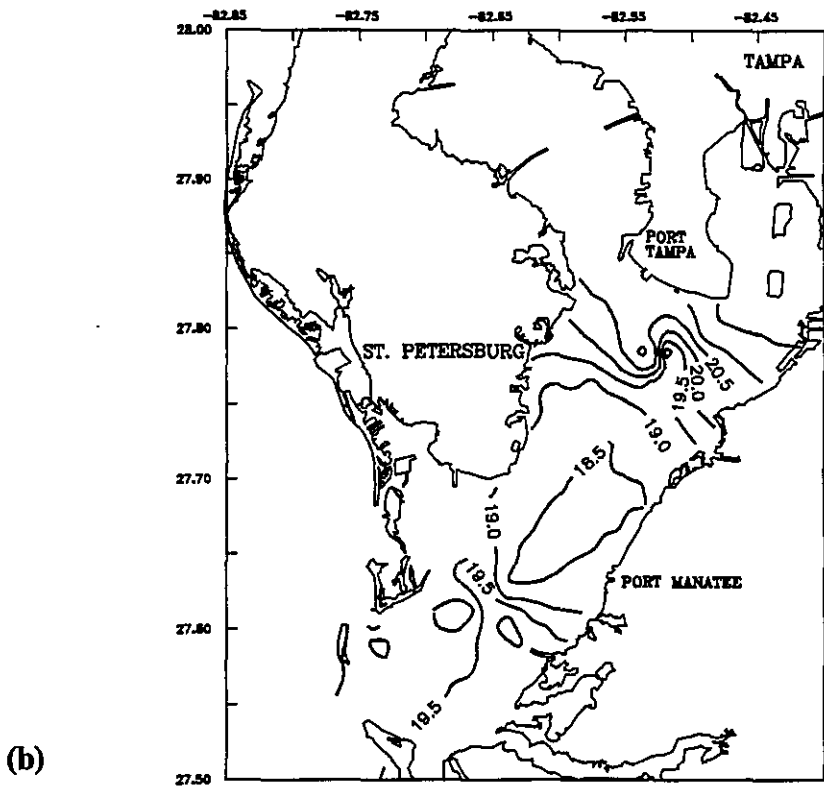
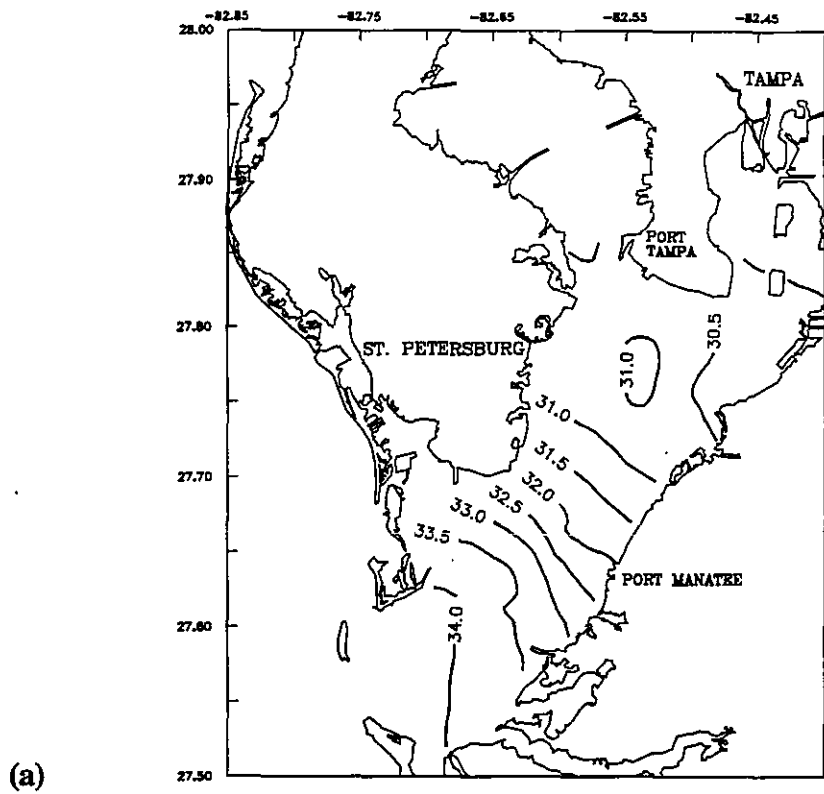


Figure 5.11. (a) Surface salinity (psu) and (b) surface temperature (°C) for Feb. 26-Mar. 5, 1991.

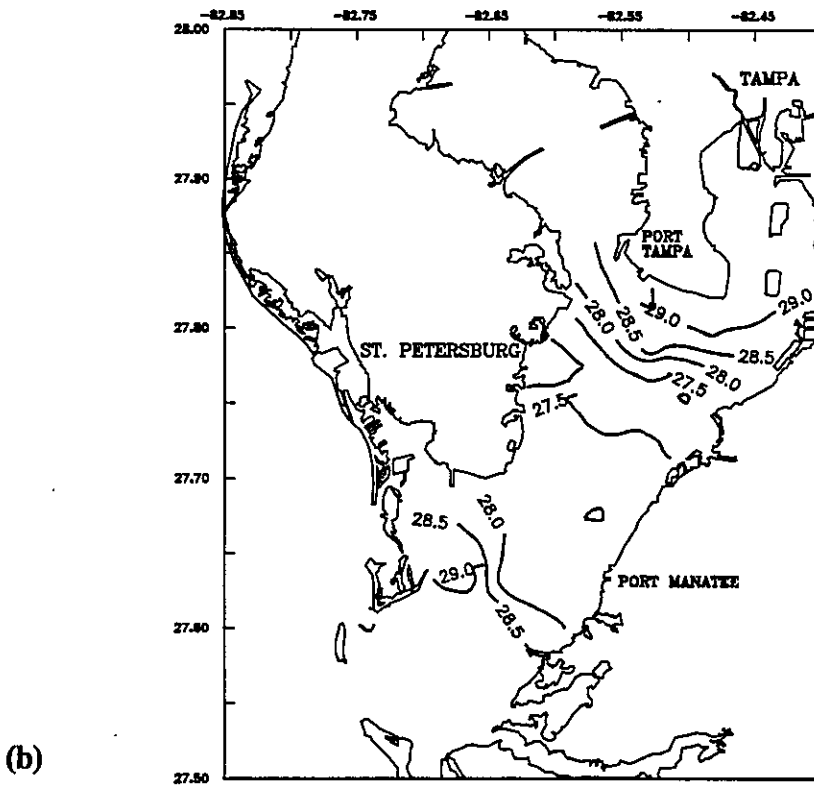
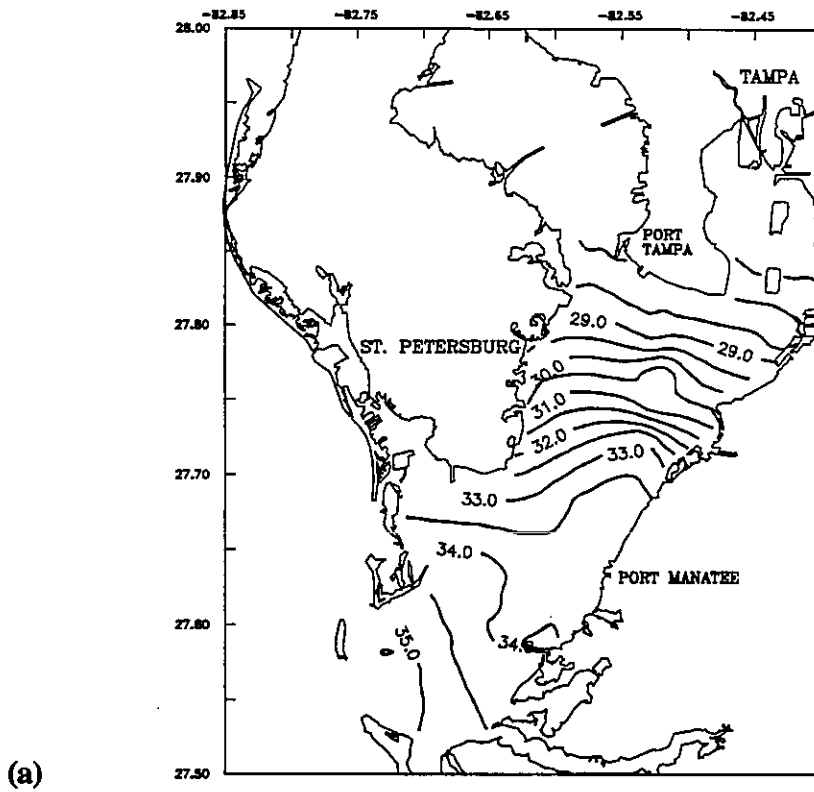
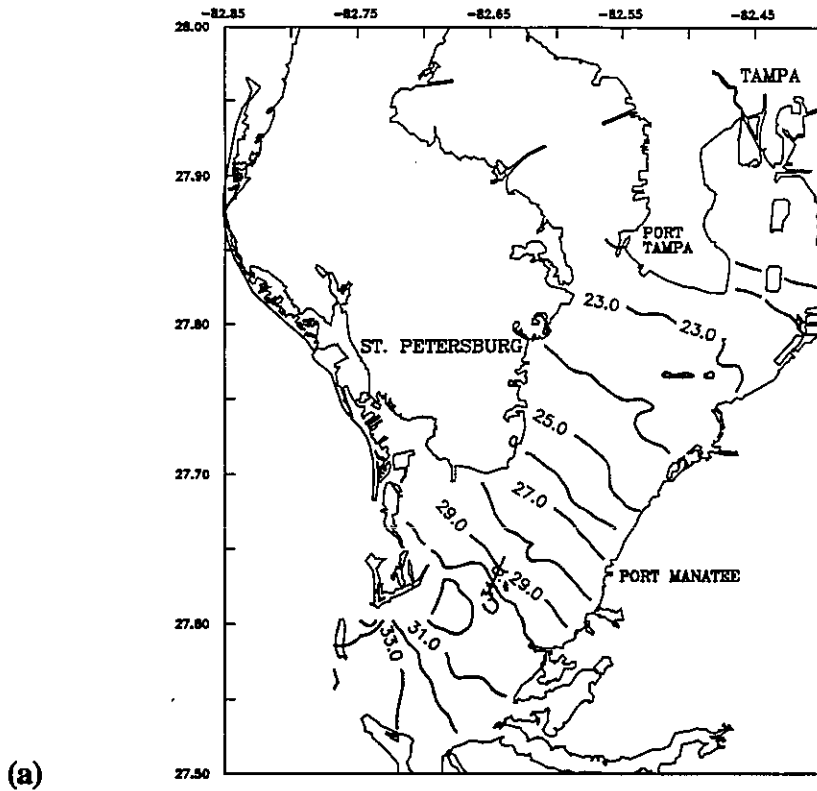
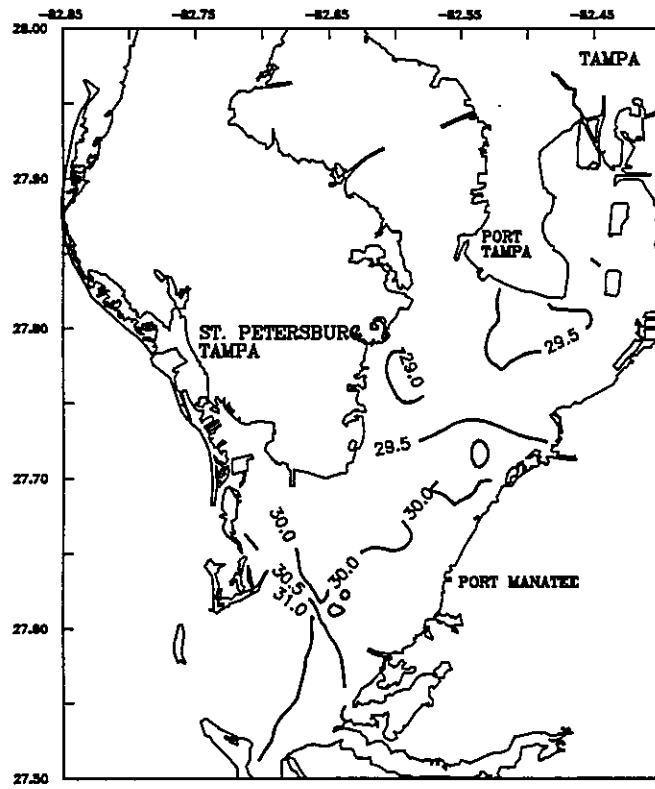


Figure 5.12. (a) Surface salinity (psu) and (b) surface temperature ( $^{\circ}\text{C}$ ) for May 24-June 4, 1991.



(a)



(b)

Figure 5.13. (a) Surface salinity (psu) and (b) surface temperature (°C) for August 17-30, 1991.

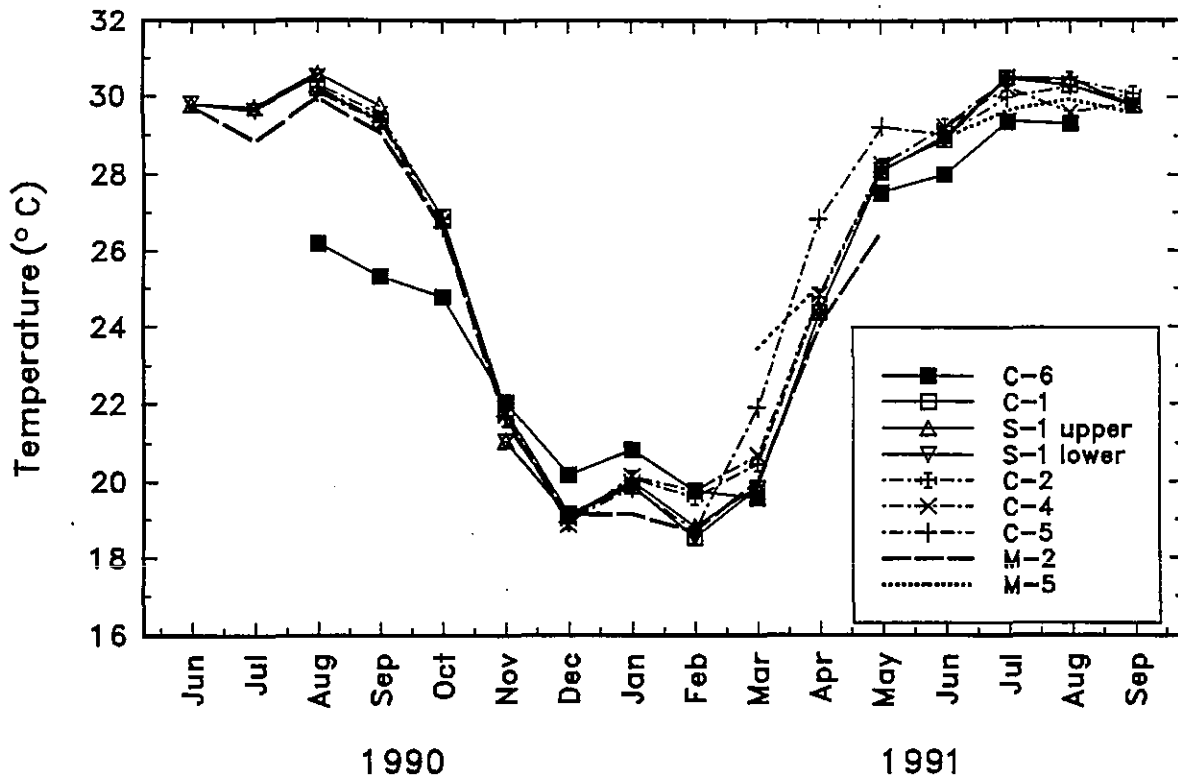
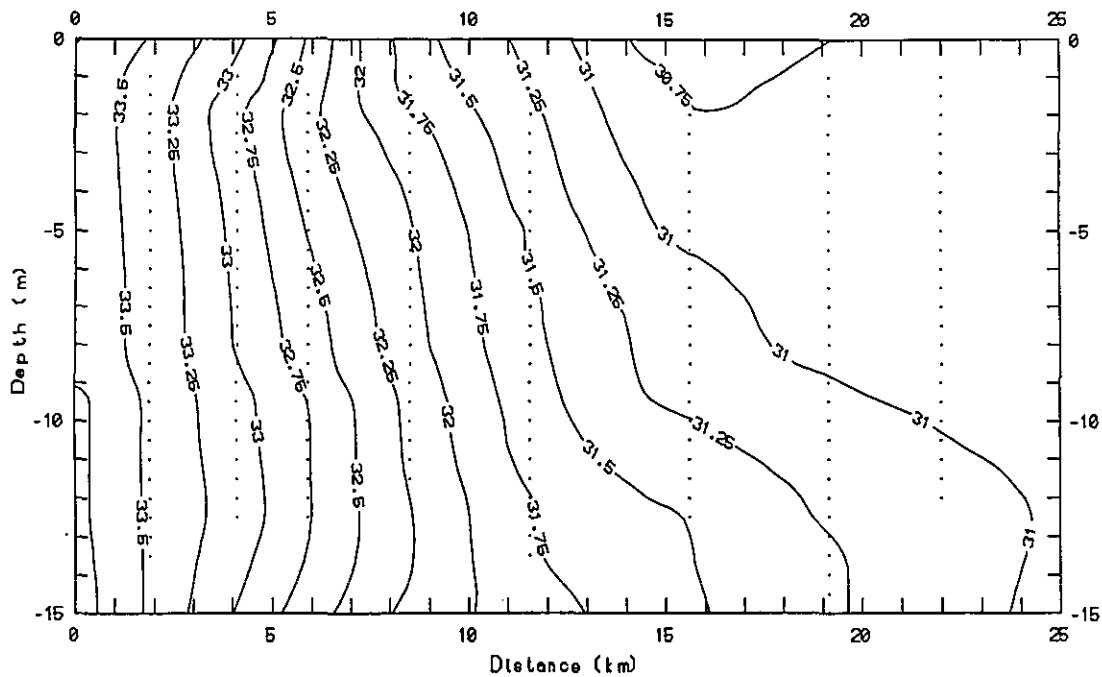
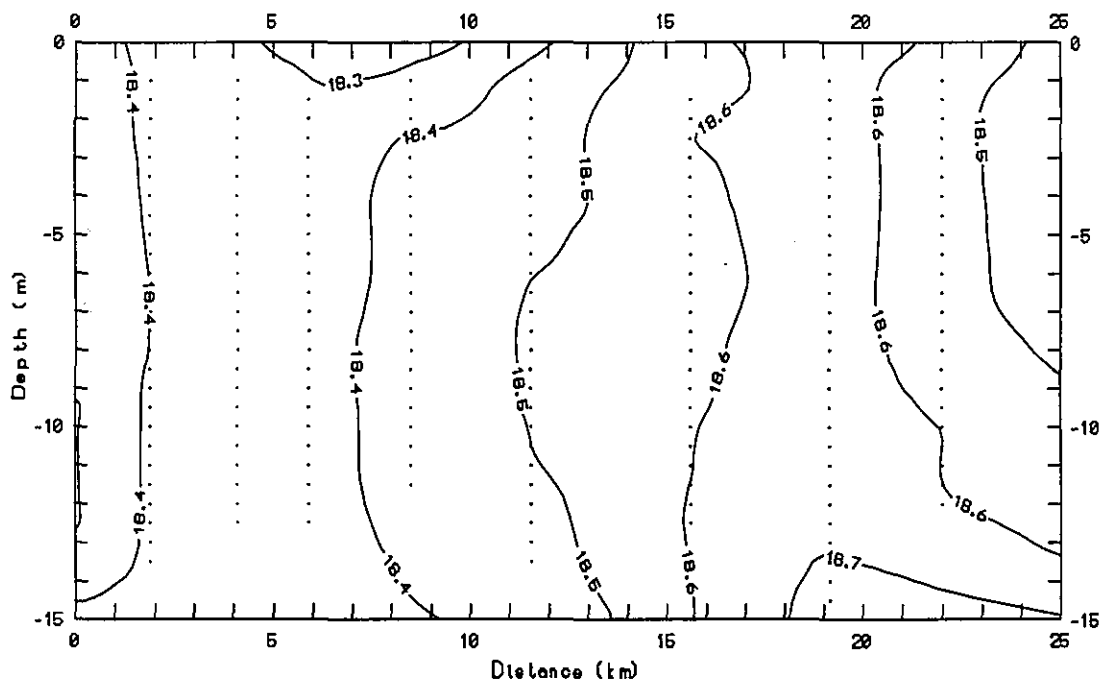


Figure 5.14. Comparison of monthly mean seawater temperature and monthly mean air temperature for June 1990 to September 1991. The monthly mean water temperature, observed at six water mass stations (C-6, C-1, S-1, C-2, C-4, and C-5), is plotted along with the air temperature observed at the real-time meteorological station (M-2). Although stations C-2 and C-5 are more than 30 km apart, the water temperature signal is spatially coherent and mirrors the air temperature signal. During the late fall and winter, the shelf (C-6) is warmer than the Bay, whereas it is cooler during the summer.



(a)



(b)

Figure 5.15. (a) Salinity versus depth along Transect 5 (contour interval is 0.25 psu). (b) Temperature versus depth along Transect 5 (contour interval is 0.1°C). These sections were taken during Cruise 3 on February 28, 1991 from 1206 UT to 1621 UT. Both salinity and temperature are very well mixed vertically.

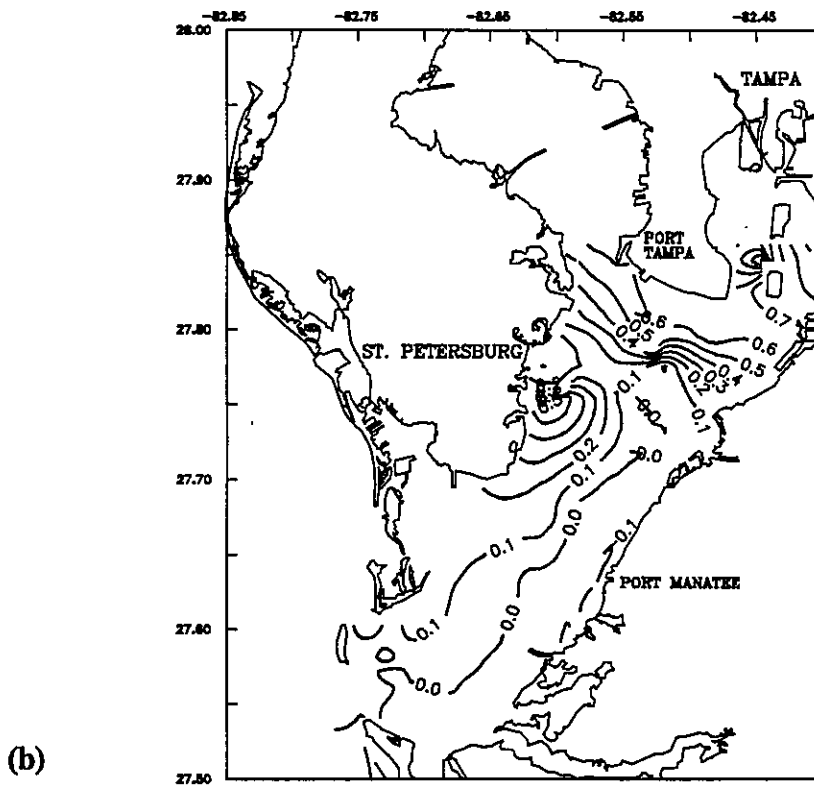
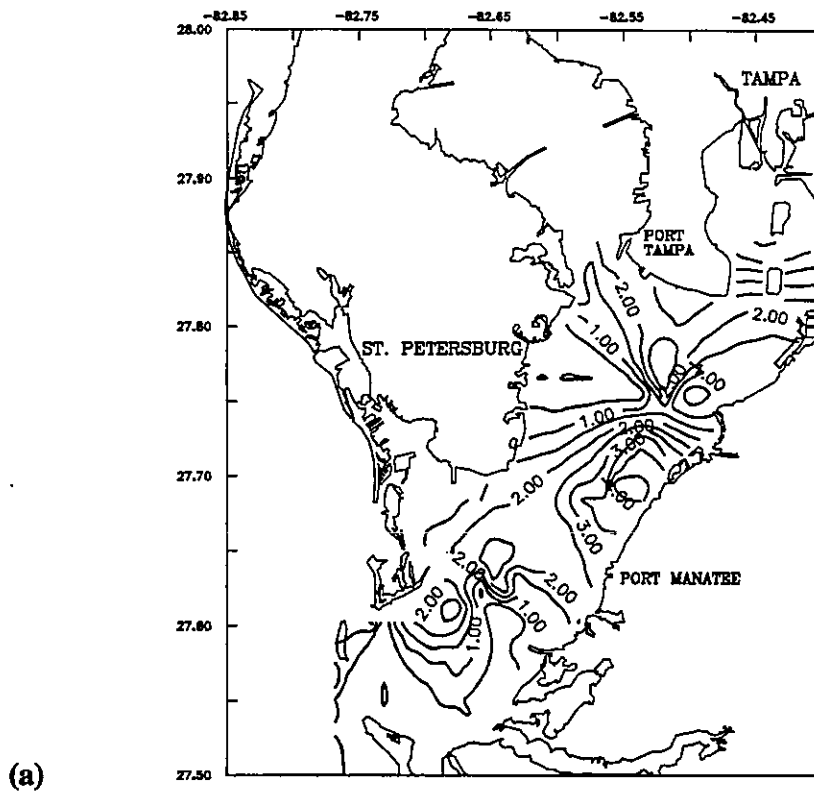


Figure 5.16. (a) Vertical salinity difference (psu) for August 17-30 and (b) vertical temperature difference ( $^{\circ}\text{C}$ ) for May 24-June 4, 1991.

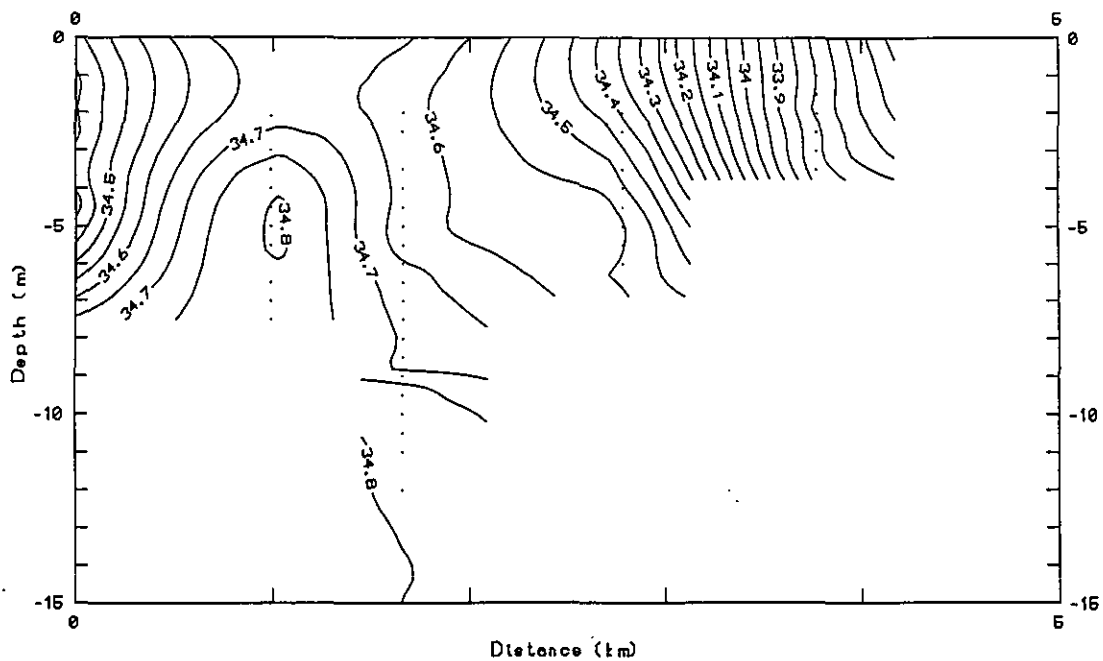
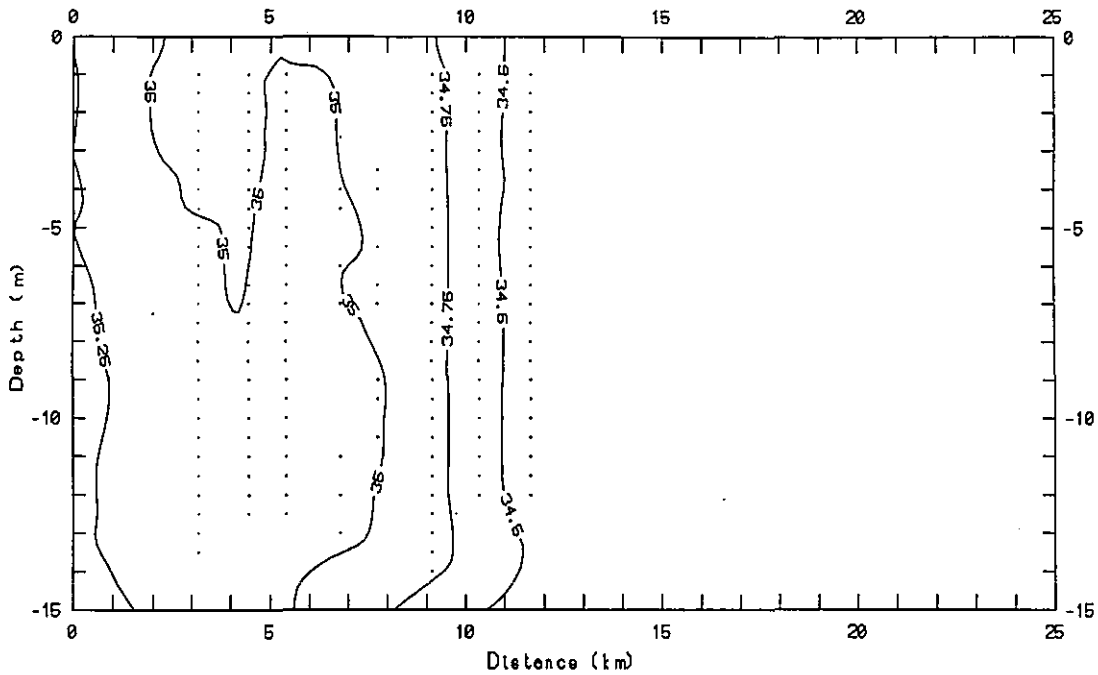
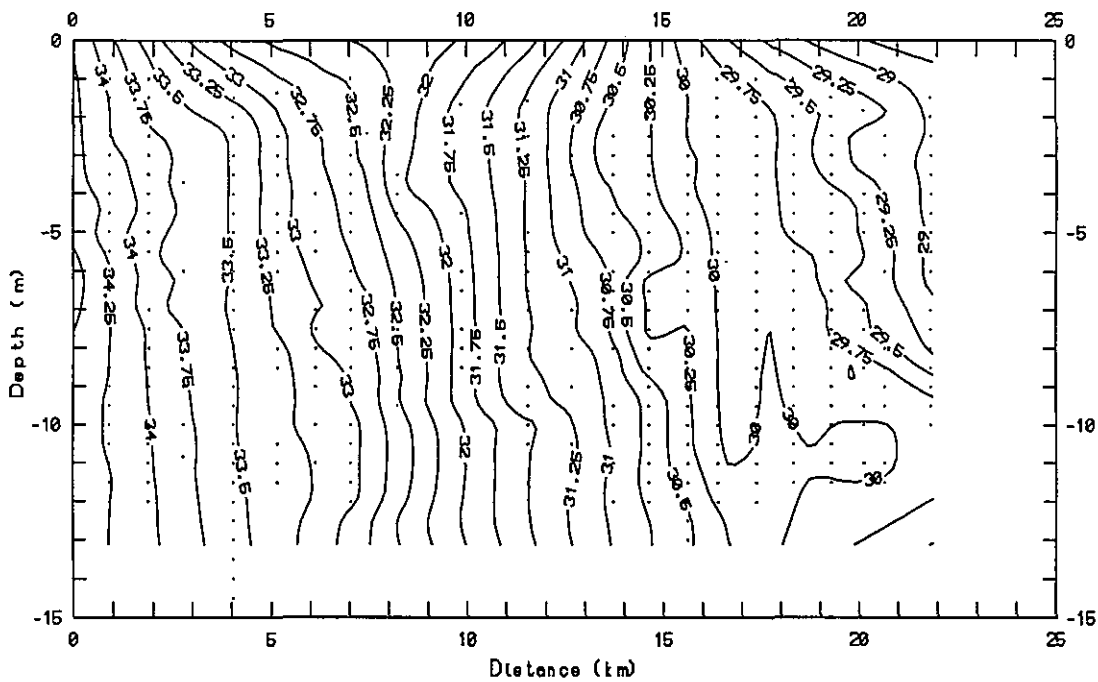


Figure 5.17. Salinity versus depth along Transect 2 (Sunshine Skyway cross-bay transect). This section was taken during Cruise 4 on June 1, 1991, from 1909 UT to 2012 UT. The contour interval is 0.05 psu. The salinity is maximum in the navigational channel and minimum at the sides of the Bay.



(a)



(b)

Figure 5.18. The variation of the strength of the salinity gradient as a function of location within the bay. (a) Salinity versus depth along Transect 4 (Outer Egmont). Generally weak horizontal salinity gradients were observed along Transect 4. (b) Salinity versus depth along Transect 5 (mid bay). Strong gradients were observed along Transect 5.

## 6. NONTIDAL CIRCULATION

Chris E. Zervas and Kathryn T. Bosley

Sections 2 and 3 documented the astronomical tidal component of the water levels and currents in Tampa Bay. Significant residual signals were found at all stations when predicted tidal water levels and currents were subtracted from observed water levels and currents. The nontidal component of the water levels and currents are examined in this section. Long-term nontidal currents are important in estuaries as the primary means of transport of dissolved and suspended matter. Two nontidal driving forces are discussed: subtidal (periods > 1 day) water level fluctuations on the west Florida continental shelf and head-to-mouth density gradients in the Bay due to freshwater input from rivers. The magnitude of these two subtidal effects on water levels and currents are quantified for each month of TOP. Some of the results in this section were discussed in Bosley (1993) and Zervas (1993).

### 6.1. SHELF WATER LEVEL EFFECT

Tidal water levels and currents in Tampa Bay are driven by the tidal water level on the west Florida continental shelf. Nontidal water level fluctuations on the continental shelf should affect the Bay in a similar manner. Nontidal water level fluctuations on the shelf are produced in part by both local and distant wind-driven currents. Where the shelf is deeper than the Ekman depth, the longshore component of the wind can raise and lower coastal water levels by Ekman transport perpendicular to the coast. As the shelf depths get shallower than the Ekman depth, the transport vector rotates toward the wind direction. Pond and Pickard (1983) calculate the Ekman depth for a 10 m/s wind at a latitude of  $27.5^\circ$  to be 63 m. This is approximately the mean depth of the west Florida continental shelf. Although the Ekman theory may not apply near the coast during the highest winds (> 10 m/s), in general, the longshore component of the wind will raise or lower coastal water levels.

The west Florida coastline and the continental slope have an orientation of about  $340^\circ$  ( $20^\circ$  west of north). When the wind blows from the south-southeast, shelf water levels should rise; when the wind blows from the north-northwest, shelf water levels should fall.

To quantify the shelf effect on Tampa Bay, four time series are considered:

- 1) 12 months of wind speed and direction measured at Tampa Airport,
- 2) 18 months of water level data measured at Clearwater Beach (E-724),
- 3) 18 months of water level data measured at St. Petersburg (E-520), and
- 4) 16 months of current speed and direction measured at C-4.

The Clearwater Beach water level station is located on a barrier island along the Gulf Coast about 45 km north of the main entrance to Tampa Bay (Figure 3.1). The St. Petersburg water level station is located on the western side of Tampa Bay and is representative of water levels

in the Bay (see Figure 3.8). Tampa International Airport (TPA), west of the city of Tampa, is equidistant from Clearwater Beach and St. Petersburg (Figure 4.1). As established in Section 4, the winds measured at the airport are representative of the synoptic scale winds over Tampa Bay and the nearby west Florida shelf.

Because of its central location, the ADCP station C-4 is used to characterize the circulation of the Bay. The current record at this station consists of seven deployments, each approximately two months long, which were combined with data from C-55 in order to produce a continuous central Bay time series. Small data gaps were filled by predicting tidal current velocities based on the tidal current constituents. The along-channel component ( $35^\circ$ ) of the C-4 current velocity at mid-depth in the water column (4.6 m below MLLW) will be considered.

### **Energy Density Spectra**

Energy density spectra for each time series are displayed in Figure 6.1 as a function of frequency in cycles per day (cpd). The energy density is the squared amplitude of the signal per frequency band. Wind energy (Figure 6.1a) is largest below 0.2 cpd (a period of 5 days and longer) and falls off exponentially at higher frequencies. There are sharp peaks at 1 and 2 cpd (24 and 12 hours) which are comparable in energy to the long-period winds and are due to the daily sea breeze cycle which often intensifies into afternoon thunderstorm activity in the summer. The 12-hour peak is likely to be a higher order harmonic of the 24-hour peak.

The water level spectra at Clearwater Beach and St. Petersburg (Figure 6.1b and 6.1c) are similar to each other. The diurnal (1 cpd) and semidiurnal (2 cpd) tidal frequencies are dominant features. The diurnal constituents  $K_1$  and  $O_1$  can be distinguished as separate peaks. The semidiurnal peak is somewhat smaller at St. Petersburg than at Clearwater Beach (see Table 3.1). Higher order overtones are also visible. The energy at the lowest frequencies is due to annual water level fluctuations (Figure 3.6). Between the annual and tidal frequencies, the spectra resemble the wind spectrum with relatively flat energy below 0.2 cpd ( $> 5$  days), falling off exponentially at higher frequencies.

In contrast, the current spectrum (Figure 6.1d) is relatively flat up to the semidiurnal tidal frequencies. The tidal energy peaks are the dominant features of the current spectrum. Higher order harmonics are also visible.

The water level and current spectra indicate the relative amplitudes of different frequency bands in the nontidal signal. For the water levels, the subtidal energy is significantly stronger than nontidal energy near the tidal and supertidal frequencies. In contrast, the relative flatness of the current spectrum indicates that a large part of the spectrum has comparable energy levels. Therefore, high frequency fluctuations are relatively more important in the current signal than in the water level signal.

## **Cross Spectral Analysis**

Cross spectral analysis can indicate how coherent two time series are as a function of frequency. The transfer amplitude is a measure of the ratio of one signal to another and the phase difference indicates the time lag of one signal relative to the other. Where the coherence is high, the transfer amplitude and the phase difference describe the relationship of one time series to another.

The longshore wind (along 340°) on the west Florida continental shelf can induce transport toward or away from the coast and result in the rise or fall of coastal water levels. When the longshore wind at Tampa Airport and the water level at Clearwater Beach are subjected to cross spectral analysis (Figure 6.2), the squared coherence is high in a band from 0.1 to 0.4 cpd (2.5 to 10 days). When the phase difference is converted to lag time in this band, it is relatively constant and corresponds to a 10-hour time lag of the water levels relative to the wind. This suggests that the synoptic scale longshore wind is causing subtidal water level fluctuations on the shelf. The large transfer amplitudes between longshore wind and coastal water level at the tidal frequencies should be ignored since coherence is low.

The water levels at Clearwater Beach and St. Petersburg were subjected to cross spectral analysis to determine the relationship between water levels on the Florida shelf and water levels inside Tampa Bay (Figure 6.3). The squared coherence is extremely high for all frequencies lower than the diurnal tidal frequency. Note that the coherence equals 1.0 at the diurnal and semidiurnal frequencies and that the transfer amplitude is near 1.0 at 1 cpd but falls to 0.7 at 2 cpd (compare Figures 6.1b and 6.1c). The phase difference converted to lag time of St. Petersburg relative to Clearwater Beach is about 2 hours for frequencies higher than 0.1 cpd (10 days or less) and the transfer amplitude is close to 1.0. This indicates that both tidal and subtidal water levels in Tampa Bay are driven primarily by water levels on the Florida shelf.

The fluctuation of the shelf water level induces currents in the Bay; therefore, the time derivative of the water level at Clearwater Beach and the along-channel current velocity at C-4 were subjected to cross spectral analysis (Figure 6.4). The coherence is high between 0.15 and 1 cpd (1 to 7 days). Coherence is 1.0 in the diurnal and semidiurnal tidal bands. The transfer amplitude is about 0.25 (cm/s)/(cm/day) between 0.15 and 1 cpd. Therefore, a water level change of 20 cm/day at Clearwater Beach would produce a current of 5 cm/s at C-4. The phase difference converted to lag time of the currents relative to the time derivative of water level is about 2 hours between 0.3 and 1 cpd (1 to 3.3 days). The high transfer amplitude at low frequencies should be ignored because the coherence is low. Long-term currents are driven by density gradients in the Bay and are discussed in Section 6.2.

## **Filtered Time Series**

The relationships described above can also be seen in the filtered time series plotted for 6-month periods in Figures 6.5, 6.6, and 6.7. The time series were low-pass filtered at 1.5 days (36 hours) to remove the tidal signal and higher frequency noise (Figure 6.1). The plots show the longshore

wind at Tampa Airport, water levels at Clearwater Beach and St. Petersburg, the time derivative of the Clearwater Beach water levels, and the along-channel current velocity at C-4.

All of the time series have higher amplitudes in the winter than in the summer due to a series of cold fronts from the continental United States that move southeast across Florida. The storm in the second week of November 1990 is typical (Figure 6.8). Before the passage of the front, the longshore wind is toward the north-northwest (positive values) and gradually builds to a maximum (see Figure 4.9). As the front passes through, the wind rapidly shifts clockwise toward the south-southeast (negative values) before gradually weakening. Water levels at Clearwater Beach and St. Petersburg follow a similar pattern; both signals gradually increase before the passage of the front to a high, fall rapidly to a low, and then slowly return to normal. The time derivative of water level and the current velocity also resemble each other. Small positive velocity values before and after the passage of the front indicate water entering the Bay. Strong negative velocity values during the passage of the front indicate rapid draining of the Bay.

The time series of filtered water level show that the high correlation between water levels on the shelf and in the Bay prevails throughout the year. However, the correlation between longshore wind and water level is strongest during the winter months and is weaker in the summer. Similarly, the correlation between the time derivative of the water levels on the shelf and the currents in the Bay is strong during the winter and weak in the summer.

### Prediction of the Shelf Effect

The relationship between water levels on the shelf and water levels and currents in the Bay should make it possible to predict the subtidal shelf effect on the Bay. The water level at St. Petersburg,  $h_{STP}[t]$ , and the along-channel current at C-4,  $u_{C4}[t]$ , can be related to the water level at Clearwater Beach,  $h_{CLR}[t]$ , as follows:

$$h_{STP}[t] = \alpha_h h_{CLR}[t-\tau_h] \quad (6.1)$$

$$u_{C4}[t] = \alpha_u \frac{dh_{CLR}[t-\tau_u]}{dt} \quad (6.2)$$

where  $\alpha_h$ ,  $\alpha_u$ ,  $\tau_h$ , and  $\tau_u$  are the as yet undetermined scaling factors and the time delays for water levels and currents.

To calculate the water level scaling factor  $\alpha_h$  and time delay  $\tau_h$  in a straightforward manner, the water level at Clearwater Beach was delayed by 1-hour time increments relative to St. Petersburg until the correlation coefficient obtained by linear regression reached a maximum. A more precise time delay could be obtained; however, since the data sampling interval is 1 hour and the data have been low-pass filtered at 36 hours, it is not meaningful to obtain greater precision. The

highest correlation coefficient (0.942) occurred when  $\tau_n$  was 2 hours. The scaling factor  $\alpha_n$  of the St. Petersburg water level relative to the delayed Clearwater Beach water level was 0.944.

The same procedure was used for the time derivative of water levels at Clearwater Beach and the along-channel current velocity at C-4. The highest correlation coefficient (0.713) was obtained when  $\tau_n$  was 1 hour. The scaling factor  $\alpha_n$  for the current velocity relative to the time derivative of water level was 0.230 (cm/s)/(cm/day).

Predicted water levels and currents were calculated using the time delays and scaling factors and then subtracted from the observed water levels and currents, respectively, to remove the subtidal effect of the Florida shelf (Figure 6.9). The residual water level time series at St. Petersburg is essentially flat (compare with Figures 6.5c, 6.6c, and 6.7c), indicating that other factors affecting subtidal water levels in Tampa Bay are minor.

The residual current velocity at C-4 shows a low amplitude current variation throughout the year (Figure 6.9). Although nontidal currents in winter have been greatly reduced, the currents in summer are essentially unchanged (compare with Figures 6.5e, 6.6e, and 6.7e). In particular, two events in late May and early June of 1991 appear to be unrelated to water levels on the coast.

## **6.2. DENSITY GRADIENT EFFECT**

Although Tampa Bay is vertically well mixed in salinity and temperature as shown in Section 5, there are strong horizontal gradients between the entrance and upper Bay. This is because several rivers contribute fresh water to the upper reaches of the Bay. Within the main channel, a classic estuarine circulation cell exists, so that in the mean, higher salinity water from the Gulf flows into the Bay near the bottom and lower salinity water flows out near the surface. The amount of fresh water input at the head of the Bay is expected to control the magnitude of the horizontal density gradient and, consequently, the magnitude of the density-driven flow.

To investigate the density-driven flow, the long-term current at C-4 was examined. Vertical profiles of the mean current for each deployment were obtained by vector averaging the observations in each 1-m bin. A continuous central Bay time series at 7 m below MLLW was created by combining the seven deployments at C-4 with one deployment at C-55. This depth was chosen because it is the deepest level common to all the deployments and the density-driven flow should be stronger near the bottom. A 15-day, low-pass filter was applied to the time series to remove the tides and storms.

Several deployments of the conductivity-temperature-depth (CTD) sensors near the entrance to Tampa Bay (at C-2, C-56, C-20, and C-21) were "blended" to construct a time series of near-bottom density at the mouth of the estuary as follows: if simultaneous records were available, the 10-min values of density were averaged; otherwise, the time series were merely appended. Small data gaps (< 3 hours) were filled by linear interpolation. In spite of the use of data from several stations, large data gaps still existed. A similar series for the head of the Bay was

constructed using data from S-3, S-4, C-46, C-31, and C-27. The two resulting series were then subtracted to obtain a time series of mouth-to-head density difference. A 15-day, low-pass filter was applied to the density difference time series to facilitate comparison with the current record.

### **Observed Long-Term Current**

Analysis of the mean current structure over depth shows that a classic estuarine circulation system is established in the central portion of the Bay. The mean current flows out of the Bay near the surface and into the Bay at depth (Figure 6.10a). The strength of this system varies over time; a weak flow was present during the winter (January-February, 1991), while the summer of 1991 (August-September, 1991) showed the strongest flow observed.

The 15-day low-pass-filtered current speed at 7 m depth (within the upper portion of the deep return flow layer) shows significant monthly and seasonal scale variability over the 16-month observation period (Figure 6.11). The speed increased during the late summer of 1990, decreased to a low near zero in the spring of 1991, and then increased to the maximum observed in September 1991.

Estuarine circulation is known to be driven by horizontal density gradients. Weisburg and Williams, (1991), investigated this relationship in Tampa Bay. Although the Bay receives relatively little freshwater compared to its tidal prism, strong head-to-mouth density gradients are observed. The seasonal variation of the along-channel salinity gradient (synonymous with density due to temperature homogeneity) was presented in Section 5. A continuous time series of density is not available at the head of Tampa Bay (in Hillsborough Bay) or at the mouth; however, some trends are still evident. The density difference increased during the summer of 1990, was minimum in the winter, and then increased to the maximum observed in the late summer of 1991 (Figure 6.12). High river discharge in late July and early August 1991 resulted in the large head-to-mouth density gradient observed at that time (Figure 6.13).

Both the mean current and density difference time series (Figures 6.11 and 6.12) show comparable annual and interannual signals, although times of the extrema are different for the two records. The maximum current appears to lag the maximum density difference by approximately 15 days. Since application of correlation techniques is not possible because of the large data gaps in density difference, another means of determining the relationship between the series is required. The following section will present a method for predicting the characteristics of the density-driven current, given a horizontal density gradient.

### **Model/Data Comparison**

A simplified version of the equations of motion was used to investigate whether the density gradients observed could cause the observed mean current vertical profile. Prandle (1991) developed an expression for density-driven currents by balancing the horizontal pressure gradient force with the along-axis frictional force. A constant eddy viscosity and a vertically homogeneous horizontal density gradient were assumed. Shear stress was zero at the surface and

defined by a linearized bed-friction formula at the bottom. An expression for density-driven flow ( $U_M$ ) as a function of depth results:

$$U_M = \frac{g}{\rho} \frac{\partial \rho}{\partial x} \frac{D^2}{ku} \left( \frac{-z^3}{6} + 0.27z^2 - 0.04z - 0.03 \right) \quad (6.3)$$

Where:

- $U_M$  = the density-driven current speed,
- $g$  = the acceleration due to gravity,
- $D$  = water depth,
- $u$  = tidal current amplitude,
- $z$  = height above bottom,
- $\rho$  = the average density,
- $\frac{\partial \rho}{\partial x}$  = the head-to-mouth density gradient, and
- $k$  = the non-dimensional eddy viscosity, ( $k = K_z / Du$ ) .

Based on the data, three values of along-channel density gradient were used in the above expression to simulate the hydrographic conditions in the summer of 1990, the intervening winter, and the summer of 1991 (0.0014, 0.0006, and 0.0029 kg/m<sup>4</sup>, respectively). In Equation 6.3 a channel depth  $D$  of 15 m, a mean tidal current amplitude  $u$  of 35 cm/s, and a non-dimensional eddy viscosity  $k$ , equivalent to a dimensional  $K_z \sim 2 \times 10^{-2}$  m<sup>2</sup>/s (Prandle, 1985), were used for all of the calculations. The resulting flow is relatively weak (2 cm/s at the surface) for the winter density gradient and is larger for both the summer values, with 12 cm/s at the surface in 1991 (Figure 6.10b).

The modeled profiles of velocity are similar to those observed at mid-Bay (Figure 6.10a); the current flows out near the surface and in at depth. Both sets of profiles exhibit a similar order-of-magnitude seasonal variation. The modeled profiles reverse from inflow to outflow at a deeper depth than the observed profiles. This difference may result from several of the model assumptions. One of the most significant oversimplifications is the vertically constant eddy viscosity. Eddy viscosity likely varies significantly over the depth of an estuary (Pritchard, 1958). Other possible contributing factors include the assumptions of no stress at the surface and a constant-depth Bay. In actuality, the Bay is broad and shallow with a deep navigation channel in the center. The inflow may be confined to the channel, while the outflow returns unrestricted both in the channel and along the sides of the Bay. Comparison of mean current profiles at two stations near mid-Bay provides evidence for horizontal variability of the flow reversal depth (Figure 6.14). At C-55, close to the main navigation channel, the mean flow is predominantly into the Bay. However, a mean outflow is observed at C-52, located nearer to the Bay shore.

Seasonal variation in the strength of the observed long-term along-channel current results from changes in the strength of the along-channel density gradient. This density gradient is established by freshwater discharge into Tampa Bay.

### **6.3. PREDICTABILITY OF CURRENTS AND WATER LEVELS**

Two forcing mechanisms have been identified as contributing to the nontidal circulation in Tampa Bay: subtidal water level fluctuations on the continental shelf and horizontal density gradients within the Bay. The subtidal shelf effect on the water levels at St. Petersburg and on the current at C-4 was calculated using Equations 6.1 and 6.2. The density gradient effect on the current at C-4 was calculated using Equation 6.3. The following discussion quantifies the effect of these two forces during TOP to provide a view of seasonal and interannual variability and the relative strength of each signal.

#### **Currents**

For the currents at mid-Bay (C-4), the monthly rms value of five time series are plotted in Figure 6.15. The time series are:

- (a) the total observed current,
- (b) the residual after subtraction from (a) of the harmonically predicted tidal current,
- (c) the residual after subtraction from (b) of the subtidal shelf effect (Equation 6.2),
- (d) the residual after subtraction from (c) of the density-driven effect (Equation 6.3), and
- (e) time series (d) after 36-hour low-pass filtering.

The monthly root mean squared (rms) value is used to estimate the reduction in variability achieved by removing the effects of tidal forcing, the subtidal shelf influence, and the horizontal density gradients in the Bay. Since the long-term mean current is a portion of the subtidal signal which has physical significance, the rms value was chosen as a representative statistic to combine the monthly mean current with the variability during the month.

The greatest reduction in variability at C-4 was achieved by removing the predicted tidal currents. According to Table 2.5, the standard deviation of the residual current at C-4 is 25.8% of the standard deviation of the observed current; the rms values in Figure 6.15 show about the same ratio with some small variations from month to month. The weakest nontidal currents were in August 1990 and the strongest nontidal currents were in September 1991 (line B).

Removing the subtidal shelf effect produces a relatively small reduction in rms velocity which is visible only in the winter months of November, December, January, and February (line C). This is consistent with the passage of strong winter storms which cause rapid changes in the water level on the shelf (see Section 6.1).

A further reduction in rms velocity is obtained after the removal of the density-driven effect. This reduction is mainly visible in the summer months of June, July, August, and September,

1991 when large head-to-mouth density gradients were observed in the Bay (line D). Note that there are no rms values for September and October 1990 due to a gap in the density-gradient data (Figure 6.12). The low values for the 36-hour, low-pass-filtered current shows that much of the remaining variability results from high-frequency forcing which was not included in the calculations of the shelf and density-driven effects (line E of Figure 6.15).

Seasonal variations in some of the tidal current constituents were noted in Section 2.2. The two constituents which show the most variation are  $S_2$  and  $K_1$ , the periods of which are closest to 12 and 24 hours, respectively. A portion of this seasonal change may be related to variations in the intensity of sea breezes (Section 4.3). The windfield at Tampa Airport was divided into 60-day periods, and clockwise and counterclockwise rotary spectra were obtained for each period. There were sharp peaks at 12 and 24 hours, and the clockwise component was significantly larger than the counterclockwise component. The magnitude of the 12 and 24 hour clockwise wind components are plotted in Figure 6.16 to provide an estimate of the sea breeze intensity during the year. The strongest sea breezes occurred during March and April while the weakest sea breezes occurred during November and December.

The variation of the 24-hour and 12-hour clockwise sea breeze components bears a strong resemblance to the variation of the amplitude of the  $K_1$  and  $S_2$  constituents in Figure 2.8. The residual rms value after the removal of currents due to tidal forcing, subtidal shelf water levels, and density gradients (line D in Figure 6.15) also resembles the 24-hour clockwise sea breeze component variation. Line D peaks in April of 1991 and is lowest in August and December of 1990. There were no values for September and October of 1990. This evidence suggests that sea-breeze-induced currents are a significant part of the nontidal current. These residual current variations are likely caused by small-scale storms and other direct wind effects on the Bay which, due to their sporadic nature, are difficult to quantify.

## Water Levels

The monthly standard deviation of three water level time series are plotted in Figure 6.17. The time series are:

- (a) the total observed water level,
- (b) the residual after subtraction from (a) of the harmonically predicted tidal levels, and
- (c) the residual after subtraction from (b) of the subtidal shelf effect (Equation 6.1).

The standard deviation from the monthly mean is used to estimate the reduction in variability achieved by removing the effects of tidal forcing and the subtidal shelf influence. The standard deviation from the monthly mean was picked as a representative statistic because the mean water level is a function of gage height and has no physical significance until it is referenced to a geodetic benchmark. Furthermore, any long-term drifts between the coastal station and the station in the Bay are eliminated.

The reduction in variability achieved by removing predicted tidal levels varies greatly during the year. According to Table 3.5, the residual standard deviation at St. Petersburg was 43.1% of the

observed standard deviation. Figure 6.17 shows that much of the residual variability occurred during the winter months from November to April (line B). The greatest nontidal signal was in March 1991 and the smallest nontidal signal was in June 1990.

When the subtidal shelf effect is removed (line C), the monthly standard deviations are reduced for every month with the greatest reductions for the winter months. The remaining variability is relatively constant during the year and is primarily due to low-frequency forcing, perhaps a result of direct wind stress on the Bay. In general, the physical system governing water levels is less complicated than that for currents, making it easier to understand the nontidal water level signal.

#### **6.4. CONCLUSIONS**

Significant nontidal signals were present in the water levels and currents recorded during TOP. Spectral analysis shows which frequencies are prominent in the nontidal signals. The water level spectra showed that subtidal energy levels (periods > 1 day) are greater than nontidal energy levels near the tidal and supertidal frequency bands. In contrast, the current spectrum showed that high frequency nontidal energy is as large as the subtidal energy. The water level fluctuations on the continental shelf and the horizontal density gradients in the Bay were quantified as subtidal driving forces. The subtraction of the shelf effect resulted in a large reduction in variability of the water level signal at St. Petersburg, especially during the winter months. A smaller reduction in variability during the winter months was observed when the shelf effect was subtracted from the current signal at C-4. The subtraction of the density-driven current resulted in a significant reduction in variability during the summer of 1991 when a strong head-to-mouth density gradient was present in the Bay. Further reduction in the variability of the residual current signal requires the quantification of the direct wind stress effect on the Bay.

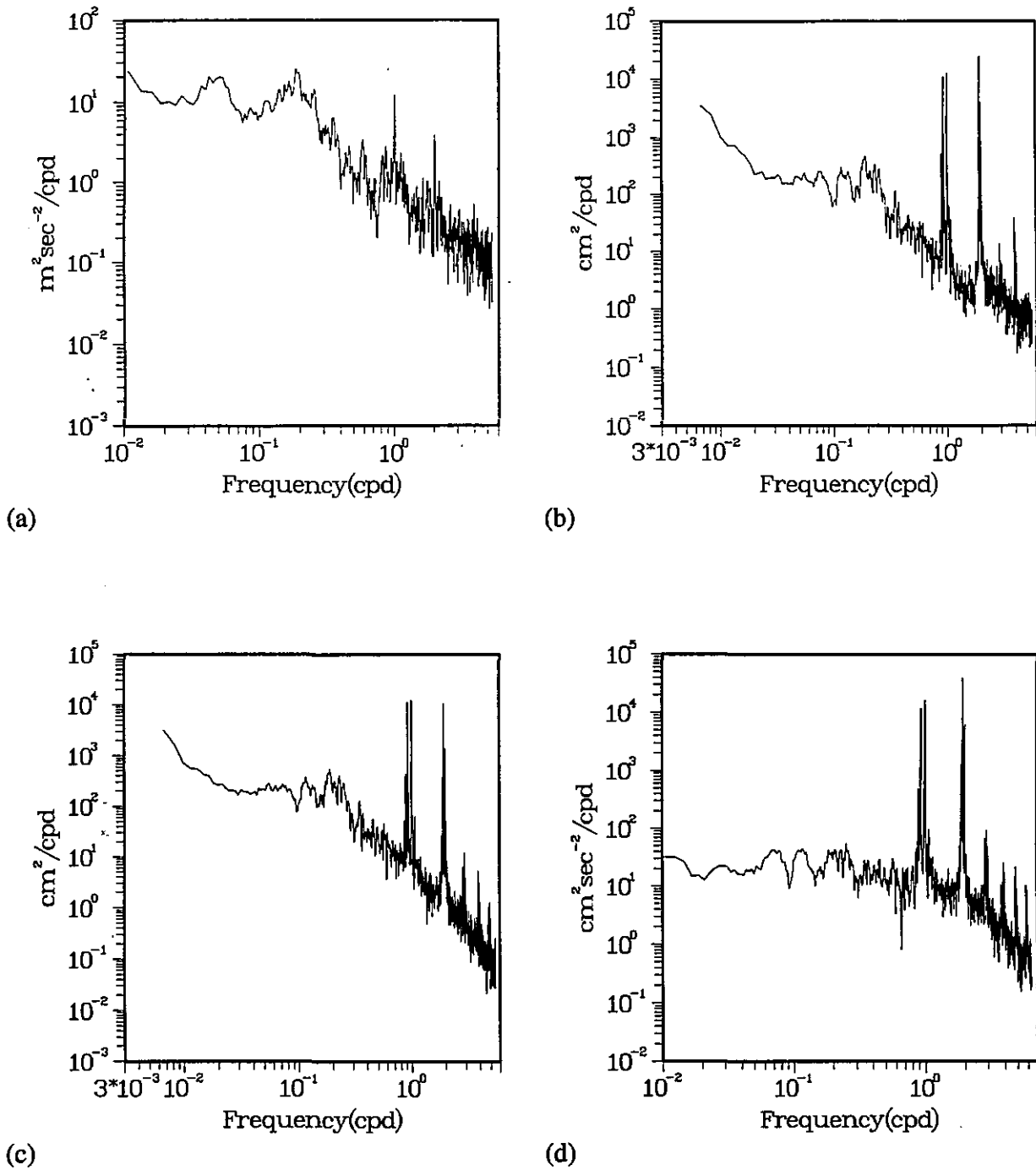


Figure 6.1. Energy density spectra of: (a) longshore wind (m/s) along  $340^\circ$  at Tampa Airport (TPA); (b) water level (cm) at Clearwater Beach; (c) water level (cm) at St. Petersburg; and (d) current along  $35^\circ$  at C-4. The bandwidth is 0.0027 cpd for (a), 0.0017 cpd for (b) and (c), and 0.0021 cpd for (d).

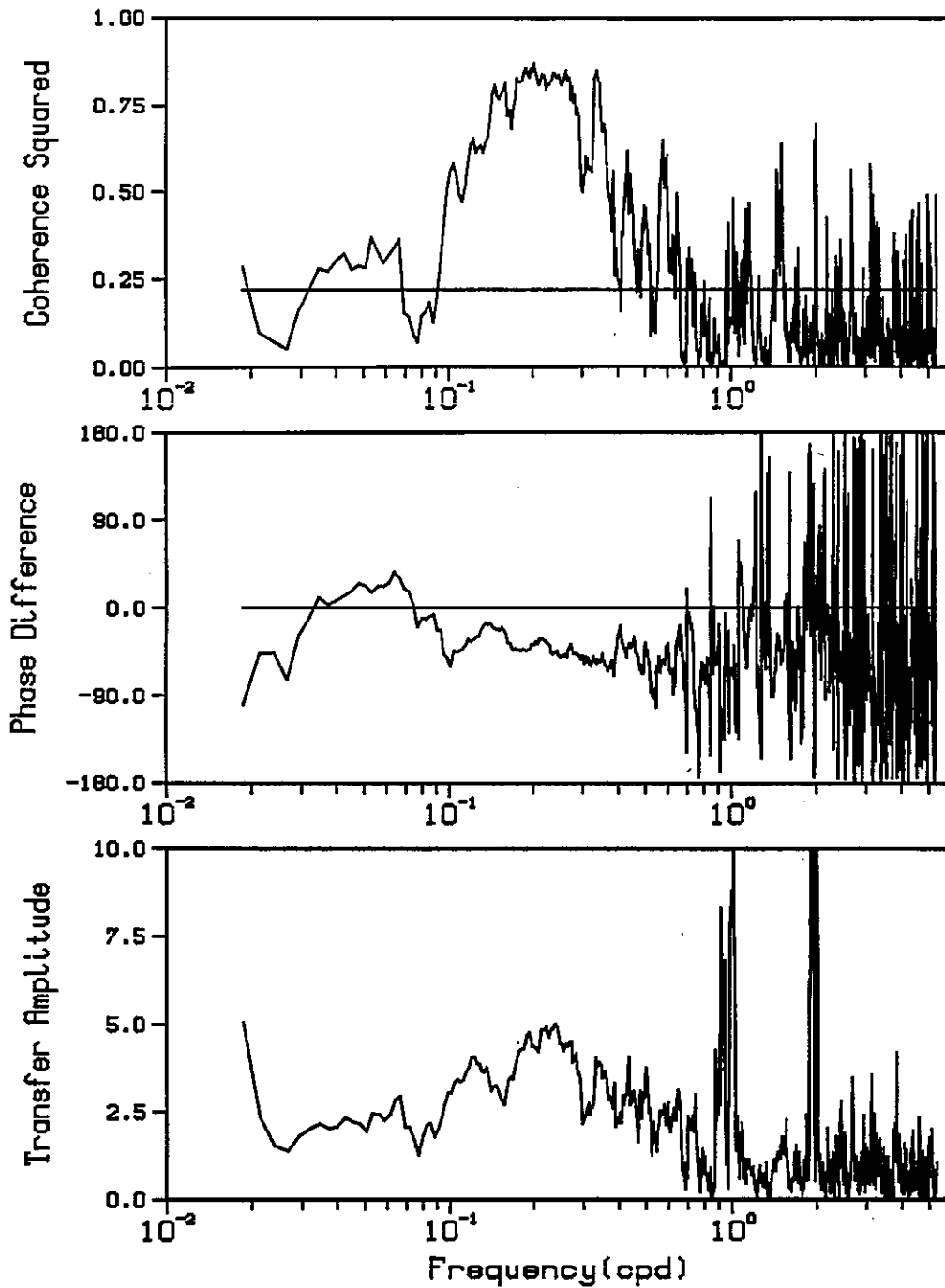


Figure 6.2. Results of cross spectral analysis between longshore wind (m/s) along  $340^\circ$  at Tampa Airport (TPA) and water level (cm) at Clearwater Beach (E-724). The figure shows coherence squared (with the 95% significance level), phase difference ( $^\circ$ ) [TPA - E-724], and transfer amplitude [E-724/TPA] in (cm)/(m/s). The bandwidth is 0.0027 cpd.

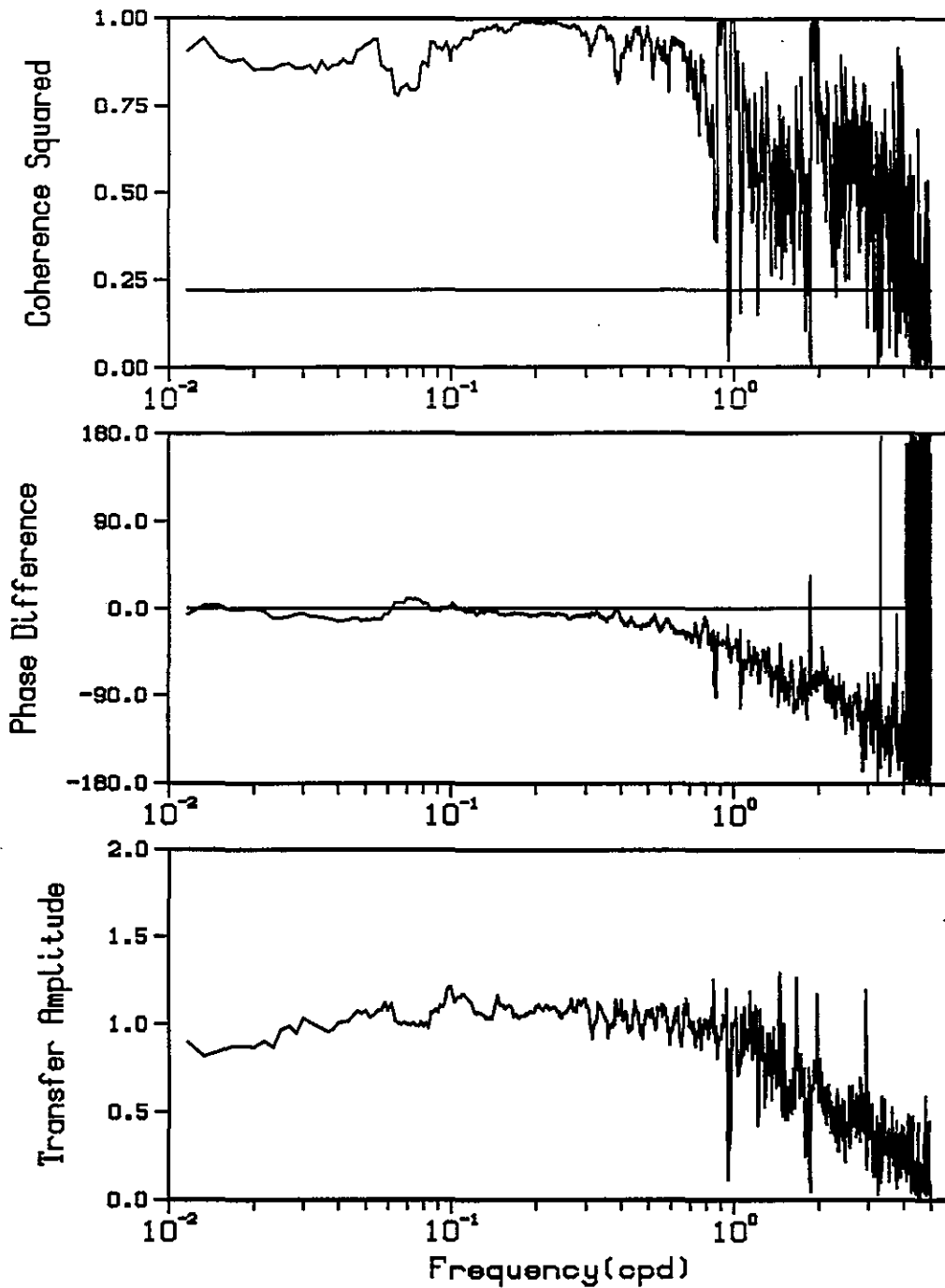


Figure 6.3. Results of cross spectral analysis between water level at Clearwater Beach (E-724) and water level at St. Petersburg (E-520). The figure shows coherence squared (with the 95% significance level), phase difference ( $^{\circ}$ ) [E-724 - E-520], and transfer amplitude [E-520/E-724] in (cm)/(cm). The bandwidth is 0.0017 cpd.

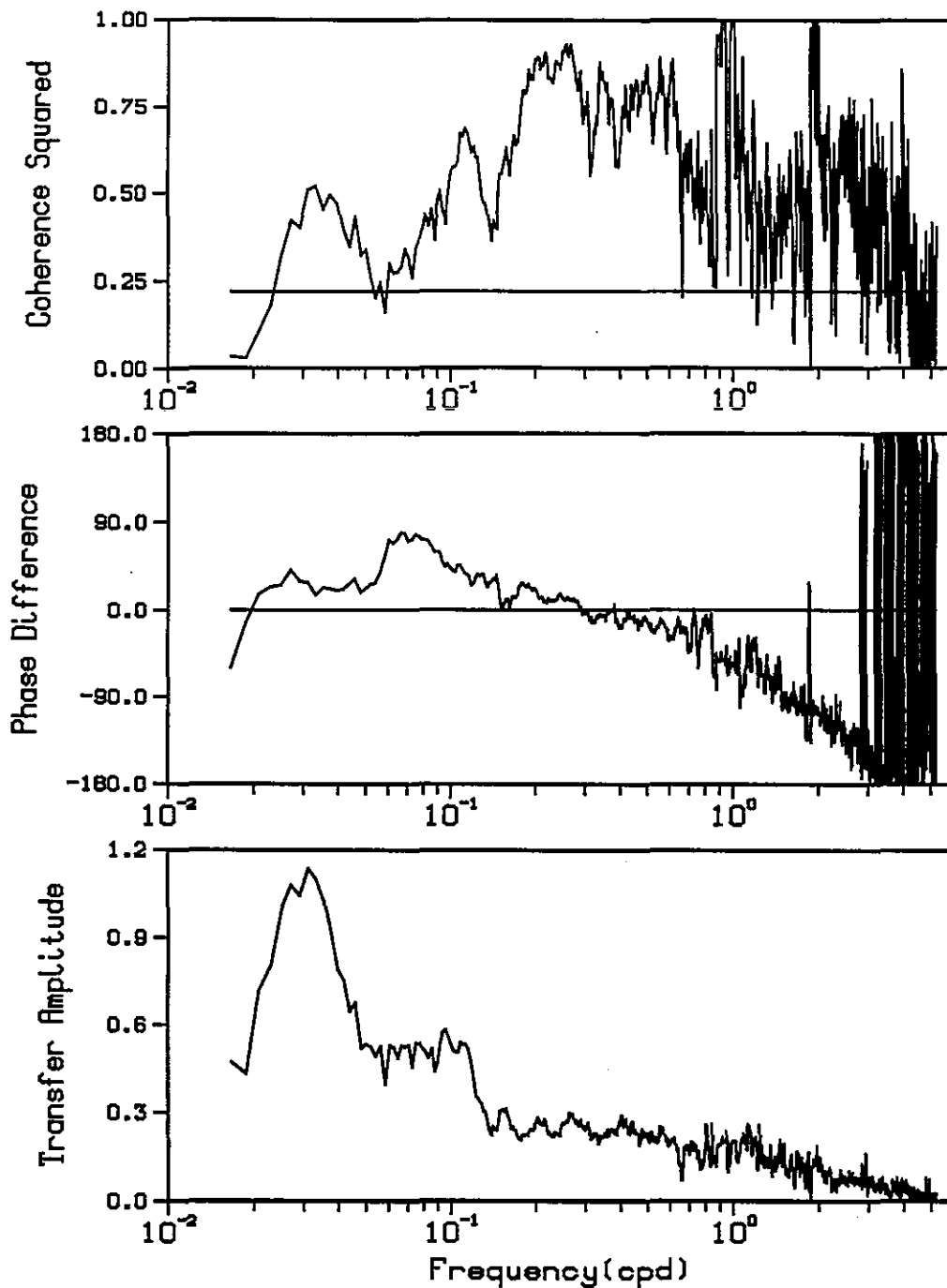
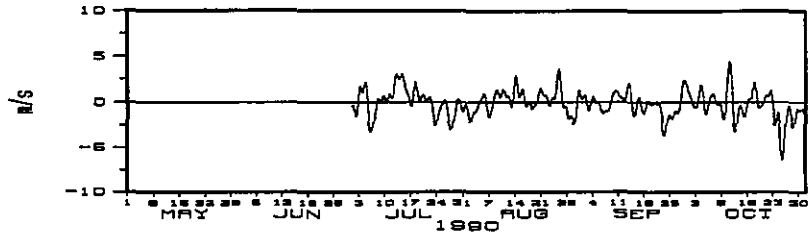
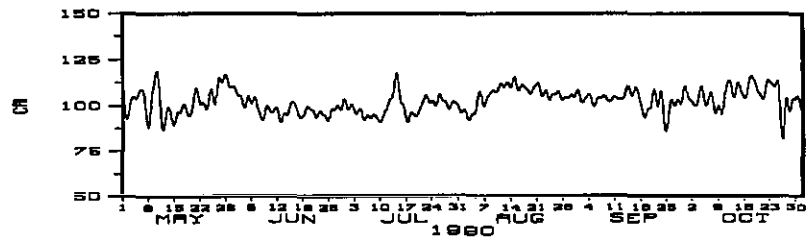


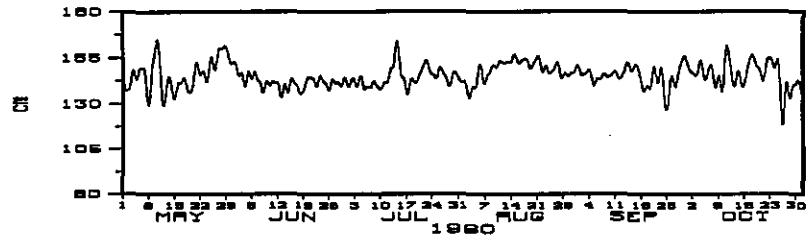
Figure 6.4. Results of cross spectral analysis between time derivative of water level (cm/day) at Clearwater Beach (E-724) and current velocity (cm/s) along  $35^\circ$  at C-4 in Tampa Bay. The figure shows coherence squared (with the 95% significance level), phase difference ( $^\circ$ ) [E-724 - C-4], and transfer amplitude [C-4/E-724] in (cm/s)/(cm/day). The bandwidth is 0.0021 cpd.



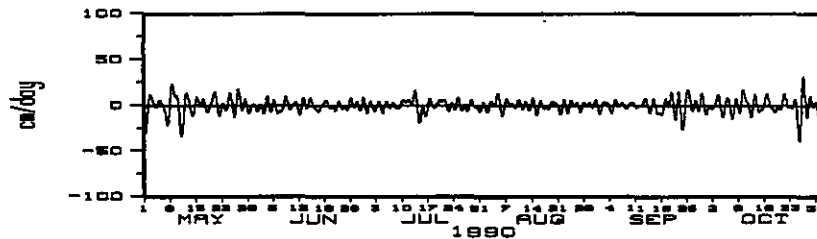
(a)



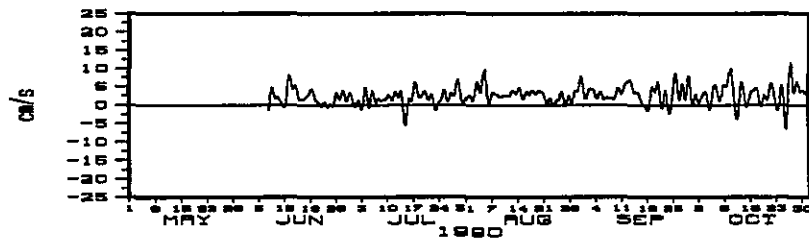
(b)



(c)

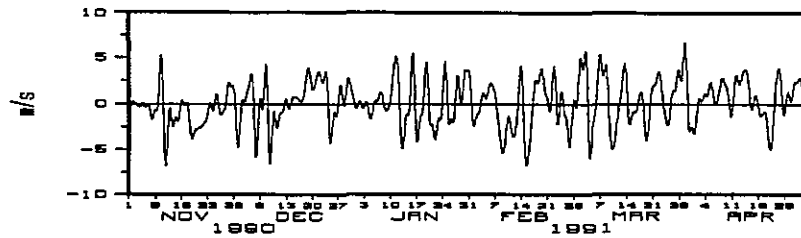


(d)

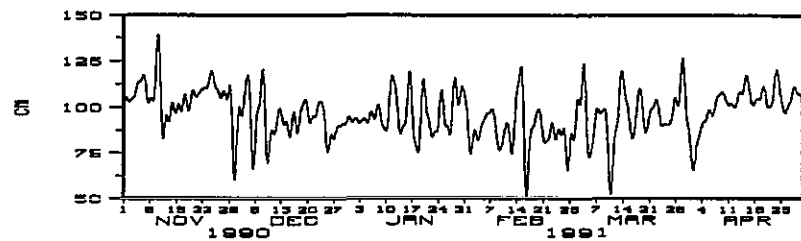


(e)

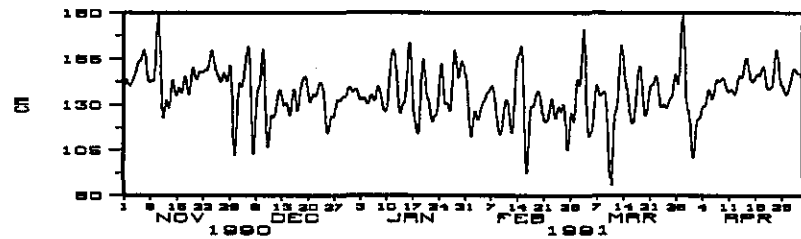
Figure 6.5. 36-hour low-pass filtered time series for summer 1990 -- (a) longshore wind ( $340^\circ$ ) at Tampa Airport, (b) water level at Clearwater Beach, (c) water level at St. Petersburg, (d) time derivative of water level at Clearwater Beach, and (e) current along  $35^\circ$  at C-4.



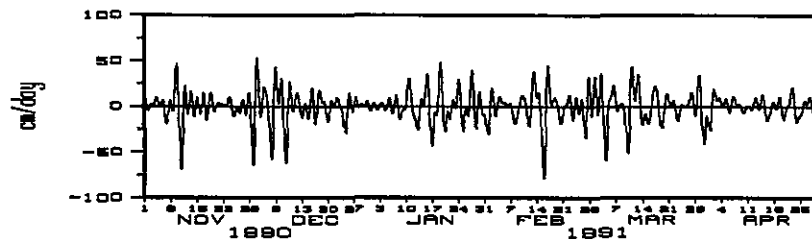
(a)



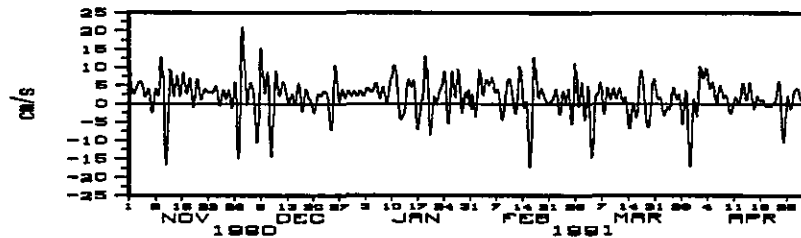
(b)



(c)

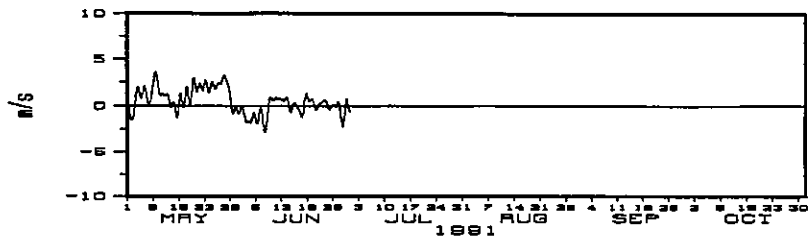


(d)

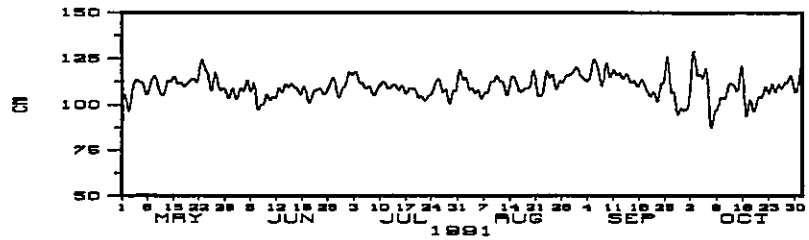


(e)

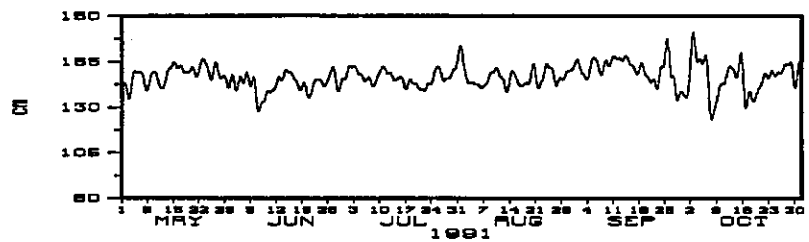
Figure 6.6. 36-hour low-pass filtered time series for winter 1991 -- (a) longshore wind (340°) at Tampa Airport, (b) water level at Clearwater Beach, (c) water level at St. Petersburg, (d) time derivative of water level at Clearwater Beach, and (e) current along 35° at C-4.



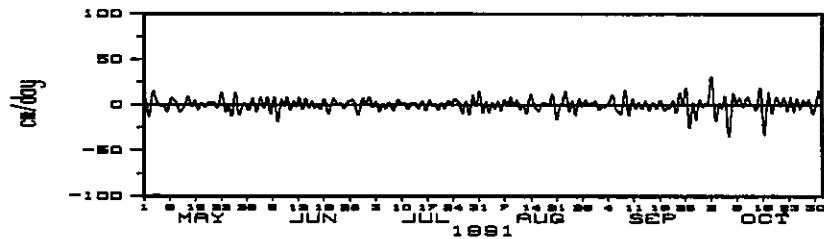
(a)



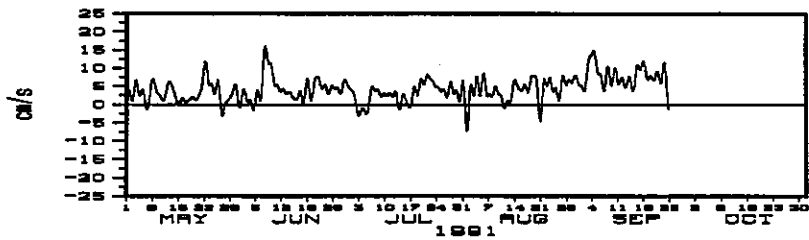
(b)



(c)

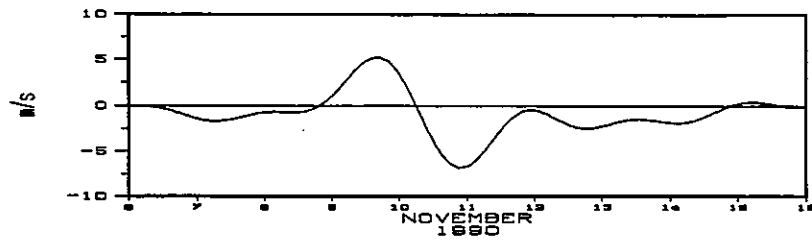


(d)

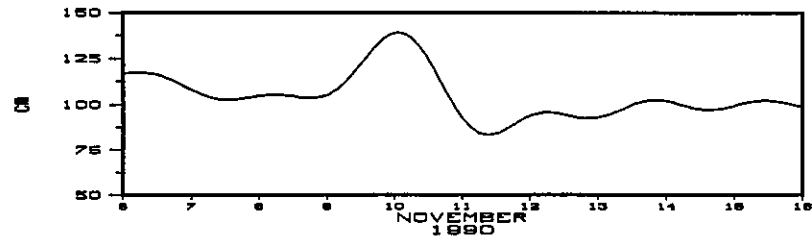


(e)

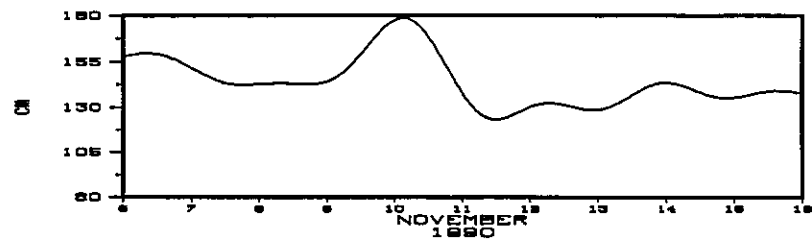
Figure 6.7. 36-hour low-pass filtered time series for summer 1991 -- (a) longshore wind ( $340^\circ$ ) at Tampa Airport, (b) water level at Clearwater Beach, (c) water level at St. Petersburg, (d) time derivative of water level at Clearwater Beach, and (e) current along  $35^\circ$  at C-4.



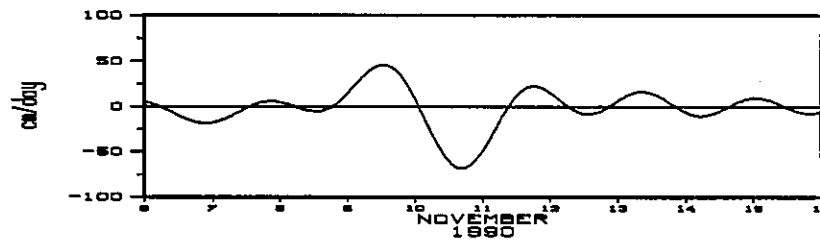
(a)



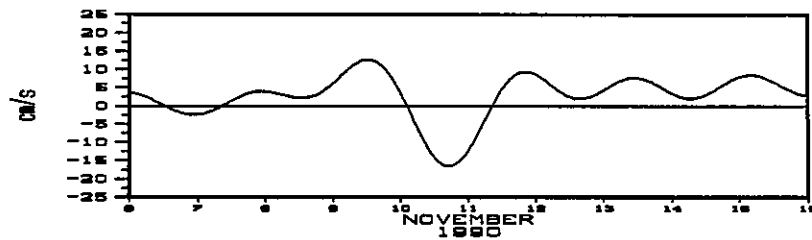
(b)



(c)



(d)



(e)

Figure 6.8. 36-hour low-pass filtered time series during a storm on November 9-11, 1990 -- (a) longshore wind ( $340^\circ$ ) at Tampa Airport, (b) water level at Clearwater Beach, (c) water level at St. Petersburg, (d) time derivative of water level at Clearwater Beach, and (e) current along  $35^\circ$  at C-4.

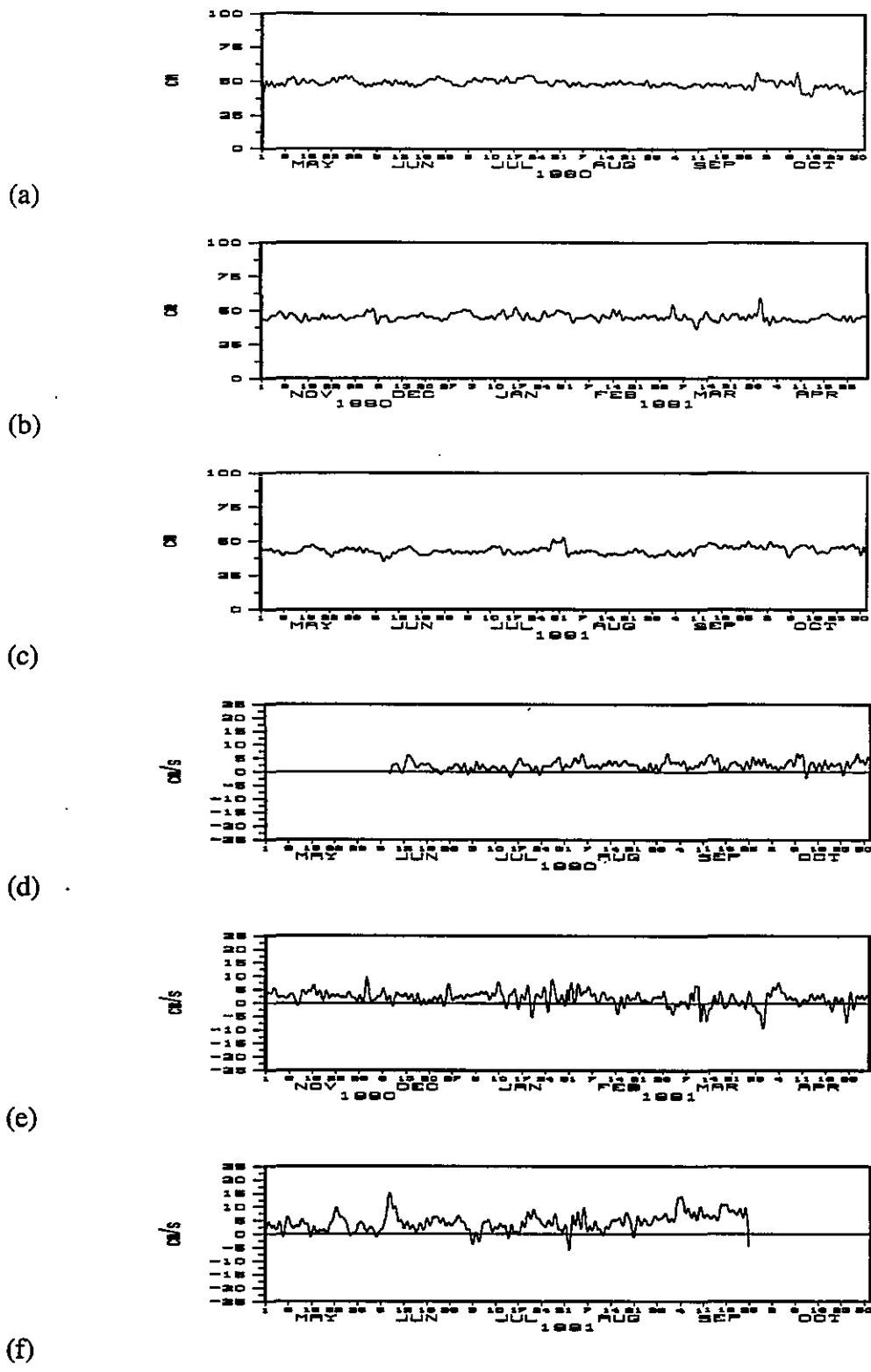
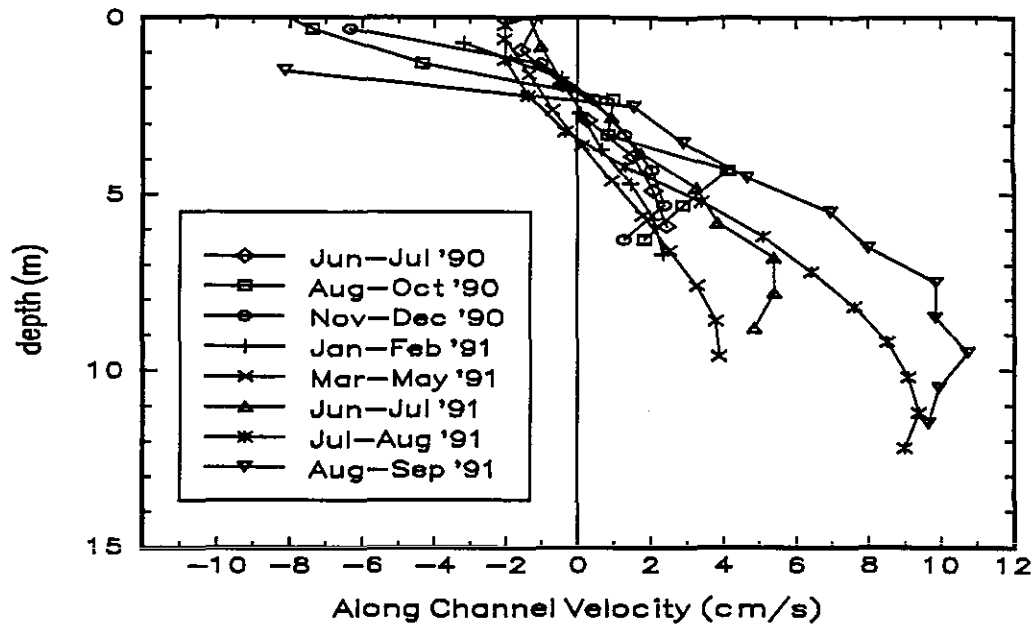
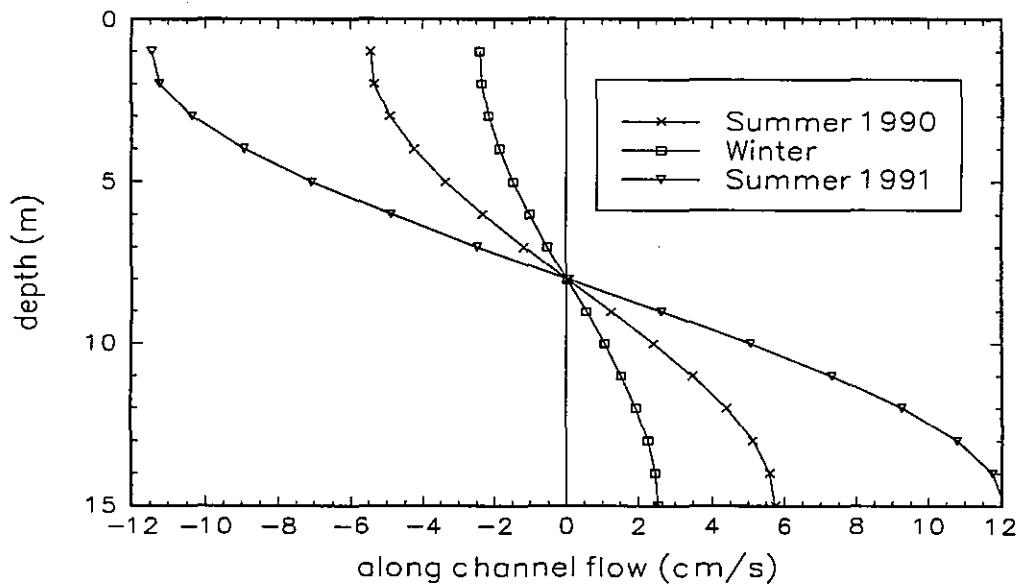


Figure 6.9. Water levels at St. Petersburg after subtraction of shelf effect for (a) summer 1990, (b) winter 1991, and (c) summer 1991. Current at C-4 after subtraction of shelf effect for (d) summer 1990, (e) winter 1991, and (f) summer 1991.



(a)



(b)

Figure 6.10. Vertical profiles of along-channel currents at mid Bay. (a) Deployment averaged velocity. (b) Modeled density-driven flow (from Equation 6.3). Seasonal variations in the strength of the mean current (a) can be understood by comparing Figures 6.11 and 6.12.

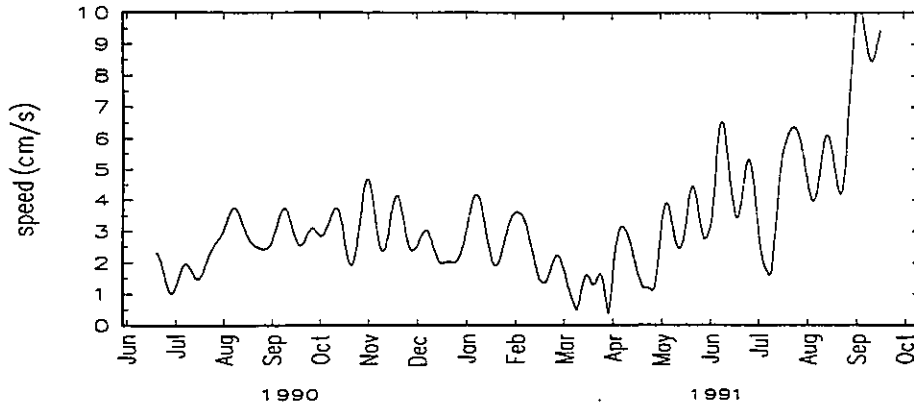


Figure 6.11. The mid Bay long-term current at C-4. The current speed at 7 m depth (in the upper portion of the deep return flow) was 15-day low-pass filtered to obtain this record.

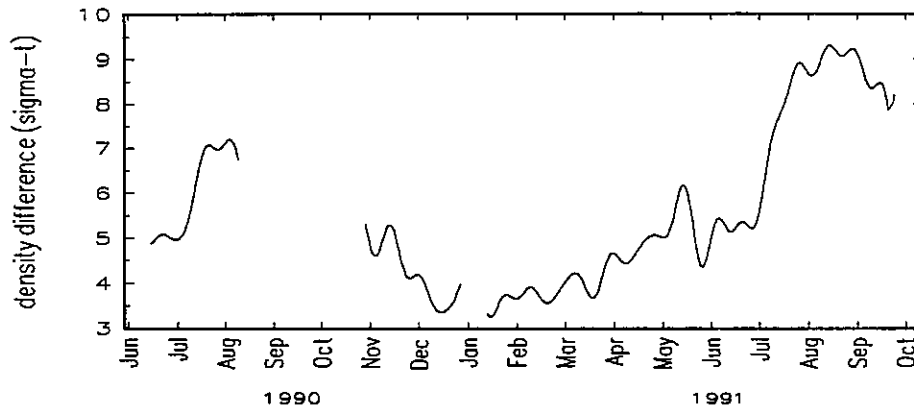


Figure 6.12. Density difference from the mouth to the head of Tampa Bay after 15-day, low-pass filtering.

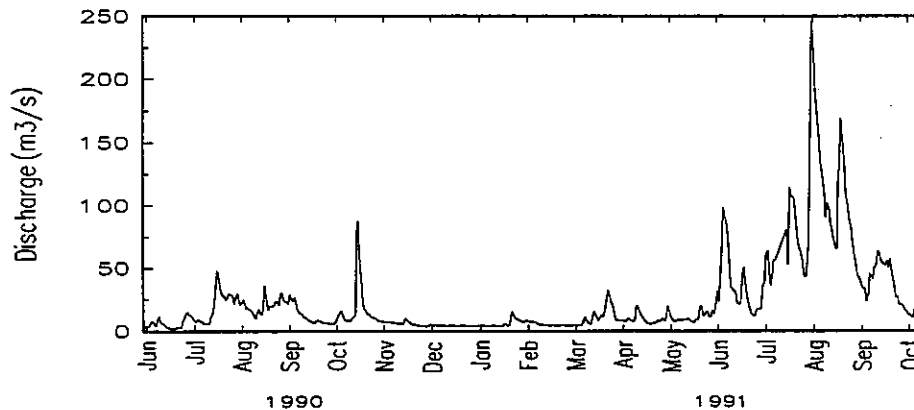


Figure 6.13. Total river discharge into Tampa Bay.

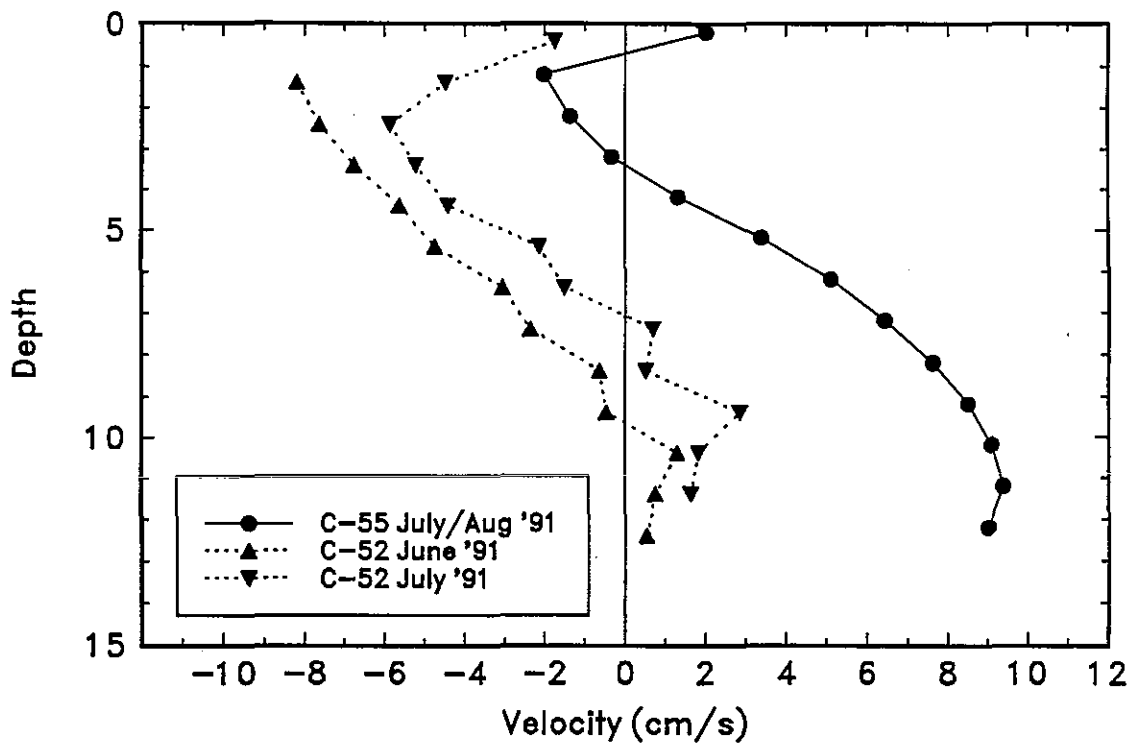


Figure 6.14. Comparison of the mean along-channel flow at mid-Bay stations (the velocities at each station were rotated to 35°). Notice that at C-55, which is closer to the main channel, the depth of current reversal is approximately 3 m; however, at C-52 which is shoreward of the main channel, the mean current changes direction closer to 8 m.

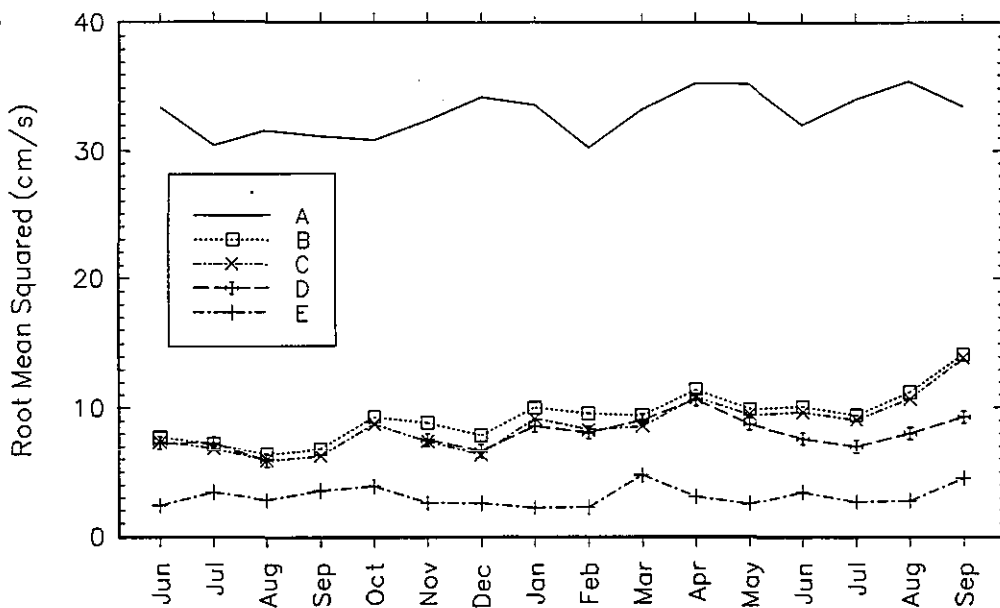


Figure 6.15. Reduction of variance in currents at mid Bay. Monthly root mean squared values are displayed. Time series A = the total observed current, B = A - the harmonically predicted tidal current, C = B - the subtidal shelf effect, D = C - the density-driven effect, and E = (D) 36-hour low-pass filtered.

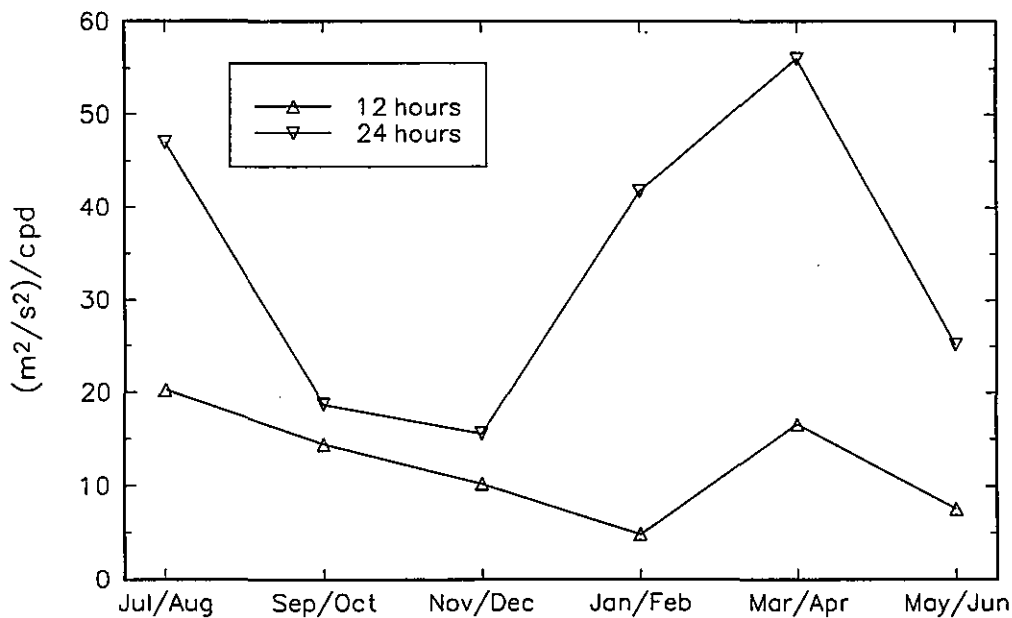


Figure 6.16. Diurnal and semidiurnal energy in the windfield at Tampa Airport. The 12- and 24-hour clockwise components of the rotary spectrum for 60-day periods are displayed. The frequency bandwidth was 0.0167 cpd.

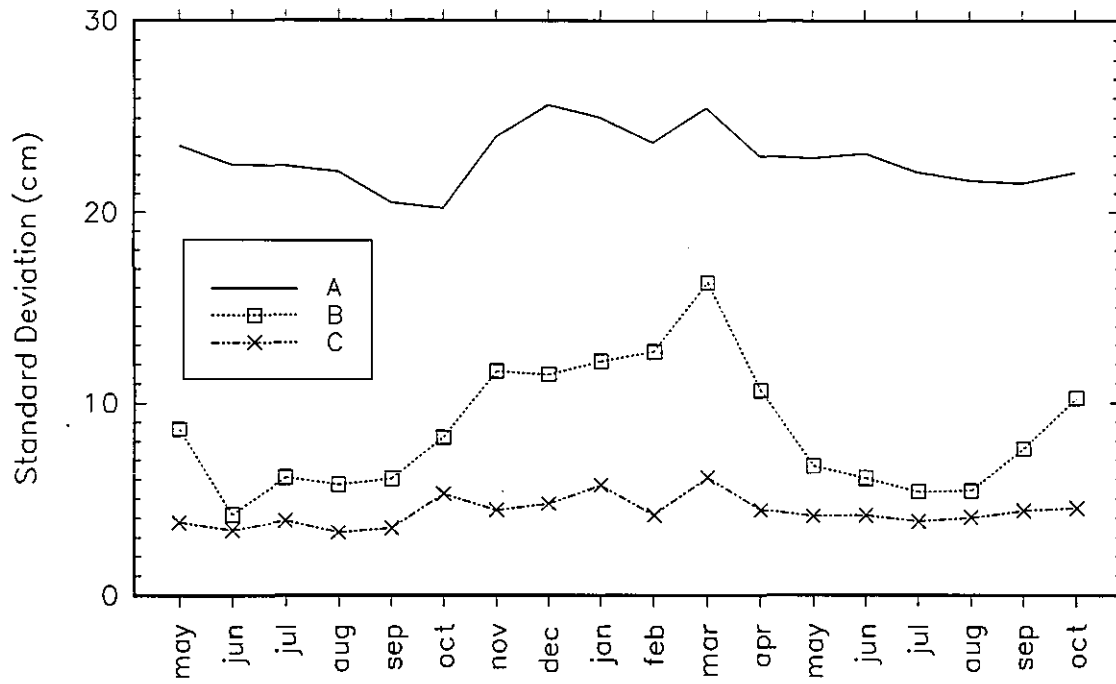


Figure 6.17. Reduction of variance in water levels at St. Petersburg. Monthly standard deviations from the mean are displayed. Time series A = the total observed water level, B = A - the harmonically predicted tidal water level, and C = B - the subtidal shelf effect.

## 7. MODELED HYDRODYNAMICS

Kurt W. Hess

### 7.1. INTRODUCTION

TOP included the development and application of a three-dimensional circulation model to Tampa Bay. The model can be a powerful tool for understanding and quantifying the Bay's dynamics, especially when used to isolate the Bay's response to specific forcing (tides, winds, or buoyancy), and in unifying the observational data by filling in spatial and temporal gaps. It was used in this synthesis to (1) estimate the Bay's natural period to attempt to find it in the current and water level spectra, (2) characterize tidal response by identifying regions of high velocities, (3) develop a more complete picture of the distribution of tidal constituent amplitudes and epochs, (4) estimate the amplitude of direct wind setup and the associated current, (5) enhance the description of salinity distribution, and (6) quantify the buoyancy current field.

The Princeton three-dimensional numerical circulation model (Blumberg and Mellor, 1987; Mellor, 1990) was applied to the Bay to produce water levels and profiles of currents and salinity at numerous locations throughout the Bay. The model has been calibrated and validated for total current and water level (Hess and Bosley, 1992) and calibrated for tidal constituents (Hess, 1993).

### 7.2. MODEL FORMULATION

The Princeton three-dimensional numerical circulation model (Blumberg and Mellor, 1987) has been successfully used in several previous studies of estuaries by numerous investigators and was adapted to the Tampa Bay study. The model includes a dimensionless sigma vertical coordinate, the level 2-1/2 turbulence closure representation, and an orthogonal curvilinear horizontal coordinate system. Since significant horizontal salinity gradients and vertical gradients in the horizontal current have been observed in Tampa Bay during the NOS survey, it is important that the model have variable density and be capable of simulation in three dimensions.

The model solves the equations of fluid motion (momentum balance, mass conservation, equation of state, salt conservation, and hydrostatic balance) at all cells in the three-dimensional grid. Salinity varies spatially and temporally but temperature, which has only a minor effect on density, is assumed to be a constant 30°C. The equations are recast in general orthogonal, curvilinear horizontal coordinates and are further transformed using a dimensionless vertical (sigma) coordinate. The code is structured to take advantage of high-speed vector processing.

The Tampa Bay model runs on an orthogonal curvilinear grid closely fitted to the Bay's lateral boundaries (Figure 7.1). A grid mesh with a total of 2,400 land and water cells was filled with depth values from bathymetric data files for Tampa Bay obtained from NOAA's National Geo-

physical Data Center in gridded (15-second interval) format. Water cell sizes range in length from 0.137 km to 4.189 km and in area from 0.068 km<sup>2</sup> to 5.39 km<sup>2</sup>.

## Boundary Conditions

All numerical model simulations require driving forces (water levels, river discharges, winds) that are applied at the open boundaries. The open boundaries on the west Florida shelf are denoted as the deep water, the up-shelf, and the down-shelf boundaries (Figure 7.1), and each cell along the boundary requires a water level value and salinity values at all vertical levels at each model time step. The river boundaries require discharge and salinity values. The wind is applied at the surface of all cells. At the closed boundaries there is zero momentum and salt transfer. At present there is no connection to Sarasota Bay or to Boca Ciega Bay north of Pinellas Bayway.

Forcing water levels at the model's deep-water, up-shelf, and down-shelf boundaries are prescribed by either a time series of equally spaced values or an analytic expression for variation over time. A time series of values during the TOP survey is available from a pressure transducer fixed to a bottom-mounted ADCP unit positioned approximately 8 km west of the entrance to Tampa Bay at C-1 (Figure 2.1). The deep-water salinity boundary condition at ebb is determined from the interior field by a simple advective equation with upstream differencing, and at flood is determined by advection from given reservoir values.

River flow data consist of daily values for several major rivers measured by the U.S. Geological Survey and adjusted to reflect ungaged portions of the watershed (Flannery, 1989). The Hillsborough, Palm, Alafia, Little Manatee, and Manatee Rivers plus several smaller tributaries (Table 4.3) were used in the simulation. Salinity in the rivers is set to 0 psu.

Winds at the real-time site, M-2, were used to estimate the wind stress for the entire Bay. The wind stress,  $\tau_s$ , is based on a drag coefficient,  $C_d$ , which is a function of wind speed,  $V$ , at 10 m above the water:

$$\frac{\tau_s}{\rho} = rC_d V^2 \quad (7.1)$$

where  $\rho$  is water density,  $r$  is the ratio of air density to water density ( $1.225 \times 10^{-3}$ ), and

$$C_d = 1.2 \times 10^{-3} \quad \text{for } V < 11 \quad (7.2a)$$

$$C_d = 0.49 \times 10^{-3} + 6.5 \times 10^{-5}V \quad \text{for } V \geq 11 \quad (7.2b)$$

Net precipitation and evaporation are neglected.

## Model Accuracy

The model has been calibrated and validated for total current and water level and calibrated for tidal constituents. Results from model validation for total water levels and currents at a limited number of stations from a 10-day run including tides, winds, and freshwater discharges are discussed in Hess and Bosley (1992). In that study, statistics were compiled for each station for time series (hourly values for water levels and 10-min values for currents) and for extrema (high and low tide or flood and ebb) and the results for all stations were combined into global statistics. For demeaned hourly water levels, rms amplitude differences between modeled and observed values were small and averaged only 0.032 m, or about 6% of the tide range. For water level highs and lows, the global model gain,  $G_w$  (i.e., the ratio of model extrema amplitude to observed amplitude), was approximately unity ( $G_w$  was 1.054), suggesting that there were no problems with excessive damping. The global mean lag time (i.e., the time of modeled extrema minus the time of observed extrema) was small (-6 min), suggesting that there were no overall bias in propagation speed errors due to incorrect water depths. The global rms time lag was 25 min. For the total currents, rms differences between modeled and observed values are 13 cm/s, or about 11% of the current range. The global model gain for flood and ebb currents was significantly less than unity (0.837) and the global mean lag was larger (-23 min) than for water levels. The global rms time difference (43 min) was also larger than for water levels.

The calibration for tidal constituents (Hess, 1993) was an improvement over the previous calibration and was used here. For 14 water level stations, the reference amplitude (based on the combined amplitudes of the four largest constituents) for the model agrees to within 4% of the observed. The rms time lag index (based on the combined differences between modeled and observed epochs of the four largest constituents) has a standard deviation of 9.7 min. For the currents at 29 locations, the reference amplitudes agree to within 9% and the rms time lag index has a standard deviation of 16.3 min.

### 7.3. THE NATURAL PERIOD

A simulation was completed to determine the natural period of Tampa Bay by a free oscillation test. If the period is nearly equal to either the semidiurnal or the diurnal tidal forcing period or to the time scale of storm passage, the water level response may be greatly amplified. Also, knowledge of the natural period of an estuary can be important for interpreting the current and water level spectra because a spectral peak at the natural frequency may be evident. An expression for the natural period (Pond and Pickard, 1983) for a rectangular, uniform-depth bay is

$$T_N = \frac{4L}{(gH_m)^{1/2}} \quad (7.3)$$

where  $T_N$  is the period,  $L$  is the length of the estuary,  $g$  is the acceleration due to gravity, and  $H_m$  is a mean depth. For  $L$  of 56 km and  $H_m$  of 3.67 m (average mean sea level depth for model cells inside the Bay),  $T_N$  was 10.37 hours.

In the simulation, the Bay was given an initial water level displacement (increasing linearly from zero at the mouth to 10 cm at the head); then the water was allowed to flow freely according to the equations of motion but with a zero water level at the mouth and outside the Bay to impose a node in the oscillation. The resulting motion was a free oscillation at the Bay's natural frequency; analysis of the time series of water levels at St. Petersburg gave a value of 10.7 hours for the natural period. It is of interest to note that the estimated natural period of the west Florida shelf offshore of Tampa Bay, assuming that  $L$  equals 220 km (the distance to the 100-m isobath) and  $H_m$  is 60 m (the average shelf depth), is 10.0 hours.

Although the estimated natural period is close to the semidiurnal tidal period, it is likely that motions at this frequency could be distinguished from tides in a frequency spectrum. However, no peak at 2.24 cpd is evident in either the current spectra (Figure 2.18) or in the water level spectra (Figure 3.9). Therefore, it is likely that either free oscillation is rare or that bottom friction is successfully damping this motion. If the natural period is close to 12 hours, its influence would be evident in the  $S_2$  tidal amplitude. An examination of the amplitude of the  $S_2$  tidal constituent for water level (Table 3.1) at the entrance (E-347) near Egmont Key (6.5 cm) and in the upper Bay (E-738) at Safety Harbor (7.4 cm) shows that there is very little amplification; therefore, it is likely that the period is significantly different from 12 h.

#### 7.4. SEMIDIURNAL TIDAL CURRENTS

The semidiurnal tidal response of the Bay was simulated by forcing the shelf water level with a single-constituent cosine tide at a period of 12 hours and an amplitude of 30 cm. This period, which equals that of the  $S_2$  constituent, was chosen primarily for modeling convenience, but it is expected that all semidiurnal constituents will have characteristics similar to this idealized cosine tide since their periods are all close to 12 hours. The 30-cm amplitude was chosen to combine the effects of the  $M_2$ ,  $S_2$ , and  $N_2$  constituents on the shelf. This amplitude gives a mean range at St. Petersburg of 49 cm, which approximates the observed mean range of 39.1 cm (Station E-520 in Table 3.3). The model was run in the three-dimensional, barotropic mode with river inflow but no wind or density forcing; after a spin-up period of 4.5 days, the last tidal period was analyzed.

The vectors representing the maximum flood current (regardless of time) for the idealized semidiurnal tide are shown in Figure 7.2. For purposes of this numerical study, flood was defined as the period of time when the average water level over the entire model grid was rising. This definition can lead to inconsistencies, since in some areas the local currents will still be flooding (i.e., directed upbay) as the average water level is falling. However, most of the flood current vectors are directed into the Bay as expected. Modeled currents described in this Section are at either (1) the standard NOS depth for predictions (15 ft or 4.6 m below mean lower low water), or (2) half the total depth below mean lower low water, whichever is closer to the surface.

Contours of the distribution of the flood current speed in Tampa Bay are shown in Figure 7.3. The modeled current speeds can be compared with the observed distribution of the  $S_2$  current

amplitude (Figure 2.4b) and the mean maximum flood speed (Figure 2.13b). While the overall correlation is good, there were some differences which may be due to scarcity of the data or the inability of a single constituent to adequately represent the tide. There are four regions of generally high currents: (1) in the lower Bay near the entrance, (2) near the Sunshine Skyway, (3) at the entrance to Old Tampa Bay near Port Tampa, and (4) at the Courtney Campbell Parkway. Analysis of the ebb current speeds shows a similar distribution.

It should be noted that the model grid may be too coarse in some locations to accurately resolve the small-scale structure of the currents, which may lead to overestimates or underestimates of current speeds in some locations. Furthermore, the contours were generated from a secondary array (30 x 40) of values that were calculated by weighting the closest values from the model grid; this procedure smooths the model values and eliminates small-scale variations.

The spatial distribution of time of maximum flood (relative to time of high water at the deep-water boundary at hour 12.0) is shown in Figure 7.4. The result compares favorably with the plot of  $S_2$  phases shown in Figure 2.5b. The modeled mid-Bay flood times occur later than at the mouth by about 0.5 hour, or (at  $30^\circ$  per hour) with a  $15^\circ$  phase shift, as shown in the data. Along the shores of the lower Bay, the flood occurs earlier. In Hillsborough Bay, floods occur earlier than at the entrance by about 0.5 hour ( $15^\circ$ ), and in Old Tampa Bay floods occur later than at the entrance by from 1.0 to 1.5 hours ( $30^\circ$  to  $45^\circ$ ). The steady increase in time of flood up to the entrance to Old Tampa Bay suggests that the tide wave is progressive in nature in the lower and middle Bay, with earlier times in the shallow water along the shore. The relative uniformity of times in Hillsborough Bay suggest that the tide there is a standing wave.

## 7.5. SEMIDIURNAL TIDES

The tidal forcing used in Section 7.4 was also used to simulate the tide range baywide. The spatial distribution of the range (computed as the maximum water level minus the minimum water level over a 12-hour period) is shown in Figure 7.5. The largest ranges occurred in the Manatee River (69.5 cm), in McKay Bay (65.7 cm), and in Safety Harbor (69.0 cm). The minimum range occurred near Point Pinellas and was 46.4 cm. This distribution can be compared to the  $S_2$  tidal amplitude plotted in Figure 3.2b and the mean tidal range in Figure 3.5c. The minimum observed  $S_2$  amplitude occurs at mid-Bay, east of St. Petersburg, near where the model places the minimum. Both model and data show gradual increases in the range farther up the Bay, indicating that the tide wave is amplified slightly as it progresses.

The spatial distribution of the time of occurrence of maximum water level in Tampa Bay relative to the high at the deep-water boundary is shown in Figure 7.6. The lag (difference between the time of local high water and the time of high water at Egmont Key) at St. Petersburg is approximately 2.2 hours, the lag at Port Tampa is 3.2 hours, the lag at Davis Island (upper Hillsborough Bay) is 2.8 hours, and the maximum lag of 4.0 hours occurs in Safety Harbor. The greatest changes occur at the entrance to Old Tampa Bay where the time lag increases from 3.0 hours to 3.75 hours over a distance of only 8 km. The observed  $S_2$  epochs (Figure 3.3b) also show a continual increase from  $350^\circ$  at the mouth to  $450^\circ$  at Port Tampa, which at the rate of

30° per hour is a difference of 3.3 hours. The modeled lag in Hillsborough Bay is relatively uniform and varies from 2.7 to 2.9 hours, supporting the conclusion in Section 7.4 that the tide there is a standing wave.

## 7.6. RESPONSE TO WINDS

Since wind setup, or rise in mean water level, is related to wind speed and fetch, winds from the southwest should produce the largest setup in the Bay. Therefore, the setup under a constant southwesterly wind of 10 m/s was simulated. An idealized wind field was defined by the speed at a height of 10 m,  $V_{10}$ , from a constant direction,  $\theta_0$ , as follows:

$$\begin{aligned}
 V_{10} &= 0 && \text{for } t < t_0 \\
 V_{10} &= V_m \frac{(t - t_0)}{(t_1 - t_0)} && \text{for } t_0 < t < t_1 \\
 V_{10} &= V_m && \text{for } t_1 < t
 \end{aligned} \tag{7.4}$$

i.e., the speed ramps up to full strength ( $V_m$ ) over 1 day ( $t_1$  minus  $t_0$ ).

For this experiment, the values chosen were as follows:  $V_m$  was 10 m/s,  $t_0$  was 2 days,  $t_1$  was 3 days, and  $\theta_0$  was 210°. Because of the importance of vertical eddy diffusion, the model was run with a semidiurnal tide (with a period of 12 hours and an amplitude of 25 cm) to provide a background level of turbulence. An analysis of the time series of water levels at Apollo Beach and Bay Aristocrat Village shows that the increase in the mean water level (as judged by the change in the maximum and minimum levels) begins at the time of application of the applied wind stress with no discernable time delay. After full wind conditions are reached, there is no apparent fluctuation in the mean level, which indicates the dominance of friction in the Bay's dynamics.

The effect of the wind on water levels at two locations is shown in Table 7.1. Before the onset of the wind, the mean water level is small (less than 1 cm). After the wind is applied, the mean range remains approximately as before, but the mean level rises. The setup at Apollo Beach was 14.9 cm. Locations of high setup were Safety Harbor (19.9 cm), Hillsborough River (19.9 cm), and upper McKay Bay (23.1 cm).

For comparison, predicted setup,  $s$ , in a bay of uniform depth,  $h$ , (Bretschneider, 1966) is

$$s = \left( \frac{2rC_dLV^2}{g} + h^2 \right)^{1/2} - h \tag{7.5}$$

where  $L$  is the distance along the bay and  $h$  is a mean depth. For Apollo Beach,  $L$  was taken to be 44 km and  $h$  was 5 m, so that Equation 7.5 gives a value of 14.0 cm for  $s$ , which is close to the modeled value of 14.9 cm.

**Table 7.1. Modeled water level characteristics (cm) at two locations in Tampa Bay before and after the imposition of a spatially-uniform 10 m/s southwesterly wind ramped up over 1 day and allowed to come to a repeatability condition. A semi-diurnal tide with a driving amplitude of 25 cm was also present to generate realistic turbulence.**

Characteristic	BEFORE WIND		AFTER WIND		DIFFERENCE	
	Apollo Beach	Bay Aristocrat Village	Apollo Beach	Bay Aristocrat Village	Apollo Beach	Bay Aristocrat Village
High Water	25.1	30.1	38.2	43.9	12.8	13.8
Low Water	-24.6	-28.3	-9.3	-12.1	15.3	16.2
Range	49.7	58.4	47.5	56.0	-2.2	-2.4
Mean Level	0.2	0.9	14.9	15.9	14.7	15.0

The wind also influences the mean currents. Table 7.2 shows the increase in mean current speed at two mid-Bay stations due to the same wind event used to study setup. Down-Bay barotropic currents increase by about 6 cm/s, which is smaller than the value of 12 cm/s predicted by Weisberg and Williams (1991) for a synoptic-scale (5-day-long) event of similar wind speed.

**Table 7.2. Mean along-channel vertically-averaged currents (cm/s) at C-3 and C-4 before and after the imposition of a steady wind of 10 m/s. Negative currents are out of the Bay.**

Condition	C-3	C-4
Before Winds	-1.4	-0.9
After Winds	-5.9	-7.3

## 7.7. SALINITY DISTRIBUTION

The mean salinity structure was studied by initializing the model with typical values and running for a 35-day period with a semidiurnal tide as described above. River discharges were the climatological mean values. After 25 days of simulation, salinity values at all cells were averaged for all time steps within the last 10 days.

The surface salinity distribution (Figure 7.7) is similar to that shown in Boler (1992) and in Figures 5.9a and 5.12a in that salinities tend to be higher in the deeper central portion of the Bay near the navigation channel. Salinities tend to be somewhat lower (by 3 or 4 psu) in Hillsborough Bay than in Old Tampa Bay due to the former's much greater river discharge. Salinities tend to be lower on the eastern side of the lower Bay, probably due to the freshwater discharge along that side.

## **7.8. MEAN BUOYANCY-DRIVEN CURRENTS**

The modeled mean buoyancy-driven currents near the surface and near the bottom are shown in Figures 7.8 and 7.9, respectively. These currents are the difference between mean currents computed with and without buoyancy forcing. The model was driven by a semidiurnal tide and annual mean river discharges and included either (1) a time-varying salinity for the buoyancy forcing case or (2) a steady, horizontally uniform but vertically (very slightly) stratified salinity field for the non-buoyancy forcing case. Mean currents were computed by averaging the layer transports over the last 10 days of the simulation and dividing the average layer transports by vertical cell thickness to get a mean velocity.

The near-surface (at a depth below the surface of 7% of the total mean sea level depth) currents are generally seaward as expected. The currents southwest of the Sunshine Skyway are generally uniform in direction, but the direction is much less uniform northeast of the bridge. This lack of uniformity is probably caused by the influence of the land supporting the bridge approaches. In the upper Bay, just south of the Interbay Peninsula, there are strong (10 cm/s) currents directed westward across the estuary (see Figure 2.16). Near the bottom, net currents are generally directed up into the Bay, especially in the natural deep channel in the lower and middle Bay.

The mean along-channel baroclinic currents under the Sunshine Skyway are shown in Figure 7.10a. The currents are generally directed out of the Bay at the surface (5 cm/s) at the center of the natural channel and have a corresponding return flow up into the Bay at three locations: near the bottom, but south of, the deep channel; near the bottom at the northern shore; and at all depths near the southern shore.

The mean isohalines modeled at the Sunshine Skyway cross section are shown in Figure 7.10b. Maximum salinities occur on the bottom-center of the section and strong horizontal gradients exist on the southern side, due possibly to the predominance of fresh water being added to that side of the estuary.

## **7.9. CONCLUSIONS**

Tampa Bay behaves like a typical coastal estuary in most respects. Tidal currents are important. The tide wave is progressive in the lower and middle Bay but changes into a standing wave (since the phase is uniform) in Hillsborough Bay. The narrow restriction at the entrance to Old Tampa Bay acts to choke off the tide, thereby increasing the currents and causing a large phase

delay there. The influence of bottom friction must be important, since the semidiurnal tidal amplitude increases only a small amount up into the Bay while being forced at a period near the natural period (10.7 h). Wind setup is rapid and steady, and vertical mixing is strong enough to nearly eliminate stratification.

In some respects, however, Tampa Bay is different from typical estuaries. Since the majority of freshwater enters along the eastern shore, water there tends to be less salty than along the axis of the Bay. This cross-estuary salinity (and therefore density) gradient can create significant cross-estuary buoyancy currents in the upper Bay, especially just south of the Interbay Peninsula.

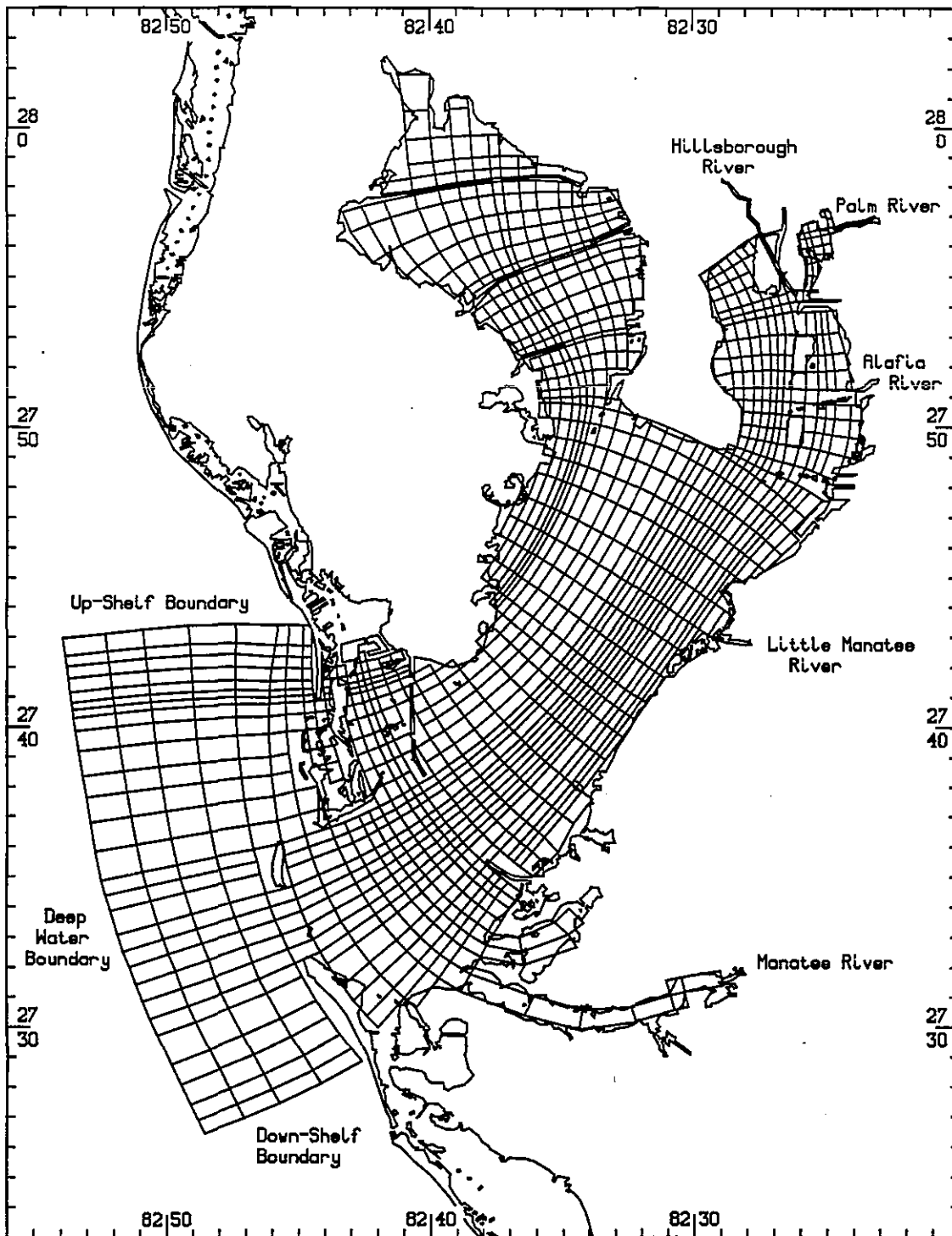


Figure 7.1. Plan view showing the orthogonal curvilinear grid for Tampa Bay used in this study.

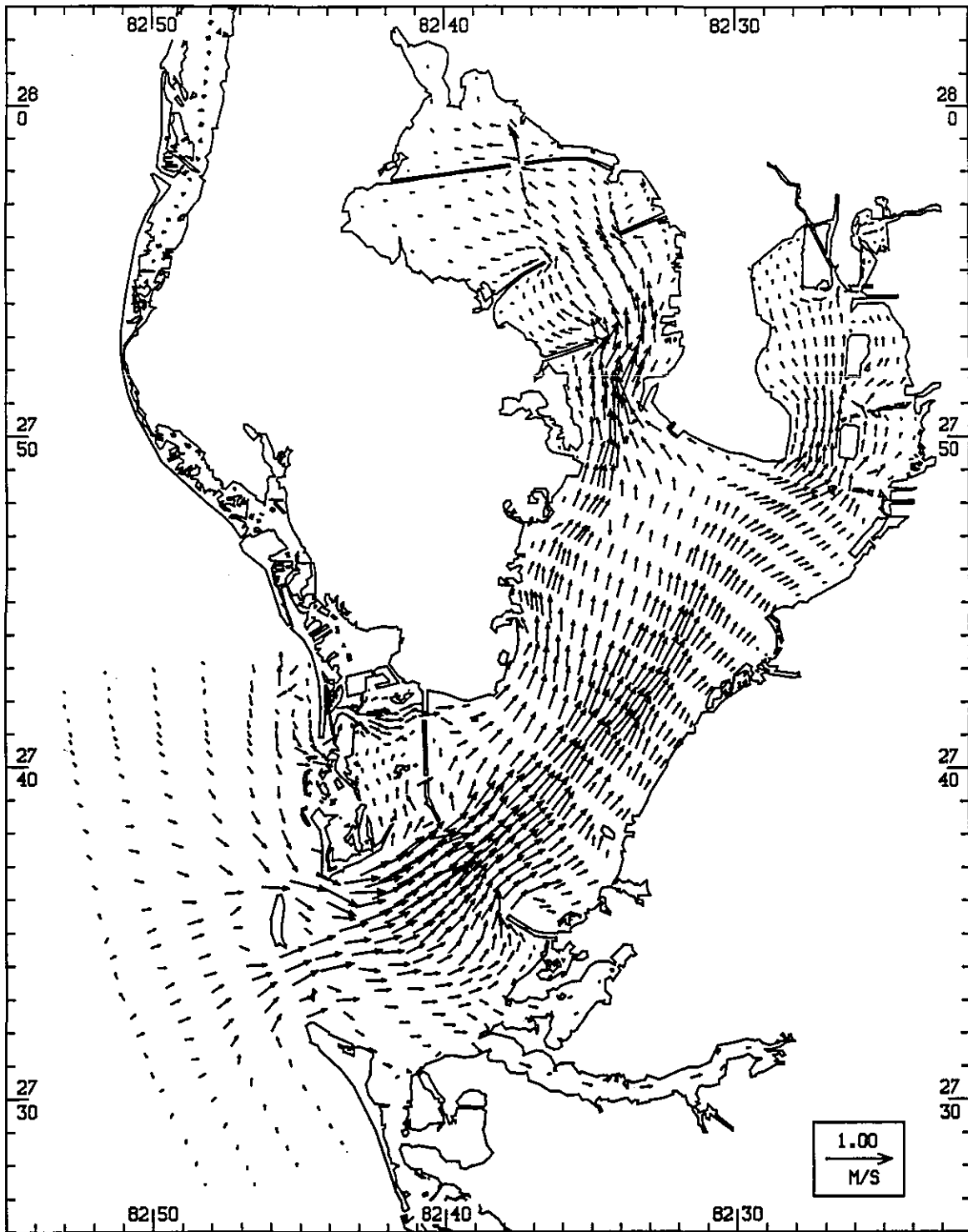


Figure 7.2. The vectors representing the maximum flood current (regardless of time) at prediction depth obtained by imposing an idealized semidiurnal tide with a 30 cm amplitude.

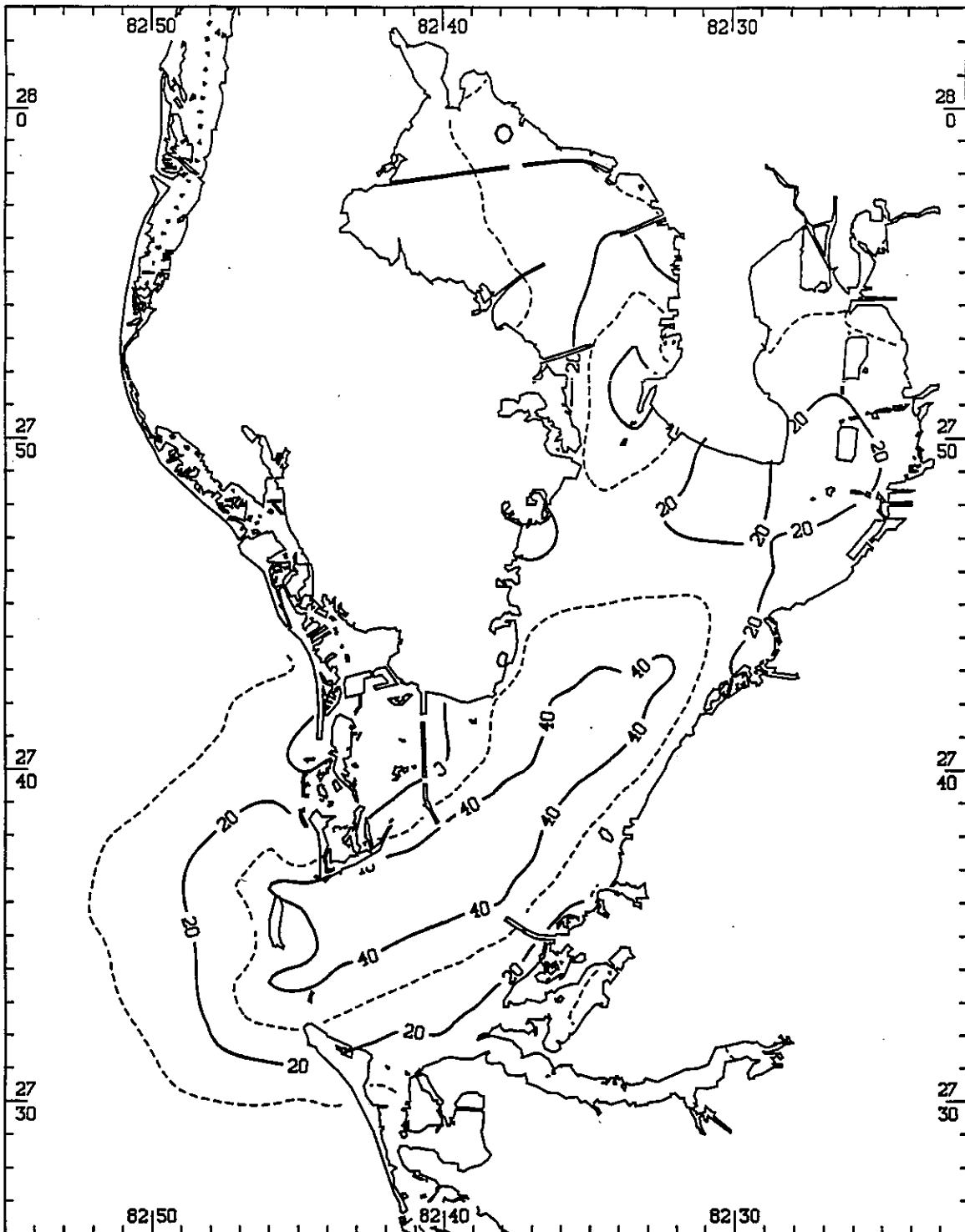


Figure 7.3. Contours of the maximum flood speed (cm/s) at prediction depth in Tampa Bay for an idealized semidiurnal tide with a 30 cm amplitude.

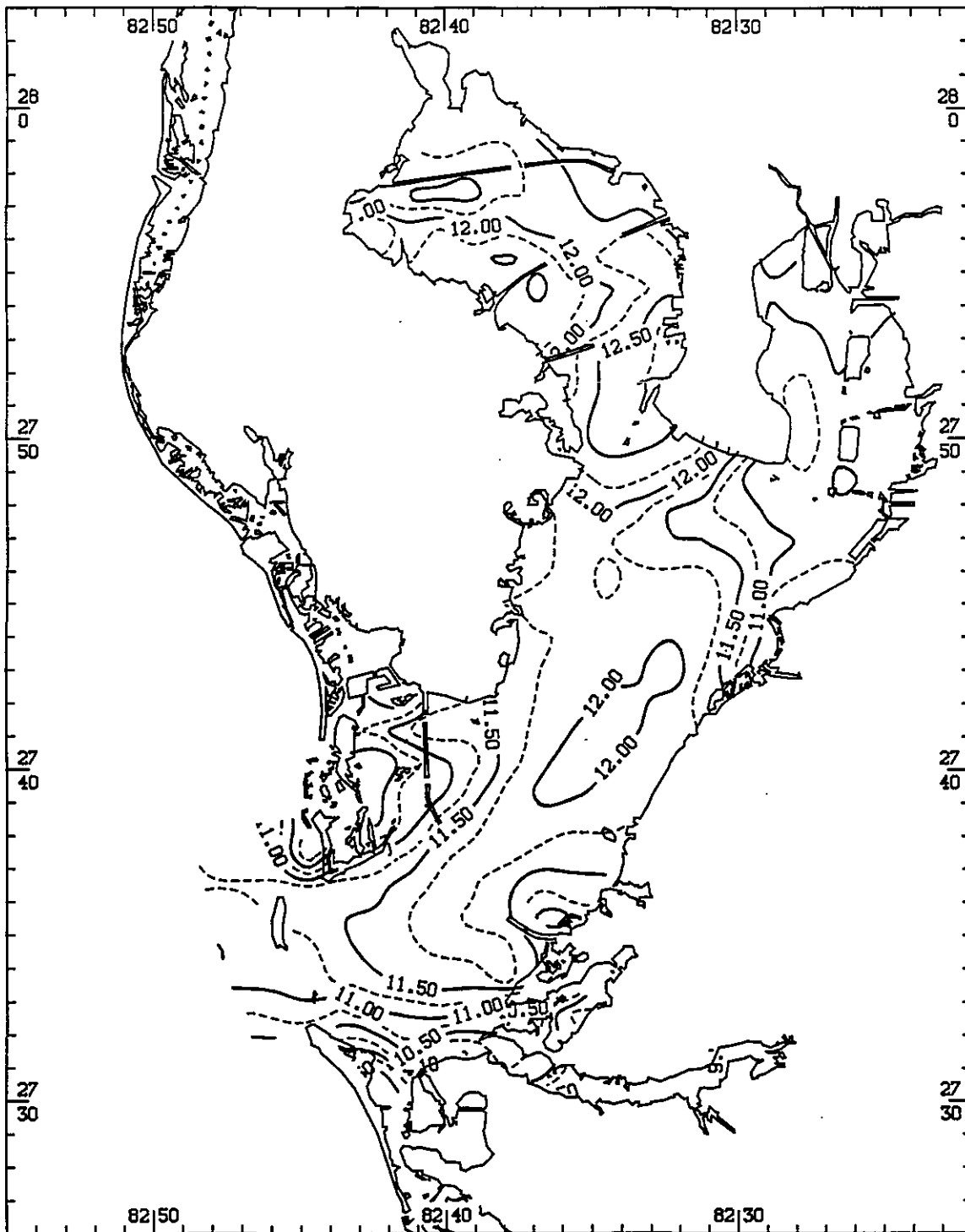


Figure 7.4. Contours of the time of maximum flood (hours) in Tampa Bay for an idealized semidiurnal tide. High water at the deep water boundary occurs at hour 12.

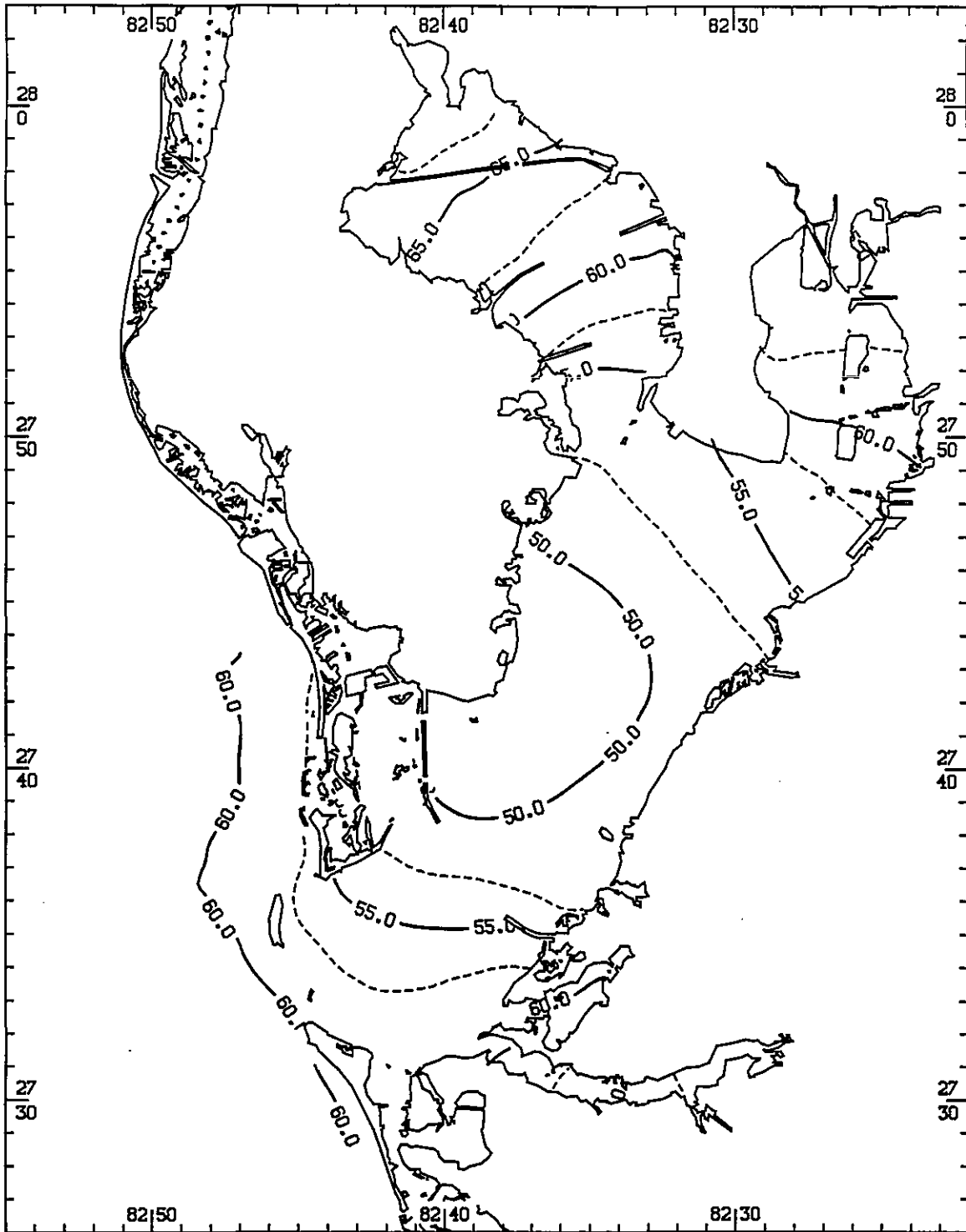


Figure 7.5. Contours of the tide range (cm) in Tampa Bay obtained by imposing an idealized semidiurnal tide with a 30 cm amplitude.

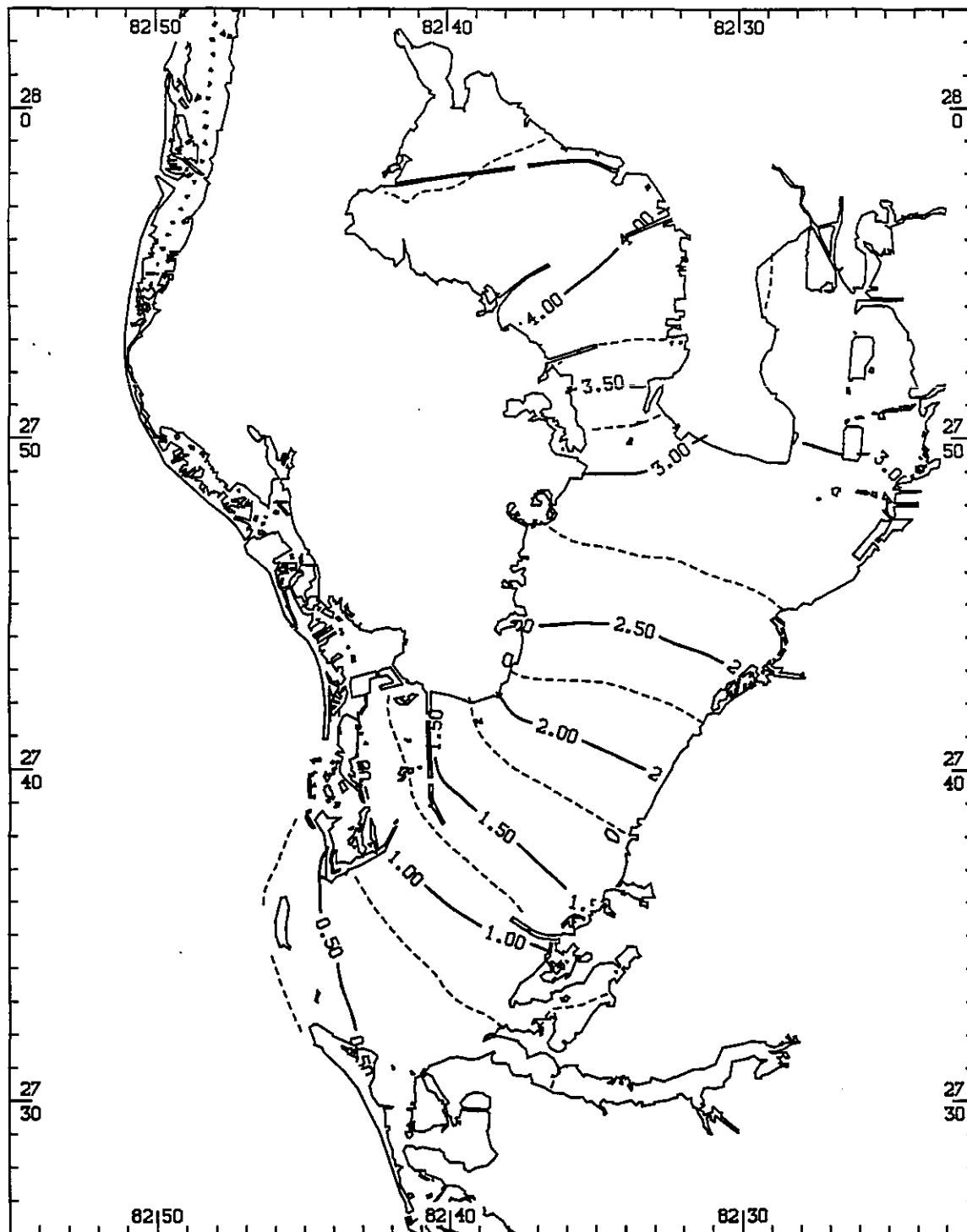


Figure 7.6. Contours of the time of maximum tide (hours) in Tampa Bay for an idealized semidiurnal tide. High water at the deep water boundary occurs at hour 00.

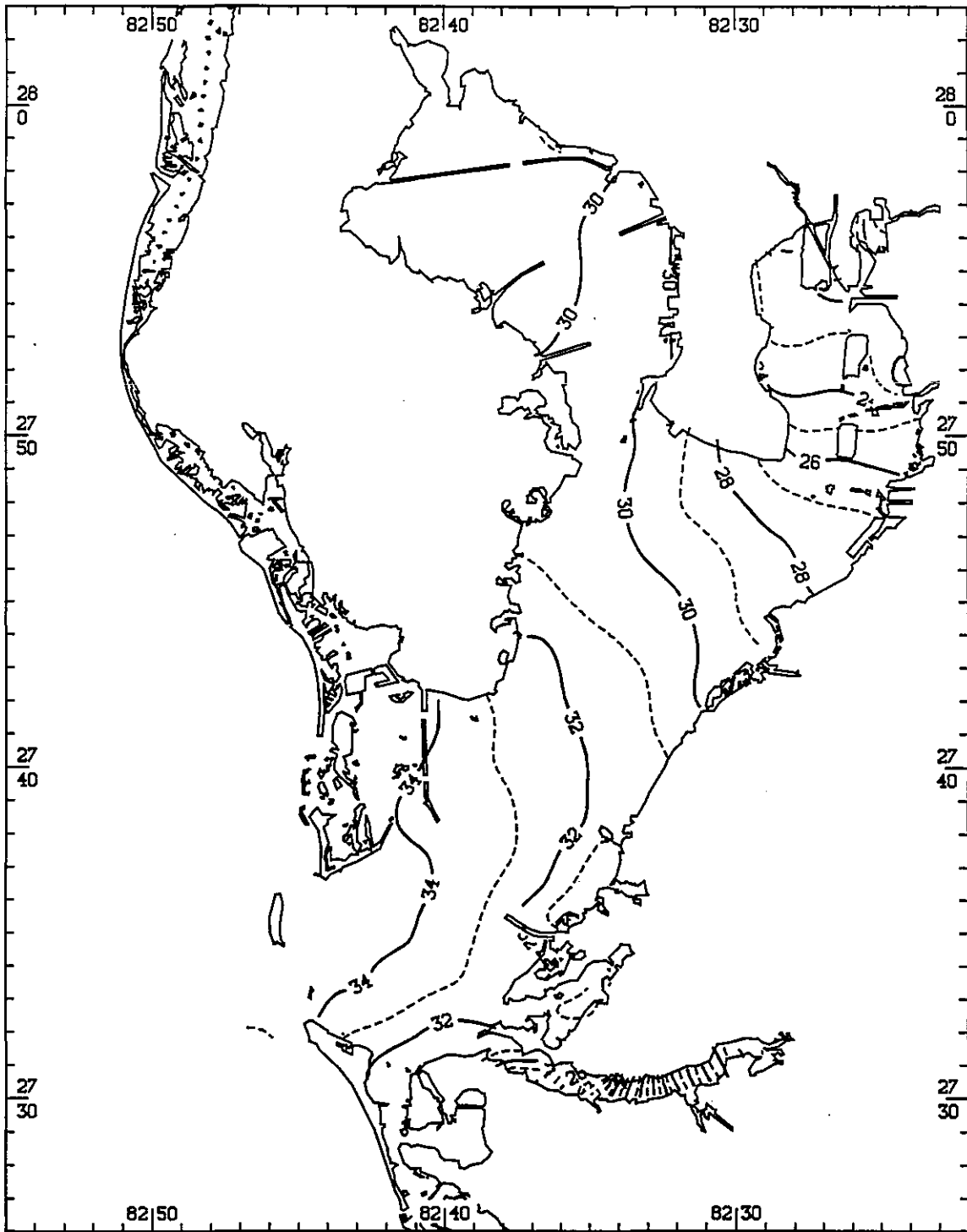


Figure 7.7. Contours of the mean surface salinity (psu) for climatological river flow.

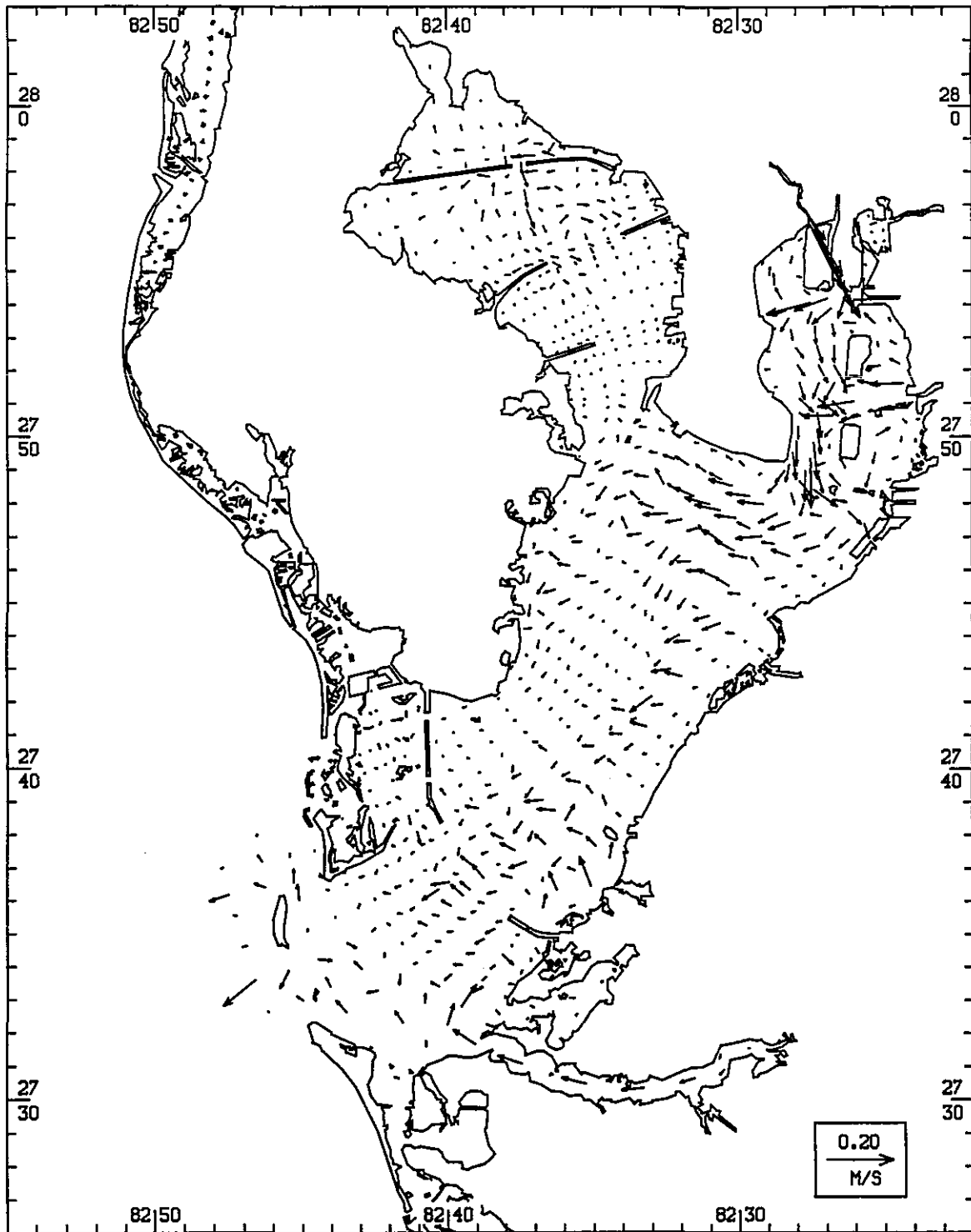


Figure 7.8. Mean near-surface buoyancy-driven circulation vectors.

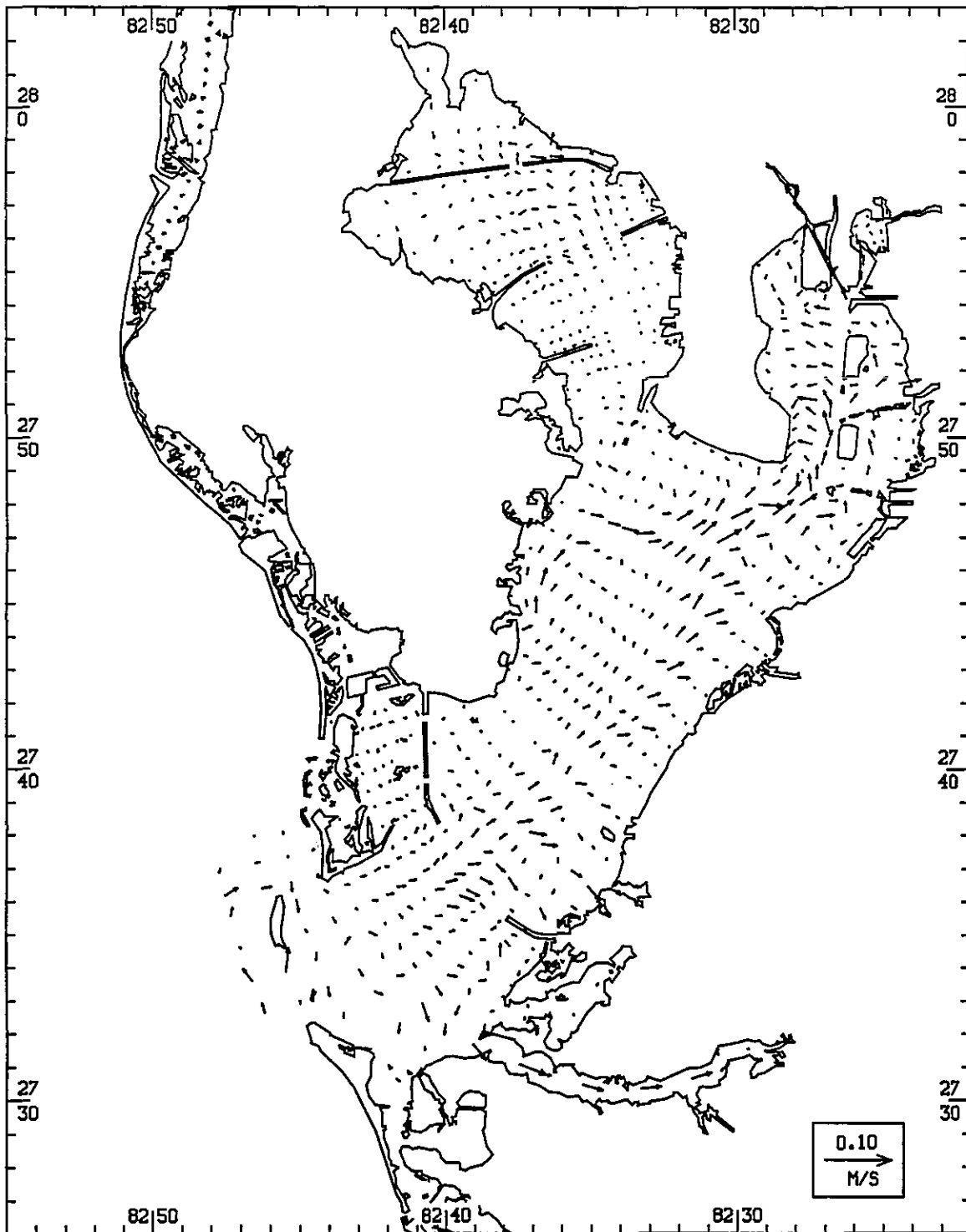
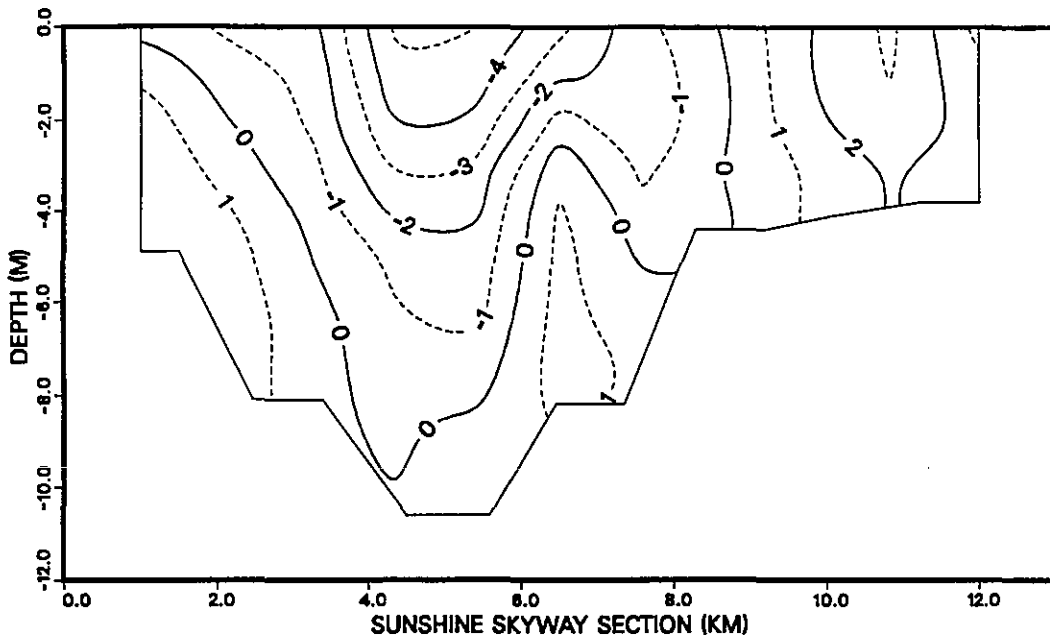
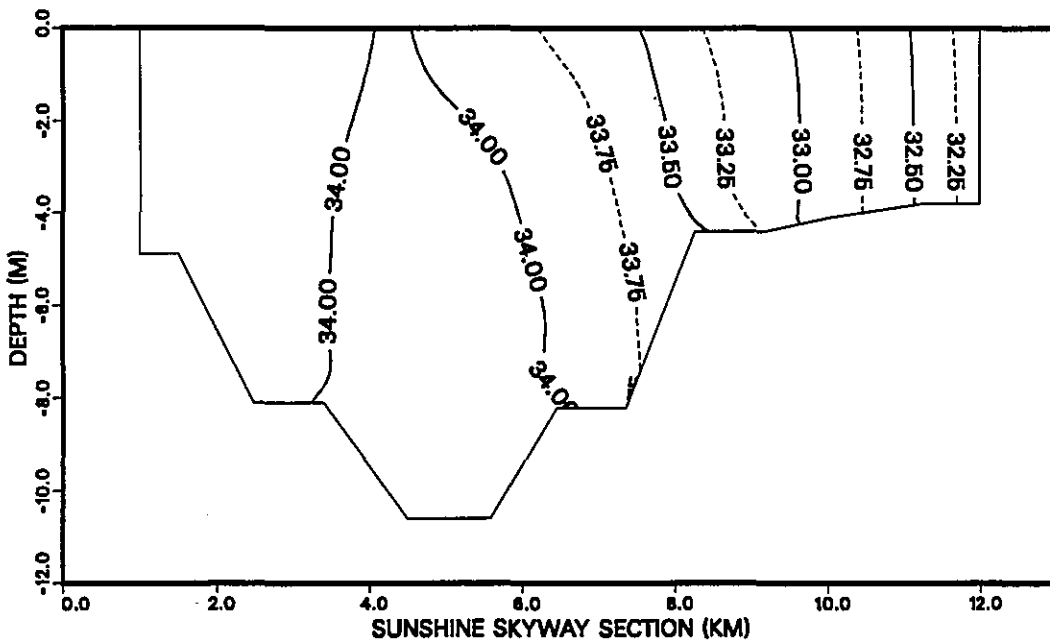


Figure 7.9. Mean near-bottom buoyancy-driven circulation vectors.

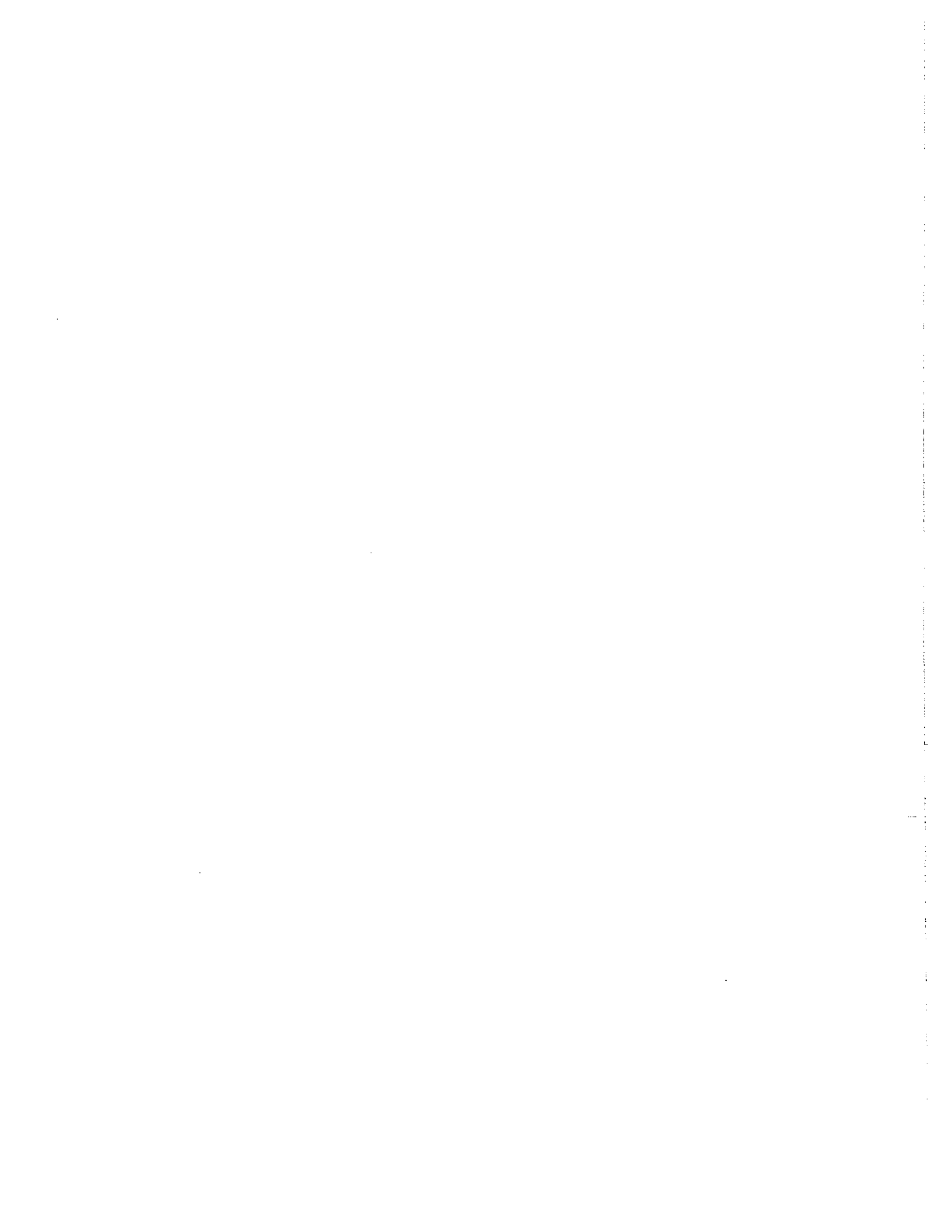


(a)



(b)

Figure 7.10. (a) Time-averaged along-channel currents (cm/s) and (b) isohalines (psu) at the Sunshine Skyway looking up the Bay. Positive currents are directed into the Bay.



## 8. OVERVIEW OF THE CIRCULATION OF TAMPA BAY

Chris E. Zervas and Richard W. Bourgerie

### 8.1. TIDAL CIRCULATION

The analysis and synthesis of the TOP data set has yielded a comprehensive view of the tidal circulation of Tampa Bay. Tidal current constituents and Greenwich intervals were computed using harmonic analysis methods. They support previous findings that the tidal currents in Tampa Bay are reversing and rectilinear (i.e. the minor ellipse axis is less than 5% of the major ellipse axis), and can be classified as mixed, mainly semidiurnal based on the ratio of the amplitudes of the two major diurnal constituents to the two major semidiurnal constituents. The largest current amplitudes occur in Egmont Channel (greater than 160 cm/s), near the Sunshine Skyway, and at the entrance to Old Tampa Bay. The weakest currents are found in Hillsborough Bay. Seasonal variation was seen in some of the tidal current constituents, perhaps due to the seasonal variation of the daily sea breeze intensity or of the density structure of the Bay. The towed ADCP measurements showed that the currents are strongest in the deeper channels, with the maximum generally near the surface. Weaker currents are found in shallower areas away from the channels. The position of the maximum current velocities varied by as much as 1.5 km from day to day and from flood to ebb.

Tidal constituent epochs indicate that the tide progresses steadily up the Bay and into Hillsborough Bay and Old Tampa Bay. Four to five hours are required for high or low tides to travel from Egmont Key to the head of Old Tampa Bay. The mean diurnal tidal range increases from about 62 cm at the mouth of the Bay to more than 82 cm at the head of Old Tampa Bay. The tide is a damped progressive wave in the lower Bay and gradually changes to a standing wave in Hillsborough Bay. The tidal constituents also showed that the tide is mixed, mainly semidiurnal throughout the Bay.

Tidal circulation has a strong impact on the water mass characteristics (salinity, temperature, and density) of Tampa Bay which exhibit significant temporal and spatial variations. Spectral analysis revealed that tidal scale fluctuations dominate the short-term temporal variability. The diurnal and semidiurnal salinity variations result from the progression of floods and ebbs, which alternatively transport saline water from the Gulf of Mexico and fresher river discharge from the upper Bay. The tidal signal is strongest at mid-Bay, where horizontal salinity gradients are large. Due to the spatial uniformity of temperature in the Bay, the diurnal signal in the temperature spectrum is dominated by the daily radiational heating and cooling cycle.

The numerical circulation model supported the observational tidal data in many respects, including the finding that the tide is a damped progressive wave from the mouth of the Bay into Old Tampa Bay and is a standing wave in Hillsborough Bay. The modeled pattern of semidiurnal current speeds was similar to, but more detailed than that found from the observations. The maximum semidiurnal current magnitudes are found in the lower Bay, in

Egmont Channel, and under the Sunshine Skyway. Large currents are also found at the entrance to Old Tampa Bay and at the Courtney Campbell Parkway.

The modeled times of flood in the lower Bay are approximately 0.5 hour after flood at the entrance, with earlier floods occurring along the shores of the Bay. In Hillsborough Bay, where the tide is a standing wave, flood occurs about 0.5 hour earlier than at the entrance of the Bay. In Old Tampa Bay, flood occurs later than at the entrance by from 1.0 to 1.5 hours. This is consistent with the observational results and may be caused by the narrow restriction at the entrance to Old Tampa Bay acting to choke off the tide and cause a large phase delay.

## **8.2. NONTIDAL CIRCULATION**

Significant nontidal components were present in the water levels and currents recorded during TOP. The standard deviation from the mean of the nontidal water level ranged from 6 to 16 cm and represented 29% to 55% of the total water level variability. The standard deviation from the mean of the nontidal current ranged from 5 to 14 cm/s and represented 17% to 88% of the total current variability. The nontidal currents were a higher percentage (greater than 55%) of the total current in locations where the tidal currents were weakest (i.e. in Hillsborough Bay and offshore on the continental shelf). Long-term nontidal currents are important in estuaries as the primary means of transport for dissolved and suspended matter. Two major nontidal driving forces in Tampa Bay were examined: subtidal water level fluctuations on the west Florida continental shelf and the horizontal head-to-mouth density gradients in the Bay. The shelf water level fluctuations are driven by longshore winds over the continental shelf and can be considered to be meteorological in origin. The density gradients in the Bay are primarily due to fresh riverine inflow and thus are considered to be hydrological in origin. In the following sections, we characterize the meteorology and hydrology of the Tampa Bay region before discussing their effects on the Bay.

### **Meteorologically-Forced Currents**

The winds over the Tampa Bay region average 3.4 m/s from the northeast and are classified as light and variable. Winds fluctuating at synoptic frequencies (periods greater than 1.5 days) are highly coherent throughout the Bay, while higher frequency winds (periods less than 12 hours) are more variable from station to station. Wind speeds increase with increasing distance from the head of the Bay toward the mouth of the Bay. Rotary spectral analyses revealed a significant amount of windfield energy at the diurnal and semidiurnal frequencies. Due to greater daily air temperature ranges over land than over water, a well-developed sea breeze system exists in the spring and fall, accounting for the diurnal and semidiurnal energy during this time. During the summer, afternoon thunderstorms are frequent and are the primary component of the diurnal and semidiurnal energy. During the winter, the passage of synoptic-scale storms results in increased energy at lower frequencies (periods greater than 1 day).

Spectral analysis of the water level and current data revealed the frequencies most prominent in the nontidal signals. The water level spectra showed that high-frequency nontidal energy levels

are much lower than subtidal (periods longer than 1 day) energy levels. In contrast, the current spectra show that high-frequency nontidal energy is as great as the subtidal energy, indicating that currents show a greater response than water levels to a wider range of frequencies.

Cross spectral analysis of wind, water level, and current data revealed the relationship between longshore wind, coastal water levels, and water levels and currents in Tampa Bay. Subtidal water level fluctuations on the west Florida continental shelf are produced by local and remote wind-driven currents. The longshore component of the wind can raise and lower coastal water levels by transport perpendicular to the coast. In response to changing water levels at the entrance to the Bay, nontidal currents develop in the Bay.

In an effort to quantify the nontidal driving forces in Tampa Bay, prediction schemes were developed for the shelf effect on water levels at St. Petersburg and currents at mid-Bay (C-4). The nontidal water level at St. Petersburg is about 94% of the nontidal water level at Clearwater Beach with a time lag of approximately 2 hours. A nontidal water level change of 20 cm/day at Clearwater Beach produces a current of approximately 5 cm/s at mid-Bay with a time lag of approximately 1 hour. Monthly rms values and standard deviations from the monthly means were calculated to evaluate the reduction in variability that the prediction schemes caused in the water level and current. The subtraction of the shelf effect resulted in a large reduction in variability of the water level signal at St. Petersburg (up to 60% in March), especially during the winter months when large-scale synoptic storms are more frequent. When the shelf effect was removed from the current signal at mid-Bay, there was also a significant reduction in variability, mainly during the winter months.

The numerical circulation model was used to determine the size of the direct wind setup and revealed that the Bay responds very rapidly to an increase in southwesterly winds with a 15 cm setup in the upper Bay caused by a 10 m/s wind directed along the axis of the Bay. The resulting sea-slope pressure gradient, in turn, induces a 6 cm/s current toward the southwest at mid-Bay. The absence of sea level oscillation during a steady wind simulation suggests the dominance of bottom friction.

### **Hydrologically-Forced Currents**

The two principle sources of freshwater into Tampa Bay are river discharge and precipitation. Over 60% of the annual rainfall and over 55% of the annual river discharge occur between June and September. During the summer months, there is significant spatial variability in the rainfall over the Tampa Bay area due to the local sea breeze/convection circulation pattern and strong, localized thunderstorms. During winter, the passage of large-scale frontal systems produces a rainfall pattern with greater spatial coherency.

June, August, and September of both 1990 and 1991 were dry compared with their historical averages. Although the 1990 and 1991 summer rainfall amounts were similar, the river discharge was considerably greater during the summer of 1991. River discharge was 51% greater than normal for May through August of 1991 and 45% less than normal for the rest of the study

period. Human factors, including controlled withdrawal and impoundment, may have caused some of this difference.

Horizontal variations are the dominant feature in the salinity distribution. During periods of high rainfall and large river discharge, a strong head-to-mouth density gradient develops. This gradient changes primarily in response to freshwater input and drives a long-term residual estuarine flow which influences the net transport of the Bay. Both the salinity and the temperature of Tampa Bay are relatively well mixed vertically, although slight vertical density stratification is occasionally evident in Hillsborough Bay during the summer season.

Measured long-term mean current profiles revealed a typical estuarine circulation pattern in the Bay; higher salinity water from the Gulf flows into the Bay near the bottom, while lower salinity water flows out of the Bay near the surface. The strength of this system varies; during the summer months the flow is markedly stronger than during the winter (12 cm/s vs. 2 cm/s).

The effect of hydrological forcing was examined with a prediction scheme that uses a simplified version of the equations of motion, balancing the horizontal pressure gradient with the bottom frictional stress. Monthly rms values of the along-axis current were calculated to evaluate the reduction in variability due to the prediction scheme. The subtraction of the predicted density-driven current resulted in a significant reduction in variability during the summer of 1991 (up to 30% in September), when a strong head-to-mouth density gradient was present in the Bay.

The numerical circulation model was employed to simulate the effects of buoyancy forcing. The model results show higher salinity in the natural channel than at the shallower sides of the Bay. The modeled salinities are also slightly greater in Old Tampa Bay than in Hillsborough Bay and generally lower on the east side of the Bay. The mean baroclinic circulation near the surface is toward the mouth of the Bay, while near the bottom, mean baroclinic currents are directed into the Bay, especially in the natural and dredged channels. Modeled density-driven currents show cross-bay flow just south of the Interbay Peninsula. In general, the mean baroclinic currents are on the order of 5 to 15 cm/s.

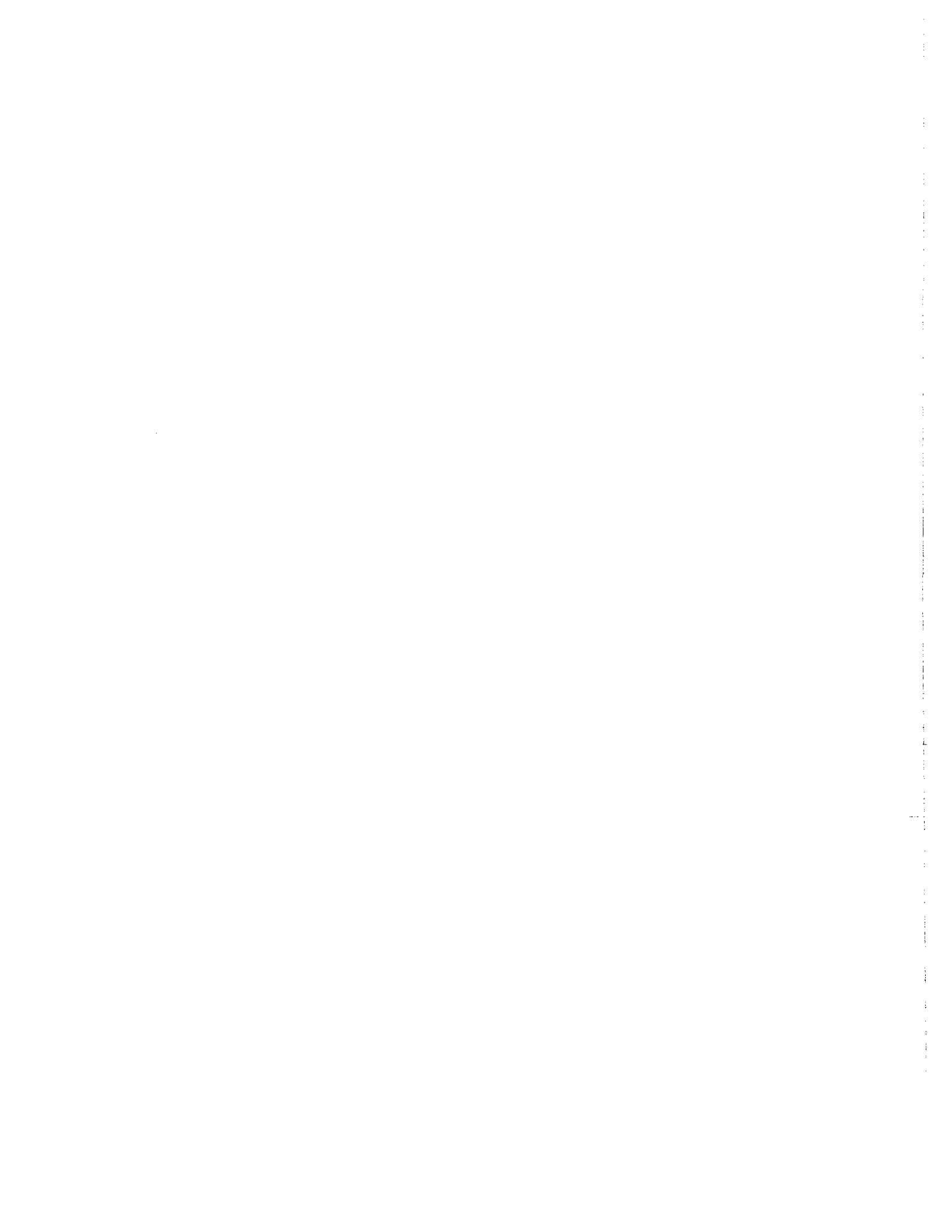
## **Summary**

Residual currents represent a substantial portion of the observed currents. During the winter months, the residual currents are strongest and are highly correlated with the passage of winter storms which cause rapid changes in the water levels on the shelf. During the summer months, the residual currents are associated with the strong horizontal density gradients resulting from the increased freshwater discharge into the Bay. Significant progress has been made toward quantifying and predicting both of these types of nontidal circulation. Various methods of improving the prediction of currents are being developed. Some of these methods include the integration of real-time current, water level, and meteorological observations provided by PORTS, and possibly the use of model-generated meteorological forecasts. These methods will be an improvement over the traditional technique of predicting only the astronomical tide and tidal current.

## ACKNOWLEDGEMENTS

The authors of this report would like to acknowledge the hard work and sustained effort by many others that went into planning and carrying out TOP. This extensive project would not have been possible without Dr. Henry Frey who organized TOP and saw it through to its completion. Extensive support was received from NOAA personnel and from numerous Tampa Bay organizations (Nowadly, 1992). Water level data were collected, processed, and analyzed by the Ocean and Lake Levels Division of NOS. Dr. Boris Galperin of the University of South Florida provided advice on numerical modeling.

Many past and present employees of the Coastal and Estuarine Oceanography Branch and its predecessor, the Estuarine and Ocean Physics Branch, assisted in the data processing and analysis phase of this project. Thanks to Dr. Charles Sun, Thomas Bethem, Barbara Rotondi, Philip Richardson, Michael Evans, and Alan Stern. Special thanks are due to Marty Welch for organizing the review process for this manuscript, and Drs. Frank Aikman, Michael Devine, and Robert Williams for their reviews of the manuscript. Technical editing was done by Patrick McHugh and Brenda Via prepared the final copy and arranged for its publication.



## REFERENCES

- Appell, G. F., T. N. Mero, and J. J. Sprenke, 1991: Design of a current, water level and meteorological information system for Tampa Bay, **Proceedings, IEEE Oceans**, 859 - 863.
- Arya, S. P., 1988: **Introduction to Micrometeorology**, Academic Press, San Diego, CA, 307 pp.
- Bethem, T. D., and H. R. Frey, 1991: Operational physical oceanographic real-time data dissemination, **Proceedings, IEEE Oceans**, 864 - 867.
- Blumberg, A. F., and G. L. Mellor, 1987: A description of a three-dimensional coastal ocean circulation model, in **Three-Dimensional Coastal Ocean Models**, Heaps, N. S. (Ed.), American Geophysical Union, Washington, DC, 1 - 16.
- Boler, R. (Ed.), 1992: Surface water quality, Hillsborough County, Florida: 1988 - 1989, Hillsborough County Environmental Protection Commission, 1900 9th Ave., Tampa, FL.
- Bosley, K. T., 1993: Density-driven residual currents in Tampa Bay, Florida, in **Proceedings, International Conference on HydroScience and Engineering**, Washington DC, June 8-11, 1993, 1521 - 1527.
- Bretschneider, C. L., 1966: Engineering aspects of hurricane surge, in **Estuary and Coastline Hydrodynamics**, Ippen, A. T. (Ed.), McGraw Hill, NY, NY, 231 - 256.
- Browne, D. R., and C. W. Fisher, 1988: Tide and tidal currents in the Chesapeake Bay, Office of Oceanography and Marine Assessment, NOS, NOAA, Rockville, MD, 84 pp.
- Clark, P. A., and R. W. MacAuley, 1989: Geography and economy of Tampa Bay and Sarasota Bays, in **Tampa and Sarasota Bays: Issues, Resources, Status, and Management**, NOAA Estuary-of-the-Month Seminar Series No. 11, 1 - 17.
- Defant, A., 1961: **Physical Oceanography**, Vol. 2, Pergamon Press, New York, NY, 598 pp.
- Dennis, R. E., and E. E. Long, 1971: A user's guide to a computer program for harmonic analysis of data at tidal frequencies, NOAA Technical Report NOS 41, Office of Oceanography and Marine Assessment, NOS, NOAA, Rockville, MD, 31 pp.
- Dinardi, D. A., 1978: Tampa Bay circulatory survey, 1963, NOS Oceanographic Circulatory Survey Report No. 2, Office of Oceanography and Marine Assessment, NOS, NOAA, Rockville, MD, 39 pp.

- Dragovich, A., and J. E. Sykes, 1967: Oceanographic Atlas for Tampa Bay, Florida, and adjacent waters of the Gulf of Mexico: 1958 - 61, U.S. Department of the Interior, Fish and Wildlife Service, Bureau of Commercial Fisheries, Circular 255, 466 pp.
- Estevez, E. D., R. R. Lewis III, S. K. Mahadevan, and J. L. Simon, 1985: The rationale for Tampa BASIS, in **Proceedings, Bay Area Scientific Information Symposium**, Tampa, FL, May 3-6, 1982, 7 - 9.
- Flannery, M. S., 1989: Tampa and Sarasota Bays: Watersheds and tributaries, in **Tampa and Sarasota Bays: Issues, Resources, Status, and Management**, NOAA Estuary-of-the-Month Seminar Series No. 11, 18 - 48.
- Frey, H. R., 1991: Physical oceanographic real-time systems for operational purposes, **Proceedings, IEEE Oceans**, 855 - 858.
- Galperin, B., A. F. Blumberg, and R. H. Weisburg, 1992a: A time-dependent three-dimensional model of circulation in Tampa Bay, in **Proceedings, Tampa Bay Area Scientific Information Symposium 2**, Tampa, FL, February 27 - March 1, 1991, 77 - 98.
- \_\_\_\_\_, \_\_\_\_\_, and \_\_\_\_\_, 1992b: The importance of density driven circulation in well mixed estuaries: the Tampa experience, in **Proceedings of the 2nd International Conference on Estuarine and Coastal Modeling**, Tampa, FL, November 13 -15, 1991, 332 - 343.
- Goodwin, C. R., 1977: Circulation patterns for historical, existing, and proposed channel configurations in Hillsborough Bay, Florida, in **Proceedings, 24th International Navigation Congress**, Leningrad, Subject 4, Section 4, 167 - 179.
- \_\_\_\_\_, 1980: Preliminary simulated tidal flow and circulation patterns in Hillsborough Bay, Florida, U.S. Geological Survey Open File Report 80-1021, 25 pp.
- \_\_\_\_\_, 1987: Tidal-flow, circulation, and flushing changes caused by dredge and fill in Tampa Bay, Florida, U.S. Geological Survey Water-Supply Paper 2282, 88 pp.
- \_\_\_\_\_, 1989: Circulation of Tampa and Sarasota Bays, in **Tampa and Sarasota Bays: Issues, Resources, Status, and Management**, NOAA Estuary-of-the-Month Seminar Series No. 11, 49 - 64.
- \_\_\_\_\_, and D. M. Michaelis, 1976: Tides in Tampa Bay, Florida: June 1971 to December 1973, U. S. Geological Survey, Tallahassee, Florida, Open File Report FL-75004, 338 pp.
- \_\_\_\_\_, and B. E. Ross, 1984: Evaluation of changes in circulation, spring tide, and hurricane surge characteristics in Tampa Bay caused by Sunshine Skyway pier protection system, (unpublished manuscript), 35 pp.

- Harris, D. L., N. A. Pore, and R. Cummings, 1963: The application of high speed computers to practical tidal problems, Abstracts of Papers 6:16, IAPO, Thirteenth General Assembly, IUGG, Berkeley, CA.
- Hess, K. W., 1990: Tampa Bay Oceanography Project: Progress Report for FY 1990, Estuarine and Ocean Physics Branch, Physical Oceanography Division, Office of Oceanography and Marine Assessment, NOS, NOAA, Rockville, MD, 38 pp.
- \_\_\_\_\_, 1992a: Numerical circulation model calibration and validation for Tampa Bay using NOS circulation survey data, in **Proceedings, Tampa Bay Area Scientific Information Symposium 2**, Tampa, FL, February 27 - March 1, 1991, 67 - 75.
- \_\_\_\_\_, 1992b: Tampa Bay Oceanography Project: Progress Report for FY 1991, Estuarine and Ocean Physics Branch, Physical Oceanography Division, Office of Oceanography and Marine Assessment, NOS, NOAA, Rockville, MD, 71 pp.
- \_\_\_\_\_, 1993: Modeling astronomical tides and currents in Tampa Bay, **Proceedings, International Conference on HydroScience and Engineering**, Washington DC, June 8-11, 1993, 1499 - 1506.
- \_\_\_\_\_, and K. T. Bosley, 1992: Methodology for validation of a Tampa Bay circulation model, **Proceedings of the 2nd International Conference on Estuarine and Coastal Modeling**, Tampa, FL, November 13 -15, 1991, 83 - 95.
- Jones, J. I., R. E. Ring, M. O. Rinkel, and R. E. Smith (Eds.), 1973: **A summary of knowledge of the eastern Gulf of Mexico, 1973**, State University System of Florida Institute of Oceanography, St. Petersburg, FL.
- Jordan, C. L., 1973: Climate, in **A Summary of Knowledge of the Eastern Gulf of Mexico, 1973**, (Eds. J. I. Jones, R. E. Ring, M. O. Rinkel, and R. E. Smith), State University System of Florida Institute of Oceanography, St. Petersburg, FL.
- Lewis, R. R., and R. L. Whitman, Jr., 1985: A new geographic description of the boundaries and subdivisions of Tampa Bay, in **Proceedings, Tampa Bay Area Scientific Information Symposium**, Tampa, FL, May 3-6, 1982, 10 - 18.
- Mellor, G. L., 1990: User's guide for a three-dimensional, primitive-equation, numerical ocean model, Princeton University Report, 50 pp.
- National Oceanic and Atmospheric Administration, 1990: Local Climatological Data: Annual Summary for Tampa, Florida, National Climatic Data Center, Asheville, NC.
- National Oceanic and Atmospheric Administration, 1991: Local Climatological Data: Annual Summary for Tampa, Florida, National Climatic Data Center, Asheville, NC.

- National Ocean Service, 1985: National Estuarine Inventory - Data Atlas, Vol. 1, Physical and Hydrologic Characteristics, Office of Oceanography and Marine Assessment, NOS, NOAA, Rockville, MD.
- \_\_\_\_\_, 1989: Tidal Current Tables 1990 - Atlantic Coast of North America, Office of Ocean and Earth Sciences, NOS, NOAA, Rockville, MD. 243 pp.
- \_\_\_\_\_, 1990a: Tampa Bay Oceanography Project - Plan for FY 1990 to FY 1992, Office of Oceanography and Marine Assessment, NOS, NOAA, Rockville, MD, 68 pp.
- \_\_\_\_\_, 1990b: Tidal Current Tables 1991 - Atlantic Coast of North America, Office of Oceanography and Marine Assessment, NOS, NOAA, Rockville, MD, 243 pp.
- Nichols, C. R., 1993: Operational characteristics of the Tampa Bay physical oceanographic real-time system, in **Proceedings, International Conference on HydroScience and Engineering**, Washington DC, June 8-11, 1993, 1491 - 1498.
- \_\_\_\_\_, C. R., R. G. Williams, and G. F. Appell, 1992: Quality assurance of Tampa Bay PORTS: Current measurements at the Sunshine Skyway Bridge, Office of Ocean and Earth Sciences, NOS, NOAA, Rockville, MD, 27 pp.
- Nowadly, F., 1992: Tampa Bay Oceanography Project: 1990 - 1991, NOS Oceanographic Circulation Survey Report No. 11, 25 pp + appendices.
- Pielke, R., 1974: A three-dimensional numerical model of sea breezes over South Florida, **Monthly Weather Review**, 102, 115 - 139.
- Pond, S., and G. L. Pickard, 1983: **Introductory Dynamical Oceanography**, 2<sup>nd</sup> Edition, Pergamon Press, New York, New York, 329 pp.
- Prandle, D., 1985: On salinity regimes and the vertical structure of residual flows in narrow tidal estuaries, **Estuarine, Coastal and Shelf Science**, 20, 615 - 635.
- Prandle, D., 1991: Tides in estuaries and embayments (Review), in **Tidal Hydrodynamics**, B. B. Parker (Ed.), Wiley and Sons, New York, New York, 125 - 152.
- Pritchard, D. W., 1955: Estuarine circulation patterns, **Proc. Amer. Soc. Civil Eng.**, 81, Separate No. 717, 1 - 11.
- Redfield, A. C., 1980: **The Tides and Waters of New England and New York**, Woods Hole Oceanographic Institution, 108 pp.

- Ross, B. E., 1973: The hydrology and flushing of the Bays, estuaries, and nearshore areas of the eastern Gulf of Mexico, in **A Summary of Knowledge of the Eastern Gulf of Mexico, 1973**, (eds. J. I. Jones, R. E. Ring, M. O. Rinkel, and R. E. Smith), State University System of Florida Institute of Oceanography, St. Petersburg, FL. Section IID, 1 - 45.
- Schureman, P., 1958: *Manual of Harmonic Analysis and Prediction of Tides*, US Department of Commerce, Coast and Geodetic Survey, Special Publication No. 98 [revised 1940 edition, reprinted 1988], 317 pp.
- Weisberg, R. H., and R. G. Williams, 1992: Initial findings on the circulation of Tampa Bay, in **Proceedings, Tampa Bay Area Scientific Information Symposium 2**, Tampa, FL, February 27 - March 1, 1991, 49 - 66.
- Williams, R. G., G. W. French, and C. R. Nichols, 1993: Nowcasting of currents in Tampa Bay using a physical oceanographic real-time system, in **Proceedings, International Conference on HydroScience and Engineering**, Washington DC, June 8-11, 1993, 1507 - 1512.
- Williams, R. G., T. D. Bethem, and H. R. Frey, 1989: Tampa Bay current prediction quality assurance miniproject, NOAA Technical Memorandum NOS OMA 50, Office of Oceanography and Marine Assessment, NOS, NOAA, Rockville, MD, 11 pp + figures.
- Wooten, G. R., 1985: Meteorology of Tampa Bay, in **Proceedings, Tampa Bay Area Scientific Information Symposium**, Tampa, FL, May 3-6, 1982, 19 - 26.
- Young, G. S., and J. W. Winchester, 1980: Association of non-marine sulfate aerosol with sea breeze circulation in Tampa Bay, **Journal of Applied Meteorology**, 419 - 425.
- Zervas, C. E., 1993: Subtidal water levels on the west Florida continental shelf and their effect on Tampa Bay, in **Proceedings, International Conference on HydroScience and Engineering**, Washington DC, June 8-11, 1993, 1513 - 1520.

## **APPENDIX A**

### **DEPLOYMENT TIME LINES FOR TOP DATA SETS**

Table A.1. Current Meter Deployments

STATION	Water Depth (m)	1990										1991									
		M	J	J	A	S	O	N	D	J	F	M	A	M	J	J	A	S	O		
C-1 A	10.7				R262			R262			R177	R262		R160	R217	R229					
C-2 A	25.0				R263			R263			R263	R263		R256	R256	R256					
C-3 A	15.1										R210										
C-4 A	8.4		R260		R160		R260			R260		R229		R217	R160	R160					
C-5 A	8.5		R229		R260		R217			R217		R217		R260	R260	R260					
C-6 A	29.3				R256		R256			R256					R263						
C-10 S	5.9		S05451472																		
C-11 S	5.7		S05451469																		
C-12 S	2.7		S05451470																		
C-13 S	6.9		S05451471																		
C-14 A	6.9		R160																		
C-15 A	7.0		R177																		
C-20 A	9.3				R177																
C-21 S	8.6				S05451472																
C-22 S	2.4				S05451471											S05451471					
C-23 A	9.1				R217																
C-24 S	5.1				S05451469																
C-26 S	5.0									S05451472											
C-27 A	11.9				S07301563		R177														
C-30 A	10.2												R160								
C-31 A	13.8									R229											
C-32 S	5.3									S05451471											
C-33 S	4.0									S05451470											
C-34 S	4.7									S07301563											
C-35 S	4.3									S05451469											
C-36 A	12.6									R160											
C-40 S	7.1											S05451470									
C-41 A	8.0											R260									
C-42 S	5.5											S05451472									
C-43 S	9.2											S05451471									
C-44 A	11.9											R177									
C-46 S	4.3											S07301563									
C-50 S	4.1														S05451470						
C-51 S	7.4														S05451471						
C-52 A	13.1																				
C-53 S	4.5												S07301563	S05451472							
C-54 S	5.7												S05451472	S07301563							
C-55 A	13.7														lost	R229					
C-56 A	14.3														R26		R217				
C-60 A	9.7																R177				

 QUALITY CONTROLLED DATA AVAILABLE  
 DATA QUESTIONABLE  
 DATA INVALID

Table A.2. Water level gage deployments

STATION	1990												1991					
	A	M	J	J	A	S	O	N	D	J	F	M	A	M	J	J	A	S
E-217 Cortez			■	■	■	■												
E-243 Anna Maria			■	■	■	■												
E-273 DeSoto Point			■	■	■	■												
E-347 Egmont Key			■	■	■	■	■	■	■	■	■	■		■	■			
E-364 Mullet Key			■	■	■	■	■	■	■	■	■	■	■	■	■	■	■	■
E-384 Port Manatee			■	■	■	■	■	■	■	■	■	■	■	■	■	■	■	■
E-428 Tierra Verde			■	■	■	■												
E-520 St. Petersburg			■	■	■	■	■	■	■	■	■	■	■	■	■	■	■	■
E-537 Apollo Beach			■	■	■	■	■	■	■	■	■	■	■	■	■	■	■	■
E-641 Gandy Bridge										■	■	■	■	■	■	■	■	■
E-657 Davis Island			■	■	■	■	■	■	■	■	■	■	■	■	■	■	■	■
E-667 McKay Bay										■	■	■	■	■	■	■	■	■
E-689 Bay Aristocrat V.			■	■	■	■	■	■	■	■	■	■	■	■	■	■	■	■
E-724 Clearwater			■	■	■	■	■	■	■	■	■	■	■	■	■	■	■	■
E-738 Safety Harbor										■	■	■	■	■	■	■	■	■
E-858 Venice Pier			■	■	■	■												

■ QUALITY CONTROLLED DATA AVAILABLE

Table A.3 Meteorological instrument deployments

STATION	1990												1991									
	A	M	J	J	A	S	O	N	D	J	F	M	A	M	J	J	A	S	O			
M-1a										M1004												
M-1b												M1004										
M-2										M7016	M1004	M7016	M0147									
M-3												M0148										
M-4												M7016							M7017			
M-5																						

 QUALITY CONTROLLED DATA AVAILABLE  
 DATA INVALID

Table A.4. CI and CTD deployments

STATION	1990							1991										
	M	J	J	A	S	O	N	D	J	F	M	A	M	J	J	A	S	O
C-1					C421		C240		C500		C682		C415	C239	C415			
C-2					C418		C411		C412		C239		C424	C237	C416			
C-4					C240		C417		C42		C237		C238	C418	C413			
C-5					C238		C412		C418		C413		C406	C818	C818			
C-6					C239		C239		C41				C682					
C-20					C412													
C-21					C411													
C-22					C424												C424	
C-23					C417													
C-24					C406													
C-26									C240								C419	
C-27							C421											
C-30											C406							
C-31									C413									
C-32									C415									
C-33									C238									
C-34									C406									
C-35									C422									
C-36									C237									
C-40											C410							
C-41											C415							
C-42											C424							
C-43											C419							
C-44											C418							
C-45											C422							
C-46											instrument lost C23							
C-51														C417	C417			
C-52														C419	C419			
C-53														C410	C406			
C-54														C240	C240			
C-55														lost C413	C424			
C-56														C420			C417	
C-60																	C23	
S-1 Upper					C500	C500	C500		C42		C410		C42	C412	C500	C817		
S-1 Lower					C501	C501	C501		C500		C500		C682	C418	C42	C418		
S-2 Upper											C424		C416	C237	C817	C500		
S-2 Lower											C419		C683	C239	C421	C406		
S-3 Upper					C502		C502				C42		C412	C500	C683	C411		
S-3 Lower					C503		C503				C239		C240	C421	C416	C683		

■ QUALITY CONTROLLED DATA AVAILABLE

▨ TEMPERATURE DATA ONLY

▩ INTERMITTANT SALINITY SPIKES

## APPENDIX B

### TYPICAL TIDAL AND TIDAL CURRENT CONSTITUENTS

**Table B.1. Harmonic constituents computed for Egmont Channel (C-2) from August 20, 1990 to September 25, 1991 (401 days) using least squares harmonic analysis.**

Constituent	Major Axis (118°)		Minor Axis (208°)	
	Amplitude (cm/s)	Epoch (°)	Amplitude (cm/s)	Epoch (°)
M <sub>2</sub>	53.7	337.6	2.5	262.6
S <sub>2</sub>	18.9	343.9	0.9	262.8
N <sub>2</sub>	9.6	333.9	0.4	269.7
K <sub>1</sub>	31.4	250.7	1.6	129.2
M <sub>4</sub>	2.2	14.4	0.5	328.2
O <sub>1</sub>	26.5	247.2	1.3	112.8
M <sub>6</sub>	0.2	239.3	0.5	319.8
MK <sub>3</sub>	2.1	261.2	0.2	113.6
S <sub>4</sub>	1.0	281.0	0.1	309.3
MN <sub>4</sub>	0.8	21.4	0.3	299.9
NU <sub>2</sub>	1.8	351.3	0.1	125.4
S <sub>6</sub>	0.2	217.2	0.1	175.6
MU <sub>2</sub>	2.1	205.2	0.5	261.3
2N <sub>2</sub>	1.0	274.9	0.2	156.1
OO <sub>1</sub>	1.1	279.9	0.2	137.6
LAMBDA <sub>2</sub>	1.5	42.4	0.2	330.4
S <sub>1</sub>	4.0	329.0	0.2	336.6
M <sub>1</sub>	0.1	281.9	0.4	214.9
J <sub>1</sub>	1.5	249.0	0.2	226.1
MM	0.5	215.5	0.2	119.8
SSA	1.8	60.2	0.5	285.1
SA	1.7	203.2	0.8	149.9
MSF	0.2	99.8	0.2	288.7
MF	0.7	107.1	0.1	296.0
RHO <sub>1</sub>	1.1	234.4	0.1	106.4
Q <sub>1</sub>	5.2	246.3	0.3	148.5
T <sub>2</sub>	1.2	353.0	0.4	327.9

**Table B.1 (continued). Harmonic constituents computed for Egmont Channel (C-2) from August 20, 1990 to September 25, 1991 (401 days) using least squares harmonic analysis.**

Constituent	Major Axis (118°)		Minor Axis (208°)	
	Amplitude (cm/s)	Epoch (°)	Amplitude (cm/s)	Epoch (°)
R <sub>2</sub>	1.3	128.8	0.2	174.1
2Q <sub>1</sub>	1.0	231.8	0.2	280.2
P <sub>1</sub>	9.8	251.3	0.2	216.7
2SM <sub>2</sub>	1.5	256.0	0.0	107.1
M <sub>3</sub>	0.7	120.1	0.4	94.9
L <sub>2</sub>	2.6	3.2	0.2	223.8
2MK <sub>3</sub>	2.0	277.2	0.4	155.6
K <sub>2</sub>	7.5	345.9	0.7	280.7
M <sub>8</sub>	0.3	307.8	0.2	176.0
MS <sub>4</sub>	1.4	.3	0.2	283.4

**Table B.2. Harmonic constituents computed for St. Petersburg (E-520) for 1990 (365 days) using least squares harmonic analysis.**

Constituent	Amplitude (cm)	Epoch (°)
M <sub>2</sub>	16.4	53.5
S <sub>2</sub>	5.2	64.2
N <sub>2</sub>	3.0	49.8
K <sub>1</sub>	15.7	335.8
M <sub>4</sub>	0.4	306.1
O <sub>1</sub>	14.8	329.4
M <sub>6</sub>	0.2	141.7
MK <sub>3</sub>	0.4	288.4
S <sub>4</sub>	0.1	28.1
MN <sub>4</sub>	0.1	317.3
NU <sub>2</sub>	0.7	65.0
S <sub>6</sub>	0.0	340.9

**Table B.2 (continued). Harmonic constituents computed for St. Petersburg (E-520) for 1990 (365 days) using least squares harmonic analysis.**

Constituent	Amplitude (cm)	Epoch (°)
MU <sub>2</sub>	0.8	254.4
2N <sub>2</sub>	0.4	137.5
OO <sub>1</sub>	0.4	16.3
LAMBDA <sub>2</sub>	0.5	89.0
S <sub>1</sub>	2.0	74.2
M <sub>1</sub>	0.8	48.3
J <sub>1</sub>	0.7	8.0
MM	0.0	0.0
SSA	2.4	63.8
SA	8.4	147.9
MSF	0.0	0.0
MF	0.0	0.0
RHO <sub>1</sub>	0.7	290.3
Q <sub>1</sub>	2.8	327.7
T <sub>2</sub>	0.3	71.8
R <sub>2</sub>	0.1	46.3
2Q <sub>1</sub>	0.3	264.6
P <sub>1</sub>	4.1	335.7
2SM <sub>2</sub>	0.2	335.8
M <sub>3</sub>	0.1	217.1
L <sub>2</sub>	0.8	57.7
2MK <sub>3</sub>	0.4	273.7
K <sub>2</sub>	2.4	59.1
M <sub>8</sub>	0.1	58.8
MS <sub>4</sub>	0.2	305.0